Coden: JPLPAY
Volume 9, Part A-2, No. 8, August 1971

Journal of Polymer Science

Part A-2: Polymer Physics

Contents

C. D. ARMENIADES and E. BAER: Structural Origin of the Cryogenic Relaxations in Poly(ethylene Terephthalate) 1345

G. M. BARTENEV: A New Relaxation Process in the High-Elastic State at Low Temperatures 1371

T. KOTAKA, N. DONKAI, and H. INAGAKI: Sedimentation Equilibrium in Non-ideal Heterogeneous Systems. I. Fundamental Equations for Heterogeneous Solute Systems and Some Preliminary Results 1379

M. YAMAMOTO and J. WHITE: Theory of Deformation and Strain-Induced Crystallization of an Elastomeric Network Polymer 1399

M. FUKUDA, G. L. WILKES, and R. S. STEIN: Stress-Optical Coefficient of Poly-1,4-butadienes 1417

H. G. OLF and A. PETERLIN: NMR Observations of Drawn Polymers. VII. Nylon 66 Fibers 1449

Y. YAMASHITA and K. MONOBE: Single Crystals of Amylose V Complexes. III. Crystals with 8_1 Helical Configuration 1471

J. L. WILLIAMS and A. PETERLIN: Transport Properties of Methylene Chloride in Drawn Polyethylene as a Function of the Draw Ratio 1483

T. GILLBRO, P.-O. KINELL, and A. LUND: ESR Single-Crystal Study of Radical and Radical-Pair Formation in Some γ-Irradiated Vinyl Monomers 1495

A. BROWN, T. GILLBRO, and B. NILSSON: Crystal Structure of Methyl Acrylate 1509

F. J. BOERIO and J. L. KOENIG: Vibrational Analysis of Poly(vinylidene Fluoride) 1517

NOTES

Y. ITO, S. KATSURA, and Y. TABATA: Application of Positron Lieftime Measurement to the Study of Solid-State Polymerization of Dimethyl Itaconate. 1525

G. L. WILKES: Technique of XYZ Photographic Light Scattering as Applied to Uniaxially Drawn Polyethylene 1531

Published by INTERSCIENCE PUBLISHERS a division of John Wiley & Sons, Inc.

Journal of Polymer Science **Part A-2: Polymer Physics**

The Journal of Polymer Science is published in four sections as follows: Part A-1, Polymer Chemistry, monthly; Part A-2, Polymer Physics, monthly; Part B, Polymer Letters, monthly; Part C, Polymer Symposia, irregular.

Published monthly by Interscience Publishers, a Division of John Wiley & Sons, Inc., covering one volume annually. Publication Office at 20th and Northampton Sts., Easton, Pa. 18042. Executive, Editorial, and Circulation Offices at 605 Third Avenue, New York, N.Y. 10016. Second-class postage paid at Easton, Pa. Subscription price, $325.00 per volume (including Parts A-1, B, and C) Foreign postage $15.00 per volume (including Parts A-1, B, and C).

JOURNAL OF POLYMER SCIENCE: PART A-2 VOL. 9, 1345–1369 (1971)

Structural Origin of the Cryogenic Relaxations in Poly(ethylene Terephthalate)

C. D. ARMENIADES, *Department of Chemical Engineering, Rice University, Houston, Texas 77001* and ERIC BAER, *Division of Macromolecular Science, Case Western Reserve University, Cleveland, Ohio 44106*

Synopsis

The effect of molecular organization (crystallinity, orientation) on the internal friction of poly(ethylene terephthalate) was studied by means of dynamic mechanical measurements at temperatures from 300 to 4.2°K, with a free-oscillating torsion pendulum at 1 Hz. It was found that crystallinity decreases the intensity of the composite γ relaxation at 210°K and gives rise to an additional loss maximum ϵ at 26°K. Uniaxial orientation broadens the γ relaxation and gives rise to an additional loss peak δ, at 46°K. The δ and ϵ losses are dependent on molecular organization, occurring only in samples containing aligned, taut chain segments and crystalline structures, respectively. They have a common activation energy of 4 kcal/mole. All three low-temperature relaxations in oriented specimens show pronounced directional anisotropy, which, in the γ loss, may be due to the preferred orientation of noncrystalline chain segments, while in the δ and ϵ losses, may be associated with the direction of defect structures. On the basis of the observed behavior of the δ and ϵ relaxations it is suggested that they may involve motions of defect structures and may thus participate in stress-transfer mechanisms at large deformations.

INTRODUCTION

It is well established that molecular motions and structural rearrangements in polymers do not cease at the onset of the glass transition. These motions are manifested macroscopically as relaxation phenomena at temperatures well below T_g and in some cases close to absolute zero.[1–4] In amorphous polymers the characteristics of the low-temperature relaxations may be directly related to the chemical structure and dynamics of the molecular chains. They have been attributed in general to small-scale motions of backbone or side-chain segments with low activation energies.[5–7] In crystalline and oriented polymers, the relaxation phenomena are more complex, showing considerable dependence on molecular organization. Sinnot has presented experimental evidence relating the α and γ relaxations in crystalline polyethylene with specific conformational arrangements, such as chain folds or lattice defects.[8] Subsequent analysis of the α, γ_c, and δ relaxations in polyethylene and polychlorotrifluoroethylene by Hoffman et al.[9] by use of barrier models suggested several mechanisms

whereby motion of specific segmental arrangements in folded lamellar crystals may give rise to discrete relaxations.

During the past three years we undertook an in-depth investigation of the internal friction and deformation behavior or ordered polymers at temperatures down to 4°K. Initial studies focused on poly(ethylene terephthalate) (PET), which can be processed to give specimens with various levels of crystallinity and chain orientation. Preliminary results of this work have been presented elsewhere.[10,11] They show a significant dependence of internal friction and deformation behavior on molecular organization. Crystalline and oriented PET samples were found to have loss maxima δ and ϵ at 46 and 26°K, respectively, which are not present in the amorphous polymer. The loss maxima were observed in addition to the previously known γ relaxation* at 210°K,[12-13] which was also found to depend on molecular organization. The crystalline oriented specimens, when subjected to tensile stress-deformation tests at temperatures down to 4°K showed a twofold increase in ductility over that of amorphous PET.

This paper discusses the results of a systematic study, aimed at elucidating the structural origin of the γ, δ, and ϵ relaxations in PET and their possible relation to cryogenic ductility.

EXPERIMENTAL

Materials and Instrumentation

The polymer used in this work, provided by courtesy of the Du Pont Co., has a number-average molecular weight of 15,000, with 1% low molecular weight (xylene-extractable) species. All samples were supplied in the form of melt-quenched sheets, which were amorphous to x-rays. Oriented specimens were characterized by means of density, birefringence, and x-ray diffraction measurements. Density was measured by a flotation-titration technique in carbon tetrachloride–*n*-heptane mixtures at 20°C. Optical birefringence was measured on a Reichert polarizing microscope using compensator plates of known birefringence. Conventional x-ray diffraction techniques with copper $K\alpha$ radiation were used for structural studies. The processing conditions and characteristic properties of the PET samples used in this investigation are listed in Table I.

The dynamic mechanical measurements were performed on a specially constructed cryogenic torsion pendulum described previously.[10] This is an inverted, free-oscillation pendulum, with the inertia arm located above the specimen and suspended by a fine monofilament and counterweight. The output of the instrument was processed by a Univac 1108 digital computer, which calculated and plotted the shear modulus G' and logarithmic decrement Δ of the specimen as a function of temperature. This computer was

* This relaxation is called β by Illers and Breuer[12] and by Takayanagi.[13] The authors of this paper follow the classification suggested by Hoffman et al.,[9] where the symbol β is reserved for the glass transition relaxation in amorphous polymers and the relaxations below T_g are named γ, δ, ϵ, etc.

TABLE I
Processing Conditions and Characteristic Properties of the PET Samples

Sample	Processing conditions	Density, g/cc[a]	Crystallinity, %	Optical birefrigence
1	Quenched from the melt[b]	1.331	0	0
2	Annealed 8 hr at 80°C	1.335	0	0
3	Annealed 70 min at 240°C	1.377	36	0
4	Annealed 2 hr at 240°C	1.406	59	0
5	Annealed 2 hr at 120°C	1.402	56	0
5a	Annealed 2 hr at 120°C and postdrawn 3.5 × at 100°C	—	—	0.121
6	Drawn uniaxially 5× at 40°C	1.368	28	0.183
6a	Drawn uniaxially 5× at 40°C and annealed taut 1 hr at 200°C	1.399	54	0.175
6b	Drawn uniaxially 5× at 40°C and annealed relaxed 1 hour at 200°C	1.401	55	0.078
7	Drawn uniaxially 5.4× at 65°C	1.372	32	0.191
7a	Drawn uniaxially 5.4× at 65°C and annealed taut 1 hr at 200°C	1.399	54	0.178
8	Drawn uniaxially 4× at 70°C	1.369	29	0.144
8a	Drawn uniaxially 4× at 70°C and annealed taut 1 hr at 200°C	1.404	58	0.165
8b	Drawn uniaxially 4× at 70°C and annealed taut 1 hr at 240°C	1.410	62	0.192
9	Drawn uniaxially 6.5× at 85°C	1.376	35	0.180

[a] Crystalline density: 1.455 g/cc[26] amorphous density, 1.334 g/cc.
[b] This is the as-received PET. All subsequent specimens were prepared from this material.

also used for smoothing and numerical differentiation of the loss modulus ($G'' = G'\Delta/\pi$) in order to resolve the components of the γ relaxation, as discussed in a subsequent section.

Analytical Treatment

The PET samples used in this work were either isotropic or uniaxially drawn. Pendulum specimens were cut from the oriented samples, with the torsion axis parallel, normal or at 45 degrees to the draw direction, as shown in Figure 1. The dynamic shear modulus of the isotropic specimens was calculated from the oscillation period (P) of the pendulum by using the standard equation[6]

$$G' = [(12\pi^2 IL/CD^3P^2) - (CT/4D^3)](1 - 0.63D/C)^{-1} \quad (1)$$

where I is the moment of inertia of the oscillating system; L, C, and D are the length, width, and thickness of the specimen, respectively, and T is the tensile load.

The torsional behavior of uniaxially oriented specimens was analyzed by the method of Hellwege et al.[15] In the case of specimens with chain orien-

tation parallel to the torsion axis (Fig. 1b) the dynamic shear modulus G_l is related to the stiffness constant of the drawn chain. It is therefore expected to be higher than the corresponding shear modulus of the isotropic specimen. Similar results are obtained for specimens with chain orientation normal to the torsion axis (Fig. 1c), because of their high aspect ratio ($C/D \approx 25$), which minimizes the effect of the transverse stiffness constant. Hence, the dynamic shear modulus G_t of these specimens is expected to be indistinguishable from G_l.

This analysis was extended to the specimens cut with the chain direction at 45 degrees to the torsion axis (Fig. 1c) by a simple rotation of the coordinate system.[16] The resulting value of the dynamic shear modulus G_{45} of these specimens approximates the tensile stiffness of the drawn chain. It is therefore expected to be much higher than G_l, approaching the value of the tensile modulus of the drawn polymer.

RESULTS

Isotropic Amorphous PET

The internal friction of isotropic amorphous PET was studied using the as-received melt-quenched film samples, as well as specimens annealed for 8 hr at 80°C and cooled slowly (2–3°C/hr) to room temperature. This annealing temperature is 13°C above the T_g of the amorphous polymer and should, therefore, be sufficiently high to remove strains frozen-in during the rapid quenching of the melt. However, the temperature is too low for crystallization. No crystallinity would be detected in the annealed speci-

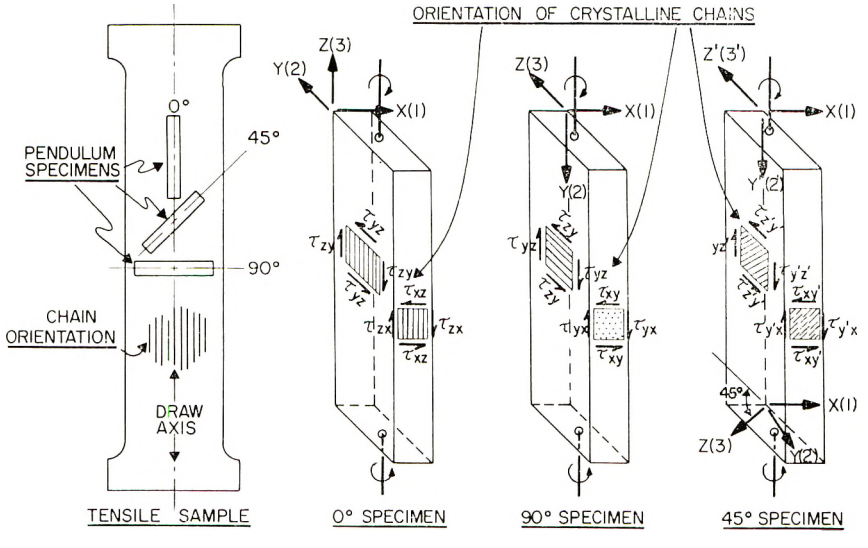

Fig. 1. Direction of torsional shear stresses with respect to crystalline chain orientation in specimens cut from uniaxially drawn PET samples at 0, 90, and 45° to the draw direction.

mens by either infrared spectroscopy or x-ray diffraction. The small increase in the density of the annealed sample, (Sample 2), from 1.331 to 1.335 g/cc, is probably due to stress relieving and volume equilibration of the glass.

The shear modulus and logarithmic decrement of an isotropic amorphous specimen (Sample 2), in the temperature range from 4 to 300°K, are shown in Figure 2. The γ loss peak occurs at 209°K and is very pronounced. Below 80°K the internal friction of the polymer is quite low and shows no loss maxima other than a shoulder at 50°K.

Effect of Crystallinity

It has been shown by Keller and co-workers[17] and by Bonart[18] that PET can develop crystalline structures of varying size and perfection by annealing of the glass at different temperatures. Samples annealed below 140°C have numerous, small spherulites and give x-ray diffraction patterns with considerable line broadening, indicating small crystallite size. In contrast, annealing above 220°C gives rise to large, well-developed spherulites, which have sharp x-ray diffraction lines indicating the presence of large, well-perfected crystalline structures. By annealing for 2 hr at 120 and 240°C we obtained isotropic specimens of approximately the same crystalline content (about 60%, as measured by density), but having the above mentioned differences in crystallite size and perfection. A sample of lower crystallinity (36%) was also obtained by annealing at 240°C for a shorter period.

Figure 2 shows the internal friction behavior of the isotropic crystalline specimens and compares it with the amorphous polymer. It can be readily seen that the strength of the γ relaxation decreases considerably with crystallinity. In addition, the crystalline samples show a new loss maximum ϵ at 22°K, which is not present in amorphous PET. This relaxation is strongest in sample 4, which has a high crystalline content as well as large, well-developed crystalline structures. Comparison of samples 3 and 5 shows that the effect of crystallinity in reducing the γ loss and enhancing the ϵ loss cannot be adequately assessed in terms of crystalline content alone, without considering the size and perfection of the crystalline structures. Indeed it is these structural factors that appear most effective in determining the γ and ϵ relaxations in semicreptalline PET.

Effect of Orientation

Molecular Organization of Drawn PET. Several authors have studied the kinetics of strain-induced crystallization of PET[19] and the resulting structure and morphology.[18–25] Of particular value for this work is Bonart's analysis[18] of the x-ray diffraction patterns of uniaxially drawn PET on the basis of Hosemann's paracrystallinity theory, since his treatment is directly applicable to several specimens used in this study.

For a systematic investigation of orientation effects on the low-temperature relaxations in drawn PET a number of samples were prepared in

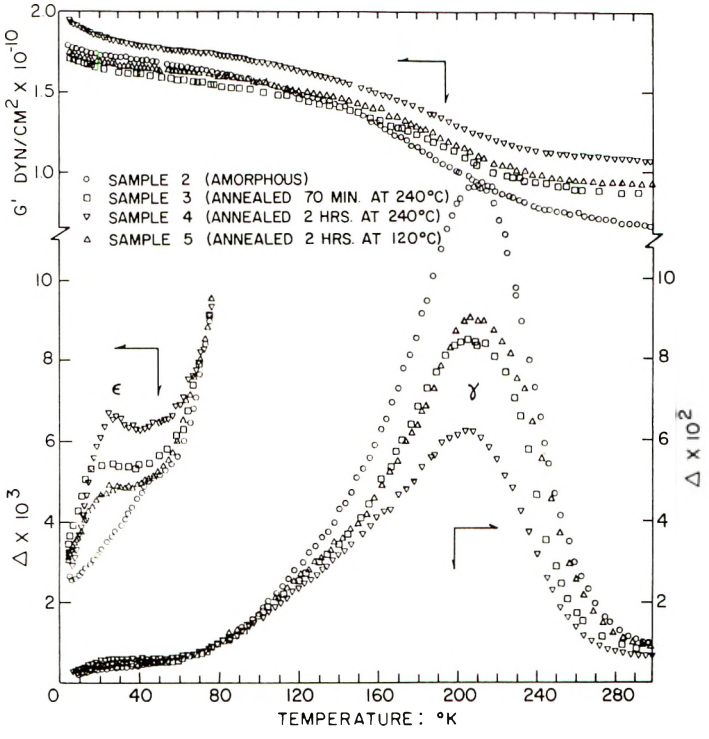

Fig. 2. Shear modulus G' and logarithmic decrement Δ of isotropic, amorphous, and semicrystalline PET samples at 1 Hz.

addition to those listed in Table I. These were drawn uniaxially at temperatures from 25 to 100°C, at different draw rates at each temperature. Samples drawn at temperatures below T_g deformed by necking and neck propagation, which was accompanied by the formation of microvoids. These voids were estimated from small-angle x-ray diffraction measurements to range in size from about 50 Å to almost 1 μ. They appear to be elongated in the draw direction. Samples drawn above T_g deformed uniformly and remained essentially free of voids.

Specific information on the molecular organization of the oriented PET samples was obtained by careful analysis of their x-ray diffraction patterns. Specimens drawn less than 4× at temperatures below 60°C show very little isotropic amorphous scatter but have intense diffuse equatorial reflections. A typical pattern with these characteristics appears in Figure 3*a*. It indicates a high degree of chain alignment in the draw direction, as suggested by the high optical birefringence of these specimens. The diffraction patterns show at least two layer lines, (001)* and (003)*, which are sharp in the meridional direction but diffuse along the equatorial plane. These cannot be indexed on the basis of the triclinic PET unit cell[26] but correspond to the chemical repeat distance of the molecular chain in the *trans* conformation (10.7 Å). According to Bonart[18] this pattern arises from a smectic arrange-

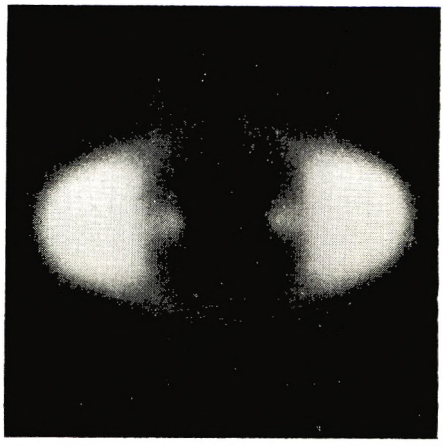

(a)

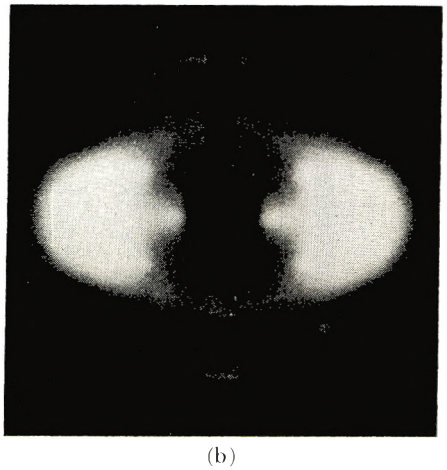

(b)

Fig. 3. X-Ray diffraction patterns of melt-quenched PET samples drawn uniaxially at 40°C: (*a*) drawn 3.8×; (*b*) drawn 5×.

ment of chain segments, where the chemical repeat units are in longitudinal register but the benzene rings are not yet parallelized, and results in an almost circular average chain cross section. The aligned chains are arranged laterally in hexagonal packing, forming a monoclinic lattice. At higher extensions the lateral order is somewhat improved and gives rise to the discrete $0\bar{1}1$ and $\bar{1}12$ reflections (Fig. 3*b*), which suffer the least amount of broadening from lateral distortion of the triclinic unit cell.

At temperatures around T_g (60–85°C) the extension rate and draw ratio become increasingly important in determining the structure of the oriented polymer. At low rates and extensions less than 4× the sample retains a substantial amount of isotropic amorphous scatter. It also shows the characteristic reflections of the smectic structure (Fig. 4*a*). These decrease in intensity with increasing draw temperatures and disappear in

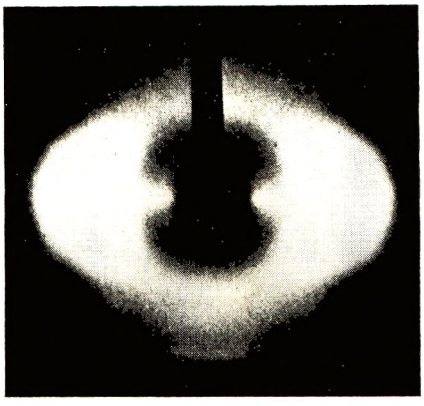

(a)

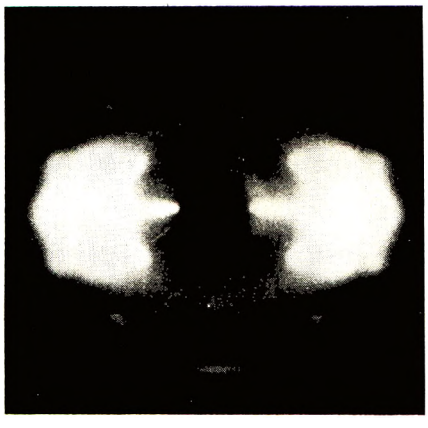

(b)

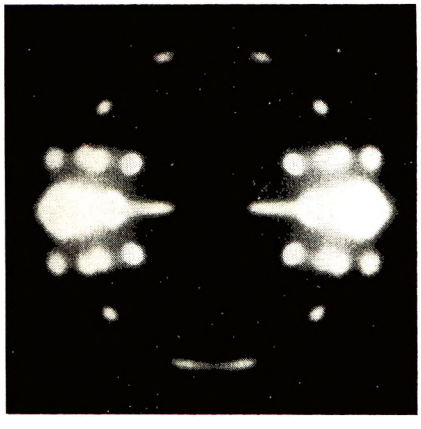

(c)

Fig. 4. X-Ray diffraction patterns of melt-quenched PET samples drawn uniaxially at temperatures near T_g: (*a*) drawn 3.5× at 70°C at a rate of 10%/min; (*b*) drawn 5.4× at 65°C; (*c*) drawn 5.4 × at 65°C and annealed taut for 1 hr at 200°C.

samples drawn above 70°C. At high rates, or extensions greater than 4×, the specimens develop a crystalline fiber pattern, which can be indexed on the basis of the triclinic unit cell[26] (Fig. 4*b*]. This pattern becomes perfected when the sample is heat-set (Fig. 4*c*). It can be reasonably postulated that at these temperatures the molecular chains possess sufficient segmental mobility to slide past each other and reorganize into crystalline structures under the influence of the drawing stress. It should be noted, however, that this stress decreases drastically with increasing temperature above T_g. As a result, the sample oriented at 85°C contains fewer taut chains than those drawn at lower temperatures.

At temperatures above 90°C the molecular chains in the now rubbery polymer possess sufficient mobility to permit several-fold extension of the specimen at low rates (100%/min) without noticeable change in molecular organization (Fig. 5*a*). Higher rates (2000%/min) result in the develop-

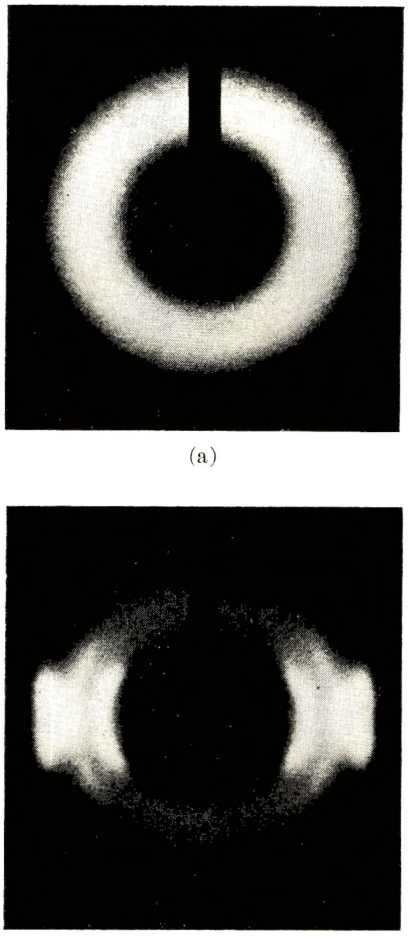

(a)

(b)

Fig. 5. X-Ray diffraction patterns of melt-quenched PET samples drawn uniaxially at 95°C: (*a*) drawn 6× at a rate of 100%/min; (*b*) drawn 4.2× at 2000%/min.

ment of crystalline structures, which are tilted 18–20° from the draw direction (Fig. 5*b*). It is known[19] that still higher rates and draw ratios give rise to structures with higher crystallinity and orientation. These rates, however, are not attainable with our present equipment.

Relaxation Behavior. The effect of molecular orientation on the low-temperature relaxation behavior of PET is illustrated best by sample 6, which has a high degree of axial chain alignment without crystalline order (Fig. 3*b*). Internal friction data on this and other samples drawn at higher temperatures are shown in Figure 6. These samples were cut and tested with the torsion axis parallel to the draw direction.

In the oriented specimens the γ relaxation shows a 5°K shift in its loss peak (from 209 to 214°K) and a substantial broadening of its high-temperature side, which extends to room temperatures (at 300°K the drawn

samples have Δ values three to four times higher than the isotropic polymer). The progressive decrease of γ peak loss strength in samples 6, 7, and 9 is probably due to the increase in strain-induced crystallinity.

An attempt was made to resolve the γ relaxation into its components with the aid of numerical differentiation of the loss functions, as shown in Figure 7. The inflection points in the plot of $\partial G''/\partial T$ and $\partial\Delta/\partial T$ versus temperature locate the peak temperature of the component relaxations.

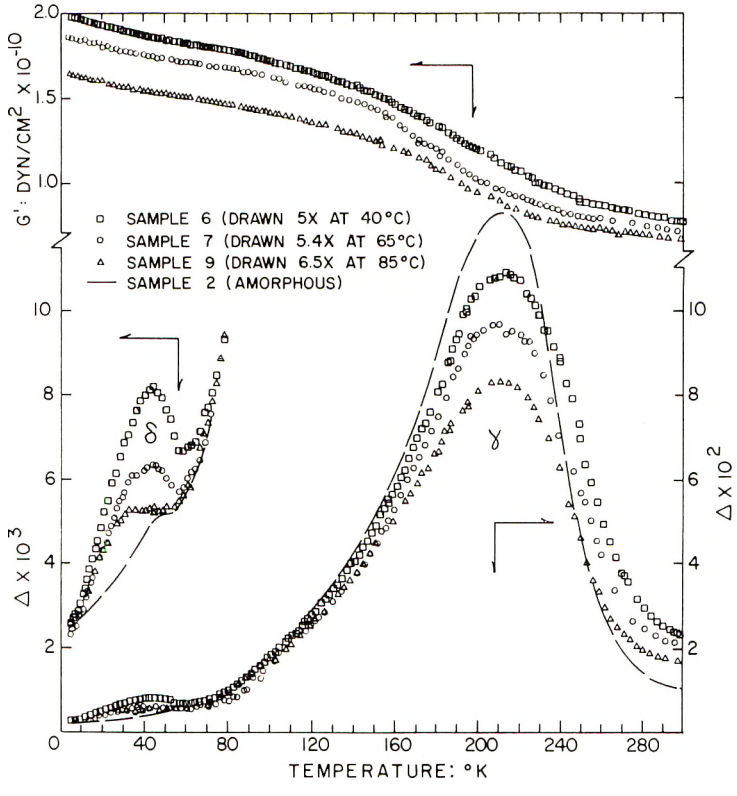

Fig. 6. Shear modulus and logarithmic decrement of uniaxially oriented PET samples, tested at 1 Hz with the torsion axis parallel to the draw direction.

These are listed in Table II. The isotropic specimens (amorphous and crystalline) show three γ loss components: γ_1 near 110°K, γ_2 around 156°K, and γ_3 at about 206°K. In the oriented samples the inflection in the loss function derivatives corresponding to the γ_3 peak occurs at a slightly lower temperature (200°K). In addition, these samples show an inflection around 235°K, indicating the presence of another subsidiary relaxation, which would account for the observed broadening of the overall γ loss.

In addition to the composite γ relaxation the drawn specimens show a sharp loss peak, δ, at 46°K. This loss is typical of oriented PET. It is

TABLE II
Inflection Temperatures of Loss Function Derivatives of the PET Specimens

Sample	Temperature, °K[a]			
	γ_1	γ_2	γ_3	
1	110, 112	156, 155	206, 206	
2	118, 119	(160)	209, 210	
3	108, 109	157, (158)	205, 209	
4	106, 107	(154)	204, 208	
5	105, 106	?	205, 208	
6	110, 110	150, (160)	202, 204	236, 236
6a	107, 108	170, (160)	198, 200	232, 234
7	106, 107	(160)	No data	
7a	109, 110	154, 156	196, 202	236, (235)
8	104, 106	159, 155	200, 210	232, (232)
8a	114, (116)	159, (160)	198, 206	233, (235)

[a] Numbers are midpoints of inflections in $\partial G''/\partial T$ and $\partial \Delta/\partial T$ respectively, Parentheses indicate ill-defined inflections.

most intense in sample 6, reaching a maximum Δ value of 8.1×10^{-3}. At this temperature the isotropic amorphous specimen has a log decrement of only 5×10^{-3}. The δ loss peak becomes broader and progressively less intense in samples 7 and 9, which were drawn at higher temperatures.

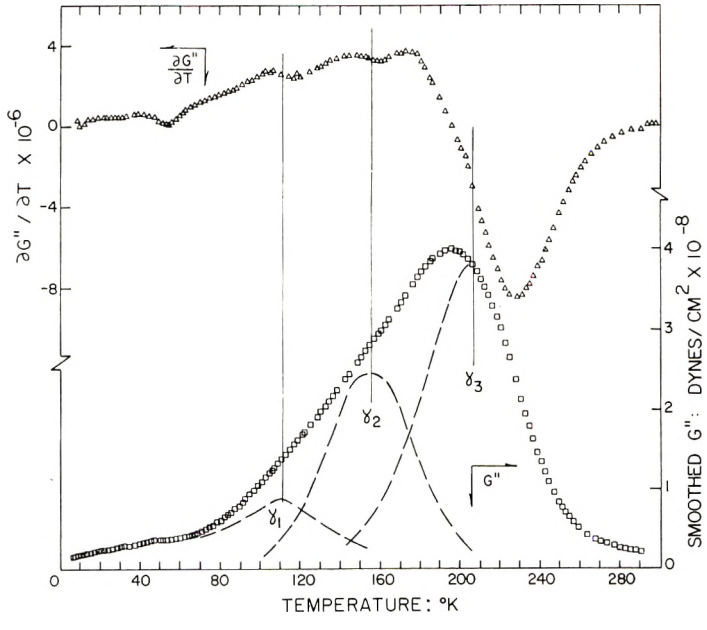

Fig. 7. Loss modulus G'' and its temperature derivative for quenched amorphous PET after smoothing and numerical differentiation of data.

Indeed, this loss peak was found to be extremely sensitive to the draw parameters of the specimen, such as temperature, extension rate and draw ratio. Since these conditions determine to a large extent the supramolecular structure of the drawn polymer it is instructive to examine their effect on the δ relaxation.

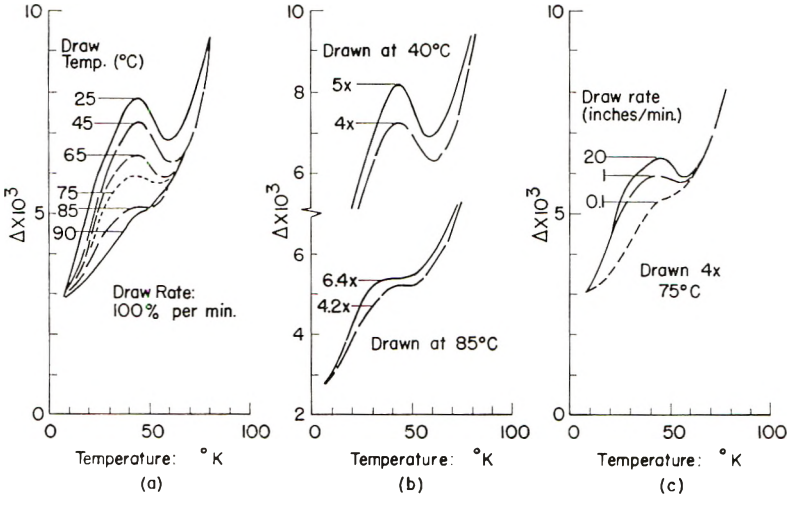

Fig. 8. Effect of draw temperature, extension, and draw rate on the relaxation: (*a*) samples drawn 4× at 100%/min at different temperatures; (*b*) samples drawn to different extensions at 40 and 85°C: (*c*) samples drawn 4× at 75°C at different rates.

Figure 8*a* compares the behavior of several specimens drawn 4× at a rate of 100%/min and different temperatures. In these samples the molecular orientation and amount of residual strain decrease as their draw temperature approaches and exceeds T_g. Correspondingly, the intensity of the δ loss decreases with increasing draw temperature. The extreme case is the sample drawn at 90°C, which shows no difference in density, birefringence or x-ray diffraction from the amorphous polymer. Its relaxation behavior is also identical to that of amorphous PET. The specimens drawn near T_g (65 and 85°C) develop, in addition to chain orientation, a certain amount of strain-induced crystallinity. These show a broad, diffuse loss maximum, which extends over the temperatures of the δ and ϵ losses. The two peaks are separated when the specimen is annealed taut, as shown in Figure 14 below. It should be noted that the δ loss is most intense in specimens drawn well below T_g, which have high residual strains, as well as large number of microvoids and defects, as a result of the drawing process.

Figure 8*b* shows the effect of draw ratio on the δ loss at two different temperatures. The intensity of the loss is enhanced by high draw ratios, which increase the degree of molecular orientation, as indicated by birefringence measurements.

Figure 8c compares the relaxation behavior of three PET samples drawn at different rates slightly above T_g. At this temperature the draw rate becomes critical in determining the degree of orientation and strain-induced crystallinity (see Figs. 5*a* and 5*b*). At high draw rates, the samples acquire a certain amount of orientation and crystallinity. As expected they show loss maxima in the temperature range of the δ and ϵ relaxations. At low extension rates, drawing produces little change in the molecular organization of the polymer, and its relaxation behavior approaches that of amorphous PET.

Directional Anisotropy of the Relaxations

The pronounced orientation dependence of the low-temperature relaxations in drawn PET raises the possibility that they may involve loss mechanisms which act preferentially along specific directions. In order to

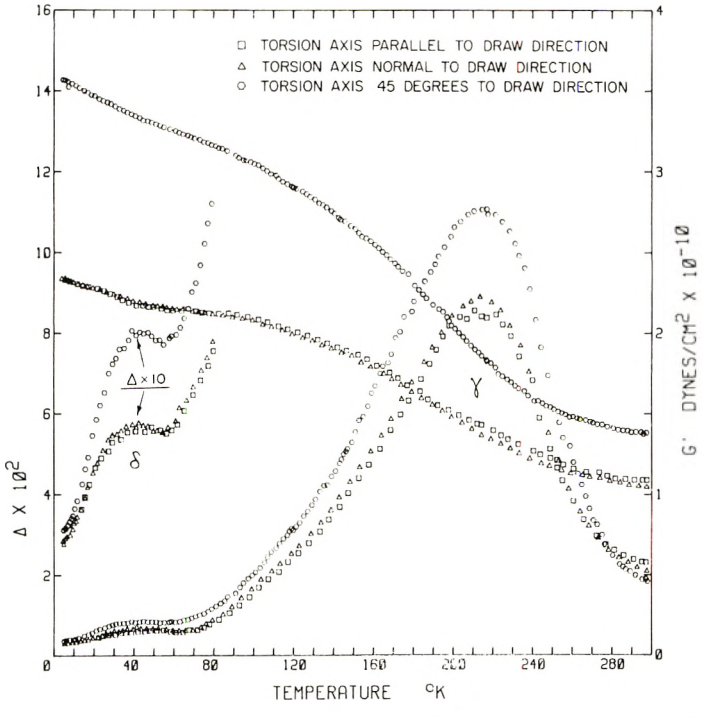

Fig. 9. Shear modulus and logarithmic decrement of specimens cut from sample 8 (drawn uniaxially 4× at 70°C).

investigate this possibility a number of specimens were cut from samples 8, 8a, and 8b, with their torsion axis parallel, normal, and at 45° to the chain orientation of the drawn film, as is shown in Figure 1. Internal friction measurements on these specimens are presented in Figures 9–11.

The observed shear moduli are consistent with expectations based on our theoretical analysis of the torsional behavior of oriented specimens. The

parallel and perpendicular specimens from the same sample have almost identical moduli, which are higher than the corresponding moduli of isotropic specimens with similar crystallinity. The 45° specimens show by far the highest modulus, since it relates to the tensile stiffness of the drawn chains.

Of considerable importance are the directional aspects of the internal friction. Within each of the three drawn PET samples the parallel and

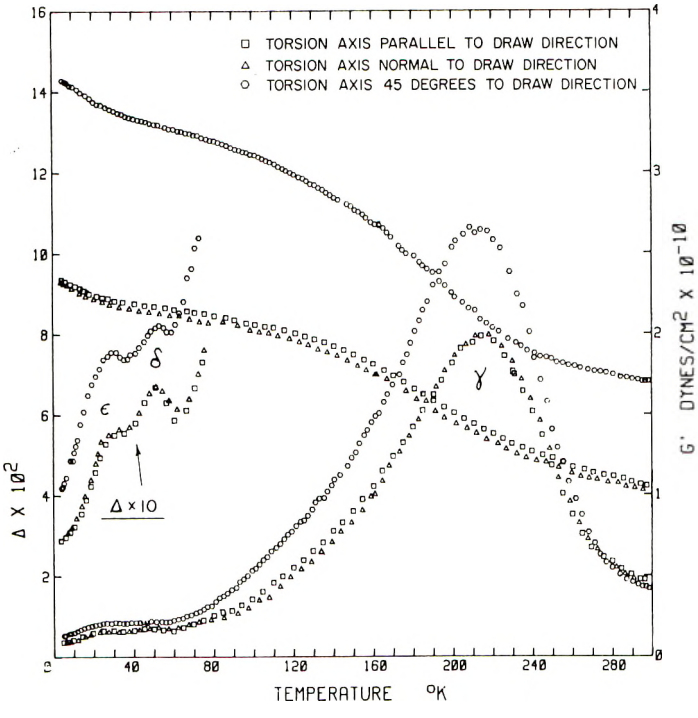

Fig. 10. Shear modulus and logarithmic decrement of specimens cut from sample 8a (drawn uniaxially 4× at 70°C and annealed taut for 1 hr at 200°C).

perpendicular specimens show very similar logarithmic decrement, which agrees with other parallel specimens of similar process history. However, the 45° specimens show a different loss behavior. In samples 8 and 8a (Figs. 9 and 10) they have substantially higher log decrement than the parallel and perpendicular specimens. This anisotropy is almost reversed in sample 8b, which was annealed at a higher temperature. Here the log decrement of the 45° specimen is slightly lower than that of the parallel and perpendicularly cut specimens, the difference becoming most pronounced near the ϵ loss peak. The intensity of all three relaxations in this drawn sample is relatively high in comparison with data on isotropic samples with similar annealing treatments, such as sample 4 in Figure 2.

The presence of directional anisotropy in logarithmic decrement within a given sample reflects a preferential action of the loss mechanism along a specific direction. Since there are no marked differences in crystalline structure or chain orientation between samples 8a and 8b, the observed variance in the directional anisotropy of the low-temperature relaxations must be attributed to differences in supramolecular structure, as a result of their respective annealing temperatures. The existence of such morphological differences is indicated by the small-angle diffraction patterns of the two samples. Sample 8a, annealed at 200°C, shows a four-point pattern oriented at 43° to the meridian. In sample 8b, annealed at 240°C, the

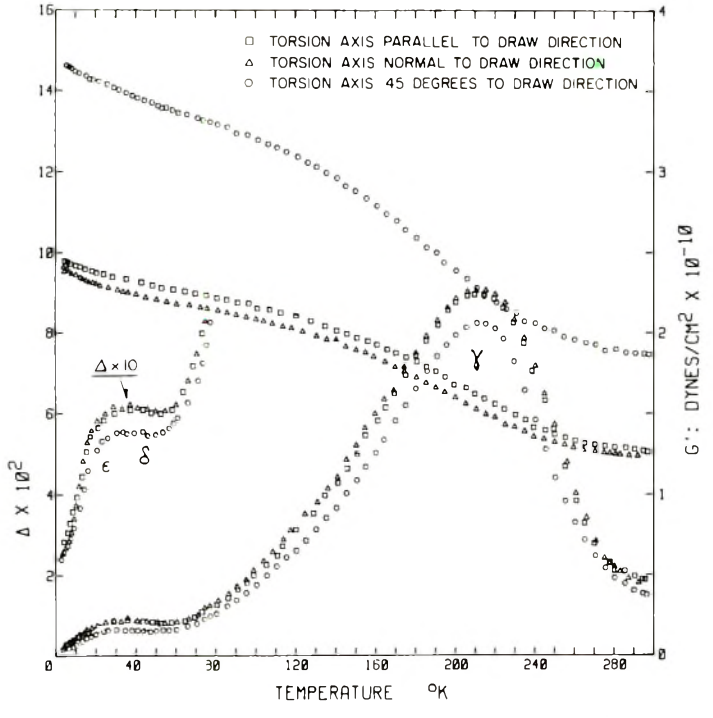

Fig. 11. Shear modulus and logarithmic decrement of specimens cut from sample 8b (drawn uniaxially 4× at 70°C and annealed taut for 1 hr at 240°C).

diffraction maxima diverge only by 11° from the meridian. Similar small-angle diffraction patterns have been observed by previous investigators[22–26] with PET specimens of similar process history. The four-point patterns reflect the existence of specific supramolecular arrangements in samples 8a and 8b, which give rise to structural periodicity. In sample 8a this periodicity occurs at an angle of 47° to the chain orientation, while in sample 8b, it is at 79.° It is noteworthy that the relaxation anisotropy of these samples is related to the direction of their structural periodicity, as indicated in Figure 12. In both samples the loss peaks are most intense when

the maximum shear stresses are in directions closest to the structural periodicity.

The exact morphological origin of this periodicity is not yet unequivocably established. Statton[23] has proposed a model for the axially oriented crystalline polymer, consisting of aligned multi-molecular fibrils, having a regular alternation of bulky (amorphous) and condensed (crystalline) regions along their length. He attributes the four-point pattern to a staggered arrangement of these regions in adjacent fibrils. Bonart[24] has suggested a staggered arrangement of aligned chain segments, while Yeh and Geil[25] have shown electron micrographs of oriented thin films where the nodular structures present in the amorphous polymer are aligned at an angle of 50° to the draw direction. They have also shown that this orientation of the nodular

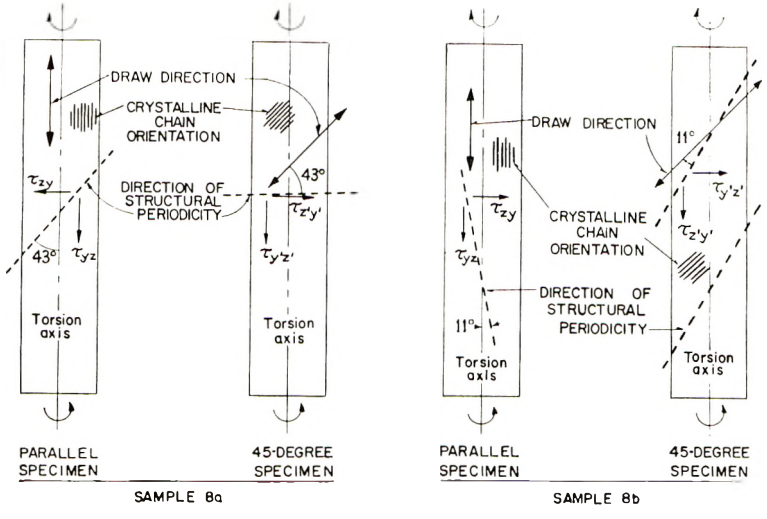

Fig. 12. Correlation of structural periodicity in samples 8a and 8b with the direction of the torsional shear stresses in the parallel and 45° specimens.

rows remains unaltered when the polymer is annealed taut at temperatures below 200°C, but shifts to a direction normal to the chain orientation at higher annealing temperatures, occurring at an angle of 80° in samples drawn at 240°C. The orientation of the nodular rows corresponds to the direction of the four-point small angle diffraction, which is attributed to a staggered arrangement of these rows. On the basis of this evidence the observed anisotropy in the low-temperature relaxation of samples 8, 8a, and 8b could be related to the arrangement of the nodular structures.

DISCUSSION

The γ Relaxation

The γ relaxation in PET has been attributed to motions involving hindered rotation of the glycol methylenes as well as motion of the carboxylene

TABLE III
Summary of the Low-Temperature Relaxation Characteristics

	γ relaxation				δ relaxation				ϵ relaxat on			
Sample	$G_U - G_R$, dynes $\times 10^{-9}$	Peak temperature, °K	Δ_{max} $\times 10^2$	Activation energy, kcal/mole	$G_U - G_R$, dynes/cm^2 $\times 10^{-9}$	Peak temperature, °K	Δ_{max} $\times 10^2$	Activation energy, kcal/mole	$G_U - G_R$, dynes/cm^2 $\times 10^4$	Peak temperature, °K	Δ_{max} $\times 10^3$	Activation energy, kcal/mole
1	9.16	206	10.90	15.8	Shoulder	49	5.64	?		None		
2	10.50	209	12.62	16.1	Shoulder	50	5.27	?		None		
3	6.60	204	8.62	15.4		None			0.71	27	5.12	4.1
4	5.55	203	6.24	16.3		None			1.47	26	6.62	4.4
5	6.88	206	9.06	15.7		None			0.67	26	4.86	4.2
5a	9.91	209	9.36	16.7	1.43	44	6.12		Shoulder	26?		
2	10.29	214	10.83	16.4	1.60	44	8.10	4.0		None		
6a	7.87	211	8.20	16.3	1.75	46	7.73	4.2[a]	Shoulder	26		
6b												
7	No data	213	8.32		1.60	44	6.34	3.7		None		
7a	8.38	211	7.80	16.6	1.67	48	6.58	3.9[a]	Shoulder	24?		
8[b]	19.13	214	12.11		3.08	42	7.98	3.9	Shoulder?			
8a[b]	15.58	212	10.53		3.00	46	7.77	4.1[a]	1.40	29	7.39	
9	8.65	209	8.10	16.4	1.47	42	5.32	4.3	Merges with δ loss			

[a] Single activation energy value, calculated for the composite δ–ϵ relaxation.
[b] Data from specimens with chains oriented 45° from torsion axis.

groups near *gauche* or *trans* chain segments.[12] The contribution of the methylene motions has been demonstrated by measurements of Farrow et al. on a series of poly(methylene terephthalates).[27] The significant role of the carboxylene motions is corroborated by the internal friction of aromatic terephthalates[28] and polycarbonates,[29] which have similar γ loss peaks, despite the absence of aliphatic chain segments. This work shows the glycol motions (γ_1) to be the weakest component of the γ relaxation in PET (Fig. 7), the bulk of the loss peak arising from the γ_2 and γ_3 components, attributed to carboxylene motions.

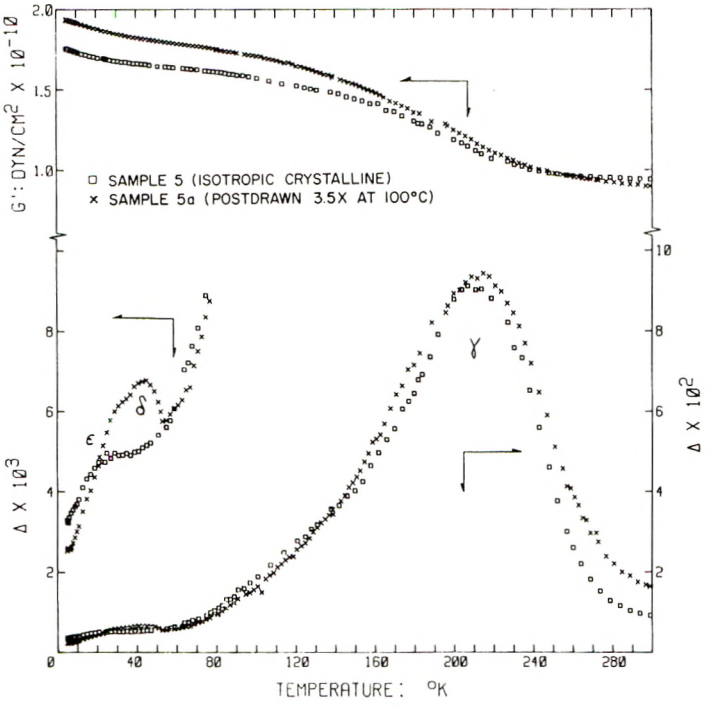

Fig. 13. Effect of postdrawing on the internal friction of crystalline PET at 1 Hz.

By use of the method of Read and Williams[30] it was possible to calculate the activation energy ΔE_γ of the relaxation of the PET samples used in this work from single-frequency measurements. The resulting values are listed in Table III, which summarizes the observed characteristics of the low temperature relaxations. ΔE_γ is about 16 kcal/mole for the isotropic polymer. It is slightly higher in the oriented samples, possibly because of the contribution of the residual stresses to the hindrance potential of the γ relaxation. These values are in agreement with the previously reported activation energy of 17 kcal/mole, calculated from mechanical and NMR measurements at various frequencies.[12]

Crystallinity Effects. The most extensive previous investigation of crystallinity effects on the γ relaxation is that of Illers and Breuer,[12] who

also used a torsion pendulum at 1 Hz. Their results can be compared directly with these measurements on samples 2, 4, and 5, if the loss modulus G'' is used as a measure of internal friction. With the exception of a consistent difference of 4°K in the peak temperature of the γ loss, the two sets of data are in substantial agreement. Both show a decrease in the intensity of the γ relaxation with crystallinity, which is more pronounced in the PET samples of this work. These have a considerably higher crystalline content than the samples of Illers and Breuer annealed at similar

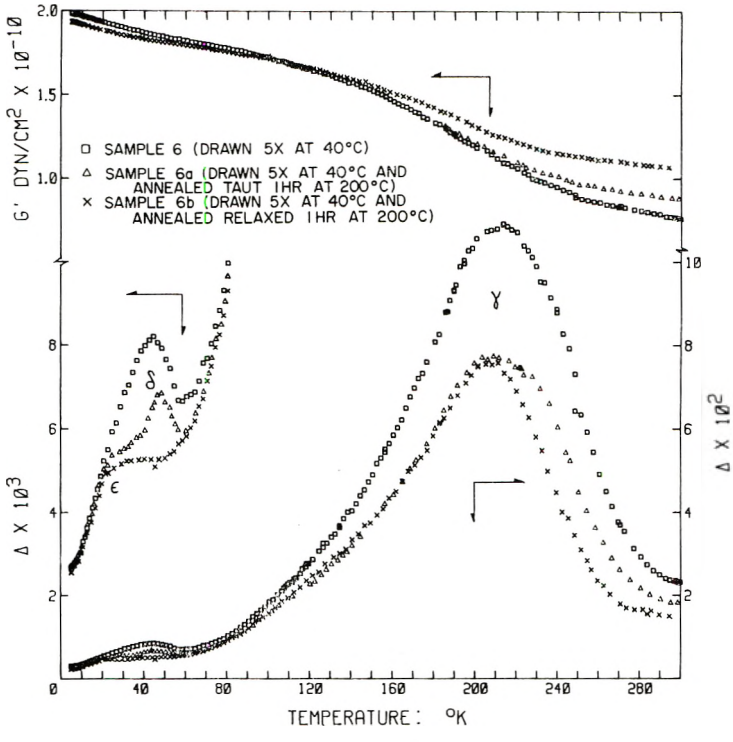

Fig. 14. Effect of annealing on the internal friction of uniaxially drawn PET at 1 Hz.

temperatures, which is not surprising, since the cold crystallization behavior of PET is substantially dependent on several parameters in addition to temperature.[16,31]

The weakening of the γ loss, first in the low, then the high temperature side of the peak, is explained by Illers and Breuer by a decrease in the population of amorphous *gauche* chain segments during nucleation, followed by a decrease in amorphous *trans* species during crystalline growth. Their data show this weakening to be most rapid at low crystallinity (0–16%) with little additional change as the crystallinity increases to 46%. This behavior is not consistent with recent morphological[32] and spectroscopic[33] evidence, which shows that cold crystallization in PET proceeds

initially by perfection of existing order within small domains with a minimum of gross morphological reorganization. Substantial growth of large spherulitic structures causing considerable reduction in *gauche* as well as *trans* amorphous content, occurs only at higher annealing temperatures. One would, therefore, expect the decrease in γ loss with crystallinity to be quite pronounced in specimens, annealed at high temperatures to high crystalline contents, as is observed in this work (Fig. 2). This is in accordance with the morphology of cold crystallized PET[17,29] and agrees with the assignment of the predominant γ loss components to carboxylene motions, which cannot occur in crystalline structures with planarized phenyl groups. At low crystallization temperatures the polymer contains numerous small, relatively imperfect crystallites, while a large fraction of the chain segments may still retain sufficient mobility to allow the loss motions. These are progressively suppressed by the growth of large, well-developed crystallites at higher annealing temperatures.

Orientation Effects. There are few published studies on the effect of orientation on the γ relaxation of PET.[34,35] These are limited to temperatures above 190°K and contain only sketchy descriptions of the specimen structure. This work shows that orientation causes a shift of the γ loss peak to higher temperatures, as well as a broadening of the high temperature region of the relaxation (Fig. 6). The peak shift can be attributed to a relative increase in the population of *trans* chain segments (which give rise to the γ_3 loss) as a result of orientation. It has been found by studies of infrared dichroism that the degree of *gauche*-to-*trans* conversion decreases with increasing draw temperature up to 100°C.[36] Correspondingly, the shift in the γ peak temperature decreases from 8 to 7 to 3°K in samples 6, 7, and 9, drawn at 40, 65, and 85°K, respectively. The process of uniaxial drawing also introduces residual axial strains on the oriented chains, which are most severe in the samples drawn below T_g. These strains are expected to increase the hindrance potential to the γ_3 relaxation and may explain the occurrence of the broadening of the γ loss at high temperature. As expected, this broadening is most pronounced in samples 6 and 7, which were drawn below T_g.

Directional Anisotropy. The directional anisotropy of the γ relaxation may be explained by considering the mechanism of strain-induced crystallization on the basis of recent morphological studies.[25] These indicate that uniaxial drawing causes alignment and perfection of the paracrystalline nodular aggregates present in the amorphous polymer. The amorphous segments originally in the draw direction can be most readily incorporated in the strain-induced crystalline structures. However, those at large angles to the draw axis are subject to the principal shear stresses due to drawing, which act at an angle of 45° to the draw direction. As a result, in the drawn polymer, the remaining amorphous chains would have a preferential reorientation at 45° to the draw axis. Accordingly, in sample 8 (Fig. 9) the 45° specimen in the torsion pendulum has its amorphous chain segments preferentially aligned in the direction of maximum shear. Hence,

it shows the most intense γ loss. The same is true for sample 8a (Fig. 10), since heat-setting at 200°C is known to leave the superamolecular arrangements largely undisturbed.[32] However, at higher annealing temperatures, where crystallization proceeds slowly, a substantial amount of amorphous material is incorporated in the aligned crystallites. This results in reorientation of most chain segments along the draw direction. Accordingly, in sample 8b (Fig. 11), the specimens cut parallel and normal to the draw direction have their noncrystalline chain segments preferentially aligned in the direction of maximum shear during the torsional experiments and show therefore, high γ loss peaks.

The δ and ϵ Relaxations

The investigation of the structural origin of the δ and ϵ relaxations in PET is hindered by the paucity of information on comparable phenomena in other polymers. Hoffman et al., in their theoretical study of polymer relaxations,[9] attempt an approximate estimate of the activation energy of the δ relaxation, based on high-frequency dielectric data of Scott et al.[37] and Hartshorn et al.[38] on polychlorotrifluoroethylene. The small number of dynamic mechanical measurements at low frequencies[39,40] have been confined to polymers with side groups. Here the observed low temperature relaxations are attributed to localized side-group motions, which probably bear no relation to the cryogenic relaxations of linear chains such as PET. The only reports of cryogenic relaxations of linear polymers are the measurements of Crissman et al.,[41] who observed a broad, low level loss maximum in poly(vinyl chloride) around 18°K at 7225 Hz. For poly(ethylene terephthalate) the previous experiments in this laboratory[10] present the first internal friction measurements at temperatures below 80°K. Recently Frosini and Woodward[42] have reported dynamic mechanical measurements from 300 to 4°K on amorphous and oriented semicrystalline PET films. Their results are similar to our measurements, with differences which probably arise from the different process history of their specimens, in the location and strength of the cryogenic relaxations.

The results of this work, presented in Table III and Figures 2 and 6 show that the δ and ϵ loss peaks have the character of true relaxations. They are associated with a decrease in shear modulus, corresponding to the loss intensity.

The most significant feature of the δ and ϵ relaxations in PET is their complete dependence on molecular organization. They are largely absent in the amorphous polymer but very distinct in crystalline and oriented specimens. The ϵ relaxation occurs in samples containing crystalline structures and increases in strength with crystalline perfection (Fig. 2). The δ relaxation occurs in drawn samples, being most intense in specimens with the highest concent of oriented taut chain segments (Fig. 6). This respective association of the ϵ loss with crystalline and the δ loss with oriented taut chains is demonstrated further by the data in Figures 13 and 14.

Figure 13 compares the internal friction behavior of the isotropic crystalline sample 5, which shows only the ϵ peak, with that of sample 5a, obtained by postdrawing sample 5 at 100°C to 3.5×. The ϵ loss is replaced by the δ peak in the postdrawn specimen. Conversely, in sample 6b (Fig. 14), obtained by annealing sample 6 at 200°C without constraint, the δ peak is replaced by the ϵ loss. In sample 6a, which was annealed taut (heat-set), the δ peak is retained, in addition to the ϵ loss, which appears as a result of the crystalline structures formed during heat-setting.

The activation energies for the δ and ϵ relaxations are listed in Table III. It should be noted that the same activation energy of 4 kcal/mole is observed for the cryogenic relaxations of all specimens, whether they show the δ or ϵ loss alone or a combination of both. This common activation energy for the two cryogenic relaxations raises the possibility that they may both relate to the same mechanism. The occurrence of the δ loss at higher temperatures may be attributed to the strained conformation of the taut chain segments in the drawn polymer. It was observed that, when the strains due to drawing are annealed away as in sample 6b (Fig. 14), the δ loss is replaced by the ϵ loss.

We have previously suggested[10,11] that the δ and ϵ relaxations in crystalline oriented PET specimens may relate to defects* in the supramolecular structure of the polymer. The observed behavior of these relaxations gives considerable evidence in support of this suggestion. The ϵ loss is most intense in samples annealed at high temperatures, which contain well-developed crystalline structures with high dislocation densities. The δ loss is highest in specimens drawn below T_g, which have a large void content and decreases in specimens drawn at higher temperatures, where fewer voids are formed. Furthermore, the directional anisotropy of the δ and ϵ relaxations indicates a preferential loss mechanism in the direction of structural periodicity. All of the morphological models proposed to account for this periodicity[23–25] involve a corresponding arrangement of defect structures. For instance, in the case of the nodular arrays observed by Yeh and Geil[25] the defect structures would be located at the nodular boundaries and the internodular regions, which contain material with a lower degree of order. Motion along these defects would depend, therefore, on the orientation of the nodular boundaries.

These characteristics of the δ and ϵ relaxations in PET are quite similar to the experimental features of the Bordoni peaks,[43,44] observed at low temperatures in the internal friction of face-centered cubic metals. These loss peaks are attributed to small scale motions of dislocation segments between adjacent potential wells under the bias of the oscillatory strains. Like the δ and ϵ relaxations, the Bordoni peaks occur at very low temperatures and have activation energies of 0.16–0.20 eV (3.7–4.6 kcal/mole). They are also dependent on the history of the material, being most pro-

* The term "defect" is used here to denote local regions of deficient molecular packing, ranging from dislocations in crystalline structures to microvoids in drawn specimens.

nounced in cold-worked specimens with high dislocation densities and decreasing as the dislocations are annealed away.[44]

An analogy between the Bordoni peaks and the cryogenic relaxations in PET may be drawn if one considers the defect regions in the oriented crystalline polymer as regions of reduced energy barrier to small-scale motion between adjacent molecular assemblies. This motion may involve cooperative conformational changes of the chain segments along the defect, occurring under the bias of the oscillatory strains. The resulting coupling between macroscopic strain and molecular motion would then give rise to the δ and ϵ relaxations.

This defect motion model is consistent with the experimentally observed behavior of the cryogenic relaxations. It is also in keeping with the results of previously reported cryogenic stress–strain measurements,[10] which show that the crystalline oriented specimens, characterized by the δ and ϵ relaxations, are substantially more ductile than the isotropic amorphous polymer, where these relaxations are largely absent. This suggests that the stress-transfer mechanism at low temperatures may involve defect motions, which contribute to the cryogenic ductility of the polymer.

CONCLUSIONS

The cryogenic relaxation studies on PET, discussed in this paper, show that, in addition to the previously known γ relaxation, the oriented and crystalline polymer has two low-level, low-temperature relaxations: δ at 46°K and ϵ at 26°K. These are largely absent in the isotropic amorphous polymer.

The γ relaxation, which is most intense in the amorphous polymer was resolved into three components, which have been previously attributed to motions of methylene and carboxylene groups. The strength of the γ relaxation decreases substantially in samples with well-developed crystalline structures. It is, therefore, attributed to motions in noncrystalline chain segments. Uniaxial drawing shifts and broadens the γ loss peak to higher temperatures.

The δ and ϵ relaxations are completely dependent on molecular organization. The δ loss occurs in samples with aligned taut chain segments while the ϵ loss occurs in crystalline specimens. These relaxations have a common activation energy of about 4 kcal/mole.

All three low-temperature relaxations show pronounced directional anisotropy in oriented and crystallized specimens. In the case of the γ loss the anisotropy may be due to the preferred orientation of noncrystalline chain segments, while the anisotropy of the δ and ϵ losses may be associated with the direction of defect structures.

It is suggested that the δ and ϵ relaxations involve a defect motion mechanism, which may be analogous to the dislocation induced Bordoni peaks in face-centered cubic metals. The proposed mechanism is consistent with the observed features of the δ and ϵ relaxations and also accounts for the mechanical behavior of the polymer at large deformations.

The financial support of this work by the National Aeronautics and Space Administration and the Manufacturing Chemists' Association is gratefully acknowledged.

References

1. N. Saito, K. Okano, S. Iwanagi, and T. Hideshima, in *Solid State Physics*, F. Seitz and D. Turnbull, Ed., Academic Press, New York, 1963, Vol. 14, p 344.

2. R. F. Boyer, *Rubber Rev.*, **34**, 1303 (1963).

3. R. F. Boyer, *Polymer Eng. Sci.*, **8**, 161 (1968).

4. M. Shen and A. Eisenberg, in *Progress in Solid State Chemistry*, H. Reiss, Ed., Pergamon Press, New York, 1967, Vol. 3, p 406.

5. N. G. McCrum, B. E. Read, and G. Williams, *Anelastic and Dielectric Effects in Polymeric Solids*, Wiley, New York, 1967.

6. A. E. Woodward and J. A. Sauer, *Physics and Chemistry of the Organic Solid State*, D. Fox, M. M. Labes, and A. Weissenberg, Ed., Interscience, New York, 1965.

7. A. E. Woodward, in *Transitions and Relaxations in Polymers* (*J Polymer Sci., C*, **4**), R. F. Boyer, Ed., Interscience, New York, 1966, p 89.

8. K. M. Sinnott, *J. Appl. Phys.*, **37**, 3385 (1966).

9. J. D. Hoffman, G. Williams, and E. Passaglia, in *Transitions and Relaxations in Polymers*, (*J. Polym. Sci. C*, **14**, R. F. Boyer, Ed., Interscience, New York, 1966, p 173.

10. C. D. Armeniades, I. Kuriyama, J. M. Roe, and E. Baer, *J. Macromol. Sci. Phys.*, **B1**, 777 (1967).

11. C. D. Armeniades and E. Baer, *Bull. Am. Phys. Soc.*, **14**, 318 (1969).

12. K. H. Illers and H. Breuer, *J. Colloid Sci.*, **18**, 1 (1963).

13. M. Takayanagi, *Mem. Fac. Eng. Kyushu Univ.*, **23**, 4, 41 (1963).

14. I. M. Ward, *Textile Res. J.*, **13**, 650 (1961).

15. K. H. Hellwege, R. Kaiser, and K. Kuphal, *Kolloid Z.*, **157**, 27 (1958).

16. C. D. Armeniades, Ph.D. Thesis, Case Western Reserve University, Cleveland, Ohio, 1969.

17. A. Keller, G. R. Lester, and L. B. Morgan, *Phil. Trans. Roy. Soc.*, **A247**, 1 (1954).

18. R. Bonart, *Kolloid Z.*, 213, 1 (1966).

19. A. B. Thompson, *J. Polym. Sci.*, **34**, 741 (1959).

20. C. J. Heffelfinger and P. G. Schmidt, *J. Appl. Polym. Sci.*, **9**, 2661 (1965).

21. W. J. Dulmage and A. L. Geddes, *J. Polym. Sci.*, **31**, 499 (1958).

22. W. O. Statton and G. Godard, *J. Appl. Phys.*, **28**, 1111 (1957).

23. W. O. Statton, *J. Polym. Sci.*, **41**, 143 (1959).

24. R. Bonart, *Kolloid Z.*, **199**, 136 (1964).

25. G. S. Y. Yeh and P. H. Geil, *J. Macromol. Sci. Phys.*, **B1**, 251 (1967).

26. R. de P. Daubeny, C. W. Bunn, and C. J. Brown, *Proc. Roy. Soc. (London)*, **A226**, 531 (1954).

27. G. Farrow, J. McIntosh, and I. M. Ward, *Makromol. Chem.*, **38**, 147 (1960).

28. J. Bussink and J. Heijboer, in *Physics of Noncrystalline Polymers* J. A. Prins, Ed., North Holland, Amsterdam, 1965, p 388.

29. J. M. Roe, M. S. Thesis, Case Western Reserve University, Cleveland, Ohio, 1970.

30. B. E. Read and G. Williams, *Trans. Faraday Soc.*, **57**, 1979 (1961).

31. K. G. Mayan, W. J. James, and W. Bosch, *J. Polym. Sci. A*, **3**, 3605 (1965).

32. G. S. Y. Yeh and P. H. Geil, *J. Macromol. Sci. Phys.*, **B1**, 235 (1967).

33. M. J. Hannon, M.S. Thesis, Case Institute of Technology, Cleveland, Ohio, 1966.

34. A. B. Thompson and D. W. Woods, *Trans. Faraday Soc.*, **52**, 1383 (1956).

35. I. Kawaguchi, *J. Polym. Sci.*, **32**, 417 (1958).

36. S. W. Cornell, M.S. Thesis, Case Institute of technology, Cleveland, Ohio, 1966.

37. A. H. Scott, D. J. Scheiber, A. J. Curtis, J. I. Lauritzen, Jr., and J. D. Hoffman, *J. Res. Nat. Bur. Stand.*, **66A**, 269 (1962).

38. L. Hartshorn, J. V. L. Parry, and E. Rushton, *J. Inst. Elect. Engrs.* **100**, Pt. IIA, No. 3 (1953).

39. K. M. Sinnott, *SPE Trans.*, **2,** 65 (1962).
40. K. M. Sinnott, *J. Polym. Sci.*, **35,** 273 (1959), *J. Polym. Sci., A2,* 2 (1960).
41. J. M. Crissman, J. A. Sauer, and A. E. Woodward, *J. Polym. Sci. A,* **2,** 5075 (1964).
42. V. Frosini and A. E. Woodward, *J. Macromol. Sci. Phys.*, **33,** 91 (1969).
43. P. G. Bordoni, *Nuovo Cim.*, **4,** 177 (1947).
44. D. H. Niblett and J. Wilks, *Phil. Mag.*, **2,** 1427 (1957); *Phil. Mag. (Suppl),* **9,** 1 (1960).

Received July 13, 1970

JOURNAL OF POLYMER SCIENCE: PART A-2 VOL. 9, 1371–1378 (1971)

A New Relaxation Process in the High-Elastic State at Low Temperatures

G. M. BARTENEV, *Department of the Physics of Solids, Lenin State Teachers' Training University, Moscow G-435, USSR*

Synopsis

A new relaxation process, explaining the change of elasticity in rubberlike polymers at critical stress (0.1–0.5 kgf/cm²) has been discovered. This process is characterized by the low value of activation energy (weak temperature dependence of relaxation times) and large sizes of kinetic units (strong dependence of relaxation time on stress). Critical stress depend on temperature and for rubberlike polymers turns to zero at 40°–60°C. Mechanism of the phenomena can be explained by the existence of the ordered molecular microregions, creating additional crosslinking points of nonchemical nature with free chains of the network, breaking up at critical stress. Observed phenomena is analogous to the process of forced rubber elasticity of those polymers in glassy state. Critical stress is analogous to the limit of forced rubber elasticity below glass transition temperature.

In elastomers various molecular ordering processes take place which lead to the formation of supermolecular amorphous structures. These are bound to affect the process of deformation of the elastomer, particularly toward the low end of the temperature region of high elasticity, even at low deformation, where these structures are not subject to failure. The low temperature region of the high elasticity of rubbery polymers has had relatively little investigation.

Experimental

Crosslinked and uncrosslinked butadiene–methylstyrene (SKMS-30) and butadiene–acrylonitrile (SKN-26) rubbers were investigated. The specimens of uncrosslinked rubbers were molded in a press at 120°C. Crosslinked rubbers were obtained by optimum vulcanization at 143°C. which for SKMS-30 required 90 min and for SKN-26, 40 min. Ingredients were added to the rubbers before vulcanization in the following amounts: for SKMS-30 (per 100 parts of rubber by weight), 2 parts sulfur, 0.3 part diphenylguanidine, 1.5 parts Altax, 2 parts Stearex and 5 parts zinc oxide; for SKN, 1.5 part sulfur, 0.8 part Captax, 1.5 part Stearex, and 0.8 part zinc oxide.

The experiments were performed over a wide temperature range by stretching strips 150 mm long, 20 mm wide, and 5 mm thick. The stretch-

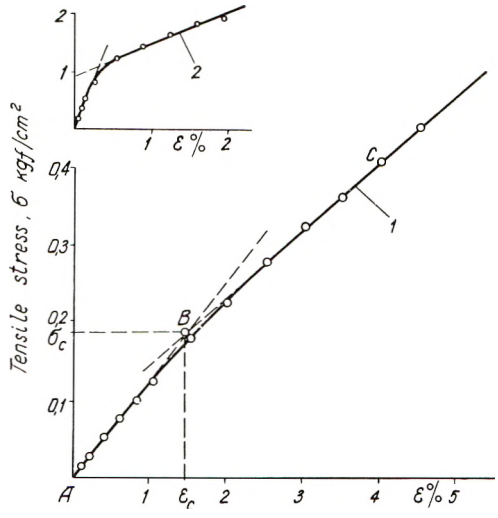

Fig. 1. Stress–strain curves obtained by slow stretching of SKMS-30 butadiene–methylstyrene rubber (*1*) at −15°C and (*2*) at −46°C.

ing was performed on an apparatus with a low inertial force measuring system which had an accuracy of 1%. The stretching was performed at fixed deformation rates of 0.01, 0.03, and 0.10% sec^{-1}. The 0.03 %/sec^{-1} rate was used in the main. The results are given in the tables. From the measured elongation and force, the relation between the actual stress σ and the strain ϵ was obtained. Before the experiment the specimen was stressed by a very small force to an elongation of 0.1%, and this state was taken as the zero point.

Typical deformation curves (true stress versus deformation) for stretching at a constant rate of 3×10^{-4} sec^{-1} are shown in Figure 1 for SKMS-30 butadiene–methylstyrene rubber at two temperatures. The deformation curves consist of an initial linear section and a subsequent section with a smaller slope. The same sort of picture is observed with SKN-26 (butadiene–nitrile) rubber.

Steel springs of various rigidities in the neighborhood of those of the specimens investigated were deformed in the control experiment. All gave straight lines without a break, in contrast to the behavior of the elastomers.

The stress and deformation which correspond to the transition from a steep to a more gently sloping section of curve may be designated respectively as the critical stress σ_c and the critical deformation ϵ_c. The physical meaning of ϵ_c may be seen from Figure 2, where we show the dependence of the slope $d\sigma/d\epsilon$ on the strain. The critical stress corresponds to the point of the greatest change in the rigidity of the material.

The temperature dependence of the critical stress is shown in Figure 3. As may be seen, the curve consists of two linear sections, 1 and 3, and a transition region, section 2. The transition region lies between the temperature T_g' and the glass transition temperature T_g. The high-tempera-

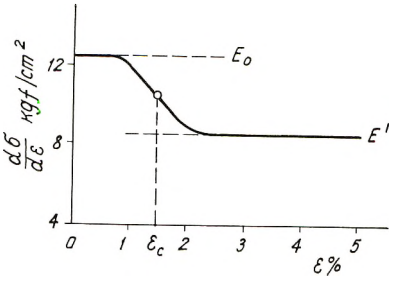

Fig. 2. Changes in the differential modulus of the butadiene–methylstyrene rubber in stretching (−15°C): E_0 initial high elastic modulus; E' differential high elastic modulus above the critical deformation.

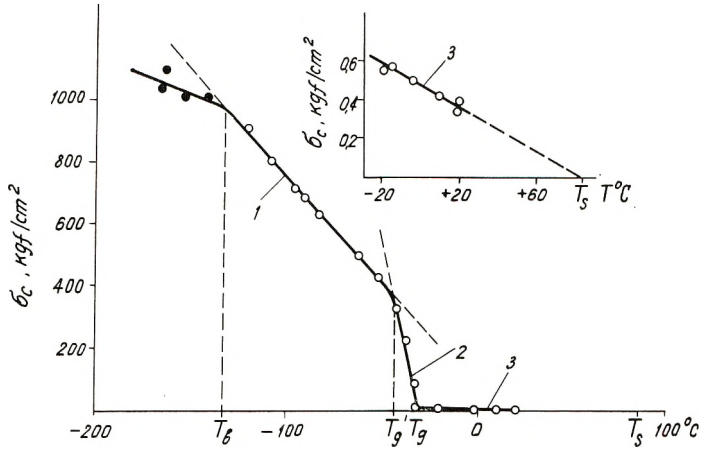

Fig. 3. Dependence of the critical stress on the temperature for vulcanized butadiene–nitrile rubber: (*1*) region of leathery elasticity (T_b to T_g'); (*2*) transition region (T_g' to T_g); (*3*) low temperature region of high elasticity (T_g to T_s).

ture part, section 3, which was obtained first, is connected with the structure of the rubbery polymers in the high elastic state. The low-temperature part of the curve, which comes between the brittleness temperature T_b and T_g', is in point of fact the temperature dependence of the limit of leathery elasticity or forced rubber elasticity σ_f as defined by Lazurkin et al.[1,2] Accordingly below temperature T_g' the critical stress σ_c is equal to σ_f.

The leathery elasticity observed in the glassy state is explained by an increase in the mobility of the kinetic units, the chain segments, with increase in the stres σ. The mobility of the segments is determined by the time of τ segmental relaxation[3–5]

$$\tau = A \exp \{(U - a\sigma)/kT\} \qquad (1)$$

where A is a constant equal to the period of vibration of a segment about the temporary position of equilibrium (it is usually assumed that $A \cong 10^{-12}$ sec), a is the volume of the segment; and U is the activation energy for mo-

tion of the segments from one temporary equilibrium position to another in the unstressed material.

As may be seen from eq. (1), the relaxation time decreases with increase in the stress. When τ becomes less than the time of observation, the segmental mobility becomes sufficient for the development of high-elastic deformation.

Equation (1) for $\sigma = \sigma_f$ may be rewritten in a convenient form for calculation:

$$\sigma_f = (U/a) - (2.3kT/a) \log (\tau/A) \quad (2)$$

From eq. (2) we get

$$d\sigma_f/dT = -(2.3k/a) \log (\tau/A) \quad (3)$$

In our experiments the time of observation is approximately equal to the time of stretching the specimen up to the critical stress. In order of magnitude it is 10 sec at all temperatures. This is why one can consider approximately, that τ is not dependent on temperature, and changes at the transition from one to the other rate of deformation.

After substitution of the indicated time for τ, and on inserting $A = 10^{-12}$ sec in eq. (2), we obtain the temperature dependence of σ_f, to which the low-temperature part of the curve corresponds (Fig. 3). From eqs. (2) and (3), we find U and a (the former by extrapolation of the part of the curve to the temperature axis at zero stress, the latter from the slope of the low-temperature part). The results are given in Table I. For the two rubbers under investigation, $a = 0.7 \times 10^{-21}$ cm^3. This figure practically coincides with the volume of the segments of the elastomers in viscous flow (ca. 10^{-21} cm^3).

TABLE I
Constants Characterizing the Relaxation Processes in Rubbery Polymers below the Glass Transition Temperature (between T_g' and T_b)

Polymer[a]	T_b, °C	T_g', °C	A, sec	a, cm^3	U, kcal/mole
SKN-26	−130	−43	10^{-12}	0.7×10^{-21}	17.0
SKS-30	−135	−62	10^{-12}	0.7×10^{-21}	16.2

[a] Vulcanized and unvulcanized rubbers have the same values.

Relaxation in Rubbery Polymers above T_g

As may be seen from Figure 1, the material is deformed more easily on reaching the critical stress σ_c. This phenomenon reminds one of the leathery elasticity in the glassy state, while the critical stress is analogous to the limit of leathery elasticity.

The critical stress σ_c, like the limit of forced elasticity σ_f in the experiments of Lazurkin,[1,2] depends on the rate of stretching (Fig. 4).

By analogy with eq. (1) we assume that for the time molecular relaxation of the kinetic units in the new relaxation process is

$$\tau = B \exp \{(U - b\sigma)/kT\} \quad (4)$$

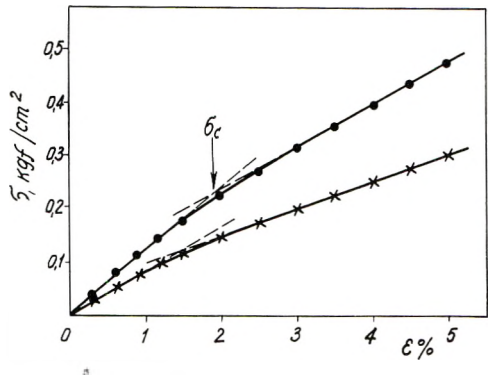

Fig. 4. Curves for stretching of SKN-26 rubber at 20°C and rates of the strain: (lower curve) 0.01%/sec. and (top curve) 0.10%/sec.

where B is a constant, U is the activation energy of the process, and b is the volume of the kinetic unit participating in this process. The nature of the kinetic units will be explained subsequently.

By analogy with eqs. (2) and (3) we may write

$$\sigma = (U/b) - (2.3kT/b) \log (\tau/B) \tag{5}$$

$$d\sigma/dT = -(2.3k/b) \log (\tau/B) \tag{6}$$

where we take $\sigma = \sigma_c$, $\tau = \tau_c$, and τ_c is the time from the beginning of the stretching until the critical deformation ϵ_c is reached (Fig. 1). In our experiments, $\tau_c \cong 10$ sec, and to this time there corresponds the critical stress $\sigma = \sigma_c$.

From the temperature dependence of the critical stress in the high elastic state (part 3 in Fig. 3) and by making use of eqs. (5) and (6), we calculated U and b. In the beginning it was assumed that the kinetic units are segments of the polymer chains, as is accepted in the theory of high elasticity. However, assuming $B = 10^{-12}$ sec and $\tau = \tau_c \cong 10$ sec, we find from eq. (6) that b is greater by three orders of magnitude than the volume of a segment. This means that the kinetic units are larger formations than a segment.

To calculate the pre-exponential coefficient, which depends on the dimensions of the kinetic units, we used in a previous study[6] the formula (7):

$$B = b^{5/6}/(6kT/\rho)^{1/2} \tag{7}$$

where b is the volume of the kinetic unit and ρ is the density of the substance. From this formula we find for a segment with $b = 10^{-21}$ cm^3, where $\rho = 1$ g/cm^3 and $T = 300°$K, the value $B = 5 \times 10^{-12}$ sec, which is close to the previously adopted value A for the calculation of leathery elastic deformation. Since in eq. (6) we have the logarithm of B, any change in the value of this constant has relatively little effect on the value of b as calculated from this formula. Accordingly, approximate values of the latter may be calculated from eq. (6) with $B = 10^{-12}$ sec (for SKMS-30, $b = 7.3 \times 10^{-19}$ cm^3; for SKN-26, $b = 8 \times 10^{-19}$ cm^3). When we substitute these

TABLE II
Constants Characterizing the Relaxation Processes in Rubbery Polymers above the Glass Transition Temperature (between T_s and T_g)

Polymer	T_g, °C	T_s, °C	B, sec	b, cm³	U kcal/mole
SKN-26	−32	42	2.0×10^{-9}	5.0×10^{-19}	14.3
Vulcanized SKN-26	−32	85	2.0×10^{-9}	5.0×10^{-19}	16.0
SKMS-30	−48	35	1.6×10^{-9}	5.5×10^{-19}	12.3

values into eq. (7), we obtain an improved value of B which, for SKMS-30 is 1.6×10^{-9} sec and for SKN-26, 2.0×10^{-9} sec. After substituting these values in eq. (7) we get a second approximation to the constant b, which differs only slightly from the previous values. For instance, for SKMS-30 the constant is equal to 5.5×10^{-19} cm³, while for SKN-26 it is 6.0×10^{-19} cm³.

From eq. (5) it is possible to calculate the activation energy. By extrapolation, we find that at a certain temperature T_s the critical stress is zero (Fig. 3).

Data on the critical temperature T_s and the activation energy of both rubbers and of crosslinked SKN-26 rubber are given in Table II. The values of the constant b exceed by two or three orders of magnitude the volume of the segments of the macromolecules. Nevertheless the activation energy of the relaxation process under investigation (Table II) is of practically the same magnitude as that of leathery elastic deformation (Table I).

The weak dependence of the constants b and U on the rate of strain as the latter changes by an order of magnitude supports the validity of eq. (4). For example, at a rate of 0.01 %/sec, $T_s = 38°C$, $b = 5 \times 10^{-19}$ cm³, and $U = 14.4$ kcal/mole; while at a rate of 0.10 %/sec, $T_s = 52°C$, $b = 4 \times 10^{-19}$ cm³, and $U = 13.8$ kcal/mole.

Nature of the New Relaxation Process

At low temperature, elements of structural ordering have been observed in rubbery polymers.[7,8] Ordered regions have also been observed in vulcanizates.[9] Recently,[10,11] ordered microregions within which the chains are in parallel arrangement have been detected by electron diffraction in melts of linear polymers. The transverse dimensions of these microblocks are 50 Å or more. In the direction of the axis of the macromolecules the dimensions are not less than 50 Å. Consequently, the minimum volume of the microblocks as measured by the above method is 1.3×10^{-19} cm³, whereas the size of the kinetic units according to the data in Table II is 5×10^{-19}–6×10^{-19} cm³. The agreement of these data confirms that in linear polymers there are microblocks of supermolecular structure with dimensions 10^{-19}–10^{-18} cm³.

The present author has suggested[12,13] that the process of break-up of the supermolecular structures explains the rheological properties of elastomers

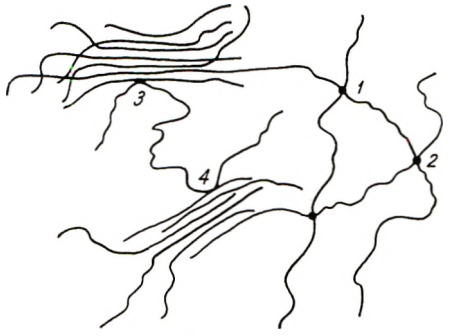

Fig. 5. Schematic representation of the structure of an unvulcanized rubbery, noncrystalline polymer: (1), (2) nonchemically crosslinked points of the network, first type; (3, 4) crosslinks of the second type.

in viscous flow. The ordered microblocks remind one of regions of short-range order in liquids but differ in their higher stability and degree of order. They take the form of structures which are constantly breaking up in some places and forming in others. In the high-elastic state, their lifetime is usually short in comparison with the time of observation but considerably longer than the time for the transition of the free segments (present in the un-ordered part of the rubber polymer) from one equilibrium position into another. With lowering of the temperature, the lifetime and the number of ordered microregions increase. The high value of the constant b indicates that the kinetic units take part in the process in the form of ordered microblocks. It may be supposed that section AB on the tensile curve (Fig. 1) corresponds to a process of deformation where there is not as yet a break-up of the microblocks.

The low value of the activation energy (Table II), coinciding with the activation energy of processes in which the kinetic units are segments of the macromolecules, indicates that in the process of deformation (Fig. 1) the segments as well as the microblocks are kinetic units

The participation of kinetic units of two different kinds in the relaxation process is explained by the following mechanism of thermal motion in rubbery polymers. To a first approximation the structure of rubbery polymers consists of ordered and disordered regions.[12–14] The ordered part consists of elements of supermolecular structures, microblocks, the chains and segments contained in the microblocks and considered as bound. The disordered part consists of free chains and segments taking part in the free thermal motion. The molecular network of unvulcanized rubber is formed by crosslinking points of two types. One comprises nonchemical crosslinks between free chains. These crosslinking points form the main network. The second comprises crosslinks forming between the free chains of the molecular network and the microblocks. These crosslinking points form a supplementary network (Fig. 5).

The thermal motion of the microblocks occurs stepwise as attached chains are removed and new free chains attach themselves. In this case the activ-

ation energy which determines the thermal motion of the microblocks is itself determined by the kinetic units, the segments, since it has already been shown that the break-up of supermolecular structures in viscous flow of linear polymers takes place by way of detachment and adherence of segments of chains from microblocks.[12,13] The stress differs in its effect on the lifetime of the crosslinks of the former and latter type. Whereas an external force acts on crosslinking points of the first type by way of the chains (crosslinking points 1 and 2 in Fig. 5), an external force acts on crosslinking points of the second type (crosslinking points 3 and 4) by way of the microblocks.

In eq. (4) the product $b\sigma$ corresponds to the elementary work of the external forces acting on each crosslinking point of the second type to detach it from the microblock. This work reduces the activation energy for rupture of the crosslinking point and consequently reduces also the time of the molecular relaxation. The elementary force acting in a stressed elastomer on a crosslinking point of the second type by way of the microblocks is considerably greater than the force acting on a crosslinking point of the first type by way of the free chains. It may be assumed that σ_c is connected specifically with the break-up of crosslinking points of the second type. The crosslinking points of the first type determine the deformability of the polymer at stresses higher than σ_c.

Thus the new relaxation process, while analogous to the phenomenon of leathery elasticity, nevertheless differs from it in its more complex molecular mechanism, in which two types of kinetic unit take part.

References

1. Yu. S. Lazurkin, *J. Polym. Sci.*, **30**, 595 (1958).
2. Yu. S. Lazurkin, G. M. Bartenev, G. P. Ushakov, and M. V. Voevodskaya, *Vysokomol. Soedin.*, **6**, 504 (1964).
3. A. P. Aleksandrov, *Proceedings of the First and Second Conferences on High-Molecular Compounds, Academcy of Sciences* USSR, Moscow, 1945, p. 57.
4. Yu. S. Lazurkin and P. L. Fogelson, *Zh. Tekh. Fiz.* **21**, 267, 1951.
5. G. I. Gurevich, *Zh. Tekh. Fiz.*, **17**, 1491 (1947).
6. G. M. Bartenev and N. V. Ermilova, *Physico-chemical Mechanics of Disperse Structures*, Academy of Sciences, USSR, Moscow, 1966, pp. 378–382.
7. V. A. Kargin, V. G. Shuravleva, and Z. Ya. Berestneva, *Dokl. Akad. Nauk. SSSR*, **146**, 3361 (1962).
8. V. A. Kargin, Z. F. Zharikova, Z. Ya. Berestneva, and E. V. Reztsova, *Dokl. Akad. Nauk. SSSR*, **158**, 697 (1964).
9. Z. F. Zharikova, M. V. Kagdan, and Z. Ya. Berestneva, *Vysokomol. Soedin. B*, **10**, 319, 1968.
10. Yu. K. Ovchinnikov, G. S. Markova, and V. A. Kargin, *Dokl. Akad. Nauk, SSSR*, **170**, 1368 (1968).
11. Yu. K. Ovchinnikov and G. S. Markova, *Vysokomol. Soedin., 9A*, 449, 1967.
12. G. M. Bartenev, *Vysokomol. Soedin.*, **6**, 2155 (1964).
13. G. M. Bartenev and L. A. Vishnitskaya, *Vysokomol. Soedin.*, **6**, 751 (1964).
14. G. M. Bartenev and L. G. Gluchatkina, *Vysokomol. Soedin. A*, **10**, 400 (1968)

Received May 12, 1970
Revised October 29, 1970

JOURNAL OF POLYMER SCIENCE: PART A-2 VOL. 9, 1379-1397 (1971)

Sedimentation Equilibrium in Nonideal Heterogeneous Systems. I. Fundamental Equations for Heterogeneous Solute Systems and Some Preliminary Results

TADAO KOTAKA, NOBUO DONKAI, and HIROSHI INAGAKI,
Institute for Chemical Research, Kyoto University,
Uji, Kyoto-fu 611, Japan

Synopsis

The sedimentation-equilibrium method is extended to treat nonideal solutions of heterogeneous macromolecules. The solute is assumed to be heterogeneous not only in molecular weight but also in other quantities such as partial specific volume, second virial coefficient and specific refractive increment. General expressions for various observable molecular weights, especially for weight-average, z-average, and number-average molecular weights, are derived. Their dependences on sedimentation parameter and solute concentration are discussed in detail. For the extrapolation of observable molecular weights, giving a type of weight-average and z-average, to infinite dilution to estimate the molecular weight and the second virial coefficient, average concentration is superior as a concentration variable to original concentration. The plots of observable molecular weight versus average concentration are usually less influenced by the choice of the sedimentation parameter, especially of rotor speed. The general expressions are applied to a few special cases; monodisperse polymer, polydisperse homologous polymer, and polymer blend. The results are compared with experiments on a monodisperse polystyrene, a polydisperse poly(methyl methacrylate), and a mixture of the two polymers, all in 2-butanone at 25°C. The agreement between the theory and experiments is satisfactory.

INTRODUCTION

The sedimentation equilibrium method has, for many years, been a standard technique for determining molecular weights and second virial coefficients in macromolecular solutions.[1-5] The method is based on the observation of solute distribution at sedimentation-diffusion equilibrium in an ultracentrifuge cell. Under specified centrifugation conditions the solute distribution is dependent not only on molecular weight of solute but also on thermodynamic quantities such as specific volume and thermodynamic nonideality. In addition, the optical system installed in an ultracentrifuge can record the solute distribution only in terms of certain optical quantities. Therefore, when a nonideal solution of a heterogeneous solute is to be examined, one should take account of the heterogeneities not only in molec-

ular weight but also in partial specific volume, thermodynamic interaction parameter, and specific refractive increment (or absorption coefficient if absorption optics is employed). Here we seek to extend the sedimentation equilibrium method for treating such nonideal solutions of a heterogeneous solute.

Several limited attempts have been already made on this problem.[1-15] Van Holde and Baldwin[10] treated heterogeneous solute systems neglecting the complication due to the thermodynamic nonideality. Many authors[1-15] treated solutions of homologous polymers, for which all solutes are assumed to have different molecular weights but identical partial specific volume and refractive increment. Hereafter, such a solution will be referred to as a homologous polymer solution, whereas a solution that consists of a mixture of solute species having different values of all these quantities will be called a heterogeneous polymer solution.

Previously we extended the Archibald ultracentrifugation method[2-5] to treat heterogeneous, nonideal polymer solutions.[16] However, the sedimentation equilibrium method is, in many respects, superior to the Archibald method; hence its extension to the general case would be interesting and worthwhile. In this article we give basic equations and results of some preliminary experiments. In doing this we have in mind application of the method to solutions of copolymers, polymer blends, and some biological macromolecules. The details of such specific applications will be reported in subsequent articles.

THEORETICAL

Basic Equations

Definitions and Differential Equation. The starting equation is based on the equilibrium condition in an ultracentrifuge cell:[1-5] The net flow of any component in a heterogeneous solute system consisting of one solvent and q solutes at equilibrium is zero anywhere in the solution column:

$$(1 - \bar{v}_i\rho)\omega^2 r - \sum_k (\partial\mu_i/\partial c_k)(\partial c_k/\partial r) = 0 \qquad \begin{matrix} a \leqq r \leqq b \\ i,k = 1,2, \ldots, q \end{matrix} \qquad (1)$$

For later convenience, we list here the definitions of some important symbols. We denote the temperature by T (°K); the angular speed of rotation by ω (radian/sec); the radial distance to a given position, to the meniscus, and to the bottom of the solution column by r, a, and b (cm), respectively. We further denote the solution density and the solvent density by ρ and ρ_s (g/ml), respectively; the molecular weight of solute i by M_i (daltons); the specific refractive increment, the partial specific volume and the apparent bouyancy factor of solute i by ν_i (ml/g), $\bar{v}_i$ (ml/g), and $\beta_i = (1 - \bar{v}_i\rho_s) = (\partial\rho/\partial c_i)_{c\to 0}$, respectively; the original and local-equilibrium concentrations of solute i by c_i^0 and c_i (g/ml), respectively; the concentration of the original solution by $c^0 = \sum c_i^0$; the local equilibrium concentration by $c = \Sigma\, c_i$; the relative abundance of solute i in the original

solution by $\gamma_i^0 = c_i^0/c^0$; the relative equilibrium distribution of solute i by $\theta_i = c_i/c_i^0$. All the quantities that should be referred to the original solution are distinguished by the superscript zero, e.g., the average partial specific volume, the refractive increment, and the apparent bouyancy factor of the original solution are denoted by $\bar{v}^0 = \sum \bar{v}_i\gamma_i^0$, $\nu^0 = \sum \nu_i\gamma_i^0$, and $\beta^0 = (1 - \bar{v}^0\rho_s) = \sum \beta_i\gamma_i^0$, respectively. The chemical potential μ_i per gram of solute i is given by

$$\mu_i = \mu_i(0) + (RT/M_i) \ln y_i c_i \tag{2a}$$

$$\ln y_i = M_i \sum_k B_{ik}c_k + 0(c_j c_k) \tag{2b}$$

where $\mu_i(0)$ is the reference potential; y_i is the activity coefficient on the c scale; and the B_{ik} are the interaction parameters. We introduce a reduced radial distance x and a sedimentation parameter λ, which are defined, respectively, as

$$x = (r^2 - a^2)/(b^2 - a^2) \tag{3a}$$

$$\lambda = (1 - \bar{v}^0\rho_s)\omega^2(b^2 - a^2)/2RT \tag{3b}$$

with R the gas constant.

Using these quantities, we rewrite eq. (1) and obtain a set of differential equations, each describing the equilibrium distribution of a solute i together with the conservation of mass statement:

$$\lambda M_i^*\theta_i = (d\theta_i/dx) + \lambda c^0 \sum_k (M_i M_k^* \bar{B}_{ik} J_{ik})\gamma_k^0 \tag{4a}$$

$$M_i^* = (\beta_i/\beta^0)M_i \tag{4b}$$

$$\bar{B}_{ik} = B_{ik} + \bar{v}_i/M_k \tag{4c}$$

$$J_{ik} = (\lambda M_k^*)^{-1}\theta_i(d\theta_k/dx) \tag{4d}$$

$$\int_0^1 \theta_i dx = 1 \qquad 0 \leqq x \leqq 1$$

$$i,k = 1,2, \ldots, q \tag{5}$$

In the above equations, the contribution of the higher virial coefficients and the concentration dependence of the ν_i and $\bar{v}_i$ are all neglected. The solution density is assumed to be $\rho = \rho_s + (1 - \bar{v}\rho_s)c$. Equation (4a) suggests that the θ_i may be expressed as a series expansion in c^0, if the solution nonideality is not too marked and if, as well, the parameter λ is not too large (cf. Appendix). The latter condition is important, because high velocity centrifugation, i.e., with large λ, necessarily results in accumulation of solute near the cell bottom and hence, a pronounced nonideality effect.

Observable Molecular Weight. We define here an observable molecular weight $\bar{M}_1^{app}$ for a heterogeneous polymer solution by analogy with the previous definition for a two-component system:[2,9]

$$\bar{M}_1^{app} = [\bar{n}(b) - \bar{n}(a)]/\lambda\bar{n}^0 \tag{6a}$$

$$\bar{n} = \sum \nu_i c_i \tag{6b}$$

$$\bar{n}^0 = \nu^0 c^0 = \sum \nu_i c_i^0 \tag{6c}$$

Here $\bar{n}^0$ and $\bar{n}$ are the original and the local-equilibrium concentrations, respectively, expressed in terms of the refractive increment scale. To correlate eq. (4a) with eq. (6a), we multiply the both sides of eq. (4a) by $(\nu_i/\nu^0)\gamma_i^0$, take the sum over all the components, and integrate the resulting equation with respect to x over the solution column. Recalling the conservation of mass statement, we finally obtain

$$\bar{M}_1^{app} = \bar{M}_1 - c^0 \sum_i \sum_k \left(\bar{M}_i M_k^* \bar{B}_{ik} \int_0^1 J_{ik} dx \right) \gamma_i^0 \gamma_k^0 \tag{7a}$$

$$\bar{M}_1 = \sum (\nu_i/\nu^0)(\beta_i/\beta^0) M_i \gamma_i^0 = \sum \bar{M}_i^* \gamma_i^0 \tag{7b}$$

$$\bar{M}_i = (\nu_i/\nu^0) M_i \tag{7c}$$

The apparent molecular weight $\bar{M}_1$ is identical to that defined previously by Van Holde and Baldwin[4,10] and to the Archibald apparent molecular weight.[16] For a homologous polymer solution, $\bar{M}_1$ is the weight-average molecular weight $\bar{M}_w$.[4,10] On the right-hand side of eq. (7a), only the term J_{ik} depends on the sedimentation conditions and reflects the equilibrium distribution of solute.

Observable Molecular Weight Versus Concentration Variable

Extrapolation with Respect to Original Concentration. To estimate $\bar{M}_1$ and the second virial coefficient from data on $\bar{M}_1^{app}$, one has to extrapolate to infinite dilution with respect to an appropriate concentration variable. From eq. (7a), the most obvious choice appears to be the original concentration c^0. Now we recast eq. (7a) in the form:

$$\bar{M}_1^{app} = M_1 - (\bar{M}_1)^2 c^0 B_{app}(1 + \Delta) \tag{8a}$$

$$B_{app} = B_{2/2} = (\bar{M}_1)^{-2} \sum \sum \bar{M}_i M_k^* \bar{B}_{ik} \gamma_i^0 \gamma_k^0 \tag{8b}$$

$$B_{app}\Delta = (\bar{M}_1)^{-2} \sum \sum \bar{M}_i M_k^* \bar{B}_{ik} I_{ik} \gamma_i^0 \gamma_k^0 \tag{8c}$$

$$I_{ik} = \int_0^1 J_{ik} dx - 1 \tag{8d}$$

To extrapolate $\bar{M}_1^{app}$ one often uses its reciprocal:

$$(\bar{M}_1^{app})^{-1} = (\bar{M}_1)^{-1} + c^0 B_{app}(1 + \Delta') \tag{9a}$$

$$B_{app}(1 + \Delta') = B_{app}(1 + \Delta)[1 - \bar{M}_1 c^0 B_{app}(1 + \Delta)]^{-1} \tag{9b}$$

The quantity $B_{2/2}$ is a type of light-scattering second virial coefficient[17-19] and is equivalent to that defined previously in the Archibald analysis.[16] In the limit of small c^0 and λ, the quantity I_{ik} may be expanded in powers of c^0 and λ^2 (cf. Appendix). Then, eq. (9a) may be written as

$$(\bar{M}_1^{app})^{-1} = (\bar{M}_1)^{-1} + c^0 B_{app} F'(\lambda) - (c^0)^2 \bar{M}_1 C'_{app} G'(\lambda) + \ldots \tag{10a}$$

$$B_{app} F'(\lambda) = B_{2/2} + (\bar{M}_1)^{-2} \sum \sum \bar{M}_i M_k^* \bar{B}_{ik} I_{ik}^{(0)} \gamma_i^0 \gamma_k^0$$
$$= B_{2/2} + (\lambda^2/12)(\bar{M}_{2/1})^2 B_{4/4} + 0(\lambda^4) \tag{10b}$$

$$\bar{M}_{2/1} = (\bar{M}_1)^{-1} \sum \tilde{M}_i^* M_i^* \gamma_i^0 \tag{10c}$$

$$B_{4/4} = (\bar{M}_1 \bar{M}_{2/1})^{-2} \sum \sum \tilde{M}_i M_k^* (M_i^* M_k^*) \bar{B}_{ik} \gamma_i^0 \gamma_k^0 \tag{10d}$$

$$C_{\text{app}} G'(\lambda) = -(\bar{M}_1)^{-3} \sum \sum \tilde{M}_i M_k^* \bar{B}_{ik} I_{ik}^{(1)} \gamma_i^0 \gamma_k^0 - [B_{\text{app}} F'(\lambda)]^2$$
$$= (\bar{M}_1)^{-3} \sum \sum \sum \tilde{M}_i M_j M_k^* \bar{B}_{ij} \bar{B}_{jk} \gamma_i^0 \gamma_j^0 \gamma_k^0 - (B_{2/2})^2 + 0(\lambda^2) \tag{10e}$$

Here $I_{ik}^{(0)}$ and $I_{ik}^{(1)}$ are the zeroth and first coefficients, respectively, in the c^0 expansion of I_{ik} (cf. Appendix). The quantity $\bar{M}_{2/1}$ is a type of z-average molecular weight, and $B_{4/4}$ a higher-average second virial coefficient. The quantities $B_{\text{app}} F'(\lambda)$ and $C_{\text{app}} G'(\lambda)$ may be called the apparent second and third virial coefficients, respectively.

Equation (10) suggests that a dual extrapolation of $(\bar{M}_1^{\text{app}})^{-1}$ with respect to λ^2 and c^0 would allow one to determine $\bar{M}_1$ and $B_{2/2}$. This was confirmed by Fujita et al.[5,20] and more recently by Utiyama et al.[13] for homologous polymer solutions. However, the dual extrapolation is tedious, and we seek another concentration variable which would be less influenced by the choice of λ than is c^0.

Extrapolation with Respect to Average Concentration. For homologous polymer solutions, a few redefined concentration variables have been already suggested.[2,5,9–15] Among them the most promising appears to be the average concentration $\bar{c} = [c(b) + c(a)]/2$. It has been shown that use of $\bar{c}$ provides an exact extrapolation, i.e., unaffected by the choice of λ, for two-component systems,[2] and also is a good approximation for homologous polymer solutions.[14,15] For a heterogeneous polymer solution the observable average concentration $\tilde{c}$ can be defined as follows:

$$\tilde{c} = [\tilde{n}(b) + \tilde{n}(a)]/2\nu^0 \tag{11}$$

The original concentration c^0 may be correlated with the average concentration $\tilde{c}$ by the identity (12):

$$c^0 = \frac{\tilde{n}(b) + \tilde{n}(a)}{2\nu^0} \frac{\tilde{n}(b) - \tilde{n}(a)}{\lambda \tilde{n}^0} \frac{2\lambda(\tilde{n}^0)^2}{\tilde{n}^2(b) - \tilde{n}^2(a)}$$
$$= \tilde{c}(\bar{M}_1^{\text{app}})[\bar{M}_1 + \sum \sum (\nu_i/\nu^0) \tilde{M}_k^* I_{ik} \gamma_i^0 \gamma_k^0]^{-1} \tag{12}$$

Inserting eq. (12) into eq. (7a) and rearranging the resulting equation, we obtain

$$(\bar{M}_1^{\text{app}})^{-1} = (\bar{M}_1)^{-1} + \tilde{c} B_{\text{app}}(1 + \delta) \tag{13a}$$

$$B_{\text{app}}\delta = \frac{\sum \sum [\tilde{M}_i M_k^* \bar{B}_{ik} - (\nu_i/\nu^0) \tilde{M}_k^* \bar{M}_1 B_{2/2}] I_{ik} \gamma_i^0 \gamma_k^0}{\bar{M}_1[\bar{M}_1 + \sum \sum (\nu_i/\nu^0) \tilde{M}_k^* I_{ik} \gamma_i^0 \gamma_k^0]} \tag{13b}$$

For a two-component system, the quantity $B_{\text{app}}\delta$ vanishes identically, regardless of nonideality. This is a generalization of the conclusion obtained earlier by Williams and Van Holde.[2,9] It is interesting to note that by definition the identity (14) always holds:

$$\sum \sum [\tilde{M}_i M_k^* \bar{B}_{ik} - (\nu_i/\nu^0) \tilde{M}_k^* \bar{M}_1 B_{2/2}] \gamma_i^0 \gamma_k^0 \equiv 0 \tag{14}$$

This implies that $B_{app}\delta$ consists of two parts which, to some extent, compensate. Consequently, $B_{app}\delta$ is always smaller than either $B_{app}\Delta$ or $B_{app}\Delta'$, as Fujita[14] suggested for homologous polymer solutions. In the limit of small c^0 and λ, eq. (13a) may be expanded in powers of $\tilde{c}$ and λ^2:

$$(\bar{M}_1^{app})^{-1} = (\bar{M}_1)^{-1} + \tilde{c}B_{app}f(\lambda) - (\tilde{c})^2\bar{M}_1C_{app}g(\lambda) + \dots \quad (15a)$$

$$B_{app}f(\lambda) = B_{2/2} + \frac{\sum\sum [\tilde{M}_i M_k^* \bar{B}_{ik} - (\nu_i/\nu^0)\tilde{M}_k^* \bar{M}_1 B_{2/2}] I_{ik}^{(0)} \gamma_i^0 \gamma_k^0}{\bar{M}_1[\bar{M}_1 + \sum\sum (\nu_i/\nu^0)\tilde{M}_k^* I_{ik}^{(0)} \gamma_i^0 \gamma_k^0]}$$

$$= B_{2/2} + (\lambda^2/12)[(\bar{M}_{2/1})^2 B_{4/4} - (\bar{M}_1\bar{M}_{2/1})B_{2/2}] + 0(\lambda^4) \quad (15b)$$

$$C_{app}g(\lambda) = C_{app}G'(0) + 0(\lambda^2) \quad (15c)$$

The concentration variable $\tilde{c}$ automatically accounts for a substantial part of the λ dependence of $\bar{M}_1^{app}$. Presumably extrapolation with respect to λ^2 will be unnecessary, unless the solute is highly heterogeneous and the sedimentation parameter λ is chosen to be large.

Various Average Molecular Weights

The sedimentation equilibrium method is well known to allow one to determine average molecular weights other than the weight-average.[1-10,21] The procedures proposed so far may be classified into two categories:[1-5,21] one utilizes data obtained from a series of experiments with varying λ; the other utilizes data of a single experiment with λ fixed. Here we examine the latter procedure. Generalization of the definition of various average molecular weights was made by Van Holde and Baldwin[4,10] for heterogeneous solute systems in the limit of vanishing nonideality.

Higher-Average Molecular Weights. Observable higher-average molecular weights may be defined as follows[4]:

$$\bar{M}_{2/1}^{app} = \frac{RT\left\{\left(\frac{1}{r}\frac{d\tilde{n}}{dr}\right)_b - \left(\frac{1}{r}\frac{d\tilde{n}}{dr}\right)_a\right\}}{(1 - \bar{v}^0\rho_s)\omega^2\{\tilde{n}(b) - \tilde{n}(a)\}} \quad (16a)$$

$$\bar{M}_{3/2}^{app} = \frac{RT\left\{\left[\frac{1}{r}\frac{d}{dr}\left(\frac{1}{r}\frac{d\tilde{n}}{dr}\right)\right]_b - \left[\frac{1}{r}\frac{d}{dr}\left(\frac{1}{r}\frac{d\tilde{n}}{dr}\right)\right]_a\right\}}{(1 - \bar{v}^0\rho_s)\omega^2\left\{\left(\frac{1}{r}\frac{d\tilde{n}}{dr}\right)_b - \left(\frac{1}{r}\frac{d\tilde{n}}{dr}\right)_a\right\}} \quad (16b)$$

etc. The subscripts a and b indicate that the values in the brackets are to be taken at the meniscus and the bottom of the solution column, respectively. Experimentally, the determination of higher average molecular weights other than $\bar{M}_{2/1}^{app}$ appears to be impractical. Hence, we discuss only the determination of $\bar{M}_{2/1}^{app}$.

Inserting eqs. (4) and (7) into eq. (16a) and rearranging the result, we obtain an expression for $\bar{M}_{2/1}^{app}$:

$$\bar{M}_{2/1}^{\text{app}} = (\bar{M}_1^{\text{app}})^{-1}\{(\bar{M}_1\bar{M}_{2/1}) - c^0 \sum\sum \tilde{M}_i M_k^* \bar{B}_{ik} \times [\lambda^{-1}\Delta J_{ik} + M_i^*(1 + I_{ik})]\gamma_i^0\gamma_k^0\} \quad (17a)$$

$$\lambda^{-1}\Delta J_{ik} = \lambda^{-1}[J_{ik}(1) - J_{ik}(0)] = (M_i^* + M_k^*)[1 + I_{ik}^{(0)}] + 0(c^0) \quad (17b)$$

Equation (17a) may be expanded in powers of c^0 and λ^2 as

$$(\bar{M}_{2/1}^{\text{app}})^{-1} = (\bar{M}_{2/1})^{-1} + 2c^0 B_z^{\text{app}} F_z(\lambda) + 0[(c^0)^2] \quad (18a)$$

$$2B_z^{\text{app}} F_z(\lambda) = 2B_z^{\text{app}}(1 + \Delta_z) \quad (18b)$$

$$2B_z^{\text{app}} = (\bar{M}_1\bar{M}_{2/1}^2)^{-1} \sum\sum \tilde{M}_i M_k^*(2M_i^* + M_k^* - \bar{M}_{2/1})\bar{B}_{ik}\gamma_i^0\gamma_k^0 = (\bar{M}_1/\bar{M}_{2/1})(3B_{3/3} - B_{2/2}) \quad (18c)$$

$$2B_z^{\text{app}}\Delta_z = (\bar{M}_1\bar{M}_{2/1}^2)^{-1} \sum\sum \tilde{M}_i M_k^*(2M_i^* + M_k^* - \bar{M}_{2/1}) \times \bar{B}_{ik} I_{ik}^{(0)}\gamma_i^0\gamma_k^0 = (\lambda^2/12)(\bar{M}_1/\bar{M}_{2/1})[3\bar{M}_{2/1}\bar{M}_{3/2}B_{5/5} - (\bar{M}_{2/1})^2 B_{4/4}] + 0(\lambda^4) \quad (18d)$$

$$3B_{3/3} = (\bar{M}_1^2\bar{M}_{2/1})^{-1} \sum\sum \tilde{M}_i M_k^*(2M_i^* + M_k^*)\bar{B}_{ik}\gamma_i^0\gamma_k^0 \quad (18e)$$

$$3B_{5/5} = (\bar{M}_1^2\bar{M}_{2/1}^2\bar{M}_{3/2})^{-1} \sum\sum \tilde{M}_i M_k^*(M_i^* M_R^*)/(2M_i^* + M_k^*)\bar{B}_{ik}\gamma_i^0\gamma_k^0 \quad (18f)$$

$$\bar{M}_{3/2} = (\bar{M}_1\bar{M}_{2/1})^{-1} \sum \tilde{M}_i^*(M_i^*)^2\gamma_i^0 \quad (18g)$$

The original concentration c^0 in eq. (18a) may be replaced by the average concentration $\bar{c}$ by using eq. (12) as before. The result reads:

$$(\bar{M}_{2/1}^{\text{app}})^{-1} = (\bar{M}_{2/1})^{-1} + 2\bar{c}B_z^{\text{app}} f_z(\lambda) + \dots \quad (19a)$$

$$2B_z^{\text{app}} f_z(\lambda) = 2B_z^{\text{app}}(1 + \delta_z) \quad (19b)$$

$$2B_z^{\text{app}}\delta_z = \frac{\sum\sum [\tilde{M}_i M_k^*(2M_i^* + M_k^* - \bar{M}_{2/1})\bar{B}_{ik} - (\nu_i/\nu^0)\tilde{M}_k^*(\bar{M}_{2/1}^2)2B_z^{\text{app}}]I_{ik}^{(0)}\gamma_i^0\gamma_k^0}{\bar{M}_{2/1}^2[\bar{M}_1 + \sum\sum (\nu_i/\nu^0)\tilde{M}_k^* I_{ik}^{(0)}\gamma_i^0\gamma_k^0]}$$

$$= \frac{(\lambda^2/12)[3(\bar{M}_1\bar{M}_{3/2}B_{5/5} - \bar{M}_1^2 B_{3/3}) - (\bar{M}_1\bar{M}_{2/1}B_{4/4} - \bar{M}_1^2 B_{2/2})] + 0(\lambda^4)}{1 + (\lambda^2/12)\bar{M}_1\bar{M}_{2/1} + 0(\lambda^4)} \quad (19c)$$

Again, for a two-component system, the additional term $B_z^{\text{app}}\delta_z$ vanishes identically regardless of nonideality.[4] The term consists of two partly compensating contributions. For extrapolating $(\bar{M}_{2/1}^{\text{app}})^{-1}$ to infinite dilution, $\bar{c}$ is better than c^0, as in the case of $(\bar{M}_1^{\text{app}})^{-1}$.

Number-Average Molecular Weight. In order to determine a type of number average molecular weight $\bar{M}_{0/-1}$ from an equilibrium experiment with a given value of λ, we must choose the value of λ so that the concentrations of all solutes go to zero at the meniscus, i.e., $n(a) = 0$.[4,5] With this

prerequisite, observable number-average molecular weight $\bar{M}_{0/-1}^{app}$ can be given as[4]

$$(\bar{M}_{0/-1}^{app})^{-1} = (\lambda/\tilde{n}^0)\left[\tilde{n}^0 - \int_0^1 x\tilde{n}(x)dx\right] \tag{20}$$

From eqs. (4a), (6b), and (20), we obtain

$$(\bar{M}_{0/-1}^{app})^{-1} = \sum (\nu_i/\nu^0)(M_i^*)^{-1}\gamma_i^0 + \lambda[1 - \sum (\nu_i/\nu^0)\theta_i(1)(\lambda M_i^*)^{-1}\gamma_i^0] - c^0 \sum\sum [(\nu_i/\nu^0)M_k^*\bar{B}_{ik}\int_0^1 xJ_{ik}(x)dx]\gamma_i^0\gamma_k^0 \tag{21}$$

The concentration of solute i at the meniscus, $c_i(a)$, is roughly $c_i^0(\lambda M_i^*)$ exp $\{-\lambda M_i^*\}$. Therefore, to satisfy the requirement, one must choose the rotor speed sufficiently high so that exp $\{-\lambda M_i^*\}$ becomes practically zero. Applying this condition to eq. (21), we obtain

$$(\bar{M}_{0/-1}^{app})^{-1} = (\bar{M}_{0/-1})^{-1} + (\lambda\bar{M}_{0/-1})c^0B_n^{app} + 0[(\lambda\bar{M}_{0/-1}c^0)^2] \tag{22a}$$

$$(\bar{M}_{0/-1}) = [\sum (\nu_i/\nu^0)(M_i^*)^{-1}\gamma_i^0]^{-1} \tag{22b}$$

$$B_n^{app} = (\bar{M}_{0/-1})^{-1} \sum\sum \bar{M}_i(M_k^*/M_i^* + M_k^*)^2\bar{B}_{ik}\gamma_i^0\gamma_k^0 \tag{22c}$$

For a two-component system, $\bar{M}_{0/-1}$ and B_n^{app} become the solute molecular weight and half of the osmotic second virial coefficient, respectively. For a homologous polymer solution, $\bar{M}_{0/-1}$ is the true number-average molecular weight M_n. On the other hand, the apparent second virial coefficient B_n^{app} cannot be correlated by a simple function with the osmotic second virial coefficient A_2. For a heterogeneous polymer solution, the quantity A_2 is:

$$A_2 = (1/2)(M_n^{-2}) \sum\sum M_iM_kB_{ik}m_i^0m_k^0 = (1/2) \sum\sum B_{ik}\gamma_i^0\gamma_k^0 \tag{23}$$

where $m_i^0 = (M_n/M_i)\gamma_i^0$ is the mole fraction of solute i in the original solution. The contrast between the two quantities is evident.

It is interesting to note that $\bar{M}_{0/-1}$ involves a factor β_i^{-1} and therefore becomes indefinite when β_i is zero. This is a consequence of an obvious fact that the requirement, $\tilde{n}(a) = 0$, cannot be satisfied at any value of λ, if the solute contains a component with $\beta_i = 0$. It should also be noted that the concentration-dependent terms of $(\bar{M}_{0/-1}^{app})^{-1}$ are directly proportional to the corresponding powers of λ. Hence the extrapolation of this quantity to infinite dilution must be done in a range of sufficiently low concentrations. Such extrapolation might be uncertain, but the difficulty in determining $\bar{M}_{0/-1}$ might be circumvented by checking whether the extrapolations with different λ give a common value of $\bar{M}_{0/-1}$.

COMPARISON WITH EXPERIMENTAL RESULTS

Experimental Procedures

Sedimentation experiments were carried out on a Hitachi analytical ultracentrifuge UCA-1A (No. S60108-1). For recording sedimentation

patterns, both Rayleigh interference and schlieren optics were employed. The light source was a high-pressure mercury lamp with an interference filter to isolate the 546 mμ line. The procedures for aligning and focusing the optics were similar to those developed by LaBar and Baldwin for a Spinco model E ultracentrifuge.[22] Sedimentation patterns[23] were photographed either on Fuji panchromatic plates or Fuji fluorographic x-ray films. The patterns were read by using a Nikon profile projector V-16 (Nihon Kogaku, Tokyo) to an accuracy of ±0.005 mm which corresponds to about 0.0025 mm in the cell. Ultracentrifuge cells used were double-sector interference cells and the Yphantis 6-channel cell,[24] all of 12 mm thickness. In either case, the amounts of solution and solvent were carefully adjusted so that the height of solution column was about 2.5 mm. Ordinary runs were performed at four rotor speeds in the range 4,800 to 10,490 rpm, and a few meniscus depletion runs at 14,400 rpm. The temperature was controlled within an accuracy of ±0.5°C.

Polymer samples used were a nearly monodisperse polystyrene and a slightly polydisperse poly(methyl methacrylate). The former was purchased from Pressure Chemical Co. (Pittsburgh, Pa.). It was designated as PST-1a and data supplied by the manufacturer show M_w = 160,000 and $\bar{M}_w/\bar{M}_n < 1.06$. The other polymer was prepared by anionic polymerization with sodium biphenyl as the initiator and tetrahydrofuran as the solvent. The sample was designated PMMA 31M.[25] All solvents used were carefully purified by appropriate procedures.[26] The equilibrium experiments were done in 2-butanone (MEK) at 25.0°C. Values of the specific volumes in MEK at 25.0°C are 0.9078 for polystyrene and 0.8002 for poly(methyl methacrylate), and the solvent density is 0.79945. Specific refractive increments were determined by synthetic-boundary cell experiments: values in MEK at 25.0°C are 0.230 for polystyrene and 0.113 for poly(methyl methacrylate).

Application to Special Cases

Two-Component System. The behavior of two-component systems is discussed in detail in Fujita's monograph.[5] Hence we give here only a brief discussion. When the effects of third and higher virial coefficients are negligible, various observable molecular weights may be reduced to the following simple forms for a two component system with a solute of molecular weight M and the second virial coefficient B.[2,4,5]

$$(\bar{M}_1^{app})^{-1} = M^{-1} + \bar{c}B \tag{24}$$

$$(\bar{M}_{2/1}^{app})^{-1} = M^{-1} + 2\bar{c}B + Mc(a)c(b)B^2 \tag{25}$$

$$(\bar{M}_{0/-1}^{app})^{-1} = M^{-1} + (\lambda M)c^0(B/4) + (\lambda M)^2(c^0)^2(MB^2/24) + \ldots \tag{26}$$

For the last relation eq. (26), the value of λM must be large enough, e.g., $\lambda M > 7$, to make the meniscus concentration practically zero.

In Figures 1 and 2, eqs. (24) and (25) are tested with data on PST-1a in MEK at 25°C. Plots of $(\bar{M}_1^{app})^{-1}$ versus $\bar{c}$ give a single composite

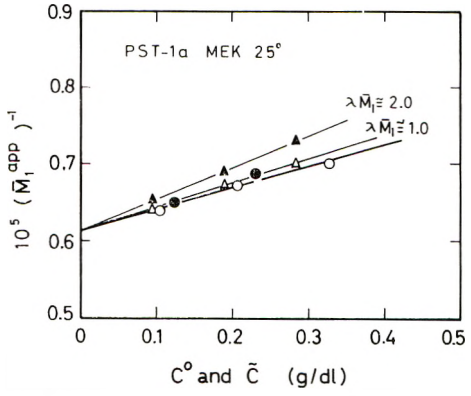

Fig. 1. Plots of $(\bar{M}_1^{app})^{-1}$ vs. (△,▲)c^0 and (○,●)$\tilde{c}$ for monodisperse PST-1a in MEK at 25°C. Values of $10^{-5}\lambda$ range from 0.592 to 0.684 for the points with $\lambda M \approx 1.00$, and from 1.12 to 1.29 for those with $\lambda M \approx 2.00$.

curve, as expected. The estimated values, $10^{-4}M = 16$ and $10^4B = 2.9$, are in excellent agreement with light-scattering data on the same system reported by Utiyama et al.[13] Also, plots of $(\bar{M}_{2/1}^{app})^{-1}$ versus $\tilde{c}$ give a single curve, which has the initial slope of roughly about $2B$. The correction due to the third term on the right-hand side of eq. (25) was negligible. In both cases, the advantage of using $\tilde{c}$ instead of c^0 as the concentration variable is obvious.

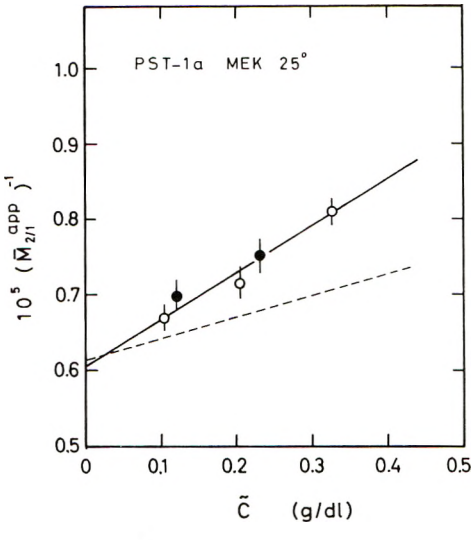

Fig. 2. Plot of $(\bar{M}_{2/1}^{app})^{-1}$ versus $\tilde{c}$ for the same systems as in Fig. 1. Vertical lines indicate error limit. The dashed curve is a plot of $(\bar{M}_1^{app})^{-1}$ vs. $\tilde{c}$ for the same systems.

Homologous Polymer System. For homologous polymers, we assume that all components have the same values of $\nu_i = \nu$ and $\bar{v}_i = \bar{v}$, and that all B_{ik} are the same as B. These assumptions are known to be good for ordinary synthetic homopolymers. Since the system is of practical interest, we discuss its behavior in somewhat detail.

Employing the above assumptions, we may rewrite eq. (8a) in a simple expansion form with respect to c^0 and λ:

$$\bar{M}_1^{\text{app}} = \bar{M}_w[1 - (\bar{M}_w c^0 B)\bar{F}(\Lambda) + (\bar{M}_w c^0 B)^2\bar{G}(\Lambda) - (\bar{M}_w c^0 B)^3\bar{H}(\Lambda) + \cdots] \quad (27a)$$

$$\begin{aligned}\bar{F}(\Lambda) &= 1 + \bar{M}_w^{-2}\sum\sum M_i M_k \bar{I}_{ik}^{(0)}\gamma_i^0\gamma_k^0 \\ &= 1 + (\Lambda^2/12)p_z^2 - (\Lambda^4/720)p_z^2(2p_{z+1}p_{z+2} - p_z^2) + 0(\Lambda^6)\end{aligned} \quad (27b)$$

$$\bar{G}(\Lambda) = \bar{M}_w^{-3}\sum\sum M_i M_k \bar{I}_{ik}^{(1)}\gamma_i^0\gamma_k^0 = 1 + (\Lambda^2/12)(5p_z^2) + 0(\Lambda^4) \quad (27c)$$

$$\begin{aligned}\bar{H}(\Lambda) &= \bar{M}_w^{-4}\sum\sum M_i M_k \bar{I}_{ik}^{(2)}\gamma_i^0\gamma_k^0 \\ &= 1 + (\Lambda^2/12)p_z^2(12 + 2p_{z+1}) + 0(\Lambda^6)\end{aligned} \quad (27d)$$

where

$$\begin{aligned}\Lambda &= \lambda\bar{M}_w \\ p_z &= \bar{M}_z/\bar{M}_w,\ p_{z+2} = \bar{M}_{z+2}/\bar{M}_w,\ p_{z+2} = \bar{M}_{z+2}/\bar{M}_w,\ \ldots\end{aligned} \quad (27e)$$

The quantity $\bar{I}_{ik}^{(n)}$ is derived from the corresponding $I_{ik}^{(n)}$ for a heterogeneous solute system, and is a function only of Λ and the molecular weight distribution of the sample. The quantities p_z, p_{z+1}, etc., as defined, reflect the latter.

In the limit of Λ^2 being zero, all the terms $\bar{F}(\Lambda)$, $\bar{G}(\Lambda)$, $\bar{H}(\Lambda)$, etc. become unity. Hence if the solution nonideality is moderate, i.e., $(\bar{M}_w c^0 B) < 1$, eq. (27a) can be written as

$$\lim_{\lambda\to 0}(\bar{M}_1^{\text{app}})^{-1} = \bar{M}_w^{-1} + c^0 B \quad (28)$$

The reciprocal of $(\bar{M}_1^{\text{app}})$ may be expanded as

$$(\bar{M}_1^{\text{app}})^{-1} = \bar{M}_w^{-1} + c^0 B\bar{F}'(\Lambda) - (c^0 B)^2\bar{M}_w\bar{G}'(\Lambda) + \cdots \quad (29a)$$

$$\bar{F}'(\Lambda) = \bar{F}(\Lambda) \quad (29b)$$

$$\bar{G}'(\Lambda) = \bar{G}(\Lambda) - [\bar{F}(\Lambda)]^2 = (\Lambda^2/12)(3p_z^2) + 0(\Lambda^4) \quad (29c)$$

Comparison of eqs. (27), (28), and (29) suggests that the plots of $(\bar{M}_1^{\text{app}})^{-1}$ rather than $\bar{M}_1^{\text{app}}$ itself would facilitate a more nearly linear plot. For example, in the limit of vanishing λ, $\bar{M}_1^{\text{app}}$ gives a hyperbola, whereas the reciprocal gives a straight line. Therefore, the extrapolation to zero λ and to infinite dilution would be easier in the reciprocal plot.

The reciprocal of $\bar{M}_1^{app}$ may also be expanded in powers of the average concentration $\bar{c}$:

$$(\bar{M}_1^{app})^{-1} = \bar{M}_w^{-1} + \bar{c}B\bar{f}(\Lambda) - (\bar{c}B)^2\bar{M}_w\bar{g}(\Lambda) + \ldots \tag{30a}$$

$$\bar{f}(\Lambda) = 1 + \frac{\bar{M}_w^{-2}\sum\sum(M_i - \bar{M}_w)M_k\bar{I}_{ik}^{(0)}\gamma_i^0\gamma_k^0}{1 + \bar{M}_w^{-1}\sum\sum M_k\bar{I}_{ik}^{(0)}\gamma_i^0\gamma_k^0}$$

$$= 1 + \frac{(\Lambda^2/12)p_z(p_z - 1) - (\Lambda^4/720)p_zp_{z+1}(2p_zp_{z+2} - p_zp_{z+1} - p_{z+1}p_{z+2}) + 0(\Lambda^6)}{1 + (\Lambda^2/12)p_z - (\Lambda^4/720)p_zp_{z+1}p_{z+2} + 0(\Lambda^6)} \tag{30b}$$

$$\bar{g}(\Lambda) = \frac{(\Lambda^2/12)[5p_z(p_z - 1)] - 0(\Lambda^4)}{[1 + (\Lambda^2/12)p_z + 0(\Lambda^4)]^3} \tag{30c}$$

On the other hand, the observable molecular weight $\bar{M}_{z/1}^{app}$ that gives $\bar{M}_z$ may be expanded in powers of c^0 and also of $\bar{c}$, respectively, as follows:

$$(\bar{M}_{z/1}^{app})^{-1} = \bar{M}_z^{-1} + 2c^0B\bar{F}_z(\Lambda) + \ldots \tag{31a}$$

$$\bar{F}_z(\Lambda) = p_z^{-1} + (\Lambda^2/12)[p_z(3p_{z+1} - p_z)/2] - (\Lambda^4/720) \times [p_z(p_zp_{z+1} + 3p_{z+2}p_{z+3} - 2p_zp_{z+2})/2] + 0(\Lambda^6) \tag{31b}$$

$$(\bar{M}_{z/1}^{app})^{-1} = \bar{M}_z^{-1} + 2c\bar{B}\bar{f}_z(\Lambda) + \ldots \tag{32a}$$

$$\bar{f}_z(\Lambda) = p_z^{-1} + \frac{(\Lambda^2/12)[p_z(3p_z - p_z - 2)/2] - 0(\Lambda^4)}{1 + (\Lambda^2/12)p_z + 0(\Lambda^4)} \tag{32b}$$

As was mentioned in the previous section, the coefficients in the $\bar{c}$ expansions, eqs. (30) and (32), consist of two compensating parts, and are smaller than the corresponding coefficients in the c^0 expansions, eqs. (27), (29), and (31). To judge from eqs. (27)–(32), one may say that impurities of low molecular weight would have little effect on the observable molecular weights. But for solutes contaminated with very high molecular weight components, even when the amount is small, p_z, p_{z+1} etc. become large and hence, the observable molecular weights would be significantly influenced by the choice of λ. Even plots against $\bar{c}$ need to be corrected for the effect of heterogeneity, unless the value of $\Lambda = \lambda\bar{M}_w$ is chosen to be sufficiently small. The same conclusion must apply to heterogeneous solute systems as well.

On the other hand, observable molecular weight $\bar{M}_{0/-1}^{app}$ that gives $\bar{M}_n$ may be written as follows:

$$(\bar{M}_{0/-1}^{app})^{-1} = \bar{M}_n^{-1} + (\lambda\bar{M}_n)c^0B\bar{F}_n - (\lambda\bar{M}_n)^2(c^0B)^2\bar{M}_n\bar{G}_n + \ldots \tag{33a}$$

$$\bar{F}_n = \bar{M}_n^{-1}\sum\sum M_i(M_k/M_i + M_k)^2\gamma_i^0\gamma_k^0 \tag{33b}$$

$$\bar{G}_n = \bar{M}_n^{-3}\sum\sum\sum M_iM_jM_k \times [\text{function of } (M_k/M_i + M_k), \text{ etc.}]\gamma_i^0\gamma_j^0\gamma_k^0 \tag{33c}$$

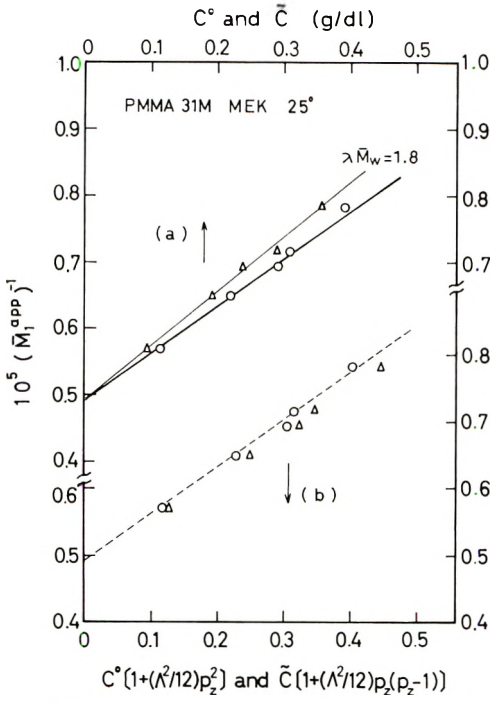

Fig. 3. (*a*) Plots of $(\bar{M}_1^{app})^{-1}$ vs. (△) c^0 and (○) $\tilde{c}$ for polydisperse PMMA 31M in MEK at 25°C: values of $10^{-5}\lambda$ range from 0.738 to 0.928 for the data with $\lambda\bar{M}_w \approx 1.8$. (*b*) The same data replotted (△) against $c^0[1 + (\Lambda^2/12)p_z^2]$ and (○) against $\tilde{c}[1 + (\Lambda^2/12)p_z(p_z - 1)]$. The dashed curve is a plot of $(\bar{M}_1^{app})^{-1}$ vs. $\tilde{c}$ for the same systems.

Obviously, $\bar{M}_{0/-1}^{app}$ is more sensitive to the presence of impurities of low molecular weight.

In Figures 3, 4, and 5, eqs. (29)–(33) are tested with the data on PMMA 31M in MEK at 25°C. In Figure 3 plots of $(\bar{M}_1^{app})^{-1}$ versus c° and $\tilde{c}$ are compared. Both plots are corrected for heterogeneity by use of $c^\circ[1 + (\Lambda^2/12)p_z^2]$ and $\tilde{c}[1 + (\Lambda^2/12)p_z(p_z - 1)]$ as the concentration variables. The value of p_z is estimated from the data shown in Figures 3 and 4. Figure 4 shows plots of $(\bar{M}_{2/1}^{app})^{-1}$ versus c^0 and $\tilde{c}$, and Figure 5 shows plots of $(\bar{M}_{0/-1}^{app})^{-1}$ versus c^0. The heterogeneity of this sample is relatively small, as judged from $\bar{M}_n$, $\bar{M}_w$, and $\bar{M}_z$. The plots against $\tilde{c}$ appear to give satisfactory estimates of $\bar{M}_w$, $\bar{M}_z$ and B.

Poly A–Poly B Blend. As a typical example of heterogeneous solute systems, we examine the behavior of a mixture of polystyrene and poly(methyl methacrylate) in MEK at 25°C. The blend consists of PST-1a and PMMA-31M mixed in a weight ratio of 0.499_7:0.500_3, and has $\bar{v}^\circ$ = 0.8940 and ν^0 = 0.171. Figures 6 and 7, respectively, show plots of $(\bar{M}_1^{app})^{-1}$ and $(\bar{M}_{2/1}^{app})^{-1}$ of this blend system. All the data are summarized in Table I, in which the values of $\bar{M}_1$ and $\bar{M}_{2/1}$ are compared with those computed by eqs. (7b) and (10c), respectively. In the computation,

we assumed that each of the constituent polymers was monodisperse and used the values listed in the table. The agreement between the experimental and the computed values appears reasonable.

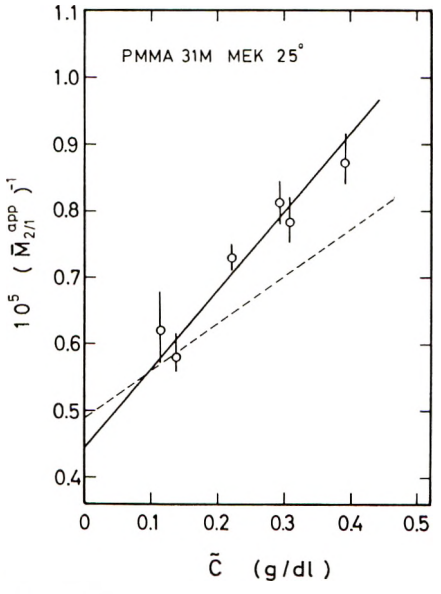

Fig. 4. Plot of $(\bar{M}_{2/1}^{app})^{-1}$ vs. $\tilde{c}$ for the same systems as in Fig. 3: Vertical lines indicate error limit. The dashed curve is a plot of $(\bar{M}_1^{app})^{-1}$ vs. $\tilde{c}$ for the same systems.

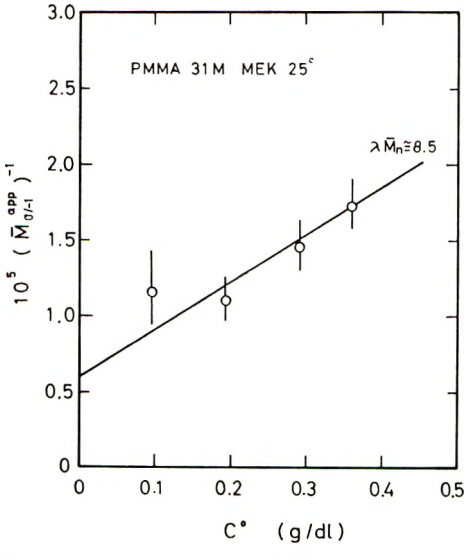

Fig. 5. Plot of $(\bar{M}_{0/-1}^{app})^{-1}$ vs. c^0 with $\lambda M_n \approx 8.5$ for polydisperse PMMA 31M in MEK at 25°C. Values of $10^{-5}\lambda$ ranges from 4.4 to 5.5. Vertical lines indicate error limits.

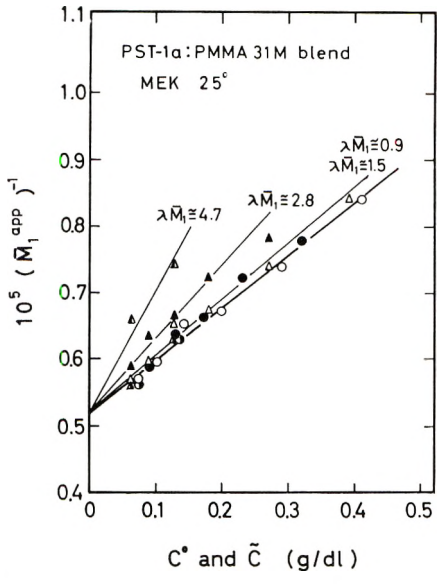

Fig. 6. Plots of $(\bar{M}_1^{app})^{-1}$ vs. (△,▲,▲)c^0 and (○,◑,●) $\tilde{c}$ for a 1:1 blend of PST-1a and PMMA 31M in MEK at 25°C. Values of $10^{-5}\lambda$ range from 0.45 to 0.526 for data with $\lambda\bar{M}_1 \approx 0.9$; from 0.687 to 0.827 for $\lambda\bar{M}_1 \approx 1.5$; from 1.36 to 1.59 for $\lambda\bar{M}_1 \approx 2.8$; and 2.46 for those with $\lambda\bar{M}_1 \approx 4.7$.

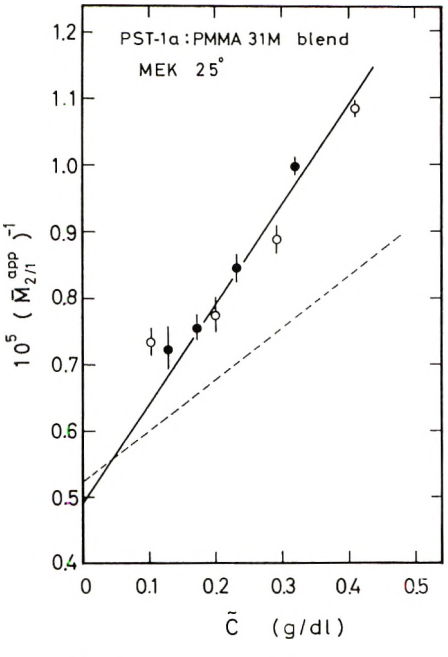

Fig. 7. Plot of $(\bar{M}_{2/1}^{app})^{-1}$ vs $\tilde{c}$ for the same system as in Fig. 6. Vertical lines indicate error limits. The dashed curve is a plot of $(\bar{M}_1^{app})^{-1}$ vs. $\tilde{c}$ for the same system.

TABLE I
Summary of Sedimentation Equilibrium Data

Polymer	$\bar{M}_n \times 10^{-4}$	$M_w \times 10^{-4}$	Sedimentation equilibrium data in MEK at 25°C					
			$\bar{M}_{0/-1} \times 10^{-4}$	$B_n^{app} \times 10^4$	$\bar{M}_1 \times 10^{-4}$	$B_{app} \times 10^4$	$\bar{M}_{2/1} \times 10^{-4}$	$B_z^{app} \times 10^{-4}$
PST-1a	15.5	16.0[a]	—	—	16.3	2.9	16.6	3.1
PMMA 31M	16.6	20.0[b]	17.2	3.2	20.4	7.4	22.6	6.5
1:1 Blend	—	—	—	—	19.1	7.9	20.8	7.4
		(computed)	—	—	(17.3)	—	(18.3)	—

[a] From light-scattering data of Utiyama et al.[13] The second virial coefficient was reported as $B_{LS} = 2.7 \times 10^{-4}$ in MEK at 25°C.
[b] From intrinsic viscosity data.[27]

For a blend of two monodisperse polymers, poly A and poly B, the light-scattering second virial coefficient $B_{2/2}$ may be expressed in terms of values for the pure polymers and the A–B interaction parameter B_{AB}:

$$B_{2/2} = (\bar{M}_1)^{-2}[\bar{M}_A M_A^* \bar{B}_{AA}(\gamma_A^0)^2 + \bar{M}_B M_B^* \bar{B}_{BB}(\gamma_B^0)^2 + (\bar{M}_A M_B^* + M_A^* \bar{M}_B)\bar{B}_{AB}\gamma_A^0\gamma_B^0] \quad (34)$$

Here the subscripts A and B refer the quantities related to the pure polymers. The parameter B_{AB} may be computed by eq. (34) by using the values for homopolymers listed in Table I. The value, $10^4 B_{AB} = 8.7$, is found to be, at least, of the right order of magnitude, as judged from the corresponding value, 8.3, found in MEK solutions of polystyrene–poly(methyl methacrylate) block copolymers.[27]

APPENDIX

The differential equation, eq. (4a), suggests that the solution θ_i may be expressed as a series function of c[5]:

$$\theta_i = \theta_i^{(0)} + c^0\theta_i^{(1)} + (c^0)^2\theta_i^{(2)} + \dots \quad (A\text{-}1)$$

Each $\theta_i^{(n)}$ must satisfy the condition conservation of mass statement, eq. (4b):

$$\int_0^1 \theta_i^{(0)} dx = 1 \quad (A\text{-}2)$$

$$\int_0^1 \theta_i^{(n)} dx = 0 \qquad \text{for } n \geqq 1 \quad (A\text{-}3)$$

Combining eq. (A-1) with eq. (4a), we obtain a set of differential equations:

$$d\theta_i^{(0)}/dx - \lambda M_i^* \theta_i^{(0)} = 0 \quad (A\text{-}4)$$

$$d\theta_i^{(1)}/dx - \lambda M_i^* \theta_i^{(1)} = -\sum M_i \bar{B}_{ij} \theta_i^{(0)} [d\theta_j^{(0)}/dx]\gamma_j^0 \quad (A\text{-}5)$$

$$d\theta_i^{(2)}/dx - \lambda M_i^* \theta_i^{(2)} = -\sum M_i \bar{B}_{ij} [\theta_i^{(0)} d\theta_j^{(1)}/dx + \theta_i^{(1)} d\theta_j^{(0)}/dx]\gamma_j^0 \quad (A\text{-}5)$$

Equations (A-4) and (A-2) describe a (hypothetical) ideal state valid only in the limit of zero concentration, wherein the effects of the $\bar{B}_{ik}$ vanish. The zero-order solution $\theta_i^{(0)}$ may be obtained easily; and with these solutions the first-order equation may be solved; and so on:

$$\theta_i^{(0)} = A_i \exp(\lambda M_i^* x) \quad (A\text{-}6)$$

with

$$A_i = \lambda M_i^* / [\exp(\lambda M_i^*) - 1] \quad (A\text{-}7)$$

$$\theta_i^{(1)} = \theta_i^{(0)} \sum M_i \bar{B}_{ij} [(A_i A_j / A_{ij}) - \theta_j^{(0)}]\gamma_j^0 \quad (A\text{-}8)$$

with

$$A_{ij} = \lambda(M_i^* + M_j^*)/[\exp\{\lambda(M_i^* + M_j^*)\} - 1] \tag{A-9}$$

$$\theta_i^{(2)} = \theta_i^{(0)} \sum_j \sum_h [M_i\bar{B}_{ih}\{M_i\bar{B}_{ij}(A_iA_j/A_{ij}) + M_h\bar{B}_{jh}(A_jA_h/A_{jh})\}\{(A_iA_h/A_{ih}) - \theta_h^{(0)}\} - M_iM_h^*(M_j^* + M_h^*)^{-1}(M_i\bar{B}_{ih}\bar{B}_{ij} + M_j\bar{B}_{ij}\bar{B}_{jh} + M_h\bar{B}_{jh}\bar{B}_{ih})\{(A_iA_jA_h/A_{ijh}) - \theta_j^{(0)}\theta_h^{(0)}\}]\gamma_j^0\gamma_h^0 \tag{A-10}$$

with

$$A_{ijh} = \lambda(M_i^* + M_j^* + M_h^*)/[\exp\{\lambda(M_i^* + M_j^* + M_k^*)\} - 1] \tag{A-11}$$

With these solutions, some important quantities such as J_{ik}, I_{ik}, etc., may also be expressed as power series in c^0:

$$(\lambda M_k^*)^{-1}\theta_i(d\theta_k/dx) = J_{ik} = J_{ik}^{(0)} + c^0J_{ik}^{(1)} + \ldots \tag{A-12}$$

$$J_{ik}^{(0)} = \theta_i^{(0)}\theta_k^{(0)} \tag{A-13}$$

$$J_{ik}^{(1)} = \theta_i^{(0)}\theta_k^{(0)} \sum_j [\{M_i\bar{B}_{ij}(A_iA_j/A_{ij}) + M_k\bar{B}_{jk}(A_jA_k/A_{jk})\} - \{M_i\bar{B}_{ij} + M_k(1 + M_j^*/M_k^*)\bar{B}_{jk}\}\theta_j^{(0)}]\gamma_j^0 \tag{A-14}$$

$$\int_0^1 J_{ik}dx - 1 = I_{ik} = I_{ik}^{(0)} + c^0I_{ik}^{(1)} + \ldots \tag{A-15}$$

$$I_{ik}^{(0)} = (A_iA_k/A_{ik}) - 1 \tag{A-16}$$

$$I_{ik}^{(1)} = \sum_j [\{M_i\bar{B}_{ij}(A_iA_j/A_{ij}) + M_k\bar{B}_{jk}(A_jA_k/A_{jk})\}(A_iA_k/A_{ik}) - \{M_i\bar{B}_{ij} + M_k(1 + M_j^*/M_k^*)\bar{B}_{jk}\}(A_iA_jA_k/A_{ijk})]\gamma_j^0 \tag{A-17}$$

In all the above quantities, the sedimentation parameter λ appears through the terms of the form $(A_iA_jA_k \ldots A_h/A_{ijk\ldots h})$, which have the following properties:

$$\lim_{\lambda \to 0} (A_i \ldots A_h/A_{i\ldots h}) = 1 \tag{A-18}$$

$$\lim_{\lambda \to \infty} (A_i \ldots A_h/A_{i\ldots h}) = (\lambda M_i^*)(\lambda M_j^*) \ldots (\lambda M_h^*)/\lambda(M_i^* + M_j^* + \ldots + M_h^*) \tag{A-19}$$

$$(A_i \ldots A_h/A_{i\ldots h}) = 1 + (\lambda^2/12)(M_i^*M_j^* + M_j^*M_k^* + \ldots\ldots + M_h^*M_i^*) + 0(\lambda^4) \tag{A-20}$$

with

$$|\lambda(M_i^* + M_j^* + \ldots\ldots + M_h^*)| \leqq 2\pi \tag{A-21}$$

The expansion in λ^2 is convergent within the region indicated in eq. (A-21) In a typical experiment, λ is of the order 10^{-5} to 10^{-6}. The applicability of the expansion is limited accordingly.

The expansion in c^0 of the θ_i and other quantities is in fact expressed in powers of $(M_i c_i^0 \bar{B}_{ik})$ etc. Hence, the series is convergent in the region $(M_i c_i^0 \bar{B}_{ik}) \ll 1$. For a typical system, say, polystyrene in MEK, $10^4 < M_i < 10^6$, $B_{ik} \approx 3 \times 10^{-4}$, and c_i^0 is taken from 10^{-3} to 5×10^{-3}. Then $M_i c_i^0 \bar{B}_{ik}$ ranges approximately from 3×10^{-3} to 1.5. These figures give some idea on the applicability of the expansion in c^0.

We wish to thank Professor Emeritus Masao Horio of this university for his encouragement and interest in the ultracentrifugation studies. For aligning and focusing the optics of the ultracentrifuge, various facilities were made available to us by Mr. Y. Gotoh of the Optical Instrument Division of Hitachi Seisakusho, Ltd., whose help is gratefully acknowledged. One of us (T. K.) acknowledges support from the Ministry of Education through grant A4037.

References

1. T. Svedberg and K. O. Pedersen, *The Ultracentrifuge*, Clarendon Press, Oxford, 1940.
2. J. W. Williams, K. E. Van Holde, R. L. Baldwin, and H. Fujita, *Chem. Rev.*, **58**, 715 (1958).
3. H. K. Schachman, *Ultracentrifugation in Biochemistry*, Academic Press, New York, 1962.
4. R. L. Baldwin and K. E. Van Holde, *Fortschr. Hochpolym. Forsch.*, **1**, 451 (1960).
5. H. Fujita, *Mathematical Theory of Sedimentation Analysis*, Academic Press, New York, 1962.
6. W. D. Lansing and E. O. Kraemer, *J. Amer. Chem. Soc.*, **57**, 1369 (1935); *ibid.*, **58**, 1471 (1936).
7. M. Wales, M. Bender, J. W. Williams, and R. H. Ewart, *J. Chem. Phys.*, **14**, 353 (1946).
8. M. Wales, *J. Phys. Colloid Chem.*, **52**, 235 (1948).
9. K. E. Van Holde and J. W. Williams, *J. Polym. Sci.*, **11**, 243 (1953).
10. K. E. Van Holde and R. L. Baldwin, *J. Phys. Chem.*, **62**, 734 (1958).
11. H. Fujita, *J. Phys. Chem.*, **63**, 1326 (1959).
12. D. A. Albright and J. W. Williams, *J. Phys. Chem.*, **71**, 2780 (1967).
13. H. Utiyama, N. Tagata, and M. Kurata, *J. Phys. Chem.*, **73**, 1448 (1969).
14. H. Fujita, *J. Phys. Chem.*, **73**, 1759 (1969).
15. R. C. Deonier and J. W. Williams, *Proc. Nat. Acad. Sci. U.S.*, **64**, 823 (1969).
16. T. Kotaka, N. Donkai, H. Ohnuma, and H. Inagaki, *J. Polym. Sci. A-2*, **6**, 1803 (1968).
17. H. C. Brinkman and J. J. Hermans, *J. Chem. Phys.*, **17**, 574 (1949).
18. J. G. Kirkwood and R. J. Goldberg, *J. Chem. Phys.*, **18**, 54 (1950).
19. W. H. Stockmayer, *J. Chem. Phys.*, **18**, 58 (1950).
20. H. Fujita, A. M. Linklater, and J. W. Williams, *J. Amer. Chem. Soc.*, **82**, 379 (1960).
21. Th. G. Scholte, *J. Polym. Sci. A-2*, **6**, 91, 111 (1968).
22. F. E. LaBar and R. L. Baldwin, *J. Phys. Chem.*, **66**, 1952 (1962).
23. T. Kotaka and N. Donkai, *J. Polym. Sci. A-2*, **6**, 1457 (1968).
24. D. A. Yphantis, *Ann. N. Y. Acad. Sci.*, **88**, 586 (1960); *Biochemistry*, **3**, 297 (1964).
25. H. Ohnuma, T. Kotaka, and H. Inagaki, *Polymer*, **10**, 501 (1969).
26. J. A. Riddick and E. E. Toops, Jr., *Organic Solvents*, Interscience, New York, 1955,
27. H. Ohnuma, Dissertation, Kyoto University, 1969.

Received November 3, 1970

JOURNAL OF POLYMER SCIENCE: PART A-2 VOL. 9, 1399–1415 (1971)

Theory of Deformation and Strain-Induced Crystallization of an Elastomeric Network Polymer

MISAZO YAMAMOTO* and JAMES L. WHITE, *Department of Chemical and Metallurgical Engineering, University of Tennessee, Knoxville, Tennessee 37916*

Synopsis

A new theory of deformation and strain induced crystallization of network polymers has been developed. The effects of lattice vacancies, variation in distribution of *trans* and *gauche* bond conformations in stretched amorphous polymers, and the crystallite orientation in the partially crystalline stretched vulcanizate were considered in the evaluation of their partition functions. Stress-extension ratio relationships were evaluated for the amorphous and semicrystalline polymers. The rise in melting temperature due to strain induced crystallization is discussed. The new theory seems to be in closer agreement with the actual strain-induced crystallization process than earlier research.

Introduction

The elastic deformation and phase transition characteristics of vulcanized rubber have long intrigued polymer researchers. One of the striking aspects of these polymers is the interaction of rheological phenomena and thermodynamic transitions. Nowhere is it more distinctive than in the crystallization of polymers during stretching. Indeed, the fact that natural rubber may crystallize was first discovered by Katz[1] in his studies of x-ray scattering patterns of stretched amorphous polymer samples.

Since the classic study of the mechanism and statistical mechanics of stretching polymer chains by Guth and Mark,[2] there has been considerable attention given to the theory of deformation of network polymers. Early research in this area has been variously reviewed by several authors.[3–7] Generally one forms a picture of a three-dimensional network of chains containing primarily single carbon–carbon bonds about which there is relatively though not perfectly free rotation. When a homogeneous force field is applied, the network deforms in an affine manner with the junctions separating uniformly. One aspect generally not considered by earlier researchers (though see Scott and Tobolsky,[8] Volkenstein,[6] Abe and Flory[9]) is the problem associated with rotational isomerism about the carbon-carbon bonds. In the unstressed amorphous state, polymer chains tend to take on a relatively random coiled configuration and there

* Permanent address: Department of Physics, Faculty of Science, Tokyo Metropolitan University, Setagaya, Tokyo, Japan.

is an equilibrium distribution of *trans* and *gauche* carbon–carbon bond conformations. Stretching the network orients the chains and causes some *gauche* bonds to be transformed into *trans* conformations.

Our view of the crystallization of an amorphous polymer is that it consists of two simultaneous phenomena. A polymer melt consists of disordered chains, with both *gauche* and *trans* conformations, which may be considered to sit in a lattice, containing a significant number of vacancies. When crystallization occurs, the chains order themselves into either an all-zigzag structure in which every carbon–carbon bond is in a *trans* conformation (as in polyethylene) or in a helical structure(as in isotactic polypropylene).[10] As this ordering takes place, the number of voids or lattice vacancies sharply decreases. The entropy of fusion is the sum of the entropy changes due to (1) the ordering of the chains and (2) the decrease in number of lattice vacancies. The energy of fusion is the sum of (1) energy changes of carbon–carbon bonds from high-energy *gauche* to low-energy *trans* conformations when zigzag crystalline structures are formed and from high-energy *trans* to low-energy *gauche* when helical structures are formed and (2) the energy change due to the decrease in the number of lattice vacancies. A theory incorporating these features has recently been published by the authors.[11]

When a force is applied to an amorphous polymer, the chains become oriented in the direction of the force and the scalar end-to-end distances are increased. The orientation, stretching, and thus partial ordering, of the polymer chains decreases the configurational entropy of the material by an amount ΔS_{def} and thus decreases the entropy of fusion. The normal melting temperature is given by:

$$T_{m,1} = \Delta H_1/\Delta S_1 \tag{1}$$

where ΔH_1 is the heat of fusion and ΔS_1 the entropy of fusion. The value of the melting temperature T_m in the stressed state will be increased by an amount

$$T_{m,\lambda} - T_{m,1} = (\Delta H_\lambda/\Delta S_\lambda) - (\Delta H_1/\Delta S_1) \tag{2a}$$

or

$$1/T_{m,\lambda} = (1/T_{m,1}) - (\Delta S_{def}/\Delta H_1) \tag{2b}$$

if the heat of fusion is independent of the deformation. This basic idea is implicit in an almost thirty-year old paper by Alfrey and Mark.[12] (Compare Krigbaum and Roe.[13–15])

Generally, polymers and especially network polymers crystallize to only a limited extent. For linear polymer chains the cause is undoubtedly largely kinetic in nature. However, the crosslinkages form such irregularities in network polymers, that the regions immediately around them will certainly not crystallize. The greater the crosslink density, the smaller will be the equilibrium degree of crystallinity. (See the remarks and experimental data, especially Figure 6.1 of Mandelkern.[16]) If a polymer crys-

tallizes only in part, then there will be oriented regions of chains in all *trans* conformation (or alternating *trans* and *gauche* for helical structures). The crystalline portions distort the amorphous sections about the crosslinks and thus, in effect, vary the extension ratios in those regions. The occurrence of this type of problem in partially crystalline polymers was first realized by Alfrey and Mark[12] and has been considered by Flory[17], Krigbaum et al.,[15] and Smith and Ciferri.[18]

In this paper, we will present what we believe to be a rather more general and thoughtful approach to the problem of deformation and strain induced crystallization of a network polymer. The effects of chain flexibility and lattice vacancies with their corresponding energetic contributions will be evaluated. An important result of this paper is the development of new and more general expressions for the partition functions of an amorphous vulcanizate and a partially crystalline vulcanizate.

Partition Function and Free Energy of an Amorphous Network Polymer

Consider a tensile specimen of crosslinked polymer subjected to an axial force F within a chamber in which there is an ambient pressure p and temperature T. The specimen consists of a network of N_p identical chains each possessing M units. We will now formulate a theory of the deformation of such a tensile specimen which will allow us to predict the relation between applied force and extension ratio and deformation-induced crystallization. To proceed, we will determine the partition function for a constant-force, constant-pressure ensemble [compare Hill[19]].

$$Z(T,p,F) = \sum_m \sum_j \sum_L \Omega_j(V_m,L,E_j) e^{-E_j/kT} e^{+FL/kT} e^{-pV_m/kT} \tag{3}$$

Here Ω_j is the number of system conformations consistent with energy E_j, volume V_m, and length L. This partition function is related to thermodynamic properties through the relation:

$$G = -kT \ln Z \tag{4a}$$

where

$$G = E - TS - FL + pV \tag{4b}$$

The partition function will be evaluated as indicated earlier by means of a lattice model. Lattice models were first applied to polymers by Meyer,[20] Flory,[4,21,22] and Huggins[23] in order to explain the thermodynamic properties of polymer solutions. Flory,[24,25] DiMarzio, and Gibbs,[26] and the present authors[11] have utilized them to analyze phase transitions in bulk polymers. DiMarzio[27] has considered the application of the lattice formulation to a deformed polymer. Consider a lattice consisting of N_0 sites in which there are N_p polymer chains taking up N_pM lattice sites and N_1 vacancies, thus:

$$V_m = v_0(N_1 + MN_p) \tag{5}$$

The energy E_j of a lattice of N_p polymer chains with N_1 holes may be written:

$$E_j = E_j^{(i)} + E_j^{(pp)} + E_j^{(flex)} \tag{6}$$

Here $E_j^{(i)}$ is the internal energy of polymer lattice units, $E_j^{(pp)}$ is the interaction energy of the adjacent polymer chain segments and $E_j^{(flex)}$ is the total bond rotation energy due to *gauche* and *trans* conformations. It may readily be seen that:

$$E_j^{(i)} = N_p M \epsilon_j^{i} \tag{7}$$

and:*

$$E_j^{(pp)} = N_p[(z - 2)M + 2]\phi_p w_{pp} \tag{8}$$

where z is the coordination number of the lattice, ϕ_p is the volume fraction of polymer, and $2w_{pp}$ is the interunit interaction energy. The total bond rotation energy of the polymer tensile specimen is:

$$E_j^{(flex)} = N_p(M - 1)[f\epsilon_G + (1 - f)\epsilon_T] \tag{9}$$

where ϵ_G is the energy of a *gauche* conformation, ϵ_T the energy of a *trans* conformation, and f the fraction of flexed bonds i.e., those in a *gauche* conformation.

The number of conformations, Ω_j, of N_p chains each of which has a fraction f of its bonds flexed, and N_1 holes is, following Flory:[22]

$$\Omega_j = (\omega_j^{i})^{N_p M} \frac{[N_p(M - 1)]!}{[N_p f(M - 1)]!\,[N_p(1 - f)(M - 1)]!} \cdot g_j \tag{10}$$

Here ω_j^{i} is the number of internal conformations per segment, g_j is the number of conformations due to lattice packing and the factorial term represents the degeneracy caused by the number of different ways $fN_p(M - 1)$ *gauche* conformations may be distributed among $N_p(M - 1)$ total conformations, the quantity g_j is:

$$g_j = \prod_{i=1}^{N_p} \nu_i \tag{11}$$

where ν_i is the number of possible conformations for the ith chain after $(i - 1)$ are already present in the lattice. In the derivation of eq. (10) it is assumed that the individual chains behave independently of each other except for the restriction that the end points of the chains are located at the crosslinks. The computation of g_j and ν_i for a network polymer is more complex than for an uncrosslinked material. First, it is noted that, unlike Flory's expression for the packing conformations in his solution theory,[4,21] no factorial term appears. This is because identical polymer chains held at their ends by crosslinks are distinguishable, like the lattice

* Volume fractions rather than the more rigorous surface fractions of sites are used in computing the interaction energy.

atoms in crystal statistics.[19] If we consider the crosslink points fixed in space, then the number of possible sites δ_i for the first segment of the ith polymer chain is simply:*

$$N_0\delta_i = N_0 - M(i-1) \tag{12}$$

For the second segment, if the conformation is *gauche*, there are $(z'-2)\ \delta_i$ possible positions, where z' is the coordination number of the sublattice of the polymer chain; if the conformation of the second segment is *trans* there will be only δ_i possible positions. If follows that:

$$\nu_i = (z'-2)^{f_i M}\delta_i{}^M P_i \tag{13}$$

where P_i is the probability that a chain beginning at the position of origin of the ith chain will have the end-to-end distance (x_i,y_i,z_i) determined by the position of the crosslink to which its last segment is attached. Thus, we obtain

$$\begin{aligned} g_j &= \prod_{i=1}^{N_p} (z'-2)^{f_i M}\delta_i{}^M P_i \\ &= \frac{(z'-2)^{fN_p(M-1)}}{N_0{}^{N_p M}} \frac{N_0!}{N_i!} \prod_{r=0}^{N_p M} P_r{}^{N_{pr}} \end{aligned} \tag{14}$$

where N_{pr} is the number of chains with end-to-end distance r having probability P_r.

The total partition function may now be written:

$$\begin{aligned} Z = q^{N_p M} \sum_{N_1} \frac{N_0!}{N_0{}^M N_1!} \exp\{-E_j^{(pp)}/kT\} \exp\{-pv_0(N_1 + MN_p)/kT\} \\ \times \sum_L \sum_f \frac{(z'-2)^{fN_p(M-1)}\,[N_p(M-1)]}{[fN_p(M-1)]![(1-f)N_p(M-1)]!} \left[\prod P_r{}^{N_{pr}}\right] \\ \times \exp\{-E^{(\text{flex})}/kT\} \exp\{FL/kT\} \end{aligned} \tag{15}$$

where q is the internal partition function of a segment;

$$q = \sum \omega_j{}^i \exp\{\epsilon_j{}^i/kT\}$$

The summation with respect to N_1 will be evaluated by the maximum term method. To do this, we form the logarithm and differentiate with respect to N_1. This gives for the maximum term:

$$\begin{aligned} \ln \phi_1 = -(1-\phi_1)\{([(z-2)M+2]/M)(-w_{pp}/kT) \\ \times (1-\phi_1) + 1\} - (pv_0/kT) \end{aligned} \tag{16a}$$

with

$$\phi_1 = N_1/(N_1 + MN_p) \tag{16b}$$

* An analysis of the effect of deformation of δ_i and packing entropy has been given by DiMarzio.[27] We neglect this correction here.

This result differs only slightly from that given in our earlier paper.[11] A term of order $1/M$ does not appear because of the crosslinking restriction. The use of the partition function Z introduces a small correction for the effect of external pressure.

We shall now devise an expression for the detailed deformation process. As a first approximation, we will presume Gaussian statistics.[3-6] In particular, we presume that:

$$P_r = v_0(3/2\pi\overline{r_0^2})^{3/2} \exp\left\{-3[(x^2 + y^2 + z^2)/2\,\overline{r_0^2}]\right\} \tag{17}$$

where v_0 is the volume of a lattice site and $\overline{r_0^2}$ is the mean-square end-to-end distance of a unperturbed polymer chain at temperature T. Further, we have

$$(2/v_0) \iiint P_r dxdydz = 1 \tag{18}$$

If we consider the set of network crosslinks to deform affinely with the tensile specimen which is stretched to extension λ in the x direction, then the fraction of end-to-end distances in volume element $dxdydz$ is:

$$N_{pr}/N_p = (3/2\pi\overline{r_i^2})^{3/2} \exp\left\{-(3/2\overline{r_i^2})[(x/\lambda)^2 + \lambda y^2 + \lambda z^2]\right\} dxdydz \tag{19}$$

where $\overline{r_i^2}$ is the initial mean-square end-to-end distance among the network chains. We distinguish between the mean square end-to-end distances $\overline{r_0^2}$ for isolated chains and $\overline{r_i^2}$ for the initial condition of the crosslinked vulcanizate; $\overline{r_i^2}$ is determined by the conditions of crosslinking.[7]

The next problem that must be resolved is the summation over f. Flory[24] has solved this problem for the case of an uncrosslinked undeformed polymer essentially by using the maximum term method. Now, f obviously depends upon the amount that the tensile specimen is stretched.[26,27] We do not yet have, however, sufficient information in eq. (15) to solve the problem. We shall try a different procedure to obtain f. This method, while in no sense a rigorous one, does, we believe, represent a reasonably good approximation to reality. Consider a system consisting of an isolated polymer chain possessing M segments which is held under a tension τ. Of the $(M - 1)$ segments which may be flexed, M_G will be taken as in a *gauche* conformation and M_T in a *trans* conformation. Our problem is to calculate $\overline{M}_G$ for a constant stress ensemble of these systems.

$$\overline{M}_G = (M - 1)\bar{f} = \frac{\sum M_G p(M_G,\tau) \exp\left\{-[(M_G\epsilon_G + M_T\epsilon_T) - \tau r]/kT\right\}}{\sum p(M_G,\tau) \exp\left\{-[(M_G\epsilon_G + M_T\epsilon_T) - \tau r]/kT\right\}} \tag{20}$$

where

$$r = M_G l_G + M_T l_T \tag{21a}$$

$$= M_G l_G + (M - 1 - M_G) l_T$$

where l_G and l_T are the effective root-mean-square projections of the *gauche* and *trans* bond vectors in the direction of the chain end-to-end distance r. l_G and l_T are, therefore, the functions of r and M_G (and M_T). Here also:

$$p(M_G,\tau) = \frac{(M-1)!}{(M-1-M_G)!M_G!}(z'-2)^{M_G}1^{M_T} \tag{21b}$$

It may be seen that:

$$M_G = (M-1)f = -kT\frac{\partial}{\partial\epsilon_G} \times \ln\left[\sum p(M_G,\tau)\exp\left\{-\frac{(M_G\epsilon_G + M_T\epsilon_T) - \tau r}{kT}\right\}\right] \tag{22}$$

By means of the binomial expansion, the sum becomes:

$$\exp\{-(M-1)(\epsilon_T - \tau l_T)/kT\} \times \left[1 + (z'-2)\exp\left\{-\frac{(\epsilon_G - \epsilon_T) - \tau(l_G - l_T)}{kT}\right\}\right]^{M-1}$$

and we immediately obtain from differentiating Eq. (22):

$$f = \frac{(z'-2)\exp\{-[(\epsilon_G - \epsilon_T) - \tau(l_G - l_T)]/kT\}}{1 + (z'-2)\exp\{-[(\epsilon_G - \epsilon_T) - \tau(l_G - l_T)]/kT\}} \tag{23}$$

Note that for $\tau = 0$ we obtain Flory's result.

We must now interpret what is meant by the difference $(l_T - l_G)$. Intuitively, we have

$$l_T - l_G = (r/Mb)(b_T - b_G) \tag{24}$$

where b is the length of the equivalent statistical segment of a bond; r is the mean end-to-end distance; and b_T and b_G are the effective projections of bond lengths of *trans* and *gauche* conformations when the chain is either all-*trans* (zigzag) or all-*gauche* (a spiral). That is, if all the bonds are in the *trans* conformation and the chain is in a fully extended conformation under this presumptive restriction, the end-to-end distance of the chain is just given by Mb_T, and if all the bonds are gauche, this is Mb_G. For small extensions of isolated polymer chains, it is readily shown from a constant tension ensemble that[19]

$$\tau = 3kTr/\overline{r_0^2} \tag{25}$$

Thus, the negative exponent in eq. (23) may be written in the form:

$$(\epsilon_G - \epsilon_T) - [3kT(b_T - b_G)/Mb](\overline{r^2}/\overline{r_0^2}) \tag{26}$$

The ensemble average, $\overline{r^2}/\overline{r_0^2}$ would seem to be the first invariant of the Finger deformation tensor:[28]

$$I_1 = \mathrm{tr}\mathbf{c}^{-1} = \lambda^2 + (1/\lambda) \tag{27}$$

Equation (23) may now be rewritten as:

$$f = \frac{(z' - 2) \exp \{-[(\epsilon_G - \epsilon_T) + (kT\Delta b/Mb)I_1]/kT\}}{1 + (z' - 2) \exp \{-[(\epsilon_G - \epsilon_T) + (kT\Delta b/Mb)I_1]/kT\}} \quad (28)$$

where

$$\Delta b = b_T - b_G$$

We believe that it is appropriate to apply eq. (28) to a vulcanizate with $\overline{r_0^2}$ interpreted as $\overline{r_i^2}$.

The stress–strain relation for a rubber vulcanizate may be computed from the partition function Z. This is accomplished by taking the partition function of eq. (15) together with eqs. (17), (19), (27), and (28), and obtaining the maximum term of the L expansion. In particular, forming ln Z, differentiating with respect to L under the condition of constant force f and setting the result equal to zero gives (compare Appendix I):

$$F = \frac{N_p kT}{L_{10}} \left[\frac{\overline{r_i^2}}{\overline{r_0^2}} + 2(M - 1) \left(\frac{3\Delta b}{Mb} \right)^2 I_1 f(1 - f) \right] \left(\lambda - \frac{1}{\lambda^2} \right) \quad (29)$$

where L_{10} is the initial length of the tensile specimen.

The correction to the kinetic-theory term in eq. (29) is inversely proportional to M and is thus undoubtedly a rather small quantity. It may seem strange that while the internal energy decreases upon stretching, the correction term increases the applied force. This is because this term includes not only energy but packing-entropy contributions.

We are now in a position to evaluate the Gibbs free energy G:

$$\begin{aligned} G = {} & N_p[(z - 2)M + 2]w_{pp}\phi_p + N_p(M - 1)[f\epsilon_G + (1 - f)\epsilon_T] \\ & + pv_0(N_1 + MN_p) - F\lambda L_{10} + N_1 kT \ln \phi_1 + N_p MkT \\ & + N_p(M - 1)kT[f \ln f + (1 - f) \ln (1 - f) - f \ln (z' - 2)] \\ & + \frac{N_p kT}{2} \frac{\overline{r_i^2}}{\overline{r_0^2}} \left[\lambda^2 + \frac{2}{\lambda} - 3 \ln \left\{ \frac{3v_0^{2/3}}{(2\pi \overline{r_0^2})} \right\} \right] - N_p MkT \ln q \end{aligned} \quad (30)$$

where we have used the maximum term for L, treated the sum arising from the products of the $P^{N_{pr}}$ as an integral and the quantity $(\overline{r_i^2}/\overline{r_0^2})$ is the so-called front factor.[7] The fraction f of flexed bonds will be taken as given by eq. (28).

Partition Function and Free Energy of Partially Crystalline Polymer

Let us presume that a fraction χ of the M units in any chain stretching between crosslinking points is crystalline. In the crystalline region carbon-carbon bonds are taken to be in the *trans* conformation. We presume that the crosslinks themselves and a certain number of segments leading away from such junctions are excluded from the crystallites. By symmetry this number must be $M(1 - \chi)/2$, for undoubtedly it will be the middle

part of the chain which occurs within the crystallite. We now have $2N_p$ chains in the amorphous polymer around the crosslinks, each chain having $M(1 - \chi)/2$ segments. The partition function Z of eq. (3) will be computed for this model.

A major problem in the evaluation of the partition function for a partially crystalline crosslinked elastomer held under tension is the direction of orientation of the crystallites. According to Flory's theory,[17] the crystallites are oriented in the direction of stretching. This is, however, not the case undoubtedly except for very large deformations. Indeed, for small deformations, the assumption leads to negative tensile forces. In this paper, we make what we believe is a better hypothesis than this though admittedly it is still an imperfect solution. The new hypothesis is that each chain crystallizes in the same direction as its end-to-end distance. It may be shown that if the chains crystallize at random, this hypothesis is valid (see Appendix II).

Turning now to the evaluation of the partition function we see that quite obviously eqs. (5)–(7) may still be used, but eqs. (8) and (9) must now take the form:

$$E_j^{(\mathrm{pp})} = N_p[(z - 2)M + 2]w_{\mathrm{pp}}[\chi + \phi_p(1 - \chi)] \tag{31}$$

and:

$$\begin{aligned} E_j^{(\mathrm{flex})} &= N_p(M - 1)[\chi\epsilon_T + (1 - \chi)\{f\epsilon_G + (1 - f)\epsilon_T\}] \\ &= N_p(M - 1)[\epsilon_T + (1 - \chi)f(\epsilon_G - \epsilon_T)] \end{aligned} \tag{32}$$

The number of conformations Ω_j becomes:

$$\Omega_j = (\omega_j^{\,i})^{N_pM} \frac{[(1 - \chi)N_p(M - 1)]!}{[(1 - \chi)fN_p(M - 1)]![(1 - \chi)(1 - f)N_p(M - 1)]!} \prod \nu_i \tag{33}$$

where

$$\nu_i = [(z' - 2)^{fi}\delta_i]^{(1-\chi)M}P_i'^{2} \tag{34}$$

Here P_i' is the probability that the ith chain beginning at a particular crosslink ends at an appropriate volume unit space on the crystallite surface.

Using eqs. (5)–(7) and (31)–(34), we may calculate Z:

$$\begin{aligned} Z = q^{N_pM} \sum_{\chi} \sum_{N_1} & \frac{[N_1 + (1 - \chi)N_pM]!}{[N_1 + (1 - \chi)N_pM]^{(1-\chi)N_pM}N_1!} \\ & \times \exp\{-E^{(\mathrm{pp})}/kT\} \exp\{-pv_0(N_1 + MN_p)/kT\} \\ \times \sum_{f} & \frac{(z' - 2)^{(1-\chi)fN_p(M-1)}[(1 - \chi)N_p(M - 1)]!}{[(1 - \chi)fN_p(M - 1)]![(1 - \chi)(1 - f)N_p(M - 1)]!} \\ & \times \exp\{-E^{(\mathrm{flex})}/kT\} \exp\{FL/kT\} (\pi p_r'^{2N_p r}) \end{aligned} \tag{35}$$

where we have summed over all possible values of degree of crystallization χ, lattices vacancies (amorphous phase only), and fraction of flexed chains (amorphous phase only).

Using the maximum-term method on Z, we may again determine the value of N_1 the number of lattice vacancies. In our treatment, such vacancies are allowed to occur only in the amorphous phase. We find that N_1 is given by

$$\phi_1 = N_1/[N_1 + (1 - \chi)N_p M] \tag{36}$$

where ϕ_1 is specified by eq. (16a). This result may be interpreted as meaning that the void fraction in the amorphous phase is independent of the extent of crystallization.

We must now evaluate the effect of crystallization upon P_r' and f. The dependence of P_r' upon χ is the critical problem for crystallization of a cross-linked polymer. It is this phenomenon, through its effect on entropy, which has a strong influence on the extent of crystallization in these materials. Because of such crystallization, the effective extension ratio in the amorphous segments is decreased. The probability of an end-to-end distance r may be seen to be (with $n = \chi M$):

$$P_r' = v_0(3/2\pi\overline{r_0^2})^{3/2}[2M/(M - n)]^{3/2} \times \exp\{-(3/2\overline{r_0^2})[2M/(M - n)][(r - nb)^2/4]\} \tag{37}$$

where it has been presumed that $\overline{r_0^2}$ is proportional to the number of units in the flexible chain[2-6] and $(r - nb)$ represents the correction of eq. (17) due to the enforced extension of a crystallized portion of the chain along the x axis. The additional factor of 4 in the denominator of the exponential term arises from the fact that we are concerned with the two flexible terminal portions of the chain rather than the chain as a whole.

The fraction of polymer chains N_{pr}/N_p in the deformed sample possessing an end-to-end distance vector in the partially crystalline polymer between (x, y, z) and $(x + dx, y + dy, z + dz)$ will again be taken to be given by eq. (19). Replacing the sum formed from the logarithm of eq. (35) with an integral, we have

$$\sum 2N_{pr} \log P_r' = -\tfrac{1}{2}N_p\{[h(\chi,\lambda)/(1 - \chi)] + 3 \ln [-(\pi\overline{r_0^2}/3)(1 - \chi)]\} \tag{38}$$

$$h(\chi,\lambda) = (\overline{r_i^2}/\overline{r_0^2})\{[\lambda^2 + (2/\lambda)] - 2Mb(6/\pi\overline{r_0^2})^{1/2}\chi\lambda g(\lambda) + 3(M^2b^2/\overline{r_0^2})\chi^2\} \tag{39}$$

with:

$$g(\lambda) = 1 + \frac{1}{2\lambda^3}\frac{1}{\sqrt{1 - 1/\lambda^3}} \ln \frac{1 + \sqrt{1 - 1/\lambda^3}}{1 - \sqrt{1 - 1/\lambda^3}} \tag{40}$$

In the natural state we have, $\lambda = 1$ and $g(1) = 2$, and in the case of large extensions $\lambda \to \infty$, $g(\lambda) \to 1$, and eq. (38) tends to Flory's result.

The next problem that must be resolved is the value of f in the amorphous regions. Equation (23) is the logical starting point and the problem is reduced to determine $\tau(l_T - l_G)$. We must determine the effective extension rates in the amorphous region. The extension of an amorphous part of a chain is just $(r - nb)/2$ and the number of segments is $(M - n)/2$. Corresponding to Eq. (26), we have

$$\begin{aligned}\Delta\epsilon' &= \overline{\tau(l_T - l_G)} \\ &= [3kTM/(M - n)^2][(b_T - b_G)/b][\overline{(r - nb)^2}/\overline{r_0^2}] \\ &= kT(1/M)[1/(1 - \chi)^2][(b_T - b_G)h(\chi,\lambda)/b] \end{aligned} \tag{42}$$

Therefore, $h(\chi,\lambda)/(1 - \chi)^2$ is utilized in place of I_1 in eq. (28).

We may determine χ by the maximum-term method. Forming $\ln Z$ and differentiating with respect to χ yields:

$$\begin{aligned}0 = &\left[\frac{(z - 2)M + 2}{M}\right]\left(-\frac{w_{pp}\phi_1}{kT}\right) + \frac{M - 1}{M}\left[\frac{f\epsilon_G + (1 - f)\epsilon_T}{kT}\right] \\ &+ \frac{\phi_1}{1 - \phi_1}\ln\phi_1 + 1 + \frac{pv_0}{kT}\left(\frac{\phi_1}{1 - \phi_1}\right) \\ &+ \frac{M - 1}{M}[f\ln f + (1 - f)\ln(1 - f) - f\ln(z' - 2)] \\ &- \frac{M - 1}{M}(1 - \chi)f(1 - f)\frac{\Delta\epsilon'}{kT}\frac{\partial(\Delta\epsilon'/kT)}{\partial\chi} - \frac{1}{2M(1 - \chi)^2}\frac{\overline{r_i^2}}{\overline{r_0^2}} \\ &\times\left[\left(\lambda^2 + \frac{2}{\lambda}\right) - 2Mb\left(\frac{6}{\pi\overline{r_0^2}}\right)^{1/2}\lambda g(\lambda) + 3\frac{M^2b^2}{\overline{r_0^2}}\chi(2 - \chi)\right] \\ &+ \frac{3}{2M(1 - \chi)}\end{aligned} \tag{43}$$

If we accept the argument of the previous paragraph:

$$\begin{aligned}\frac{\partial(\Delta\epsilon'/kT)}{\partial\chi} = &\left(\frac{b_T - b_G}{b}\right)\frac{2}{M(1 - \chi)^3}\left[\left(\lambda^2 + \frac{2}{\lambda}\right) - Mb\left(\frac{6}{\pi\overline{r_0^2}}\right)^{1/2}\right. \\ &\left.\times(1 - \chi)\lambda g(\lambda) + 3\frac{M^2b^2}{\overline{r_i^2}}\chi\right]\end{aligned} \tag{44}$$

This form is rather more general than that of Flory.[17]

If we note that the number of crosslinks in our lattice of N_p chains with N_pM total units is $N_p/2$ or $(N_pM)/2M$, it may be seen that the quantity M in the above equations represents an inverse crosslink density. Solution for χ as a function of M is equivalent to finding the effect of crosslink density on degree of crystallinity.

For large values of M,

$$\Delta\epsilon' \backsimeq 3kT[(b_T - b_G)/b][\chi^2/(1 - \chi)^2] \tag{45}$$

$$\partial(\Delta\epsilon')/\partial\chi \backsimeq 6kT[(b_T - b_G)/b][\chi/(1 - \chi)^2]$$

and if we omit terms higher than χ^2,

$$(z - 2)\left(-\frac{w_{pp}}{kT}\phi_1\right) + f\frac{\epsilon_G}{kT} + (1 - f)\frac{\epsilon_T}{kT} + \frac{\phi_1}{1 - \phi_1}\ln\phi_1$$

$$+ \frac{pv_0}{kT}\frac{\phi_1}{1 - \phi_1} + [f\ln f + (1 - f)\ln(1 - f) - f\ln(z' - 2)]$$

$$= B$$

$$= [3\chi(2 - \chi)/2(1 - \chi)^2]^{-1} \tag{46}$$

where the relation $\overline{r_0^2} = Mb^2$ has been used. From this equation we have for small B:

$$\chi \simeq 1 - \sqrt{3/5} + \sqrt{3/125}B = 0.225 + 0.155B \tag{47}$$

We may determine the force-deformation relationship for the partially crystalline polymer by using the maximum-term method. This is:

$$F = \frac{N_p}{L_0}kT\frac{1}{1 - \chi}\left[\left(\lambda - \frac{1}{\lambda^2}\right) - Mb\frac{b}{\pi\overline{r_i^2}}\chi g^*(\lambda)\right] \tag{48}$$

with

$$g^*(\lambda) = g(\lambda) - \lambda g'(\lambda)$$

$$= 1 + \frac{3x}{2(1 - x)} - \frac{x}{(1 - x)^{3/2}}\left(1 - \frac{x}{4}\right)\ln\frac{1 + \sqrt{x - 1}}{1 - \sqrt{1 - x}} \tag{49}$$

where

$$x = 1/\lambda^3$$

The function $g^*(\lambda)$ has the limiting values

$$\lambda \to 1,\ g^*(1) = 0$$

$$\lambda \to \infty,\ g^*(\infty) = 1 \tag{50}$$

Near the undeformed state, $g^*(\lambda)$ tends to zero, and for large deformations eq. (50) becomes the same as Flory's stress–strain relation. In this way we avoid the paradox of negative stress in the small elongation region.

At this point we may write down our final expression for the free energy G:

$$G = N_p[(z-2)M+2]w_{pp}[\chi+(1-\chi)\phi_p] + N_p(M-1)[\epsilon_T+(1-\chi)f(\epsilon_G-\epsilon_T)] + N_1kT\ln\phi_1 + (1-\chi)N_pMkT + pv_0(N_1+MN_p) - FL_1 + (1-\chi)N_p(M-1)kT[f\ln f+(1-f)\ln(1-f) - f\ln(z'-2)] + (N_pkT/2)(\overline{r_i^2}/\overline{r_0^2})[1/(1-\chi)][\lambda^2 + (2/\lambda) - 2(6Mb^{1/2}/\pi\overline{r_i^2}) + (3M^2b^2/\overline{r_i^2})\chi^2] + 2N_pkT\ln[v_0(3/2\pi\overline{r_0^2})^{3/2}/(1-\chi)^{3/2}] - N_pkT\ln q \quad (51)$$

Effect of Extension Ratio on Crystallization

The theory of the elevation of the crystalline melting point of a polymer network on stretching is outlined in eqs. (1) and (2).

It is of interest to first look at a model in which the crosslinks do not interfere with crystallization. For such a model, the canonical partition function is given by:

$$Q = q^{N_pM}\exp\{-N_p[(z-2)M+2]w_{pp}/kT\} \quad (52)$$

Here $A = -kT\ln Q$. If one accepts this model of the crystalline state and neglects variations in packing entropy and the distribution of *trans* and *gauche* conformations in the polymer network as well as variations in the structure of the stretched and unstretched vulcanizate, then it readily follows from Eqs. (30) and (49) that:

$$1/T_{m,\lambda} = (1/T_{m,1}) - (N_pk/\Delta H_1)(\overline{r_i^2}/\overline{r_0^2})[\lambda^2+(2/\lambda)-3] \quad (53)$$

This result has been published by several authors, but is more general as it explicitly considers the sources of the energy of fusion, namely the formation of *trans* conformations and the disappearance of holes. The melting temperature $T_{m,1}$ will be in essence that derived in our earlier paper.[11]

To compute the value of $T_{m,\lambda}$ for the more complex model takes more serious consideration. One way of viewing the problem is that χ is a decreasing function of temperature and an increasing function of extension ratio. When an amorphous elastomer is stretched, a characteristic extension ratio is reached when crystallization begins and χ takes on nonzero positive values. Such a $T_{m,\lambda}$ is obtained when one equates χ to zero in Eq. (43). This is the approach of Flory.[17] This procedure may be unrealistic, and it actually denies that there is a temperature at each extension ratio (or an extension ratio at each temperature) at which a finite amount of crystalline material is formed. The results of the previous two sections yield expressions for the Gibbs free energy* of an amorphous and a partially

* The free energy defined by $E + pV - TS$ as distinct from that defined by eq. (4).

crystalline phase. If these become equal at finite values of χ, something like a true phase transition will occur and give:

$$T_{m,\lambda} = \frac{\left\{[(z-2)M+2](-\epsilon_{pp}) + \dfrac{pv_0M}{(1-\phi_1)}\right\}\chi\phi_1}{k\left\{(M-1)\ln\left[\dfrac{1-f_a}{(1-f_c)^{1-\chi}e^{\chi}}\right] + \dfrac{\chi M\phi_1}{1-\phi_1}\ln\dfrac{1}{\phi_1} - \Phi\right\}} \tag{54}$$

where

$$\Phi = \frac{1}{2}\frac{\chi}{1-\chi}\frac{\bar{r}_i^2}{\bar{r}_0^2}\left[\lambda^2 + \frac{2}{\lambda} - \left(\frac{24}{\pi\bar{r}_i^2}\right)^{1/2} Mb\lambda g(\lambda) - \frac{3M^2b^2}{\bar{r}_i^2}\chi^2\right]$$

$$+ 3\ln(1-\chi) + \frac{3(M-1)\Delta b}{Mb}\left[f_aI_1 - (1-\chi)f_c\frac{h(\chi,\lambda)}{1-\chi}\right] \tag{55}$$

We call $T_{m,\lambda}$ the incipient crystallization temperature.

Here we have assumed that the internal partition function of a segment of polymer is the same in the crystalline and amorphous states; and f_a and f_c represent, respectively, the fractions of flexed bonds in the amorphous vulcanizate and in the amorphous portions around the crosslinks in a semicrystalline polymer. Quite obviously f_c is greater than f_a.

Two effects may be seen in eq. (54). Stretching of the vulcanizate increases the equilibrium melting temperature. However, the presence of distorted regions around the crosslinks decreases the melting temperature.

There is a major difference between eqs. (53) and (54) in their predictions of the dependence of the incipient crystallization temperature on extension ratio. Equation (53) predicts a far more rapid increase in this temperature with extension ratio than the former equation. This is due to the restriction on crystallization by the junctions between chains. An experimental study of this dependence for a *trans*-polychloroprene vulcanizate has been made by Gent,[29] who finds the dependence to be much weaker than would be predicted by eq. (53). Gent interprets this as giving support to the early theory of Flory,[17] which indeed it does. However, detailed agreement would undoubtedly be improved through comparison with the more sophisticated formulation of this paper wherein bond flexing, packing entropy, and crystalline orientation variations are considered. The superiority of the theory outlined in this paper is perhaps best shown where the force-deformation relationship for a partially crystalline polymer is developed. Here it is shown that the problem with Flory's theory at small strains does not arise.

It is of interest to discuss the effect on the equilibrium melting temperature of stretching and drawing in an uncrosslinked polymer. While such a process is not an equilibrium one and the statistical mechanical methods of this paper cannot be rigorously utilized, some interesting conclusions may be made. As such a polymer will have no distorted amorphous region around crosslinks, there will be no tendency of this sort of imperfec-

tion to decrease the melting temperature. For this reason, it would be expected that the melting temperature for such linear polymers should approach the dependence of eq. (53) rather than eq. (54) if the extension ratio were replaced by some sort of recoverable strain.

Conclusions

A new statistical mechanical theory of deformation and strain induced crystallization of a network polymer has been devised. The increase in melting temperature with extension ratio has been evaluated. As intermediates in this development, new and more general forms of the partition functions for stretched amorphous and partially crystalline network polymers have been devised.

APPENDIX I

An alternate approach to obtaining the applied force F is possible. We may write:

$$F = (\partial A/\partial L_1) = \partial(G - pV + FL_1)/\partial L_1 \tag{A-1}$$

where A is the Helmoltz free energy.

For an incompressible isotropic elastic material, the free energy is a function of the first two principal deformation invariants I_1 and I_2 which may be expressed in terms of the principal extension ratios as[5,27]

$$\begin{aligned} I_1 &= \lambda_1^2 + \lambda_2^2 + \lambda_3^2 \\ I_2 &= \lambda_1^2\lambda_2^2 + \lambda_2^2\lambda_3^2 + \lambda_3^2\lambda_1^2 \end{aligned} \tag{A-2}$$

For uniaxial extension, the first invariant is given by eq. (27). The second invariant is:

$$I_2 = 2\lambda + (1/\lambda^2) \tag{A-3}$$

From eq. (A-2) we may write:

$$\begin{aligned} F &= (\partial A/\partial I_1)(\partial I_1/\partial L_1) + (\partial A/\partial I_2)(\partial I_2/\partial L_1) \\ &= \frac{1}{L_{10}}\left[\left(\frac{\partial A}{\partial I_1}\right)\left(\frac{\partial I_1}{\partial \lambda}\right) + \left(\frac{\partial A}{\partial I_2}\right)\left(\frac{\partial I_2}{\partial \lambda}\right)\right] \qquad \text{(A-4)} \\ &= \frac{2}{L_{10}}\left[\frac{\partial A}{\partial I_1} + \frac{1}{\lambda}\left(\frac{\partial A}{\partial I_2}\right)\right]\left[\lambda - \left(\frac{1}{\lambda^2}\right)\right] \qquad \text{(A-5)} \end{aligned}$$

From eqs. (27), (29), and (A-3), it may be seen that A is a strong function of I_1, but is independent of I_2. It may be shown that:

$$\partial A/\partial I_1 = N_p kT(\overline{r_i^2}/\overline{r_0^2})[1/2 + (M - 1)(3\Delta b/Mb)^2 I_1 f(1 - f)] \tag{A-6}$$

$$\partial A/\partial I_2 = 0 \tag{A-7}$$

This result is, of course, the same as that given by eq. (29).

APPENDIX II

Consider a chain with its end points at O and P, and possessing a crystalline portion at its center. The coordinate system is arbitrarily chosen such that OP is in the x axis. We denote the angular coordinates of the crystalline part of the length nb as θ and ϕ with respect to the polar axis x. The amorphous part of this chain has $(M - n)/2$ segments. If the crystallization occurs at random, the probability that the crystalline part will have a direction θ, ϕ is given by

$$P_r(\theta,\phi) = \left(\frac{3}{2\pi\overline{r_0^2}}\frac{2M}{(M-n)}\right)^{3/2} \exp\left\{-\left(\frac{3}{2\overline{r_0^2}}\frac{2M}{(M-n)}\right) \times \frac{1}{4}\left[(x - nb\cos\theta)^2 + (nb\sin\theta\cos\phi)^2 + (nb\sin\theta\sin\phi)^2\right]\right\} \quad \text{(A-8)}$$

The average value of $\cos\theta$ is

$$\langle\cos\theta\rangle = \frac{\iint \cos\theta P_r(\theta,\phi)\sin\theta\, d\theta\, d\phi}{\iint P_r(\theta,\phi)\sin\theta\, d\theta\, d\phi} = \mathcal{L}\left\{(3/2r_0^2)[Mn/(M-n)]bx\right\} \quad \text{(A-9)}$$

Here $\mathcal{L}(x)$ is the Langevin function

$$\mathcal{L}(x) = \coth(x) - 1/x \quad \text{(A-10)}$$

Now, we have

$$\overline{r_0^2} \simeq Mb^2$$
$$x \simeq \sqrt{M}b$$
$$n \simeq M$$
$$\frac{3}{2\overline{r_0^2}}\left(\frac{Mn}{M-n}\right)bx \simeq \frac{n\sqrt{M}}{M-n} > 1 \quad \text{(A-11)}$$

Therefore

$$\langle\cos\rangle\,\theta \simeq 1 \quad \text{(A-12)}$$

This means that each chain crystallizes essentially in the direction of its end-to-end vector.

References

1. J. R. Katz, *Naturwiss.*, **13**, 410 (1925); *Kolloid-Z.*, **36**, 300 (1925).
2. E. Guth and H. Mark, *Monatsh.*, **65**, 93 (1934).
3. E. Guth, H. M. James, and H. Mark, in *Advances in Colloid Science*, Vol. 2, Interscience, New York, 1946.
4. P. J. Flory, *Principles of Polymer Chemistry*, Cornell Univ. Press, Ithaca, N. Y., 1953, Chaps. 10–12.
5. L. R. G. Treloar, *Physics of Rubber Elasticity*, 2nd ed., Oxford Univ. Press, 1958.

6. M. Volkenstein, *Configurational Statistics of Polymeric Chains*, Interscience, New York, 1963.
7. A. Ciferri, *J. Polym. Sci.*, **54**, 149 (1961).
8. K. W. Scott and A. V. Tobolsky, *J. Colloid Sci.*, **8**, 465 (1953).
9. Y. Abe and P. J. Flory, *J. Chem. Phys.*, **52**, 2814 (1970).
10. P. Geil, *Polymer Single Crystals*, Interscience, New York, 1961, Chap. 1.
11. J. L. White, and M. Yamamoto, *J. Phys. Soc. Japan*, **28**, 891 (1970).
12. T. Alfrey and H. Mark, *J. Phys. Chem.*, **46**, 112 (1942).
13. W. R. Krigbaum and R. J. Roe, *J. Polym. Sci. A*, **2**, 4391 (1964).
14. W. R. Krigbaum and I. Uematsu, *J. Polym. Sci. A*, **3**, 2915 (1965).
15. R. J. Roe, K. J. Smith, and W. R. Krigbaum, *J. Chem. Phys.*, **35**, 1306 (1961).
16. L. Mandelkern, *Crystallization of Polymers*, McGraw-Hill, New York, 1964, Chap. 6.
17. P. J. Flory, *J. Chem. Phys.*, **15**, 397 (1947).
18. K. J. Smith, A. Greene, and A. Ciferri, *Kolloid Z. Z. Polym.*, **194**, 49 (1964).
19. T. L. Hill, *Introduction to Statistical Thermodynamics*, Addison-Wesley, Boston, 1960.
20. K. H. Meyer, *Z. Physik. Chem.*, **B44**, 383 (1939).
21. P. J. Flory, *J. Chem. Phys.*, **10**, 51 (1942).
22. P. J. Flory, *J. Chem. Phys.*, **12**, 425 (1944).
23. M. L. Huggins, *J. Amer. Chem. Soc.*, **46**, 151 (1942).
24. P. J. Flory, *Proc. Roy. Soc.* (London), **A234**, 60 (1956).
25. P. J. Flory, *J. Polym. Sci.*, **49**, 105 (1961).
26. E. A. DiMarzio and J. H. Gibbs, *J. Chem. Phys.*, **28**, 807 (1958).
27. E. A. DiMarzio, *J. Chem. Phys.*, **35**, 658 (1961); *ibid.*, **36**, 1563 (1962).
28. A. C. Eringen, *Non-linear Theory of Continuous Media*, McGraw-Hill, New York, 1962.
29. A. N. Gent, *J. Polym. Sci. A*, 3787 (1965).

Received April 24, 1970
Revised January 29, 1971

JOURNAL OF POLYMER SCIENCE: PART A-2 VOL. 9, 1417–1447 (1971)

Stress-Optical Coefficient of Poly-1,4-butadienes

M. FUKUDA,* G. L. WILKES,† and R. S. STEIN,‡
Polymer Research Institute and Department of Chemistry, University of Massachusetts, Amherst, Massachusetts 01002

Synopsis

The stress-optical coefficient of poly-1,4-butadiene is measured as a function of strain, *cis/trans* ratio, and degree of swelling. Deviations from the Kuhn-Grün theory are found which are reduced upon swelling. Results are interpreted in terms of the Shindo-Stein theory of birefringence of polymers containing statistical segments of different sizes. This interpretation for the unswollen polymer leads to the unreasonable conclusion that the *cis* segment is considerably longer than the *trans*. Reinterpretation for the swollen polymer leads to the more reasonable conclusion that the *trans* segment is slightly longer than the *cis*. The dependence of the stress-optical coefficient on the nature of the swelling solvent is similar to the observations of Gent and Nagai and is believed to result from the effect of internal field from anisotropic solvent molecules. It is felt that the value of the stress-optical coefficient for the dry rubber is modified by the internal field from somewhat locally ordered neighboring polymer molecules.

INTRODUCTION

The stress-optical coefficient (SOC) of a rubber network may be described in terms of the statistical segment model of Kuhn and Grün[1] and Treloar[2,3] as

$$C = \frac{\Delta n}{\sigma} = \frac{2\pi}{45kT} \frac{(\bar{n}^2 + 2)^2}{\bar{n}} \Delta\Gamma \tag{1}$$

where Δn is the birefringence of the uniaxially stretched rubber subjected to a stress σ (on unit area in the stretched state), k is Boltzmann's constant, T the absolute temperature, and $\bar{n}$ is the average refractive index of the rubber. The anisotropy of the statistical segment $\Delta\Gamma$ is given by

$$\Delta\Gamma = (b_1 - b_2)_s \tag{2}$$

where b_1 and b_2 are the polarizabilities parallel and perpendicular respectively, to the axes of the segment.

* Present address: Central Research Laboratory, Denki Kagaku Kogyo Company, Limited, Tokyo, Japan.

† Present address: Department of Chemical Engineering, Princeton University, Princeton, New Jersey 08540.

‡ To whom correspondence should be sent.

Equation (1) is derived upon the assumption of tensor additivity of polarizabilities. That is, the difference of polarizabilities parallel and perpendicular to the stretching direction is given by

$$P_1 - P_2 = N_s \Delta\Gamma f_s \tag{3}$$

where N_s is the number of segments per cubic centimeter and f_s is the orientation function of the segments defined by

$$f_s = (3\langle\cos^2\theta_s\rangle_{\mathrm{av}} - 1)/2 \tag{4}$$

where θ_s is the angle between the segment axis and the stretching direction. This function is calculated by the techniques of the kinetic theory of rubber elasticity.

It is presumed that the induced dipole moments of the segments are independently additive and do not influence each other. We shall present some evidence that this assumption may not be fulfilled.

More recently, a more satisfying formulation of the theory of the SOC of rubbers has been carried out by Flory et al.[4,5] and by Nagai[6] in which (in terms of Nagai's formulation) $\Delta\Gamma$ is given in terms of the principal polarizabi ities of bonds by

$$\Delta\Gamma = {}^1/_2\langle r^2\rangle^{*-1} \sum_{i,k} (\alpha_1 - \alpha_2)_k (3\langle r^2 \cos^2 \Phi_{ik}\rangle - \langle r^2\rangle) \tag{5}$$

where $\langle r^2\rangle$ is the mean-square end-to-end length of the unconstrained polymer chain, $\langle r^2\rangle^*$ is the part of $\langle r^2\rangle$ which is proportional to chain length, $(\alpha_1 - \alpha_2)_k$ is the difference between the principal polarizabilities of the kth bond and $\Phi_{i,k}$ is the angle between the end-to-end chain displacement vector and the unit vector along the kth bond of the ith structural unit. The average values of these functions of angles may be calculated in terms of the rotational isomer model. This calculation again involves the assumption of independence of induced dipole moments of the bonds.

Shindo and Stein[7] have generalized the Kuhn-Grün formulation to the case of chains having more than one type of statistical segment and have shown that eq. (1) is applicable, provided $\Delta\Gamma$ is replaced by its average value $\overline{\Delta\Gamma}$ defined by

$$\overline{\Delta\Gamma} = \sum_i N_{si}(\Delta\Gamma_i) L_i^2 / \sum_i N_{si} L_i^2 \tag{6}$$

where N_{si} is the number of segments of type i per chain, $(\Delta\Gamma_i)$ is the anisotropy and L_i is the length of such a segment. While a general formulation in terms of molecular quantities of this case of more complex structures has been proposed by Nagai,[8] specific solutions applicable to the experimental data in this paper are not yet available so that our analysis will be in terms of the statistical segment approximation.

An application of eq. (6) has been made to the analysis of the birefringence and dichroism of partially dehydrohalogenated poly(vinyl chloride) containing polyene segments as well as poly(vinyl chloride) segments.[9] In this paper we shall attempt to apply the analysis to a more straightforward

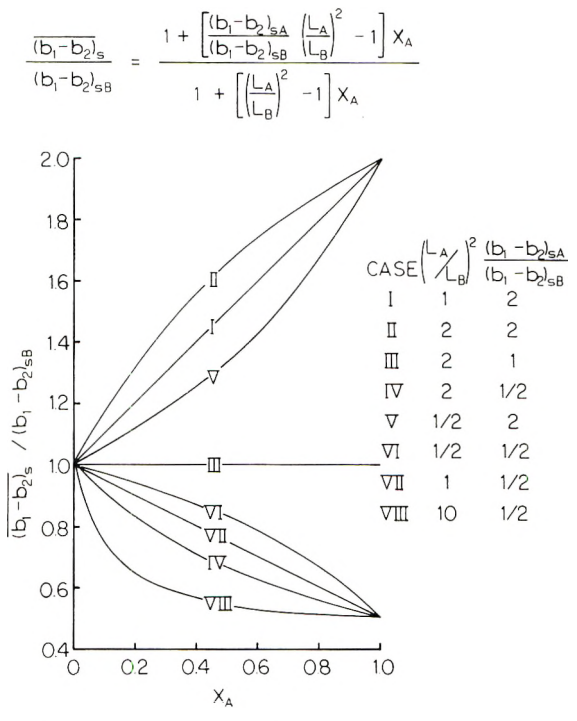

Fig. 1. Theoretically calculated variation of statistical segment anisotropy with copolymer composition for different ratios of monomer segment anisotropies and of monomer statistical segment lengths.

case, that of poly-1,4-butadiene containing monomer units having both *cis* and *trans* configurations. We shall show that such a copolymer must be represented by a chain possessing more than one type of segment.

If we consider the chain to be composed of two types of segments, A and B, of lengths L_A and L_B, where X_A is the fraction of segments of type A, a plot of the ratio of the segment anisotropy of the copolymer to that of component B is given by[7]

$$\frac{\overline{\Delta\Gamma}}{\Delta\Gamma_B} = \frac{\overline{(b_1 - b_2)_s}}{(b_1 - b_2)_{sB}} = \frac{1 + \left[\frac{(b_1 - b_2)_{sA}}{(b_1 - b_2)_{sB}}\left(\frac{L_A}{L_B}\right)^2 - 1\right]X_A}{1 + \left[\left(\frac{L_A}{L_B}\right)^2 - 1\right]X_A} \tag{7}$$

It is seen from this equation and its plot in Figure 1 that unless $L_A = L_B$, $\overline{\Delta\Gamma}$ will vary in a nonlinear manner with composition. We shall try to test this prediction by determination of the SOC of poly-1,4-butadiene as a function of *cis/trans* ratio.

EXPERIMENTAL

Sample Preparation

High *cis*-1,4 (93%) and high *trans*-1,4 (91%) polybutadiene samples were obtained from Phillips Petroleum Company (Bartlesville, Oklahoma). These polymers are referred to by Phillips as Cis-4 and Trans-4. Copolymer samples of different *cis*/*trans* ratios were prepared from the high-*cis* polymer by the photoisomerization technique of Golub,[10] as described by Berger and Buckley.[11]

The starting polymer, which is purified by precipitation from benzene solution by methanol, is dissolved in benzene to give a concentration of 5 g/100 ml. Phenyl disulfide sensitizer at a concentration of 55% by weight of the polymer is added. The solution is irradiated with ultraviolet light for 30 min to 10 hr at room temperature after which an antioxidant, 2,2′-methyl bis(4-methyl-6 *tert*-butyl)phenol, is added to a concentration of 2% of the polymer. The polymer is repurified by repeated precipitation from benzene solution with methanol after which 1% more antioxidant is added and the polymer is dried in a vacuum oven at 30°C for 24 hr. The composition of isomeric components was determined from infrared spectra using the extinction coefficients reported by Hampton[12] listed in Table I. All analyses were obtained on films of thickness about 8 μ cast from benzene solution on rock salt plates.

TABLE I
Extinction Coefficients of Polybutadiene Isomers

Isomer	Frequency, cm^{-1}	Extinction coefficient
cis-1,4	724	0.608
trans-1,4	967	2.608
Vinyl	911	3.285

TABLE II
Properties of Polybutadiene Samples

Sample	*cis*/*trans*/vinyl	SOC (100°C) $\times 10^6$, cm^2/g	$\Delta\Gamma$ $\times 10^{25}$, cm^2	Dicup, phr
cis	93/5/2	2.33 2.28	70.8 69.2	0.20
trans	5/91/4	3.38	102	0.50
01	23/73/4	2.92	88.7	0.20
04	85/12/3	2.28	69.2	0.20
05	70/27/3	2.55 2.62	77.3 79.3	0.20
06	62/35/4	2.28	69.2	0.20
35	35/58/7	2.71	82.2	0.20
Blend 1	70/30/0	2.68	81.0	0.20
Blend 2	25/75/0	3.38	102	0.30

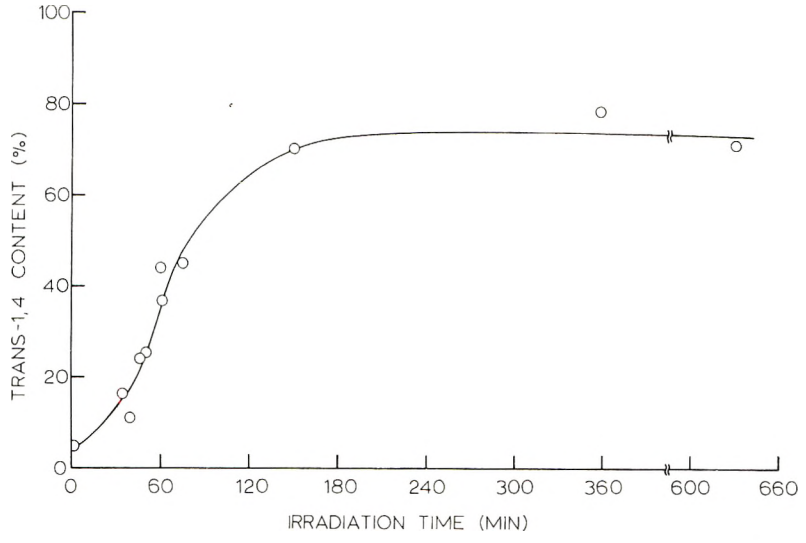

Fig. 2. Variation of *trans* isomer content with time during the isomerization of the high-*cis* 1,4 polybutadiene.

The *trans*-1,4 content was found to increase with time and approach an equilibrium value of about 67% after about 6 hr as shown in Figure 2. Properties of the polymer samples used are summarized in Table II.

A curing agent, 5 g/100 ml dicumyl peroxide (Dicup), was added to the rubber in solution in benzene and then films 10 to 25 mils thick were cast on a Teflon-coated pan. These were crosslinked at 140°C at 3000 psi for 60 min in a small laboratory press holding the films between sheets of cellophane.

Samples for measurement were cut from these cured films of 15 mm × 40 mm and were examined for local strain by using a Babinet compensator.

Birefringence Measurements

Birefringence measurements were carried out by using the optical system shown in Figure 3 with a Babinet compensator. The samples were held in an air thermostat through which a flow of oxygen-free nitrogen gas was maintained to retard oxidation at higher temperatures. Measurements were made with monochromatic light from a mercury lamp at a wavelength of 5461 Å.

Samples were stretched by a weight hanging from the lower end. Weights up to 250 g were used, which gave elongation ratios up to $\lambda = 1.4$. For measurements of the temperature variation of birefringence, the cell was heated at a rate of 1°C/3 min while keeping the sample under load. The sample length was simultaneously measured by using a cathetometer external to the chamber to determine the distance between clamps. The elongation ratio was defined as $\lambda = l/l_0$, where l is the actual length of the sample and l_0 the length in the absence of load. The dimensions of the sample in the

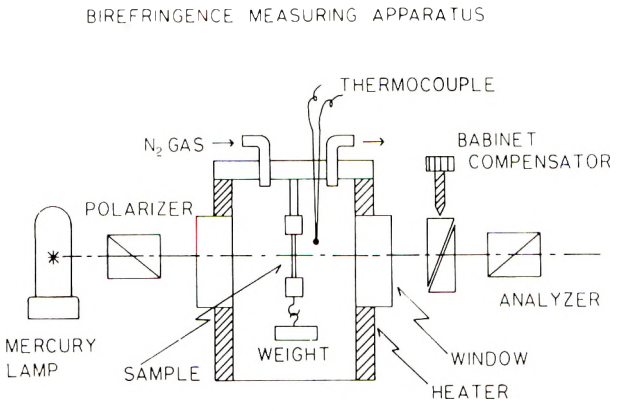

Fig. 3. Schematic diagram of the optical system for birefringence measurements.

stretched state were calculated by assuming uniaxial extension at constant volume so that, for example, the thickness t in the stretched state is related to that t_0 in the unstretched state by $t = t_0\lambda^{-1/2}$. Stress and birefringence in the stretched state were calculated on the bases of the attained cross-sectional area and thickness in this state. A plot of the birefringence against stress was linear for the range of stresses encountered (up to 4 kg/cm^2), and the SOC was determined from the slope of such a plot. Values of $\Delta\Gamma$ were then calculated by using eq. (1).

RESULTS

Values of the SOC multiplied by temperature are plotted against temperature in Figure 4 along with data on swollen samples to be discussed later.

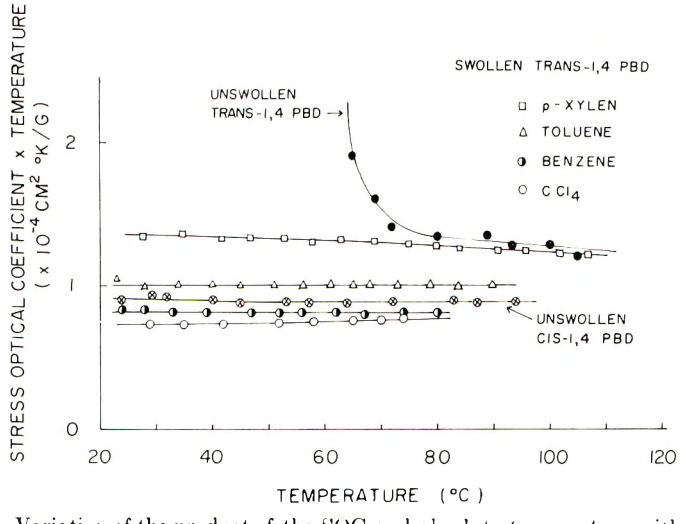

Fig. 4. Variation of the product of the SOC and absolute temperature with temperature during the heating of unswollen high-*cis* and high-*trans* 1,4 polybutadiene. Data on samples of the *trans* polymer swollen with different solvents is also included.

The constancy of this quantity for the high-*cis* isomer indicates that $\Delta\Gamma$ is essentially independent of temperature. If a weight is hung from the high-*trans* sample at room temperature, the sample does not deform very much because of its high crystallinity; consequently, the birefringence is low. If this sample is not heated, the birefringence increases rapidly at about 60°C as the sample softens and elongates. With further heating, the crystals begin to melt and the SOC decreases rapidly with increasing temperature and achieves a constant value at temperatures above about 90°C. This decrease is a consequence of the melting and loss of orientation of crystals of the *trans*-1,4-polybutadiene and occurs at a temperature about 20°C lower than the melting point as determined by differential scanning calorimetry (DSC). The melting point is quite dependent upon the degree of crosslinking and occurs at about 64°C (measured at a heating rate of 10°C/min) for the degree of crosslinking characteristic of the sample in Figure 4 as compared with a measured value of 100°C for the high-*trans* uncrosslinked sample and 141–148°C reported in the literature[13] for the pure *trans* isomer.

The degree of crosslinking of a series of samples was varied by changing the amount of dicumyl peroxide (Dicup) added prior to curing, as shown in Table III. The molecular weight between crosslinks M_c was determined from the coefficient C_1 in the Mooney-Rivlin plot of the stress–strain data, as discussed later, by using $M_c = \rho RT/2C_1$, where ρ is the density of the rubber.

As expected, M_c decreases with increasing concentration of Dicup. Correspondingly, the volume fraction of rubber in the equilibrium swollen rubber with benzene at 25°C increases. It is noted that M_c is considerably greater for the *trans* isomer at the same concentration of Dicup, indicating a lower efficiency of the crosslinking reaction for this isomer.

In Figure 5, the melting point T_m for the higher-*trans* isomer as determined by DSC is plotted against the volume fraction of rubber v_2 in a network swollen to equilibrium in benzene. The quantity v_2 is a measure of the degree of crosslinking which increases with decreasing M_c. The temperature T_b at which birefringence rapidly decreases is also plotted. Both

TABLE III
Properties of Rubbers Crosslinked to Different Degrees

Rubber	Dicup, phr	M_c	v_2	SOC (100°C) × 10^7, cm²/g	T_m, °C (DSC)	T_b, °C
High-*cis*	0.18	16900	0.150	2.36	—	—
	0.50	10480	0.206	2.31	—	—
	2.00	3690	0.292	2.25	—	—
	5.00	975	0.413	1.77	—	—
High-*trans*	0.50	30400	0.097	3.35	87	42
	2.00	4050	0.219	3.22	67	47.5
	5.00	2401	0.339	2.63	Unobservable	

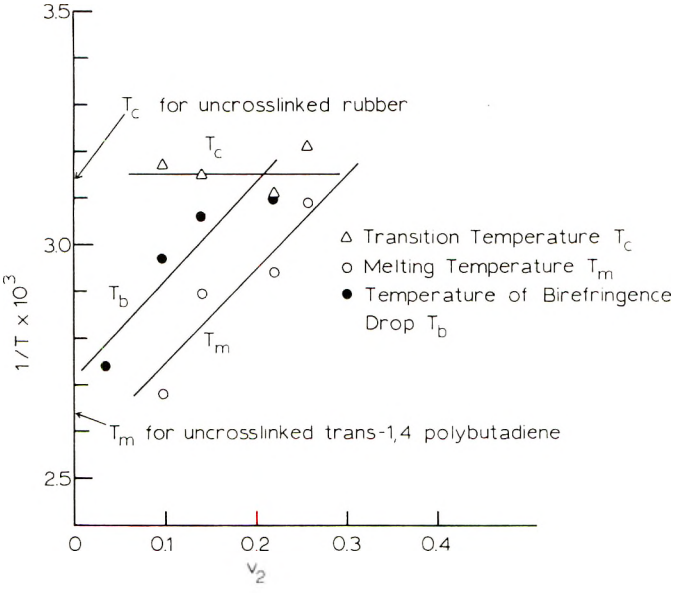

Fig. 5. Variation of the melting point T_m determined by DSC and the temperature T_b of decrease in birefringence with equilibrium fraction of rubber, v_2 in the benzene swollen polymer for the high-*trans* polybutadiene. The temperature of the crystal phase transition is also plotted against v_2.

temperatures are seen to decrease with increasing crosslinking. In consideration of this variation, all measurements of the SOC for various *cis*/*trans* ratios have been made at 100°C (unless otherwise indicated), at which temperature crystallinity should not affect measurements. Melting points for the samples with lower *trans* content should, of course, be lower than that for the high-*trans* sample.

The observation that $T_b < T_m$ may be understood if one assumes that the first material that melts is quite highly oriented and also that its melting allows the orientation of the remaining crystalline and amorphous material to decrease. The melting point determined by DSC is that of the highest melting crystals. By the time these melt, there is little effect on the SOC.

The temperature T_c of a lower-temperature DSC maximum which has been attributed to a crystal-phase transition[14] is also plotted here as a function of v_2. It is noted that T_c is independent of v_2, confirming the assignment of this transition to the crystal phase. The temperature T_c is close to T_b so that the drop in birefringence at about 60°C may in part be related to the crystal-phase transition. However, the observations that T_b depends upon degree of crosslinking and T_c does not indicate that other factors must affect T_b.

It has been proposed[15] for *trans*-1,4-polyisoprene that the corresponding transition involves a melting of the low-temperature form followed by a recrystallization in the high temperature form. There is a disappearance of

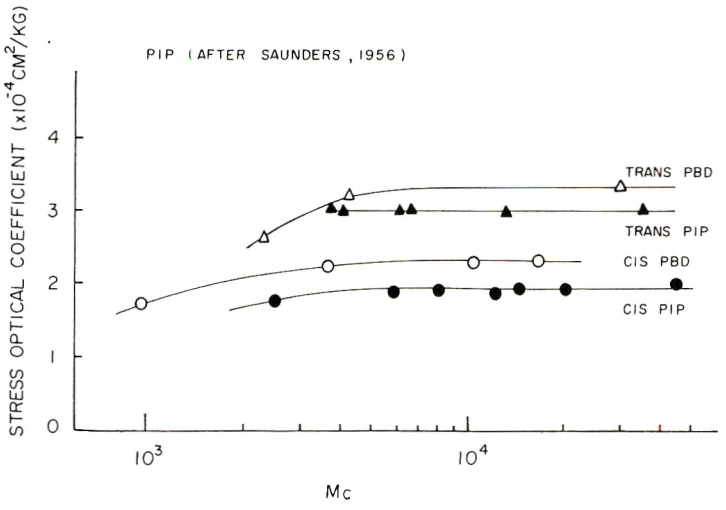

Fig. 6. Variation of the SOC with M_c for the high-*cis* and high-*trans* 1,4-polybutadiene measured at 100°C as compared with values for *cis* and *trans* 1,4-polyisoprene as reported by Saunders.[16]

spherulite birefringence at the transition temperature. If a similar process occurs with *trans*-1,4-polybutadiene, the loss of birefringence at T_c is understandable.

The variation of the SOC of the high-*cis* and high-*trans* 1,4-polybutadiene is plotted against M_c in Figure 6, where it is compared with values

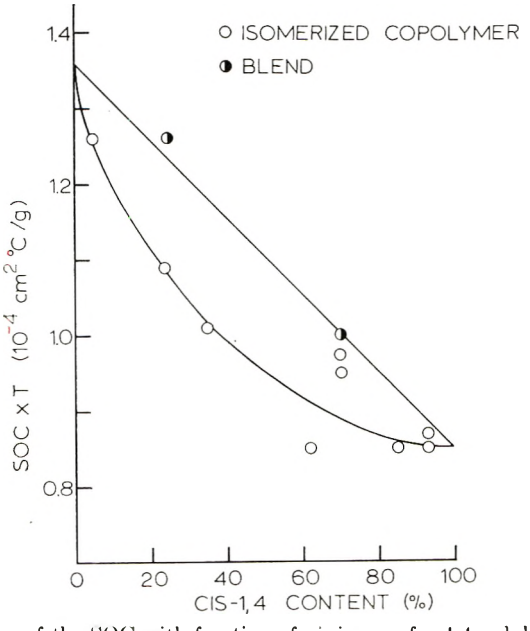

Fig. 7. Variation of the SOC with fraction of *cis* isomer for 1,4-polybutadiene samples. Data for a crosslinked blend of *cis* and *trans* polymer is also given.

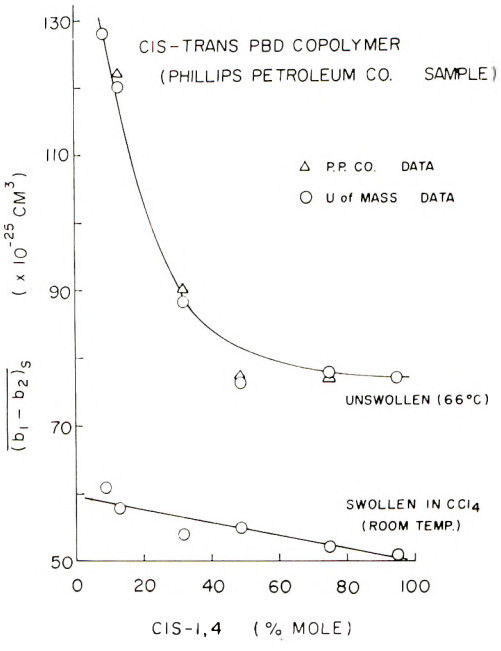

Fig. 8. Variation of the anisotropy of the statistical segment with mole percent *cis* isomer for the Phillips 1,4-polybutadiene. Measurements at 66°C by Phillips and ourselves are indicated. Values obtained on CCl_4 swollen samples at room temperature are also given.

reported by Saunders[16] for *cis*- and *trans*-1,4 polyisoprene. It is noted that the SOC is independent of M_c above values of M_c of about 5000. At lower values of M_c, network chains are sufficiently short that non-Gaussian contributions must be considered. A similar effect has been observed by Saunders for polyethylene.[16]

A plot of the variation of the SOC of the polybutadienes as a function of their *cis* content is given in Figure 7, where it is seen that this variation is nonlinear. Data is included in the plot for two blended samples, described in Table II, which were prepared by mixing the designated amounts of high-*cis* and high-*trans* isomer in solution along with Dicup, preparing a film of the blend, and curing it. It is noted that the SOC values for the blend varies linearly with composition, as predicted by the Shindo-Stein theory.[7]

For comparison, a series of 1,4-polybutadienes of varying *cis*/*trans* ratio were provided by Dr. G. Kraus of the Phillips Petroleum Co. (Bartlesville, Okla.) which were prepared by a polymerization technique and are described in Table IV. Values of the $\Delta\Gamma$ calculated from the SOC measured at 66°C by Kraus and by us are plotted in Figure 8 as a function of *cis* content. It is noted that Kraus's values and ours are in good agreement and that both show the same sort of nonlinear variation as do the isomerized samples in Figure 7. However in these measurements on the Phillips' samples at 66°C the values for the two high-*trans* samples (48581 and

TABLE IV
Properties of Phillips Butadiene Samples

Sample No.	(*Cis*/*trans*/vinyl	SOC × 10^7, cm^2/g	$\Delta\Gamma$ × 10^{25}, cm^3	Dicup, phr
48576	95/3/2	2.80	76.9	0.2
48579	75/20/5	2.83	77.7	0.2
48580	32/65/3	3.25	88.2	0.4
48581	13/85/2	4.38	120	0.6
48582	9/89/2	4.65	128	0.7
48583	49/42/9	2.77	76	0.3

48582) are higher than those for our isomerized samples at 100°C. From considerations of the effect of composition and degree of crosslinking on crystal melting points, we believe crystallinity persists in these two samples at 66°C.

A comparison of Figures 7 or 8 with Figure 1 indicates that the segment length of the *cis* isomer is longer than that of the *trans*. In fact, a comparison of the data with eq. (7) indicates that the best fit is achieved for $L_{cis}/L_{trans} = 2.0$. This conclusion is somewhat surprising in that there is much evidence which indicates $L_{trans} > L_{cis}$. For example, this is indicated by theoretical calculations based on the free rotation model by Wall[17] and on the rotational isomer model by Mark[18] and more recently by Ishikawa and

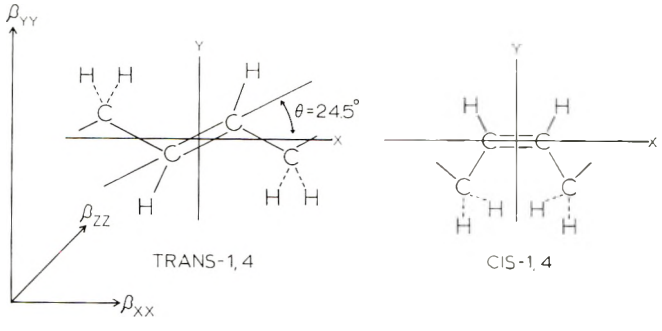

Fig. 9. Conformations and principal polarizability axes for the monomer units of *cis*- and *trans*-1,4 polybutadiene.

Nagai.[19,20] Similar conclusions are arrived at by Wagner and Flory[21] on the basis of intrinsic viscosity measurements on polyisoprene having similar structure. Saunders[22] concludes that the segment of *trans*-polyisoprene is longer than that of *cis* isomer by comparing $\Delta\Gamma$ values calculated from the SOC values with the anisotropies of the monomer units. Conclusions similar to those of Saunders are obtained on the basis of $\Delta\Gamma$ values calculated from streaming birefringence by Poddubnyi et al.[23] By using the same statistical weighting factora as used for the calculation of the dimensions of polybutadiene, Ishikawa and Nagai,[19,20] are able to reproduce the measured values of $\Delta\Gamma$.

TABLE V
Anisotropies of the Monomer Units of *Cis*- and *Trans*-1,4 Polybutadienes

	Trans	*Cis*
b_{xx}, cm³	98.6×10^{-25}	96.0×10^{-25}
b_{yy}, cm³	73.1×10^{-25}	77.5×10^{-25}
b_{zz}, cm³	51.5×10^{-25}	51.1×10^{-25}
$(b_1 - b_2)_m$, cm³	36.3×10^{-25}	31.7×10^{-25}
$\Delta\Gamma$, cm³	108.0×10^{-25}	70.0×10^{-25}
q	3.0	2.2

It is of interest to extend the calculations of Saunders[3,22] for polyisoprene to polybutadiene. The principal polarizabilities of the monomers of *cis*- and *trans*-1,4-polybutadiene are calculated relative to the conformations of these molecules shown in Figure 9 by using the equation

$$b_k = \sum_i [(b_{1i} - b_{2i}) \cos^2 \theta_{ik} + b_{2i}] \tag{8}$$

where b_{1i} and b_{2i} are the longitudinal and transverse polarizabilities of the ith bond and θ_{ik} is the angle between the axis of this bond and the kth principal polarizability axis. The sum is over all bonds of the monomer unit. The bond polarizabilities proposed by Denbigh were used.[24] The anisotropy of the monomer unit is then defined as

$$(b_1 - b_2)_m = b_{xx} - [(b_{yy} + b_{zz})/2] \tag{9}$$

and the ratio q, called the number of monomer units per statistical segment, is defined as

$$q = \Delta\Gamma/(b_1 - b_2)_m \tag{10}$$

The results of this calculation are given in Table V.

The calculated lengths of monomer units in the conformations shown in Figure 9 are 4.57 and 5.57 Å for the *cis* and *trans* isomers, respectively, so that multiplying these by the respective values of q gives 10.1 and 16.7 Å for the lengths of the *cis* and *trans* segments, respectively. Thus it is seen that $L_{cis}/L_{trans} = 0.61$, in contrast to the value of 2.0 found by fitting to the Stein-Shindo theory.

It is evident that there is an inconsistency. A clue to the difficulty comes from the recent results of Gent[25] and Ishikawa and Nagai[19,20] who believe that values of $\Delta\Gamma$ measured in the bulk polymer are not representative of the isolated polymer molecule as required by the Kuhn-Grün theory, but are modified through interaction with neighboring molecules. Some evidence for such interaction comes from the observation of deviations from the kinetic theory of rubber elasticity.

Mooney-Rivlin Equation Considerations

For uniaxial elongation, it has been proposed by Mooney and Rivlin[26,27] that the stress σ_0 based upon the unstretched cross-sectional area may be represented by the equation

$$\sigma_0/(\lambda - \lambda^{-2}) = 2C_1 + 2C_2\lambda^{-1} \tag{11}$$

The constant C_2 represents deviations from kinetic elasticity theory. It is independent of the degree of crosslinking but is time-dependent, representing, in part, nonequilibrium behavior. The constant C_1 is dependent upon the degree of crosslinking.

A Mooney-Rivlin (MR) plot for the *cis*-1,4-polybutadiene at 33°C crosslinked with various concentrations of Dicup is given in Figure 10. The data were determined by using an Instron tensile tester with a crosshead speed of 2 in./min on a 1-in. sample. The dependence of the intercept on degree of crosslinking but independence of the slope is evident.

It has been observed that C_2 is substantially reduced by swelling and often approaches zero for volume fractions of rubber less than about 0.2.[28] It was proposed that in the swollen state, the NR equation should be modified as

$$\sigma_{0u} v_2^{1/3}/(\lambda - \lambda^{-2}) = 2C_1 + 2C_2\lambda^{-1} \tag{12}$$

to account for the effect of the diluent upon the modulus. The stress σ_{0u} in this equation is the stress based on the unswollen unstretched area. When plotted in this way, it was found that C_1 is essentially independent of v_2 and depends upon crosslink density and that C_2 decreases linearly with decreasing v_2 but is independent of the nature of the swelling agent. This suggests that C_1 represents the modulus resulting from constraints upon the polymer chains due to the chemical crosslinks but that C_2 represents deviations arising from entanglements (and other interactions between chains) which are reduced upon swelling.

It has been pointed out[29] that part of this reduction in C_2 is a geometric effect, in that $C_{2s} = C_{2d} v_2^{4/3}$, where C_{2s} and C_{2d} are values of C_2 in the swollen and dry states, respectively. The quantity C_{2d} is the measure of nonideality. We feel that the observed reduction of C_{2d} upon swelling is sufficiently great to indicate a decrease in departure from ideality.

It has recently been reported[30] that if a rubber is crosslinked while swollen and then dried, C_2 is substantially reduced. Also stress-temperature studies indicate that deviations from kinetic elasticity theory arising from internal energy contributions to stress principally affect the C_1 term.

It might be noted that additional deviations from the MR equation are observed at elongations greater than those shown in Figure 10. They presumably arise from deviations from the Gaussian distribution of distances between chain ends as a consequence of the finite extensibility of such chains.

Gent and Vickroy[31] point out that there is an appreciable dependence of the SOC of amorphous crosslinked polyethylene upon swelling. Gent[25] and Ishikawa and Nagai[19,20] independently report appreciable swelling effects on the SOC of 1,4-polyisoprenes and 1,4-polybutadienes. The latter authors propose that an equation analogous to the MR equation applies to birefringence. This is

$$(\Delta n) v_2^{-1/3}/(\lambda^2 - \lambda^{-1}) = B_1 + B_2\lambda^{-1} \tag{13}$$

where the constant B_2 is dependent upon deviations from the Kuhn–Grün birefringence theory. As with stress, they find that a plot, in accordance

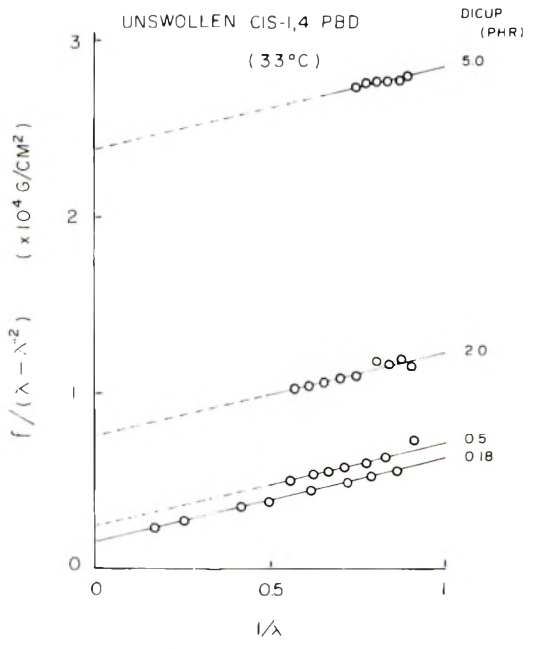

Fig. 10. Mooney-Rivlin plots for *cis*-1,4-polybutadiene at 33°C crosslinked with several different concentrations of Dicup.

with this equation is linear with a value of B_2 which is reduced by swelling. In contradiction to the stress equation, however, B_1 does depend upon the kind of solvent.

It is evident that the SOC will be affected by swelling and that values measured in the unswollen state are not accounted for by the kinetic theory. This suggests that the contradictions reported in the first part of this paper may be related to these deviations from this theory for isolated chains. Consequently we undertook a study of the effect of swelling upon the stress and birefringence of the series of polybutadienes of varying *cis*/*trans* ratio.

Techniques for Swelling Studies

Samples were prepared as in the first part of this study. They were then swollen with carbon tetrachloride, cyclohexane, benzene, toluene, and *p*-xylene to equilibrium. The air thermostat for birefringence measurements was replaced by a liquid bath composed of the swelling solvent and containing a heater, thermoregulator and stirrer. Since the weights hanging from the sample were immersed in the liquid, it was necessary to correct for buoyancy. Unless otherwise reported, all values of SOC were determined at room temperature (21–28°C). This was possible since the melting point of the crystals of the *trans*-1,4-polybutadiene were sufficiently reduced by swelling so that there was no crystalline contribution to birefringence for the samples studied at room temperature.

The volume fraction v_2, of rubber in the swollen polymer was measured by quickly removing the sample from the swelling bath, wiping off the surface, and weighing. While it has been reported[32] that v_2 varies with λ, our measurements indicated little effect over the range of elongations studied.

To calculate the birefringence in the swollen state from the retardation R of light, it was necessary to use the thickness of the sample t_s in the stretched swollen state according to

$$\Delta n = R\lambda_0/t_s \tag{14}$$

where λ_0 is defined as the ratio of the length of the swollen stretched polymer to that of the swollen unstretched polymer. The stress σ is calculated as the force per unit area of the swollen stretched sample.

The SOC for the swollen stretched sample is $C = \Delta n/\sigma$ and is still related to $\Delta\Gamma$ by eq. (1), since v_2 cancels upon dividing the birefringence of the swollen rubber by the stress.[30] The SOC is obtained from the slope of the plot of Δn against σ.

In order to calculate $\Delta\Gamma$ from the SOC, the value of $\bar{n}$ must be adjusted for the change in the average refractive index of the rubber with swelling. The mixing equation

$$\bar{n} = n_1v_1 + n_2v_2 \tag{16}$$

was assumed, where n_1 and n_2 are the refractive indices of the pure solvent and the rubber, respectively, and v_1 and v_2 are their volume fractions in the swollen rubber. It was also assumed that the refractive indices of the rubvers varied linearly with the *cis* content. Values of the polymer and solvent refractive indexes are given in Table VI. Values of $\bar{n}$ and degree of swelling are included in Table VII.

TABLE VI
Refractive Indices and Anisotropies

	Refractive index (25°C)	$(b_1 - b_2)_0 \times 10^{24}$, cm^3
Cis-1,4-PB	1.520	—
Trans-1,4-PB	1.515	—
Carbon tetrachloride	1.459	0
Cyclohexane	1.424	1.0
Benzene	1.498	3.0
Toluene	1.494	4.4
p-Xylene	1.493	5.8

Swelling Studies

The MR plots for the high-*cis* and high-*trans* 1,4-polybutadienes in the unswollen and swollen states are given in Figures 11 and 12. The data for the unswollen *trans* polymer is taken at 100°C to avoid the effect of crystallinity. These 100°C data were determined with an Instron tester. Other

TABLE VII
Properties of Swollen Samples

Swelling agent	Sample *cis*/*trans*	Dicup phr	Temp, °C	$\bar{n}$	v_2	SOC × 10^7, cm^2/g	$\Delta\Gamma$ × 10^{25}, cm^3
Carbon tetrachloride	0/100	0.50	27	1.467	0.121	2.40	61.1
	22/72	0.20	25	1.465	0.0866	2.33	58.9
	68/27	0.40	21	1.464	0.0508	2.20	54.8
	51/45	0.20	21	1.466	0.082	2.28	56.8
	100/0	0.20	25	1.467	0.117	2.13	53.5
Cyclohexane	0/100	0.50	26	1.435	0.136	2.64	68.0
	51/45	0.20	23	1.436	0.135	2.46	62.7
	100/0	0.20	24	1.436	0.149	2.35	57.3
Benzene	0/100	0.50	24	1.500	0.132	2.88	70.4
	51/45	0.20	27	1.500	0.0955	2.60	64.0
	100/0	0.20	25	1.501	0.133	2.56	62.7
Toluene	0/100	0.50	26	1.498	0.138	3.30	81.6
	51/45	0.20	28	1.497	0.0917	2.90	72.2
	100/0	0.20	27	1.498	0.135	2.90	72.0
p-Xylene	0/100	0.50	28	1.496	0.124	4.82	101
	51/45	0.20	28	1.495	0.0894	3.64	91.0
	100/0	0.20	24	1.497	0.147	3.54	86.9

values are at room temperature. Values for v_2 for the swollen samples are included in Table VII.

It is noted that the slopes of the MR plots are negligible over the rather limited range of elongations that are possible with the swollen samples. There appears to be some variation of the intercepts with the various sol-

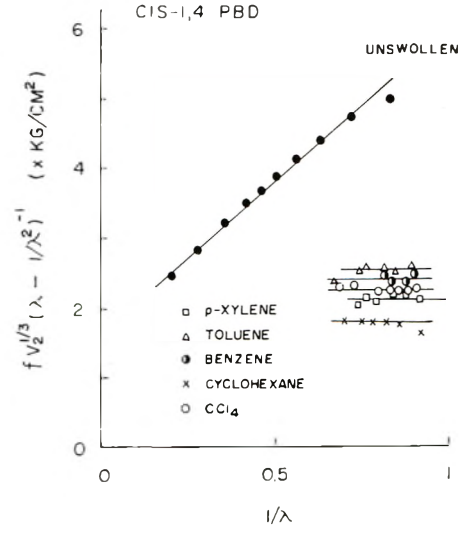

Fig. 11. Mooney-Rivlin plots for *cis*-1,4-polybutadiene in the unswollen and swollen states with various solvents.

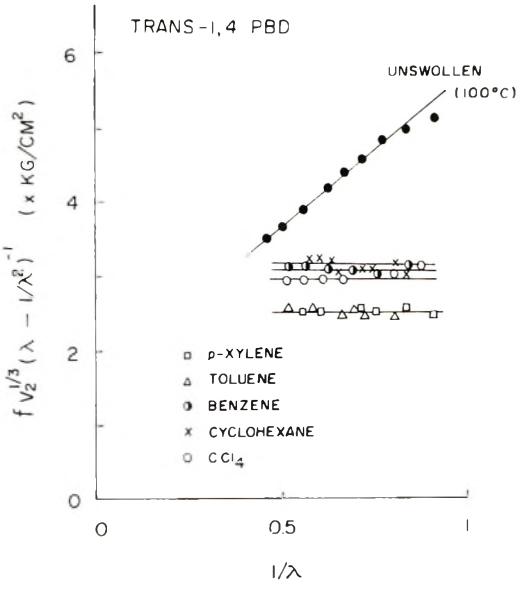

Fig. 12. Mooney-Rivlin plots for *trans*-1,4-polybutadiene in unswollen (100°C) and swollen (room temperature) states with various solvents.

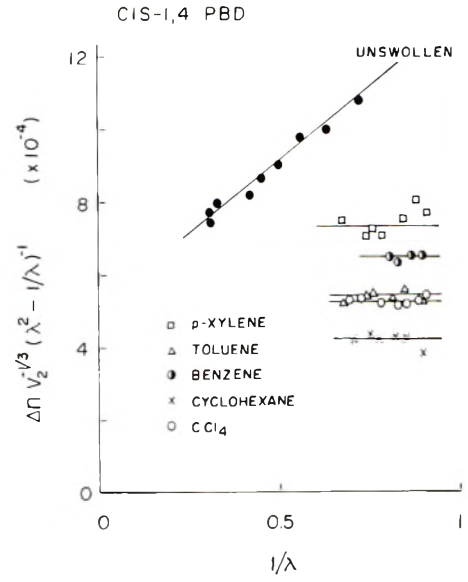

Fig. 13. Mooney-Rivlin type plots for birefringence of unswollen and swollen samples of *cis*-1,4-polybutadiene.

vents in contradiction to previous observations.[28] This may be an experimental error but might also be related to the dependence of the end-to-end chain length on the swelling solvent, as suggested by Tobolsky.[33]

The MR-type plots for the birefringence of the swollen rubbers are given in Figures 13 and 14. It is noted that as with the stress plots, the slopes of

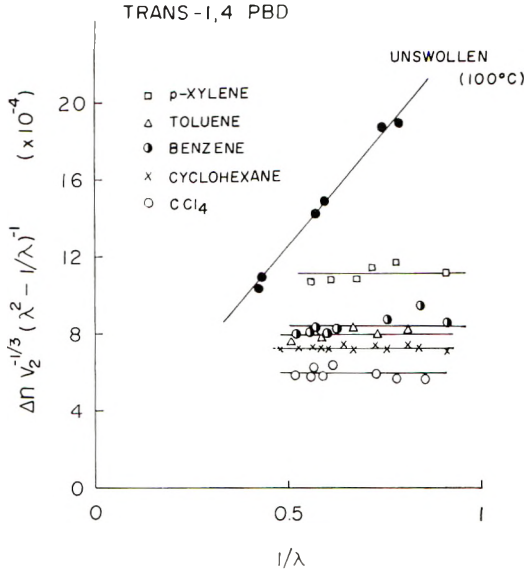

Fig. 14. Mooney-Rivlin type plots for birefringence of unswollen and swollen samples of *trans*-1,4-polybutadiene.

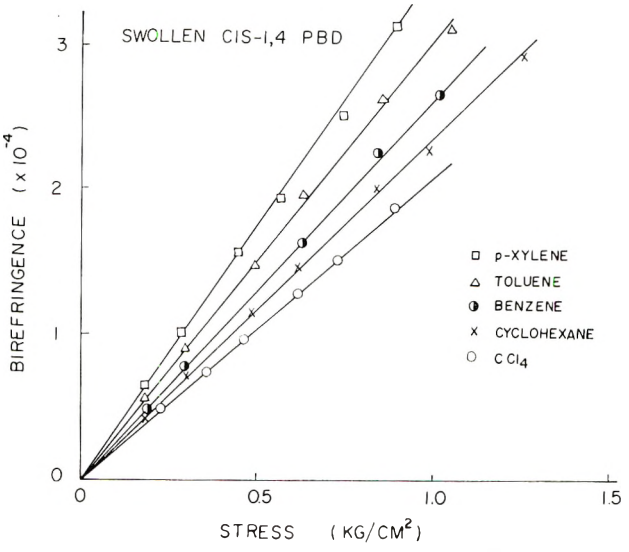

Fig. 15. Plot of birefringence against stress for high-*cis* crosslinked 1,4-polybutadiene rubber swollen in a variety of solvents.

these plots are reduced essentially to zero upon swelling. The intercepts are more highly dependent upon the swelling solvent than in the case of stress. While data for the unswollen *trans* polymer was taken to 100°C to avoid contributions from crystallinity, it was possible to obtain data on the swollen *trans* samples at room temperature since the crystal melting point was lowered to less than room temperature upon swelling. Further evi-

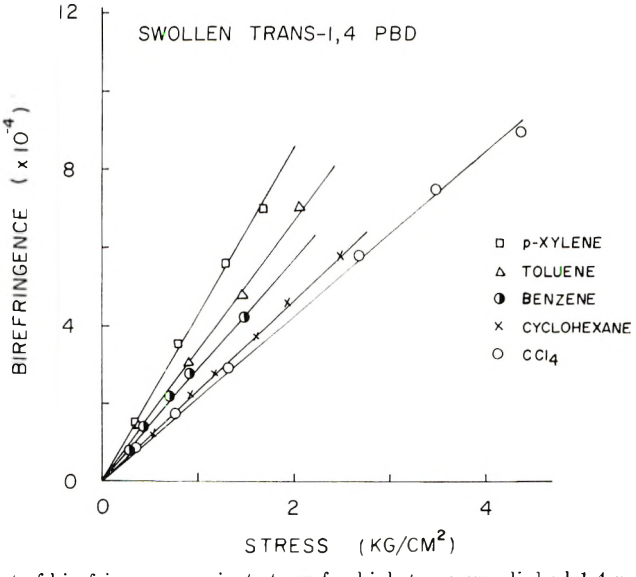

Fig. 16. Plot of birefringence against stress for high-*trans* crosslinked 1,4-polybutadiene rubber swollen in a variety of solvents.

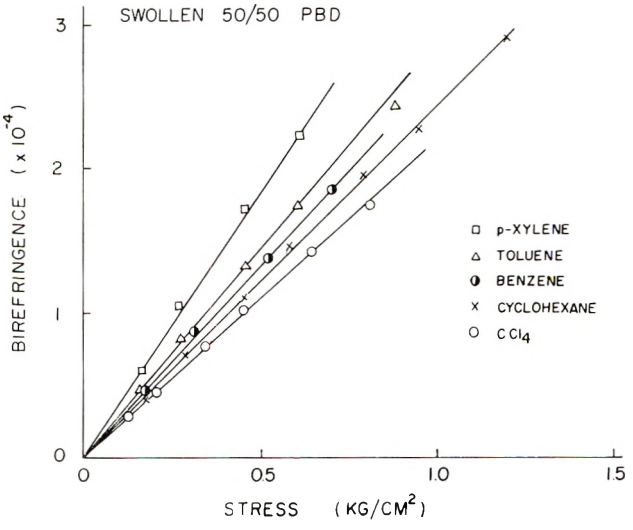

Fig. 17. Plot of birefringence against stress for a 50/50 *cis*/*trans* crosslinked 1,4-polybutadiene rubber swollen in a variety of solvents.

dence for this is seen in Figure 4 where the variation with temperature of the product of SOC and temperature is given for these swollen samples. There is no SOC maximum at lower temperatures, as is seen for the unswollen *trans* sample.

Thus, it is evident that both stress and birefringence exhibit significant deviations from kinetic elasticity and birefringence theory, and that these deviations are substantially reduced by swelling. It seems apparent that it is best to compare experiment and theory in the swollen state.

As has been pointed out by Ishikawa and Nagai,[19,20] there is a proportionality between stress and birefringence even in the unswollen state, but this proportionality, while predicted by the kinetic theory is not itself a sufficient proof that the theory is applicable. The finite slopes of the MR stress and birefringence plots are more sensitive indications of nonideality.

The SOC can be obtained by taking the ratio of intercepts of the respective birefringence and stress MR plots. However, this procedure proves not to be very accurate because of the fairly extensive extrapolation required for for the data taken in the swollen state. We prefer obtaining the SOC from slopes of birefringence-stress curves. Such plots are given for the high-*cis*, high-*trans* and 50/50 copolymer samples in Figures 15, 16, and 17, respectively. It is noted that quite good straight lines are obtained, the slope of which gives the SOC. It is apparent that this slope depends upon the nature of the swelling solvent as Gent[25] and Ishikawa and Nagai[19,20] also found.

If we assume that eq. (1) is applicable in the swollen state, we may then calculate $\Delta\Gamma$ which depends upon the *cis* content of the polymer and upon the kind of swelling solvent but is relatively independent of the degree of

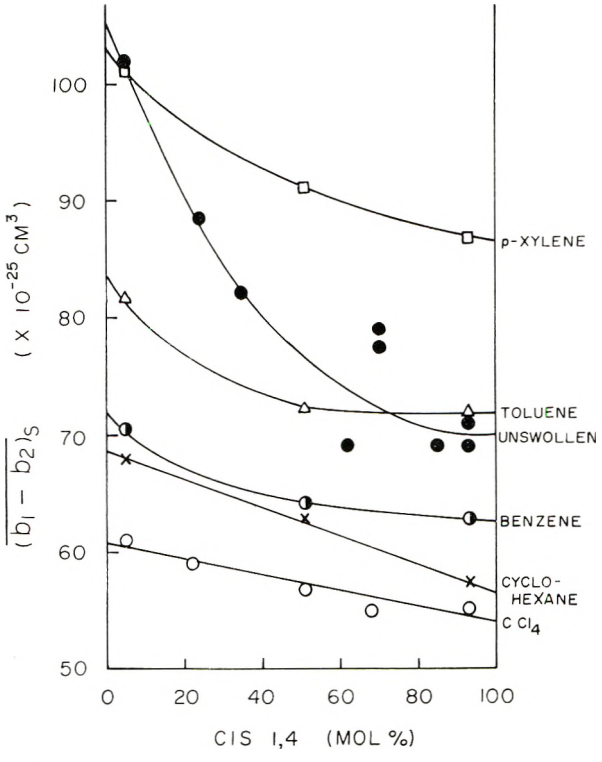

Fig. 18. Variation of the segment anisotropy, $\Delta\Gamma$ with *cis* content for 1,4-polybutadiene rubbers swollen with a number of solvents.

swelling provided that $v_2 < 0.2$ (which is true in all cases studied) and is also independent of M_c provided M_c is above ca. 5000. Values of the SOC obtained in this way are enumerated in Table VII, and calculated valuesof $\Delta\Gamma$ are given in Table VII and plotted in Figure 18.

It is seen that both $\Delta\Gamma$ and its dependence upon *cis* content are very dependent upon the type of solvent. Values for the unswollen rubber are also included on the plot and these prove to have the greatest composition dependence. Values for $\Delta\Gamma$ for the high-*cis* and high-*trans* samples are in approximate agreement with those published by Ishikawa and Nagai.[19,20]

Two significant observations may be drawn from this curve: (1) the lowest values of $\Delta\Gamma$ are obtained with the symmetrical solvent, carbon tetrachloride; (2) the variation of $\Delta\Gamma$ with composition is most linear with this solvent. It is seen in Figure 8 that similar linearity is found with the samples of poly-1,4-butadiene from Phillips Petroleum Company when they are swollen with carbon tetrachloride.

DISCUSSION

We believe, as do Gent[25] and Ishikawa and Nagai,[19,20] that the values of $\Delta\Gamma$ most representative of the isolated molecule are those determined for

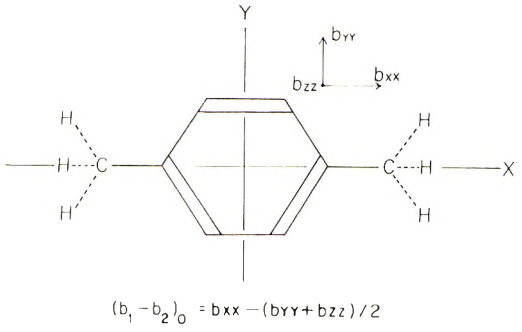

Fig. 19. Coordinate system for principal polarizabilities of solvent molecules.

polymer swollen with an isotropic solvent. Values obtained in the dry state are not correct, in part because of the same deviations from kinetic elasticity theory that lead to a finite C_2 in the MR plots. The exact nature of these deviations is still not clear but there is no reason to expect that the deviations will be the same for stress and birefringence behavior, so that the SOC in the unswollen state at finite elongations will differ from that of the ideal rubber.

In principle one might expect an ideal value to be approached by obtaining the SOC from the ratio of the extrapolated stress and birefringence MR type plots or else by obtaining the SOC at each elongation and carrying out the MR extrapolation of this ratio. Actually, there is no theoretical reason for believing that the intercept of the MR birefringence plot is the ideal value. Even if in this idealized state described by the extrapolation, the chains may statistically behave in the manner described by kinetic theory, the value of $\Delta\Gamma$ may not be the value characteristic of an isolated segment because of the environmental effect of the internal field of the neighboring chains (see below).

The dependence of the SOC upon the nature of the swelling solvent is a point of interest. It has been pointed out by Gent[25] and Ishikawa and Nagai[19,20] that this variation depends upon the anisotropy of shape and of the polarizability of the solvent. This effect may be seen in our data for different solvents. These were composed of molecules similar in shape but varying in saturation and in substituent groups.

The polarizabilities of the molecules were calculated from the Denbigh bond polarizabilities[24] by using eq. (8) and referring the principal polarizabilities to the coordinate system defined in Figure 19. The anisotropy of the solvent $(b_1 - b_2)_0$ is then defined as in eq. (9). Values are listed in Table VI. It is noted that this anisotropy is not referred to the optic axis of the molecule (which would be perpendicular to the plane of the aromatic ring in benzene, for example) but rather to the long or b_{zz} axis which is thought to be the axis of alignment of the solvent with respect to the polymer chain.

The values of $\Delta\Gamma$ are plotted against $(b_1 - b_2)_0$ in Figure 20 for the three polybutadienes. It is seen that the plots are similar and lead to an increase

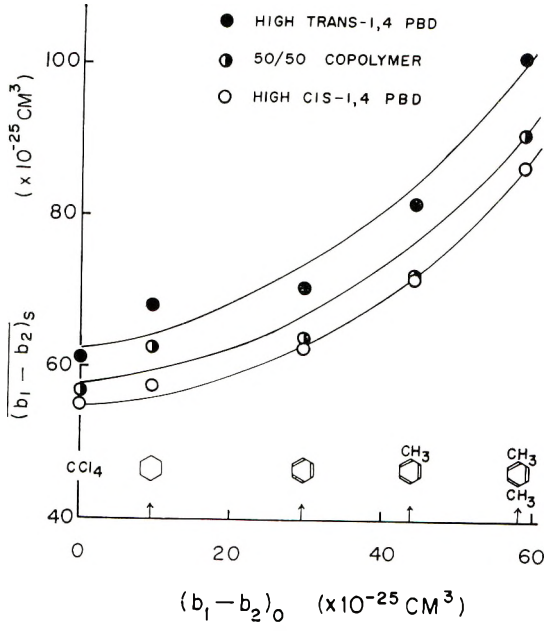

Fig. 20. Variation of $\Delta\Gamma$ of the high-*cis*, high-*trans* and 50/50 *cis*/*trans* 1,4-polybutadiene samples with the anisotropy of the solvent.

in $\Delta\Gamma$ with an increase in $(b_1 - b_2)_0$, suggesting that part of the perturbation of $\Delta\Gamma$ for the swollen polymer results from the optical anisotropy of the solvent molecule. It should be pointed out that Gent[25] finds that the shape anisotropy of a solvent molecule correlates better with changes in $\Delta\Gamma$ than does the anisotropy of polarizability.

Gent[25] says that "it is not clear, however, to what degree the enhanced optical anisotropy is due to partially ordered solvent molecules or to changed conformational properties of the polymer molecules in a condensed anisotropic medium." It may be that the enhanced birefringence with anisotropic solvents comes in part from the orientation of the anisotropic solvent molecule with the polymer. Some evidence for this effect may be seen in the infrared dichroism studies of Gotoh et al.,[34] who demonstrate that when plasticized poly(vinyl chloride) is stretched, the plasticizer orients along with the polymer.

It seems unlikely that major changes in the conformational properties of chains are occurring, since the principal effect of the solvent according to the kinetic theory of rubber elasticity is to change the "front factor" in the equation for stress based on the swollen cross-sectional area[35]

$$\sigma = N_c kT v_2^{1/3}(\langle r_i^2\rangle/\langle r\rangle^2)(\lambda^2 - \lambda^{-1}) \tag{17}$$

where N_c is the number of chains per cubic centimeter in the unswollen state, $\langle r_i^2\rangle$ is the mean-square distance between crosslinking points in the unswollen, unstretched network, and $\langle r^2\rangle$ is the mean-square distance be-

tween these points for the free chain. The elongation λ is the length of the stretched swollen polymer divided by that of the unstretched swollen polymer.

Since the same factor $\langle r_i^2\rangle/\langle r\rangle^2$, appears in the equation for birefringence,[36] it cancels when Δn is divided by σ to obtain the SOC. Any effect of the solvent on chain conformation would be reflected in its effect on $\Delta\Gamma$ which depends on the length of the statistical segment and is related through eq. (5) to the potentials associated with rotation about bonds. This chain conformation effect would also influence $\langle r_i^2\rangle/\langle r^2\rangle$ and consequently would be seen in a measurement of f_e/f where f is the total force on the stretched network and f_e is the portion of that force contributed by internal energy changes.[4] This ratio is found to be independent of the swelling solvent[30] and in fact is found, at least in some cases, to be almost the same for an unswollen polymer and a polymer in dilute solution in a theta solvent.[37] Whether or not is is generally true has been questioned.[38,39] Thus $\Delta\Gamma$ calculated through use of eq. (5) should not depend upon the solvent, and the observed variation must arise from factors not allowed for in this equation or in eq. (1), which relates $\Delta\Gamma$ to the measured SOC.

It is our point of view that the problem arises through the use of the Lorenz-Lorentz equation in obtaining eq. (1).[3] This equation corrects for the effect of the internal field of dipoles of surrounding molecules upon the molecule in question by assuming that the molecule resides within a spherical cavity in a dielectric and calculating the surface charge on this cavity.[40-42] This procedure is satisfactory for a spherical molecule but cannot be exactly true for an extended statistical segment having a more nearly cylindrical shape. It has been shown[42,43] that such considerations can account for the rather large difference in $\Gamma_{CH_2} = (b_1 - b_2)_{CC} - 2(b_1 - b_2)_{CH}$ calculated for n-paraffin molecules from gas-phase data ($\Gamma_{CH2} = 1.4$ Å^3) and from crystal refractive indices ($\Gamma_{CH_2} = 0.3$ Å^3) and for the differences between Γ_{CH_2} applicable to polyethylene and polypropylene crystals.[44]

The need for modification of the Lorenz-Lorentz field in describing anisotropic light scattering by liquids has been pointed out by Kielich[45] who states that the internal field can be exactly calculated from a knowledge of the position and orientation of all neighboring molecules, but that practically it is more convenient to replace the molecular field by a cavity field, as was done, for example, by Raman and Krishnan,[46] who assumed an ellipsoidal cavity. Nagai[47] has pointed out the abnormally high anisotropies of the n-alkanes in the pure liquids as seen in the data of Clement and Bothorel.[48] He ascribes these abnormally large anisotropies of n-alkanes to the "orientational order" existing among geometrically asymmetric molecules in the condensed phase.

The need for introducing internal field considerations in the stress-birefringence theory has been expressed by Bullough,[49,50] who extends the work of Rosenfeld[51] on the generalization of the Lorenz-Lorentz relation and shows that the "birefringence of all anisotropic fluid systems is determined in part by any intrinsic anisotropy of polarizability of the constituent par-

ticles (orientation birefringence) and in part by anisotropic correlations between particles (environmental birefringence)." The Kuhn-Grün theory [eq. (1)] gives only the orientation birefringence. He represents this orientation birefringence by a factor C_0 and divides the environmental birefringence into a contribution C_1 from pairs of chain elements on the same chain of the network and to a contribution C_2 from pairs of elements on different chains. (It should be noted that these C_i terms are different from those of the MR equation). He shows that C_0 "is necessarily accompanied by a relatively large value of C_1" and that for small stresses, C_1 "shows the same dependence on strain as C_0." He also concludes that "the effect of C_2 is to reduce C_1 and at the same time to increase the similarity between the strain dependence of C_0 and that of $(C_1 + C_2)$ at larger strains."

It is evident that if conformations are not affected by solvent, C_0 should be solvent-independent but C_1 and C_2 will depend upon the shape of both the solvent and the polymer segment and upon both their anisotropies and average polarizabilities. The solvent effect will depend upon (1) the correlation of orientation of solvent molecules with the segment axis and (2) the distribution of centers of solvent molecules about the center of the segment. For isotropic solvent molecules, orientation correlation is of no consequence, but a solvent effect resulting from the second contribution may still persist. That is, the field at the center of a segment surrounded by isotropic solvent molecules which are anisotropically distributed, will differ from that for an isolated segment. Thus, while a solvent effect may be small for CCl_4, there still might be an effect which may be different from what would be obtained for CBr_4, for example.

One sees from Figure 18 that $\Delta\Gamma$ for unswollen butadienes is considerably greater than the minimum values found in CCl_4. This may, in part, be due to nonequilibrium chain conformations resulting from entanglements and local order in the dry polymer. We believe, however, that the principal contribution does not come from perturbation of the conformations of a given chain by the neighboring chains but arises through an internal field effect of the sort described by the C_2 term in Bullough's theory[49,50] in which there is correlation of the orientation and position of neighboring segments of a given chain with that of the segment in question. This C_2 contribution may be increased or decreased upon swelling depending upon the anisotropy, orientation and position correlation of the solvent molecules. It must be realized that even in swelling with an isotropic solvent, the C_1 contributions, arising from the field of segments on the same chain, persist. (The solvent may influence this slightly through its effect upon the dielectric constant.) The fact that such interactions can be appreciable has been demonstrated by the calculations of Rowell and Stein.[52] Thus the $\Delta\Gamma$ obtained is not that of the isolated segment, even in the absence of interchain interaction, but rather the $\Delta\Gamma$ of the segment residing in the field of other segments of the same chain.

It should be noted that these internal field effects diminish rapidly with distance so that the intersegment correlation necessary to account for it is

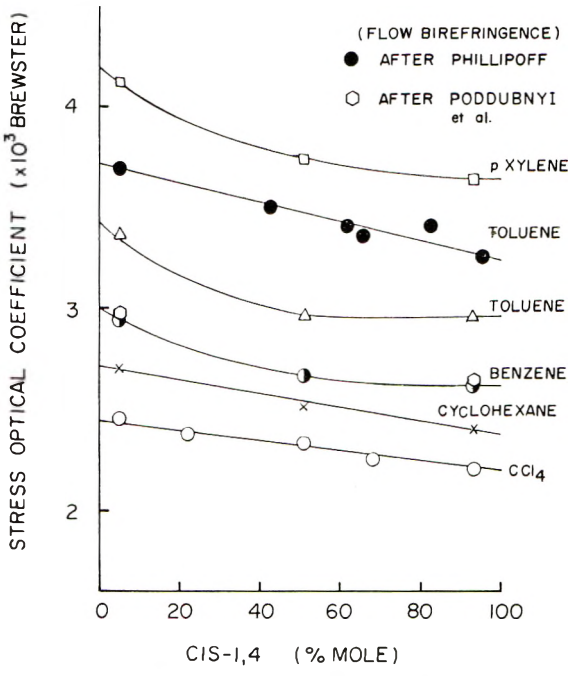

Fig. 21. The variation of the segment anisotropy with *cis* content for 1,4-polybutadiene rubbers swollen with a number of solvents as compared with streaming birefringence results of Poddubnyi *et al.* and of Phillipoff.

quite short-range and may not appreciably influence the thermodynamic properties. The diminution of $\Delta\Gamma$ occurring upon swelling with CCl_4 is much greater for *trans*-1,4-polybutadiene than for the *cis* isomer, indicating, as seems reasonable, that internal field effects may be greater with the more extended trans isomer since local parallel packing of chains is more likely.

The influence of solvent upon optical anisotropy has long been realized with streaming birefringence studies, as described, for example, in the paper by Frisman and Dadivanian.[53] The effect of solvent on the birefringence of swollen polymers has been discussed by Tsvetkov and Grishchenko,[54] the solvent being subdivided into a macroform and microform anisotropy. The macroform contribution "arises from non-spherical distribution of masses in a Gaussian coil and optical interaction from distant segments of the chain,"[55,56] whereas "microform anisotropy is the consequence of the optical interaction of adjacent chain segments."[57] While the macroform effect is clearly of importance in a dilute solution where separated polymer molecules may be imbedded in a solvent of differing refractive index, the application of such a term to a crosslinked network appears questionable to us in that the molecules are interpenetrating and connected together by crosslinks so that no distinct polymer–solvent boundaries can be found. The equation for macroform anisotropy is dependent upon the molecular weight and intrinsic viscosity which are clearly not significant variables for a crosslinked network. Also, the equations of Tsvetkov and Grishchenko do not involve

the solvent anisotropy; hence it appears that they do not include the contribution arising from the orientation of the solvent with respect to the polymer. These authors investigate the dependence of stress-birefringence upon concentration and attempt to resolve the solvent effect into macro- and microform contributions.

It is of interest to compare in Figure 21 the values of SOC which we determined on the networks swollen with different solvents with values determined by Poddubnyi et al.[23] from streaming birefringence measurements on dilute solutions in benzene solution and by Phillipoff[58] on dilute solutions in toluene. The values in benzene are in quite good agreement, while the toluene values are in fair agreement. It should be realized that complete agreement is not expected, because a macroform contribution should occur in the streaming birefringence measurements but not in the stress birefringence measurements. Also, the effects of correlation between solvent and polymer segment orientation are possibly different in the shear field of the streaming measurements and in the static case of strain birefringence studies Poddubnyi et al.[23] indicate that up to a 30% correction was applied to their data for the birefringence of benzene but do not give details as to how this was done. Also, they mention that little difference was found for measurements made in CCl_4 in contrast to our SOC results, but say without clarification that the "shape effect" was taken into account in the comparison.

Calculation of Segment Sizes in Swollen Polymers

If we assume that the SOC measurements in the CCl_4 swollen polymers closely represent the values for the isolated polymer chains, we may then repeat the calculations of the factor q originally given following Table V,

TABLE VIII
Statistical Segment Anisotropies and Sizes of *Cis*- and *Trans*-1,4 Polybutadiene

	Trans-1,4-PB	*Cis*-1,4-PB
$\Delta\Gamma$, cm^3		
This work	61.1×10^{-25}	53.5×10^{-25}
Ishikawa and Nagai[a]	58.1×10^{-25}	55.2×10^{-25}
Poddubnyi et al.[b]	71×10^{-25}	63×10^{-25}
$(b_1 - b_2)_m$		
This work	36.3×10^{-25}	31.7×10^{-25}
Poddubnyi et al.[c]	37.4×10^{-25}	30.8×10^{-25}
q		
This work	1.68	1.69
Poddubnyi et al.[d]	1.9	2.0
L		
This work, Å	9.4	7.8

[a] Values of Ishikawa and Nagai[19,20] determined in CCl_4 at 20°C for *cis* isomer and at 60°C for *trans* isomer.

[b] Values of Poddubnyi et al.[23] determined in benzene by streaming birefringence.

[c] Values calculated by Poddubnyi et al.[23] by using Denbigh bond polarizabilities.

[d] Values calculated from ratio of $\Delta\Gamma$ to $(b_1 - b_2)_m$ (Poddubnyi's data [23]).

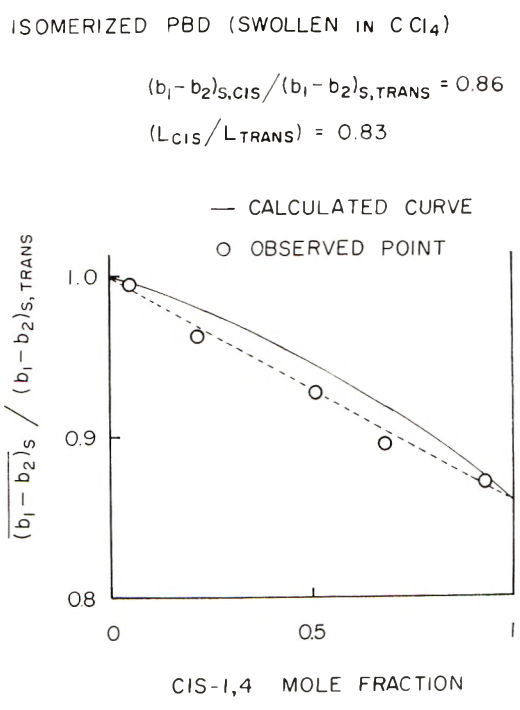

Fig. 22. The variation of $\Delta\Gamma$ with *cis* content for 1,4-polybutadiene rubbers swollen with CCl_4 compared with values calculated by using the Stein-Shindo theory.

again using the values of the monomer anisotropies $(b_1 - b_2)_m$ calculated from the Denbigh polarizabilities.[24] These results are summarized in Table VIII.

It is noted that quite good agreement is achieved between the values of $\Delta\Gamma$ obtained by us and by Ishikawa and Nagai[19,20] for samples swollen with CCl_4. The values of $\Delta\Gamma$ given by Poddubnyi et al.[23] are higher but these were determined in benzene solution and agree quite well with our values determined from SOC measurements on networks swollen with benzene as shown in Figure 21.

The values of the number of monomer units q per statistical segment are quite close for *cis*- and *trans*-1,4-polybutadiene. The results of the calculation of Poddubnyi et al. are also quite close to each other but larger than ours, principally as a result of the larger $\Delta\Gamma$ values which were derived from measurements in benzene and which we believe still contain a significant contribution from a solvent effect. The values of monomer anisotropy, $(b_1 - b_2)_m$, calculated by us and by Poddubnyi et al., both from Denbigh bond polarizabilities, are in good agreement.

It is of interest to compare the variation of $\Delta\Gamma$ with *cis* content experimentally measured in CCl_4 solution with values calculated from the Shindo-Stein theory using values of L_{cis}/L_{trans} of 0.83 obtained from Table VIII from data on the high-*cis* and high-*trans* isomers and of $(b_1 - b_2)_{s,cis}/(b_1 -$

$b_2)_{s,trans} = 0.88$ calculated by using Denbigh bond polarizabilities. The results are shown in Figure 22. We believe that differences are within experimental error. Thus if data obtained in CCl_4 solution is used, there is good agreement between the experimental results and the predictions of the theory. The approximate equality of statistical segment sizes for the two isomers leads to an almost linear variation of $\Delta\Gamma$ with composition. The non-linear results obtained for the dry polymers are a consequence of non-linearity of the deviations from ideality.

Furukawa et al.[59] have observed that SOC values for styrene-butadiene copolymer rubbers vary linearly with styrene content. Similar observations have been made by Kraus.[60] It would be of interest to extend their work to swollen systems to determine whether the linear-variation still persists.

Our analysis of our data in terms of the Stein-Shindo theory involving two different kinds of segments implies that one type of segment is associated with the *cis* isomer and the other with the *trans*. This will be true if q is close to unity so that a statistical segment is identical with the monomer unit. If $q > 1$ so that a segment may include more than one type of monomer, then more than two types of segments may be required. For example, if $q = 2$, we may have three types of segments, one of length L_1 containing two *cis* monomer units, one of length L_2 containing two *trans* units, and one of length L_3 containing a *cis* and a *trans* unit. The relative numbers of these segments depends upon the stereosequence distribution as well as upon the *cis* content. Thus a polymer having more block character has a lower relative number of L_3 type segments. This suggests the interesting experimental possibility of determining $\Delta\Gamma$ for a series of polymers having the same *cis* content but of varying block character. In fact, if the stereoblocks are sufficiently long so that their molecular weight becomes comparable with M_c, then the polymer behaves as a crosslinked blend for which $\Delta\Gamma$ varies linearly with composition regardless of L_1/L_2.

CONCLUSIONS

This work confirms the conclusions of Gent and of Ishikawa and Nagai that the SOC values for rubbers are quite solvent dependent. We feel that the dependence is principally a result of orientation of the solvent by the polymer and of internal field effects arising because of local correlation in orientation of polymer segments on neighboring molecules. The measurements on dry polymer are inconsistent when interpreted in terms of the Stein-Shindo theory, but measurements in the CCl_4 swollen state are quite consistent.

The authors appreciate the help of Prof. R. W. Lenz of the University of Massachusetts in supplying samples and advising about procedures for isomerization. The suggestions, samples, and data supplied by Dr. G. Kraus of Phillips Petroleum Co. are appreciated. We also appreciate receiving unpublished data from Dr. W. Phillipoff of Esso Research and Engineering Labs. One of us (RSS) appreciates the advice and discussion with Dr. K. Nagai of the Government Industrial Research Laboratories of Osaka, Japan.

This study was supported in part by a contract with the Office of Naval Research and in part by Grants from the General Tire and Rubber Company and the Petroleum Research Fund of the American Chemical Society.

References

1. W. Kuhn and F. Grün, *Kolloid Z.*, **101**, 248 (1942).
2. L. R. G. Treloar, *Trans. Faraday Soc.*, **43**, 277 (1947); *ibid.*, **50**, 881 (1954).
3. L. R. G. Treloar, *The Physics of Rubber Elasticity*, Oxford Univ. Press, 2nd ed., 1967.
4. P. J. Flory, R. L. Jernigan, and A. E. Tonelli, *J. Chem. Phys.*, **48**, 3822 (1968).
5. P. J. Flory, *Statistical Mechanics of Chain Molecules*, Interscience, New York, 1969.
6. K. Nagai, *J. Chem. Phys.*, **40**, 2818 (1964); *ibid.*, **49**, 4212 (1968).
7. Y. Shindo and R. S. Stein, *J. Polym. Sc . A-2*, **7**, 2115 (1969).
8. K. Nagai, *J. Chem. Phys.*, **47**, 2052 (1967).
9. Y. Shindo, R. S. Stein, and B. E. Read, *Makromol. Chem.*, **118**, 272 (1968).
10. M. A. Golub, *J. Polym. Sci.*, **25**, 373 (1957).
11. M. Berger and D. J. Buckley, *J. Polym. Sci. A*, **1**, 2945 (1963).
12. R. R. Hampton, *Anal. Chem.*, **21**, 923 (1949).
13. G. Natta and G. Morgalio, *Rubber Plastics, Age*, **44**, 42 (1963).
14. G. Natta and P. Corradini, *Nuovo Cimento* (Suppl.) **1**, 9 (1960).
15. E. G. Lovering and D. C. Wooden, *J. Polym. Sci. A-2*, **7**, 1639 (1969).
16. D. W. Saunders, *Trans. Faraday Soc.*, **52**, 1414, 1425 (1946).
17. F. T. Wall, *J. Chem. Phys.*, **11**, 67 (1943).
18. J. E. Mark, *J. Amer. Chem. Soc.*, **88**, 4354 (1966); *ibid.*, **89**, 6829 (1967).
19. T. Ishikawa and K. Nagai, *J. Polym. Sci. A-2*, **7**, 1123 (1969).
20. T. Ishikawa and K. Nagai, *Polymer J. (Japan)*, **1**, 116 (1970).
21. H. L. Wagner and P. J. Flory, *J. Amer. Chem. Soc.*, **74**, 195 (1952).
22. D. W. Saunders, *Trans. Faraday Soc.*, **36**, 860 (1957).
23. I. Ya. Poddubnyi, Ye. G. Erenburg, and M. A. Yeremina, *Vysokomol. Soedin.*, **A10**, 1381 (1968).
24. K. G. Denbigh, *Trans. Faraday Soc.*, **36**, 936 (1940).
25. A. N. Gent, *Macromolecules*, **2**, 262 (1961).
26. M. Mooney, *J. Appl. Phys.*, **19**, 434 (1948).
27. R. S. Rivlin, in *Rheology*, Vol. I, F. R. Eirich, Ed., Academic Press, New York, 1956.
28. S. M. Gumbrell, L. Mullins, and R. S. Rivlin, *Trans. Faraday Soc.*, **49**, 1495 (1953).
29. B. M. E. van der Hoff, *Polymer*, **6**, 397 (1965).
30. C. Price, (Univ. of Manchester), private communication, 1970.
31. A. N. Gent and V. V. Vickroy, Jr., *J. Polym. Sci. A-2*, **5**, 47 (1967).
32. P. J. Flory and J. Rehner, *J. Chem. Phys.*, **12**, 412 (1944).
33. A. V. Tobolsky, private communication, 1970.
34. J. Uemura, T. Takenaka, S. Hayashi, and R. Gotoh, *Bull. Inst. Chem. Res. Kyoto Univ.*, **46**, 228 (1968).
35. P. J. Flory, C. A. J. Hoeve, and A. Ciferri, *J. Polym. Sci.*, **34**, 337 (1959).
36. D. W. Saunders, D. R. Lightfoot, and D. A. Parsons, *J. Polym. Sci. A-2*, **6**, 1183 (1968).
37. J. E. Mark and P. J. Flory, *J. Amer. Chem. Soc.*, **87**, 1423 (1965).
38. A. Ciferri, *J. Polym. Sci. A*, **2**, 3089 (1964).
39. D. Puett, *Makromol. Chem.*, **100**, 200 (1967).
40. H. A. Lorentz, *The Theory of Electrons*, Dover, New York, 1952; *Ann. Physik*, **9**, 641 (1880).

41. L. Lorenz, *Ann. Physik*, **11**, 70 (1880); *Videnskapsselskapets-Strifter* **8**, 205 (1869); *ibid.*, **10**, 485 (1875).
42. R. S. Stein, *J. Polym. Sci. A-2*, **7**, 1021 (1969).
43. M. F. Vuks, *Optika Spektroskopie*, **2**, 494 (1957).
44. D. A. Keedy, J. Powers, and R. S. Stein, *J. Appl. Phys.*, **31**, 1911 (1960).
45. S. Kielich, *J. Chem. Phys.*, **46**, 4090 (1967).
46. C. W. Raman and K. S. Krishnan, *Phil. Mag.*, **5**, 498 (1928).
47. K. Nagai, *J. Chem. Phys.*, **47**, 4690 (1967).
48. C. Clement and P. Botherel, *J. Chem. Phys.*, **61**, 878 (1964).
49. R. K. Bullough, *J. Polym. Sci.*, **46**, 517 (1960).
50. R. K. Bullough, private communication.
51. L. Rosenfeld, *Theory of Electrons*, North Holland, Amsterdam, 1951, Chapt. 6.
52. R. L. Rowell and R. S. Stein, *J. Chem. Phys.*, **47**, 2985 (1967).
53. E. V. Frisman and A. K. Dadivanian, in *Macromolecular Chemistry, Prague 1965* (*J. Polym. Sci. C*, **16**), B. Sedlàček and O. Wichterle, Eds., Interscience, New York, 1967, p. 1001.
54. V. N. Tsvetkov and A. E. Grishchenko, in *Macromolecular Chemistry, Prague 1965* (*J. Polym. Sci. C*, **16**), B. Sedlàček and O. Wichterle, Eds., Interscience, New York, 1968, p. 3195.
55. V. N. Tsvetkov, and E. V. Frisman, *Dokl. Akad. Nauk SSSR*, **97**, 647 (1954).
56. M. Copic, *J. Chem. Phys.*, **26**, 1382 (1957).
57. V. N. Tsvetkov, *Vysokomol. Soedin.*, **5**, 740 (1963).
58. W. Phillipoff, private communication, 1970.
59. J. Furukawa, T. Kotani, and S. Yamashita, private communication, 1969.
60. G. Kraus, private communication, 1969.

Received October 15, 1970
Revised January 25, 1971

JOURNAL OF POLYMER SCIENCE: PART A-2 VOL. 9, 1449–1469 (1971)

NMR Observations of Drawn Polymers. VII. Nylon 66 Fibers*

HEINZ G. OLF and A. PETERLIN, *Camille Dreyfus Laboratory, Research Triangle Institute, Research Triangle Park, North Carolina 27709*

Synopsis

Wide-line NMR spectra have been obtained on an oriented sample of drawn nylon 66 fibers at temperatures between −196°C and 200°C and at alignment angles between the fiber axis and the magnetic field of 0°, 45°, and 90°. At −196°C, 20°C, and 180°C, the complete angle dependence of the NMR spectrum has been measured. The second moments of these spectra have been compared to theoretical second moments calculated for various models of chain segmental motion in an attempt to elucidate the mechanisms involved in the low-temperature segmental motion (γ process) and the high-temperature segmental motion (α_c process). In agreement with earlier suggestions, the present results indicate that the γ process consists of segmental motion in noncrystalline regions. The overall decrease in second moment caused by the γ process is consistent with a model in which all noncrystalline segments rotate around axes nearly fixed in space. Furthermore, this decrease shows a pronounced dependence on the alignment angle. It is believed that this is due to tie molecules which become highly oriented along the fiber axis during drawing; their axes of rotation will therefore be nearly parallel to the fiber axis. The segments in noncrystalline entities such as chain folds and chain ends are less well oriented along the fiber axis and make an essentially isotropic contribution to the second moment decrease. The second moment at 180°C indicates the presence of considerable motion in the crystalline regions, and this motion is denoted the α_c process. The second moment S_c of the crystalline regions is strongly dependent on the alignment angle, the predominant feature being a relatively high value of the second moment when the fiber axis is directed parallel to the magnetic field. This is in qualitative, but not quantitative, agreement with the motional model recently advanced by McMahon, which assumes full rotation of the chains around their axes. Excellent quantitative agreement with experiment has been obtained by superimposition of rotational oscillation around the chain axis of amplitude roughly 50°, and torsion of the chains with neighboring CH_2 groups oscillating around the C-C bond with a relative amplitude of about 40°. A model in which the chains perform rotational jumps of 60° between two equilibrium sites has also been considered (60° flip-flop motion). A distinction between this model and rotational oscillation has not been possible.

INTRODUCTION

The processes of molecular motion giving rise to the well-known relaxation phenomena in polyamides[1] still pose many unanswered questions although they have been studied extensively by dielectric and mechanical methods[2,3] as well as by nuclear magnetic resonance (NMR) techniques.[4–22]

* Presented in part at the Meeting of the American Physical Society, Dallas, Texas, March 1970.

Inferences regarding molecular motion can also be drawn from x-ray,[23–29] infrared,[30,31] and calorimetric[32,33] data. The purpose of this paper is to present wide-line NMR data on oriented nylon 66 and to discuss these in view of some of the remaining problems, notably molecular mechanisms of the motions involved.

Since the dynamic-mechanical loss modulus of polyamides exhibits up to three maxima[1,8] when measured as a function of temperature it is customary to designate the three relaxation processes as the α, β, and γ processes in order of decreasing temperature.[3] Although the underlying molecular mechanisms are uncertain or unknown, there seems to be general agreement that these relaxations originate from molecular motion in noncrystalline regions.[3] The x-ray[5,25,26,28,29] and NMR[6,8,9,17,18] data suggest, however, that in addition there exists a process of molecular motion in crystalline regions. This motion causes no conspicuous effects in dynamic-mechanical experiments, although Woodward et al.[34] have mentioned the possibility that it may be responsible for the observed asymmetry (high-temperature tail) of the α loss peak. We shall denote this motion the α_c process and refer to the motion previously called α as the α_a process.

Of the four motional processes α_c, α_a, β, and γ, only the γ and α_c processes will be discussed. Since the β process in nylon 66 depends on the presence of water and other polar liquids,[35–39] this process is not present in our carefully dried samples. The α_a process, often associated with the glass transition, is clearly observed in our NMR experiments (10^4Hz, 80°C), but little will be said about it.

The low-temperature γ process (10^4 Hz, -100°C) has been attributed to motion of the —CH_2— sequences of nylon 66 in noncrystalline regions.[1] The similarity of this process to the γ process in polyethylene has already been noted in mechanical experiments.[1,3] The present NMR results also bear out this similarity and the discussion of this process can in fact be regarded as a continuation of a recent consideration of the γ process in polyethylene.[40–42]

Information on the α_c process, that is chain motion in the crystalline regions, has come in the main from x-ray and wide-line NMR studies. From these methods it appears that motion in the crystallites starts at about the same temperature as the α_a relaxation and is fully excited at about 160°C. In the temperature range of the α_c process, nylon 66, according to x-ray studies, undergoes a gradual and reversible transition from its room-temperature triclinic form to a different high-temperature triclinic form[25,28] which may be called pseudohexagonal because the projections a' and b' of the lattice constants a and b on a plane perpendicular to the chain direction become equal and the angle between them becomes 60°. It has been suggested that this transition may be caused by rotation of the chains in the crystal around their long axes.[5] Appreciable narrowing of the NMR spectrum has been ascribed to the same kind of motion.[5,18]

Another mechanism of molecular motion for the α_c process has been proposed based entirely on x-ray observations. The room-temperature

triclinic form is characterized by planar arrays of molecules hydrogen-bonded to one another, thus making a two-dimensional network of hydrogen bonds.[43] Within such hydrogen-bonded sheets the distance between neighboring molecules has the relatively large value $a' = 4.8$ Å, since the hydrogen bonds act as spacers. The crystal structure of nylon 66 can be imagined as a regular stacking of these sheets such that the distance b' between two nearest molecules in neighboring sheets is only 4.1 Å. During transition to the pseudohexagonal high-temperature form, a' scarcely changes, whereas b' increases gradually to a final value of 4.8 Å. This value is suggestive of hydrogen bonds between sheets, of course, and led Brill[25,26] and Schmidt and Stuart[28] to postulate a dynamic three-dimensional network of hydrogen bonds in the pseudohexagonal structure. The crystalline chain segments are thought to perform rotational jumps of 60° around their long axes, breaking the hydrogen bonds in their own sheet and making new ones with molecules in the neighbor sheet. The time between breaking and reformation of hydrogen bonds can be extremely small, which would make understandable the infrared evidence that on a time average nearly all hydrogen bonds remain intact up to the melting point.[30,31] We refer to this mechanism as the "60° flip-flop."

The effect of the two motional mechanisms, rotational oscillation and 60° flip-flop, on the anisotropy of the NMR second moment in axially oriented nylon 66 will be predicted quantitatively and these predictions will be compared with experimental second moment data in an attempt to distinguish between the two mechanisms.

The angle dependence of the wide-line NMR spectrum of a number of polymers has already been studied by several authors.[18,42,44–60] Nylon 66 has also been treated in this manner.[17,18] The present paper as outlined above is an experimental and theoretical extension of previous work on nylon 66 in the following respects: The temperature range covered is −196°C to 200°C and thus includes the γ process. The theoretical calculations of the second moment are more rigorous in that intermolecular contributions and the nonideal orientation of the samples are taken into account. The models of chain-segmental motion considered include oscillation of general amplitude, containing full rotation as a limiting case, the 60° flip-flop motion, and chain torsion.

THEORETICAL

The NMR second moment of a fiber sample has been shown[59] to depend on the alignment angle γ subtended by the fiber axis and the NMR magnetic field as follows:

$$S(\gamma) = A \cos^4 \gamma - B \cos^2 \gamma + C \tag{1}$$

where A, B, and C are independent of γ. They depend on the degree of orientation of the sample, which enters through the parameters C_2 and C_4 defined by $C_2 = \langle \cos^2 \alpha \rangle$ and $C_4 = \langle \cos^4 \alpha \rangle$, α being the angle between the

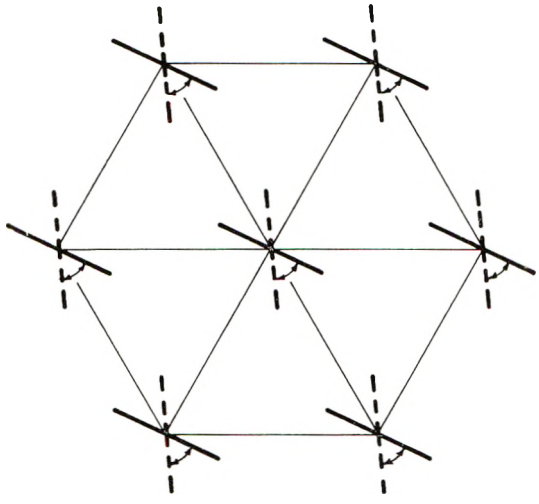

Fig. 1. Illustration of the 60° flip-flop motion in the high temperature pseudohexagonal lattice of nylon 66 in a projection onto a plane perpendicular to the chain axis. The two equilibrium positions of the chain are indicated by the solid line (low-temperature position of the carbon backbone plane) and the broken line. The arrows symbolize the 60° rotational jumps of the molecules.

fiber axis and the molecular axis.[59] Furthermore, A, B, and C are functions of molecular and crystal structure as well as of molecular motion, these variables entering in the form of time-average lattice sums which have been defined elsewhere.[59] The second moment of an unoriented sample (powder average) is given by[59]

$$S_{uo} = A/5 - B/3 + C \tag{2}$$

We shall use these general results to predict the angle dependence of the second moment in the presence of either of the motional mechanisms discussed in connection with the α_c process. The motions to be considered are best described in terms of the probability $pd\chi_1 d\chi_2$ of finding two neighboring molecules at angular displacements near χ_1 and χ_2 around their axes away from their equilibrium positions. For rotational oscillation we use

$$p(\chi_1, \chi_2) = (1/2\pi\delta^2) \exp\left\{-(\chi_1^2 + \chi_2^2)/2\delta^2\right\}$$

where δ is half the width of the assumed normal distribution and will be called the angular amplitude of oscillation. Other models for rotational oscillation have also been used[59] but need not be considered here, since they lead to rather similar results.

The 60° flip-flop motion consists of rotational jumps of crystalline chain segments between two equilibrium sites 60° apart as shown in Figure 1. Also, the possibility of oscillation with angular amplitude δ around each site before the molecule jumps to the other one is taken into account. The case characterized by $\delta = 0°$ may be denoted pure 60° flip-flop motion. Schmidt and Stuart have made the reasonable assumption that neighboring segments

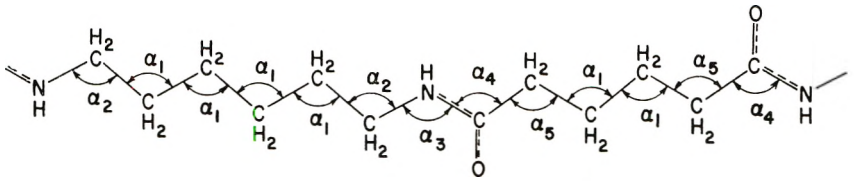

Fig. 2. Bond angles and bond lengths used for calculating theoretical second moments. Numbers are given in Table I.

perform these jumps simultaneously. This leads to the following expression for the probability density

$$p(\chi_1, \chi_2) = (1/4\pi\delta^2)\,[\exp\{-(\chi_1^2 + \chi_2^2)/2\delta^2\} + \exp\{-[(\chi_1 - \pi/3)^2 + (\chi_2 - \pi/3)^2]/2\delta^2\}]$$

The molecular chains are first assumed to be rigid; the possibility of torsion will be considered in the discussion.

As the needed atomic coordinates in the nylon 66 chain are not well established, they were estimated from the literature on low molecular weight compounds. They are given in Figure 2 and Table I in terms of bond angles and bond lengths. The pseudohexagonal crystal structure has not been determined in detail, but since the main contribution to the second moment arises from intramolecular interactions, this is not serious. The parameters $a' = b' = 4.85$ Å were used,[25] and it was assumed that the relative longitudinal arrangement of the chains is the same as in the room-temperature triclinic form.[43]

Some results of the calculations are shown in Figures 3 and 4. The angle dependence of the second moment of nylon 66 fibers for different motions appears in Figure 3. The powder average second moment in the presence of rotational oscillation or 60° flip-flop motion is shown in Figure 4 as a function of the oscillation amplitude δ. Full rotation of the chains around their axes in either case corresponds to $\delta \to \infty$. Also shown is the value for the rigid lattice with the low-temperature triclinic structure.

TABLE I
Bond Lengths and Bond Angles in Nylon 66 (see Figure 1)

	Angle	Bond length, Å	Reference
Bond angles			
α_1	110° 36′		
α_2	113°		61
α_3	123°		62
α_4	114°		62
α_5	113° 54′		63
Bond lengths			
HN—CH_2		1.47	62
H_2C—CH_2		1.541	64
HN=—CO		1.32	62
OC—CH_2		1.53	62

In applying these results to a semicrystalline polymer such as nylon 66 it will prove useful to consider a two-phase model which allows one to express the total second moment S through S_c and S_a, the second moments of crystalline and noncrystalline regions, respectively:

$$S = \alpha_m S_c + (1 - \alpha_m) S_a \tag{3}$$

where α_m is the mass fraction of crystalline material.

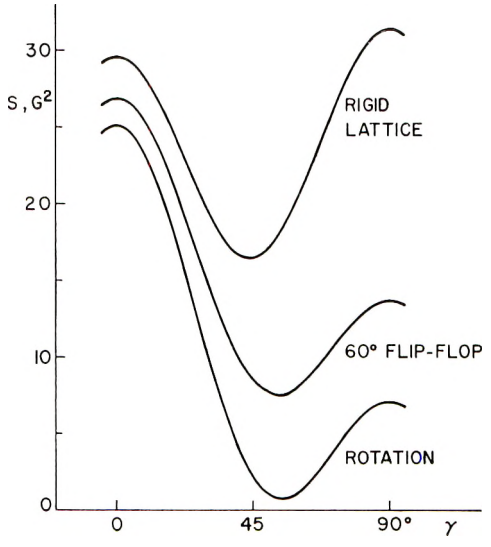

Fig. 3. The dependence of second moment on the alignment angle γ in a perfectly oriented nylon 66 fiber, calculated for the low-temperature triclinic rigid lattice and for 60°-flip-flop motion and full rotation of the chains in the pseudohexagonal lattice.

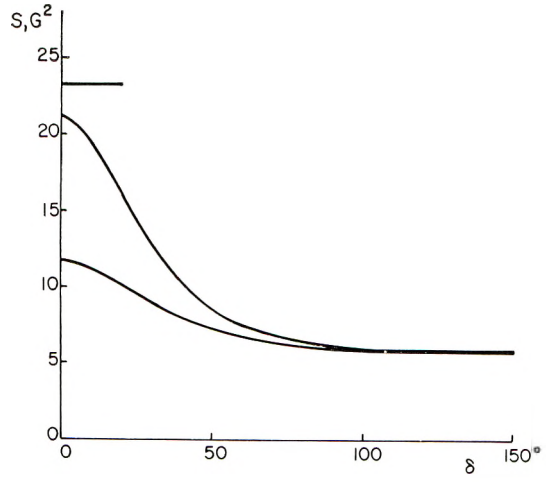

Fig. 4. The second moment of an unoriented nylon 66 sample (powder average) as a function of the amplitude of oscillation δ calculated for rotational oscillation (upper curve) and for 60°-flip-flop motion (lower curve).

EXPERIMENTAL

Sample

Nylon 66 monofilaments, drawn to a ratio 5:1, were used as an axially oriented sample. The fibers as well as molecular weight data ($\bar{M}_n \approx 17.5 \times 10^3$ from endgroup analysis, $\bar{M}_w \approx 34.4 \times 10^3$ from light scattering) were kindly supplied by Dr. G. W. Sovereign of the Chemstrand Research Center. The density of the fibers was 1.144 g/cm^3 which corresponds to a crystalline mass fraction α_m of 0.53, according to the density values of Starkweather and Moynihan[65] for crystalline and noncrystalline nylon 66. The x-ray scattering at small angles showed an intensity maximum corresponding to a long period of 88 Å along the fiber. The fibers were thoroughly dried in a vacuum better than 10^{-4} torr at 100°C for four weeks.

NMR Measurements

NMR spectra were obtained by using a Varian DP-60 spectrometer. The nylon 66 fibers were inserted into an opening cut in a Teflon rod sample holder so that the fiber axis was directed perpendicular to the rod axis. By turning the rod around its axis the fiber axis could be set at any alignment angle γ with respect to the magnetic field. The angle was read on a goniometer.

The magnetic audio modulation field generally employed in wide-line NMR was of frequency 40 Hz in all measurements. The amplitude was varied between 0.5 and 2.2 G peak-to-peak and so chosen in each case as to yield a satisfactory signal-to-noise ratio of the recorded spectrum. The speed of scanning through resonance was 3.5 G/min. Steps taken to prevent saturation, as well as calibration and evaluation procedures, are described elsewhere.[41,53] A general discussion of the application of wide-line NMR to polymeric solids can be found in the review article by Powles.[66]

X-Ray Measurements

The fibers were found to possess the well-known triclinic structure in the α-form.[43] Bunn and Garner have established that drawing of a nylon 66 fiber causes the crystallites to preferentially align themselves with their c-axis, and therefore their molecular axes, parallel to the draw direction or fiber axis.[43] Letting α be the angle subtended by the crystallite c-axis and the fiber axis, the degree of crystallite orientation will be expressed by the averages $C_{2c} = \langle\cos^2 \alpha\rangle_c$ and $C_{4c} = \langle\cos^4 \alpha\rangle_c$, where the subscript (c) refers to the crystallites. These parameters were obtained from measurements of the X-ray intensity distribution $I(\alpha)$ of a set of diatropic lattice planes so that $I(\alpha)$ is proportional to the plane normal or c-axis distribution. The (1, 3, 14) planes of nylon 66 were used since they are nearly perpendicular to the c-axis, their normal deviating only about 2° from the latter. $I(\alpha)$ was determined by an x-ray diffractometer in the symmetrical transmission arrangement[67] with point counting for 10^4 counts, with the use of Ni-

filtered CuKα radiation at 35 kV and 15 mA. Numerical integration according to

$$C_{nc} = \langle \cos^n \alpha_c \rangle = \int_0^{\pi/2} I(\alpha) \cos^n \alpha \sin \alpha d\alpha \Big/ \int_0^{\pi/2} I(\alpha) \sin \alpha d\alpha$$

where $n = 2, 4$, yielded $C_{2c} = 0.97$ and $C_{4c} = 0.94$.

Birefringence Measurements

The birefringence of the fibers as determined on a Leitz polarization microscope with Berek compensator was 0.055. Stein has shown that the birefringence Δ of drawn, axially oriented material may be expressed as:[68]

$$\Delta = \alpha_m f_c \Delta_c^\circ + (1 - \alpha_m) f_a \Delta_a^\circ$$

if the small contribution arising from form birefringence is neglected. In this expression α_m is the crystalline mass fraction, Δ_c° and Δ_a° are the birefringences of segments in the crystalline and noncrystalline regions, and f_c and f_a are orientation parameters for the crystalline and noncrystalline regions. These are related to $\langle \cos^2 \alpha \rangle$ by $f = (3 \langle \cos^2 \alpha \rangle - 1)/2$.

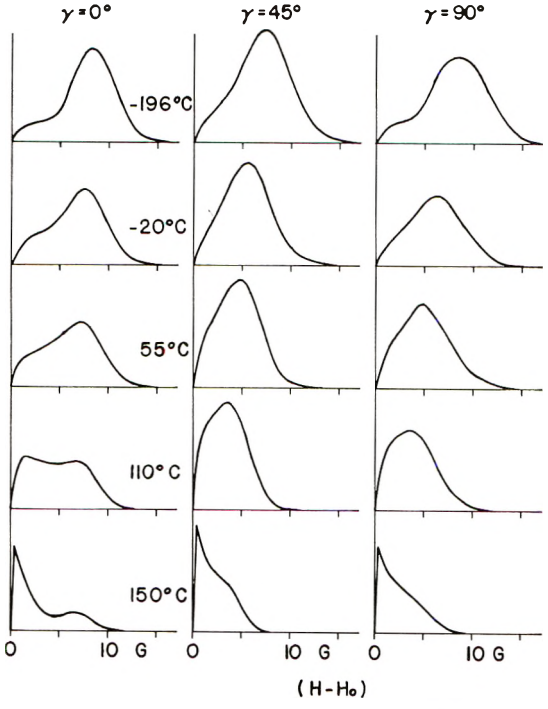

Fig. 5. Experimental first derivatives of the proton NMR absorption in nylon 66 fibers at alignment angles $\gamma = 0°, 45°, 90°$ of the fiber axis with respect to the magnetic field H at the temperatures indicated. As these spectra are symmetrical with respect to the origin, only one-half is shown. The center of the resonance is at $H = H_0$. Data taken from Olf and Peterlin.[17]

Taking for both Δ_c° and Δ_a° the value 0.073 of Culpin and Kemp,[69] and the measured birefringence, one obtains the following estimates: $f_a = 0.52$ or $C_{2a} = 0.68$. Assuming a normal distribution function over the angle α one obtains $C_{4a} = 0.52$.

RESULTS

Wide-line NMR spectra of the oriented nylon 66 fibers were obtained between −196°C and 200°C at alignment angles $\gamma = 0°$, 45°, and 90°. A selection of these spectra, as usual in their first derivative representation,[66] is shown in Figure 5. At elevated temperatures a narrow line develops as a consequence of vigorous segmental motion in noncrystalline regions, i.e., the α_a process. The distinction between broad and narrow lines is particularly easy in the spectra taken at $\gamma = 0°$ but is much less clear in the spectra taken at other angles. The variation of the peak-to-peak linewidth of these spectra with temperature appears in Figure 6. Whereas the linewidths at $\gamma = 0°$ are considered fairly accurate, those at 45° and 90° are only rough estimates, particularly at high temperatures, because of the uncertainty in locating the peaks of the broad line.

The experimental total second-moments, determined from these spectra, are shown in Figure 7 as a function of temperature, again at three alignment angles. It has been shown recently[42,59] that the second moment of an unoriented sample can be calculated from these data according to $S_{uo} = (1/15)[S(0°) + 8S(45°) + 6S(90°)]$, and this is represented by the thin

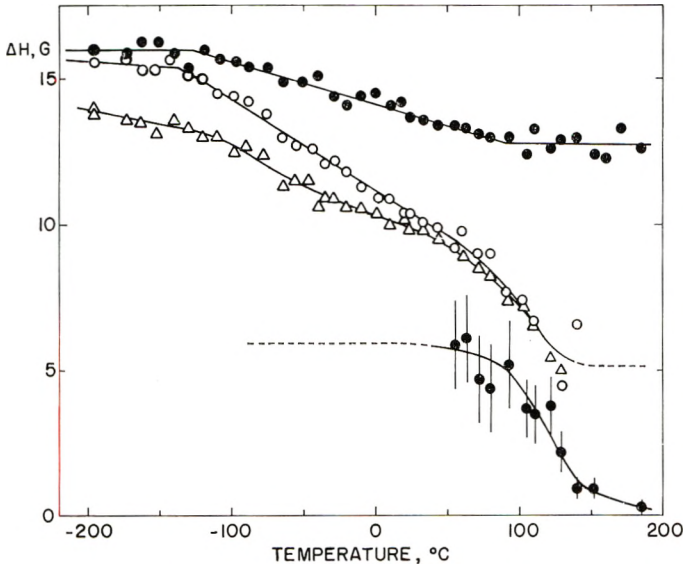

Fig 6. Linewidths for nylon 66. The 3 upper curves represent the apparent peak-to-peak width (in Gauss) of the broad line as a function of temperature at various alignment angles: (●) 0°; (△) 45°; (○) 90°. The bottom curve represents the width of the narrow line. Data from Olf and Peterlin.[17]

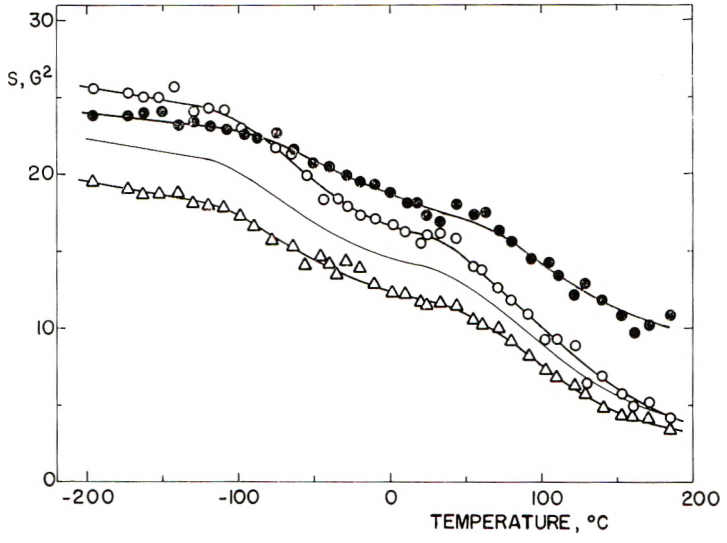

Fig. 7. Total second moment S (in Gauss^2) as a function of temperature at various alignment angles: (●) 0°; (△) 45°; (○) 90°. Data from Olf and Peterlin.[17]

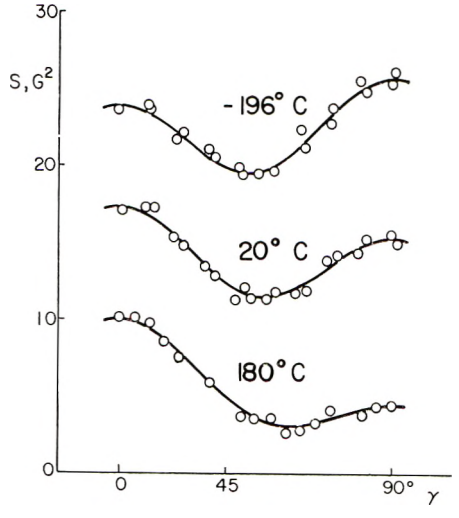

Fig. 8. Second moment for nylon 66 as a function of the alignment angle γ, measured at the indicated temperatures. Data from Olf and Peterlin.[17]

line in Figure 7. The second moments are seen to fall with rising temperature in two steps; the low-temperature decrease commences at about -100°C and is due to the γ process as has already been mentioned. The high temperature decrease begins at approximately 40°C and is caused by both the α_a and the α_c process. It will be shown in the discussion that the largest part of this decrease is due to the α_c process. Both the high and the low-temperature decreases of second moment are strongly dependent on

the alignment angle γ, the decrease at 90° always being greatest and that at 0° smallest.

At −198°C, 20°C, and 180°C the complete angle dependence of the second moment has been measured, as shown in Figure 8, the curves representing least-squares fits of eq. (1) to the data points. The values of A, B, and C were found to be 21.4, 23.2, and 25.7 at −196°C; 19.5, 17.4, and 15.3 at 20°C; and 14.6, 8.9, and 4.4 at 180°C. As shown previously,[42] estimates of C_2 and C_4 can be obtained from the values of A and B at −196°C, at which temperature molecular motion may be assumed to be frozen out (rigid lattice):

$$C_2 = 0.66$$

$$C_4 = 0.57.$$

These values characterize the overall orientation of the sample. The NMR value for C_2 can be compared with a value for C_2 derived from the birefringence, namely $C_2 = 0.84$. The disagreement is probably due to the approximations implicit in both methods.

DISCUSSION

The γ Process

The great similarity of the γ processes in nylon 66 and polyethylene is readily apparent from the present NMR results. One aspect of this is shown in Figure 9, where the relative decrease of second moment between −196°C and 20°C appears as a function of noncrystalline mass fraction $(1 - \alpha_m)$ for a number of linear polyethylene samples and for the nylon 66 fiber sample. The straight line is a least-squares fit to the polyethylene data and the point for nylon 66 falls rather close to this line. Extrapolation

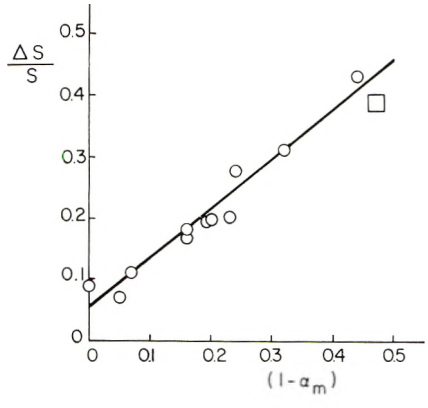

Fig. 9. Relative decrease of the powder-average second moment $\Delta S/S$, where ΔS is the decrease between −196°C and 20°C and S is the second moment at −196°C, as a function of the noncrystalline mass fraction $(1 - \alpha_m)$ for (○) polyethylene[42] and (□) nylon 66.

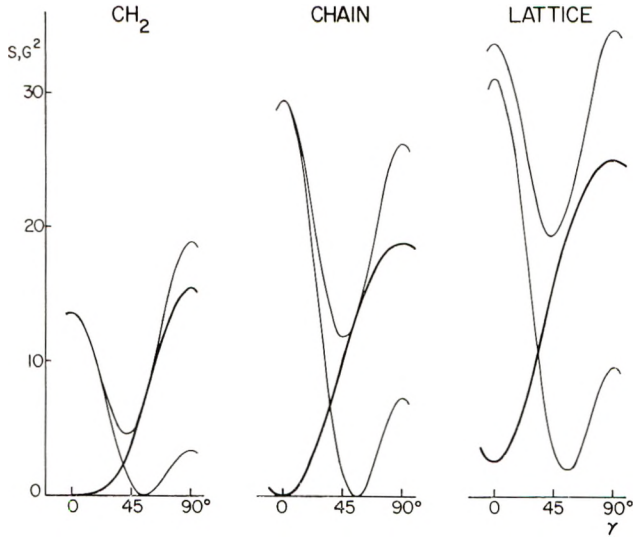

Fig. 10. Polyethylene as an example of a planar-zigzag chain of CH_2 groups. Assuming fiber symmetry and ideal orientation, the second moment of isolated CH_2 groups, of isolated chains, and of the whole crystal lattice is shown as a function of the alignment angle γ. The thin lines represent the rigid case (top) and full rotation around the chain axis (bottom). The heavy line represents the difference between these curves, that is the decrease of second moment due to rotation.

of the straight line to a completely crystalline sample yields a relative decrease in second moment which is entirely due to thermal lattice expansion and contains no motional contribution. The motional decrease of second moment is proportional to the noncrystalline fraction and hence the γ process arises from motion in noncrystalline regions.[41,42] Furthermore, it has been shown recently[41,42] that these results are consistent with full rotation of all noncrystalline chain segments around axes which remain nearly fixed in space. This immediately rules out the crankshaft mechanism[59,70] and the kink model[71,72] as discussed in a previous paper.[42] Since nylon 66 fits so well the plot for polyethylene (Fig. 9), it is suggested that these conclusions apply to the γ process of nylon 66 as well.

Another aspect to be considered is the dependence of this second-moment decrease on the alignment angle γ. This angle dependence has been investigated for the γ process in oriented polyethylene, specifically in cold-drawn polyethylene[53] and in oriented mats of polyethylene single crystal.[42] Drawn polyethylene exhibited a pronounced angle dependence which in fact was quite similar to that in nylon 66 (Figs. 7 and 8). Clearly, an angle-dependent γ process requires that the noncrystalline chain segments be oriented to some extent and that motion occur around axes which have a preferred orientation with respect to the fiber axis. In both drawn polyethylene and nylon 66 fibers the greatest decrease of second moment occurs at $\gamma = 90°$, the smallest at $\gamma = 0°$. This is consistent with rotating

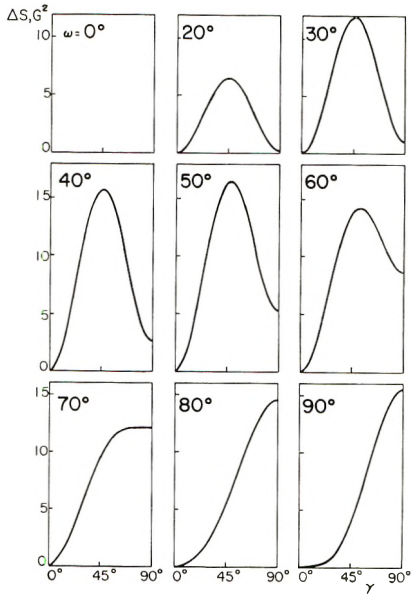

Fig. 11. Decrease in second moment due to rotation of an isolated CH_2 group as a function of the alignment angle γ between the fiber axis (or axis of rotation) and the magnetic field. The angle depeendence of this decrease is sensitive to the angle ω between the proton-proton vector and the axis of rotation.

planar-zigzag chains oriented along the fiber axis, the axis of rotation being parallel to the fiber axis. This is shown in Figure 10, where polyethylene is used as an example. The salient features are exhibited even by isolated CH_2 groups, a fact we shall use below.

At this point the objection may be raised that the noncrystalline regions are not made up by planar-zigzag chains, as implied above, but that strongly bent and tortuous chain conformations must prevail. The observation that the maximum decrease of second moment occurs at $\gamma = 90°$, however, poses a clear limit on randomness of conformation for a substantial fraction of the noncrystalline segments, as can be shown by the following argument. Consider, for example, a model fiber composed of isolated CH_2 groups which rotate around fixed axes parallel to the fiber axis. The decrease of second moment due to this rotation exhibits a certain dependence on the alignment angle γ between the fiber axis or axis of rotation and the magnetic field and this dependence is different for each angle ω the proton-proton vector subtends with the axis of rotation. This is shown in Figure 11, where ω assumes values between 0° and 90°. Only when ω lies from approximately 70° to 90°, as in segments with nearly extended planar-zigzag conformation, will the maximum second-moment decrease occur at the alignment angle $\gamma = 90°$; this condition is observed for the γ process in Figure 7, which supports the idea that those rotating segments responsible for the observed anisotropic decrease in second moment are close to their extended conformation.

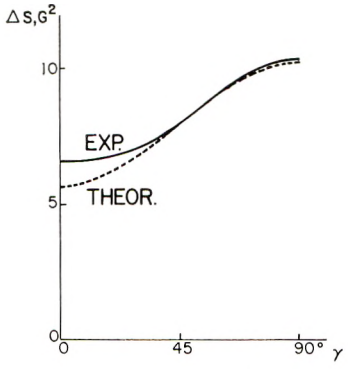

Fig. 12. Comparison of the experimental and the theoretical decrease of second moment due to the γ process, both as functions of the alignment angle γ.

It is believed that these noncrystalline chain segments are identical to the now well-established tie molecules which connect neighboring crystallites. During drawing these tie molecules become highly extended and oriented along the draw direction or fiber axis.[73–84] That a system without tie molecules, such as polyethylene single crystals, shows no angle dependence of the decrease in second moment due to the γ process[42] is, of course, in support of our contention. It has been argued recently that in polyethylene single crystals the noncrystalline component consists largely of chain folds and chain ends on the crystal surfaces. In agreement with the mentioned isotropic decrease in second moment it is reasonable to assume that the chain segments in these entities are nearly unoriented. A certain amount of chain folds and chain ends certainly exists in fibers and drawn material, and this may explain the fact that in the nylon 66 fibers, for example, the noncrystalline orientation ($C_{2a} \approx 0.68$) is smaller than the crystallite orientation ($C_{2c} \approx 0.97$).

Finally, a quantitative comparison of the model of rotating noncrystalline segments with experiment is made in Figure 12. The experimental decrease of second moment, shown as a function of γ, is the difference between the two upper curves in Figure 8. The theoretical decrease is obtained by using eq. (3) in the form

$$\Delta S(\gamma) = \alpha_m \Delta S_c(\gamma) + (1 - \alpha_m)\Delta S_a(\gamma)$$

where ΔS_c is the decrease due to the thermal lattice expansion in crystalline regions, for which 1 G² is used as a reasonable estimate. The motional decrease $\Delta S_a(\gamma)$ due to the γ process in noncrystalline regions is calculated with the orientation parameters obtained from birefringence measurements. The agreement can be considered satisfactory in view of the simplicity of the model and the uncertain orientation of the noncrystalline regions.

With respect to the line width data in Figure 6 the question may be raised as to how the γ process can possibly cause the narrowing of the broad line observed in the temperature range from approximately -120°C to

20°C, when the γ process is due as suggested to segmental motion in noncrystalline regions, while the broad line at 20°C presumably arises from immobile crystalline segments. The following explanation of this apparent paradox is offered. The γ process leads to a pronounced change of the line shape, as is shown by a comparison of the spectra at −196°C and −20°C in Figure 5. There is little doubt that this change is due to the presence of a line of intermediate width at −20°C. The linewidth is difficult to estimate but is probably between 5 G and 6 G. This has been indicated by the broken line at low temperatures in Figure 6. In unoriented samples this line is difficult to detect and, therefore, has escaped notice. The intermediate line corresponds to segments which become mobilized in the course of the γ process; it is transformed into a true narrow line only around 100°C because of the micro-Brownian motion excited at these temperatures (α_a process). As 47% (noncrystalline fraction) of the sample contributes to the intermediate line, one can readily visualize its effect of shifting the observed or apparent width of the broad line toward smaller values. The actual width of the broad line unfortunately cannot be extracted from the spectra (Fig. 5) without further assumptions, but is believed to remain essentially unchanged throughout the γ process.

Why is the apparent narrowing of the broad line (Fig. 6) dependent on the alignment angle? First, it is the appearance of the intermediate line in nylon 66 which causes the decrease in second moment associated with the γ process, just as in polyethylene.[85] Second, this decrease is greatest at $\gamma = 90°$ (Fig. 12), implying that the intermediate line is narrowest at this alignment angle. Finally, if one considers that the amplitude of a first-derivative line varies inversely with the square of its width, assuming no change in shape, then one realizes that the biasing effect of the intermediate line on the apparent width of the broad line must be most pronounced at $\gamma = 90°$ and least pronounced at $\gamma = 0°$, as is shown in Figure 6.

The α_c Process

As mentioned earlier, the decrease in second moment above room temperature results from the simultaneous onset of the well established micro-Brownian motion in the noncrystalline regions (α_a process) as well as motion in the crystalline regions (α_c process). The existence of these two separate processes can be shown as follows. Assume that at 180°C segmental motion in noncrystalline regions is so effective that their second moment S_a has vanished. If there were no motion in crystalline regions at all, then according to eq. (3) the powder-average second moment would be given by $S = \alpha_m S_c \approx 9.9$ G², if we use for S_c the value for the pseudohexagonal rigid lattice from Figure 4. In actuality, it is 4.4 G² (Fig. 7), and this divergence implies considerable segmental motion in the crystallites. In this argument it has been assumed that the crystalline fraction at 180°C is still 0.53, the value measured at room temperature. Justification for this assumption derives from two considerations. First, 180°C is still 80°C below the melting point[28] of nylon 66, so partial melting is not expected to occur to an

appreciable degree. Second, it has been reported by McCall and Anderson[13] and by McMahon[19] that the fraction of segments not engaged in micro-Brownian motion remains constant in the temperature range between the α_a process and temperatures well above 180°C. This fraction would have varied with temperature if α_m had changed.

There remains the difficulty of distinguishing in the experimental second moment data between the noncrystalline and the crystalline contributions, S_a and S_c. To do this, the following simple procedure has been adopted. One must only realize that the narrow line at 180°C has a fairly small second moment. An estimate based on the narrow line of the spectrum

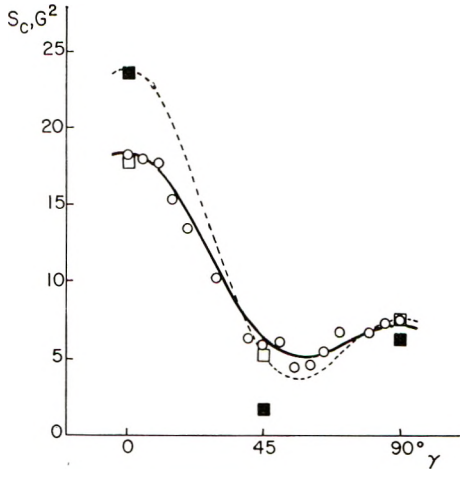

Fig. 13. Variation of the second moment $S_c(\gamma)$ in crystalline regions with alignment angle γ: (——) theoretical curve; (□) McMahon's[18] experimental values and (■) theoretical predictions.

taken at $\gamma = 0^c$, where the separation is relatively straightforward (Fig. 5), yielded 0.9 G^2. Furthermore, the low value of the second moment of the narrow line as well as its sharpness make it clear that a rather general type of motion (micro-Brownian) is taking place at 180°C in noncrystalline regions. Therefore, it is safe to assume that S_a is independent of the alignment angle γ at 180°C. With these considerations in mind, the second moment of the crystalline regions can be expressed by rearranging eq. (3),

$$S_c(\gamma) = [S(\gamma) - 0.9(1 - \alpha_m)]/\alpha_m$$

Application of this expression to the second moments $S(\gamma)$ measured at 180°C (Fig. 8) yields the data points for $S_c(\gamma)$ shown in Figure 13. The powder-average second moment turns out to be (7.5 ± 1.5) G^2, where the error given arises from the experimental uncertainties in S, S_a, and α_m. This value is well below the second moment 21.2 G^2 for the pseudohexagonal rigid-lattice, which again indicates the presence of segmental motion in crystalline regions.

These data will now be compared to theoretical predictions based on the motional models of rotational oscillation and 60° flip-flop motion. First, the two motions must be shown to be effective enough to account for the experimental decrease in second moment. If this condition is fulfilled, the oscillation amplitude δ consistent with the above-mentioned powder-average second moment is determined. The final test of these motional models consists of deciding whether or not they correctly describe the experimentally observed angle dependence of $S_c(\gamma)$ shown in Figure 13.

Pure 60° flip-flop motion would lower the powder average second moment to a value of only 11.7 G^2 (Fig. 4) and hence is not vigorous enough. Evidently, additional oscillation around each of the two equilibrium sites in the manner described earlier is needed to reduce the second moment to the observed value of (7.5 ± 1.5 G^2). Rotational oscillation as well as the 60° flip-flop motion are found to be capable of accounting for the powder average second moment, rquiring amplitudes of $\delta = (59^{+40}_{-15})°$ and $\delta = (47^{+40}_{-15})°$, respectively (Fig. 4). By using the crystallite orientation parameters determined by x-ray scattering, theoretical predictions of the dependence of second moment on alignment angle are obtained. It is found that rotational oscillation and the 60° flip-flop motion result in very nearly the same angle dependence shown in Figure 13 by the broken curve. The reason for this similarity lies in the fact that the angular amplitudes δ required for both motions are so large that their effect on the second moment is quite similar to that of full rotation, the limiting case in which the two models become strictly identical. For this reason a distinction between the two models by the present method is not possible. In the following it will therefore suffice to discuss only one of the models, for instance rotational oscillation.

The agreement of the broken theoretical curve with experiment (Fig. 13) is qualitative at best; quantitatively there is considerable disagreement at $\gamma = 0°$, where the theoretical prediction exceeds the experimental value by nearly 6 G^2. It is believed that this disagreement is due to the neglect of chain torsion in the calculations. That torsion is undoubtedly present to an appreciable extent at 180°C is suggested, for example, by the pronounced shortening of the identity period along the chain which has been reported by Slichter.[5] Excellent quantitative agreement between theory and experiment is in fact achieved when torsion is taken into account at the expense of rigid rod oscillation, as can be judged by the close fit of the solid theoretical curve to the experimental points in Figure 13. This curve has been obtained by assuming rotational oscillation of angular amplitude 52° with superimposed harmonic chain torsion in which neighboring CH_2 groups oscillate around the carbon-carbon bond with an amplitude of 40° relative to each other.

For comparison, experimental second moments at 150°C and theoretical predictions of a previous study[18] have been included in Figure 13. Whereas the experimental values are in agreement with the present results, the theoretical predictions are not, owing to their approximate nature and particularly because of the neglect of chain torsion.[18]

A final comment on the 60° flip-flop model is in order. It does not seem reasonable to consider this motion for the CH_2 sequences in nylon 66, since the large amplitude required essentially destroys the two-site character of the motion. This, however, does not altogether rule out the possibility that the chain molecules engage in this motion in the manner suggested by Schmidt and Stuart.[28] It is conceivable that the amide groups, in particular, perform nearly pure 60° flip-flop motion since their equilibrium sites should be relatively sharply defined by the hydrogen bonds which effectively restrict their oscillation around each equilibrium site. In the paraffinic sections of the chains, however, there is torsional motion in addition to any pure 60° flip-flop motion as shown by the present experiments as well as by x-ray results.[5] This torsion appears to be of considerable amplitude and, as can be shown, would also result in a pronounced component of oscillation of a given CH_2 group around the segment axis. The main features of this description are compatible with our experimental results.

CONCLUSION

The NMR second moment data at temperatures between −196°C and 20°C indicate that the γ process in nylon 66 consists of segmental motion in noncrystalline regions, in agreement with earlier suggestions.[1-3] The magnitude of the overall decrease in second moment is in agreement with all noncrystalline chain segments rotating around axes fixed in space, as in the γ process of polyethylene.[42] The dependence of this decrease on the alignment angle between fiber axis and magnetic field shows that a sensible fraction of the rotating segments are close to a planar zigzag conformation and well oriented along the fiber axis. It is suggested that these segments are identical with tie molecules.

The second moment at high temperatures shows the presence of considerable motion in crystalline regions, and this is referred to in this paper as the α_c process. By a simple straightforward scheme the second moment S_c of the crystalline regions was extracted from the experimental second moment at 180°C and the angle dependence was analyzed in terms of motional models. As a result it is found that simple oscillation or 60° flip-flop motion of rigid chain segments around their axes cannot account quantitatively for the observed angle dependence; when torsion of the chains is admitted and superimposed on these motions excellent agreement between theory and experiment is obtained. The amplitudes for both oscillation and torsion are appreciable, approximately 50° and 40°, respectively. It has not been possible to distinguish between rotational oscillation and the 60° flip-flop motion of the paraffinic portion of the nylon 66 molecule, that portion "seen" by the NMR method. Pure 60° flip-flop motion is not efficient enough to account for the large decrease in S_c due to the α_c process. Considerable amplitudes of oscillation around each of the two equilibrium sites as well as torsion are needed so that the two-site character of the motion is lost. This does not exclude the possibility that the amide groups

which engage in extensive hydrogen bonding might perform pure 60° flip-flop motion in a manner suggested by Schmidt and Stuart.[28]

The authors gratefully acknowledge the support of this work by the Camille and Henry Dreyfus Foundation and by the U.S. Air Force Materials Laboratory, Wright-Patterson Air Force Base, Ohio, under Contract No. AF 33(615)-2244 effective during 1965/66. They also wish to thank Dr. G. W. Sovereign of the Chemstrand Research Center, Research Triangle Park, N. C., for supplying the nylon 66 fiber sample, and Dr. N. Morosoff of this laboratory for his help with the x-ray experiments.

References

1. K. Schmieder and K. A. Wolf, *Kolloid-Z.*, **134**, 149 (1953).
2. A. E. Woodward and J. A. Sauer, in *The Physics and Chemistry of the Organic Solid State*, D. Fox, M. M. Labes, and A. Weissberger, Eds., Interscience, New York, 1965, Vol. II, Chap. 7.
3. N. G. McCrum, B. E. Read, and G. Williams, *Anelastic and Dielectric Effects in Polymeric Solids*, Wiley, New York–London, 1967.
4. W. P. Slichter, *J. Appl. Phys.*, **26**, 1099 (1955).
5. W. P. Slichter, *J. Polym. Sci.*, **35**, 77 (1959).
6. A. E. Woodward, R. E. Glick, J. A. Sauer, and R. P. Gupta, *J. Polym. Sci.*, **45**, 367 (1960).
7. R. E. Glick, R. P. Gupta, J. A. Sauer, and A. E. Woodward, *J. Polym. Sci.*, **42**, 271 (1960).
8. K. H. Illers and R. Kosfeld, *Makromol. Chem.*, **42**, 44 (1960).
9. D. J. Shaw and B. A. Dunnell, *Can. J. Chem.*, **39**, 1154 (1961).
10. D. W. Jones, *Polymer*, **2**, 203 (1961).
11. R. P. Gupta, *J. Phys. Chem.*, **65**, 1128 (1961).
12. D. W. Jones, *J. Polym. Sci.*, **59**, 271 (1962).
13. D. W. McCall and E. W. Anderson, *Polymer*, **4**, 93 (1963).
14. S. N. Zhurkov and E. A. Yegorov, *Dokl. Akad. Nauk SSSR*, **152**, 1155 (1963).
15. Y. Sekita and K. Kawasaki, *Repts. Progr. Polym. Phys. Japan*, **7**, 283 (1964).
16. R. E. Glick and R. C. Phillips, *J. Polym. Sci. A*, **3**, 1885 (1965).
17. H. G. Olf and A. Peterlin, Technical Report AFML-TR-67-6 to the Air Force Materials Laboratory, 1966.
18. P. E. McMahon, *J. Polym. Sci. A-2*, **4**, 639 (1966).
19. P. E. McMahon, *J. Polym. Sci. B*, **4**, 75 (1966).
20. P. E. McMahon, *J. Polym. Sci. B*, **4**, 43 (1966).
21. P. E. McMahon, *J. Polym. Sci. A-2*, **4**, 501 (1966).
22. P. F. Dismore and W. O. Statton, in *Small Angle Scattering from Fibrous and Partially Ordered Systems* (*J. Polym. Sci. C, 13*) R. H. Marchessault, Ed., Interscience, New York, 1966, p. 133.
23. C. S. Fuller, W. O. Baker, and N. R. Pape, *J. Amer. Chem. Soc.*, **62**, 3275 (1940).
24. W. O. Baker and C. S. Fuller, *J. Amer. Chem. Soc.*, **64**, 2399 (1942).
25. R. Brill, *J. Prakt. Chem.*, **161**, 49 (1943).
26. R. Brill, *Makromol. Chem.*, **28/29**, 294 (1956).
27. I. Sandemann and A. Keller, *J. Polym. Sci.*, **19**, 401 (1956).
28. G. F. Schmidt and H. A. Stuart, *Z. Naturforsch.*, **13a**, 222 (1958).
29. H. W. Starkweather, J. F. Whitney, and D. R. Johnson, *J. Polym. Sci. A*, **1**, 715 (1963).
30. D. S. Trifan and I. F. Terenzi, *J. Polym. Sci.*, **28**, 443 (1958).
31. E. Bessler and G. Bier, *Makromol. Chem.*, **122**, 30 (1969).
32. P. W. Allen, *Research*, **5**, 492 (1952).
33. R. C. Wilhoit and M. Dole, *J. Phys. Chem.*, **57**, 14 (1953).

34. A. E. Woodward, J. A. Sauer, C. W. Deeley, and D. E. Kline, *J. Colloid Sci.*, **12**, 363 (1957).
35. C. W. Deeley, A. E. Woodward, and J. A. Sauer, *J. Appl. Phys.*, **28**, 1124 (1957).
36. K. H. Illers, *Makromol. Chem.*, **38**, 168 (1960).
37. K. H. Illers and H. Jacobs, *Makromol. Chem.*, **39**, 234 (1960).
38. K. H. Illers, *Materialprüfung*, **2**, 269 (1960).
39. J. Kolařik and J. Janáček, in *Macromolecular Chemistry Prague 1965* (*J. Polym. Sci. C*, **16**), O. Wichterle and B. Sedláček, Eds., Interscience, New York, 1967, p. 441.
40. H. G. Olf and A. Peterlin, *Kolloid-Z. Z. Polym.*, **212**, 12 (1967) (Part II of this series).
41. H. G. Olf and A. Peterlin, *Kolloid-Z. Z. Polym.*, **215**, 97 (1967).
42. H. G. Olf and A. Peterlin, *J. Polym. Sci. A-2*, **8**, 771 (1970).
43. C. W. Bunn and E. V. Garner, *Proc. Roy. Soc.* (London), **A189**, 39 (1947).
44. L. H. Meyer, Thesis, University of Illinois, 1953.
45. W. P. Slichter, *J. Polym. Sci.*, **24**, 173 (1957).
46. D. Hyndman and G. F. Origlio, *J. Polym. Sci.*, **39**, 556 (1959).
47. D. W. McCall and W. P. Slichter, *J. Polym. Sci.*, **26**, 171 (1957).
48. D. Hyndman and G. F. Origlio, *J. Appl. Phys.*, **31**, 1849 (1960).
49. D. Hyndman and G. F. Origlio, *J. Polym. Sci.*, **46**, 259 (1960).
50. K. Yamagata and S. Hirota, *Repts. Progr. Polym. Phys. Japan*, **5**, 236 (1962).
51. A. Peterlin and H. G. Olf, *J. Polym. Sci. B*, **2**, 409 (1964) (Part I of this series).
52. A. Peterlin and H. G. Olf, *J. Polym. Sci. B*, **2**, 769 (1964) (Part III of this series).
53. H. G. Olf and A. Peterlin, *J. Appl. Phys.*, **35**, 3108 (1964) (Part IV of this series).
54. A. I. Koltsov and M. W. Volkenstein, *Vysokomol. Soedin.*, **7**, 250 (1965).
55. J. B. Lando, H. G. Olf, and A. Peterlin, *J. Polym. Sci. A-1*, **4**, 941 (1966).
56. A. Peterlin and H. G. Olf, *J. Polym. Sci. A-2*, **4**, 587 (1966) (Part V of this series).
57. H. G. Olf and A. Peterlin, *Makromol. Chem.*, **104**, 135 (1967) (Part VI of this series).
58. V. J. McBrierty and I. M. Ward, *Brit. J. Appl. Phys.* [2], **1**, 1529 (1968).
59. H. G. Olf and A. Peterlin, *J. Polym. Sci. A-2*, **8**, 753 (1970).
60. H. G. Olf and A. Peterlin, *J. Polym. Sci. A-2*, **8**, 791 (1970).
61. H. A. Stuart, *Die Physik der Hochpolymeren*, Vol. 1, Springer-Verlag, Berlin-Göttingen-Heidelberg, 1952, p. 173.
62. L. Pauling, *The Nature of the Chemical Bond*, Cornell Univ. Press, Ithaca, N. Y., 3rd ed., 1960.
63. D. R. Davies and R. A. Pasternak, *Acta Cryst.*, **9**, 334 (1956).
64. *International Tables for X-ray Crystallography*, N. F. M. Henry and K. Lonsdale, Eds., The Kynoch Press, Birmingham, England, 1962.
65. H. W. Starkweather and R. E. Moynihan, *J. Polym. Sci.*, **22**, 363 (1956).
66. J. G. Powles, *Polymer*, **1**, 219 (1960).
67. B. F. Decker, E. T. Asp, and D. Harker, *J. Appl. Phys.*, **19**, 388 (1948).
68. R. S. Stein and F. H. Norris, *J. Polym. Sci.*, **21**, 381 (1956).
69. M. F. Culpin and K. W. Kemp, *Proc. Phys. Soc.*, **69**, 1301 (1956).
70. T. Schatzki, *J. Polym. Sci.*, **57**, 496 (1962).
71. W. Pechhold and S. Blasenbrey, *Kolloid-Z. Z. Polym.*, **216/217**, 235 (1967).
72. W. Pechhold, *Kolloid-Z. Z. Polym.*, **228**, 1 (1968).
73. G. Meinel and A. Peterlin, *J. Polym. Sci. B*, **5**, 197 (1967).
74. G. Meinel and A. Peterlin, *J. Polym. Sci. A-2*, **6**, 587 (1968).
75. G. Meinel, A. Peterlin, and K. Sakaoku, in *Analytical Calorimetry*, R. S. Porter and J. F. Johnson, Eds., Plenum Press, New York, 1968, pp. 15–22.
76. W. Glenz and A. Peterlin, *J. Macromol. Sci. (Phys.)*, **B5**, 473 (1970).
77. A. Peterlin, in *Structure and Properties of Polymers* (*J. Polym. Sci. C*, **9**), A. V. Tobolsky, Ed., Interscience, New York, 1965, p. 61.
78. A. Peterlin, in *U.S.-Japan Seminar in Polymer Physics* (*J. Polym. Sci. C*, **15**), R. S. Stein and S. Onogi, Eds., Interscience, New York, 1967, p. 427.

79. A. Peterlin, in *The Meaning of Crystallinity in Polymers* (*J. Polym. Sci. C*, **15**), F. P. Price, Ed., Interscience, New York, 1967, p. 123.
80. A. Peterlin, *Kolloid-Z. Z. Polym.*, **216/217**, 129 (1967).
81. A. Peterlin, *Man-Made Fibers*, H. Mark, S. M. Atlas, and E. Cernia, Eds., Interscience, New York, 1967, Vol. I, pp. 283–340.
82. G. Meinel, N. Morosoff, and A. Peterlin, *J. Polym. Sci. A-2*, **8**, 1723 (1970).
83. A. Peterlin, *Polym. Eng. Sci.* **9**, 172 (1969).
84. W. Glenz and A. Peterlin, *J. Polym. Sci. A-2*, **9**, 1191 (1971).
85. K. Bergmann and K. Nawotki, *Kolloid Z. Z. Polym.*, **219**, 132 (1967).

Received October 19, 1970
Revised January 25, 1971

JOURNAL OF POLYMER SCIENCE: PART A-2 VOL. 9, 1471–1481 (1971)

Single Crystals of Amylose V Complexes. III. Crystals with 8_1 Helical Configuration

YUHIKO YAMASHITA and KAZUO MONOBE, *School of Engineering, Okayama University, Okayama, Japan*

Synopsis

Single crystals of amylose V complexes with the 8_1 helical configuration can be obtained from aqueous solutions of amylose by using α-naphthol as a complexing agent. Morphological observations suggest that the differences in crystallization behavior among the α-naphthol complex and other complexes with alcohols are due to differences in solubility of the complexes in water. Electron diffraction studies indicate a two-dimensional tetragonal unit cell with $a = b = 22.9$ Å. It is deduced that the space group providing a satisfactory arrangement of two helices is one of the enantiomorphs $P4_12_12$ and $P4_32_12$. From x-ray diffraction it was found that the c axis spacing of the α-naphthol complex is equivalent to that in 6_1 and 7_1 helical amylose crystals. Consequently, the geometry of the helical configuration requires an integral number of glucose residues per turn. The true helical diameters of the *n*-butanol, isopropanol, and α-naphthol complexes were calculated from experimental data. The ratio was 6:7:8 and indicated that the helix of the α-naphthol complex has eight glucose residues per turn. The diversity of helical configurations in V amylose crystals is discussed.

INTRODUCTION

Amylose has the interesting property of forming crystalline complexes with low molecular weight substances, such as iodine, alcohols, ketones and fatty acids. Studies on the properties and structures of these complexes were carried out extensively by Bear[1] and Rundle[2–5] in the 1940's. However there remain unsolved problems, such as (1) the mechanism of the formation of these complexes; (2) the stability and conformation of the low molecular weight substances in the interior of the amylose helix; (3) the conformation of the glucopyranose rings and the ether linkages of the amylose molecule in the helical structure.

It may seem rather surprising, considering the wide natural occurrence and importance of amylose and increasing interest in the clathrate compounds, that only little attention has been directed to structural study of amylose V complexes. In part, this may be accounted for by difficulties encountered in producing oriented specimens of amylose V crystals and to the limitations on structural information obtainable from x-ray and other physical techniques applied to powder specimens.

In recent years, the morphology and structure of single crystals of amylose V complexes formed by precipitation from aqueous solution with

straight-chain and branched-chain alcohols have been reported[6,7] from our laboratory. In the first paper it was shown that the crystals obtained with a straight-chain alcohol (*n*-butanol) consisted of lamellae about 100 Å in thickness and had many features in common with lamellar crystals from linear synthetic polymers. Thus it was confirmed that the concept of chain folding could be applied to lamellar crystals of amylose V complexes with the large helix diameter of 13.7 Å. The hexagonal electron diffraction pattern from single crystals provided strong support for the helical structure pictured by Rundle[5] as close-packed helices with six glucose residues per turn (6_1 helix). In the second paper it was demonstrated that lamellar crystals of amylose V complexes with 7_1 helical configuration can be obtained by using branched chain alcohols (isopropyl, isobutyl, *sec*-butyl and *tert*-butyl alcohols).

The occurrence of cyclic oligomers (the α, β, and γ Schardinger dextrins[8] which correspond to cyclohexaglucose, cycloheptaglucose and cyclooctaglucose) composed of glucose residues bonded by α-1,4-glucosidic linkages as in amylose,[9,10] lead us to expect amylose V crystals with 8_1 helical configuration. Accordingly, we tried to prepare these crystals by precipitation from aqueous solution of amylose with α-naphthol, which has a larger molecular cross section than straight-chain and branched-chain alcohols.

The purpose of the present paper is to report results of morphological and structural studies on single crystals of amylose V with 8_1 helical configuration. Ultimately it is hoped that studies of single crystals will supply some answer for the above-mentioned unsolved problems.

EXPERIMENTAL

Preparation of Amylose V Complexes with α-Naphthol

Amylose V complexes with α-naphthol were prepared as follows. A 10-g portion of potato starch was dispersed in 800 ml. of water by heating the mixture at 70°C for 1 hr. in a thermostat. The hot turbid starch dispersion was filtered rapidly. The resulting amylose solution was heated to 95°C again, a 0.2 g portion of α-naphthol was added to 100 ml of the above solution, and the whole was stirred gently. The solution was kept at a constant temperature of 95°C for 10 hr and then cooled slowly to room temperature. After a few days the resulting crystals of the α-naphthol complex were examined by electron microscopy and x-ray and electron diffraction. To obtain the degree of polymerization of the leached potato amylose, the intrinsic viscosity in 1*N* NaOH at 22.5°C was measured. This value was 115 ml/g and corresponds to an average degree of polymerization of 850 from the viscosity–molecular weight relation derived by Greenwood et al.[11]

Morphological Observations and Electron Diffraction Studies

Drops of the above crystal suspension were placed on carbon-coated grids and the solvents were evaporated. The specimens were shadowed with Pt–Pd and examined by direct transmission in a HU 11B electron

microscope. Selected-area electron diffraction experiments were carried out in the same instrument. Calibration of the diffraction spots was made with the aid of a thin evaporated layer of aluminum on the same specimens.

X-Ray Diffraction Studies

The film was obtained by filtering the crystal suspension of the α-naphthol complex carefully. The x-ray diffraction photographs for the oriented films of the sedimented lamellar crystals were obtained in a cylindrical camera with nickel-filtered CuKα radiation.

RESULTS AND DISCUSSION

Morphology and Crystallization Behavior of Amylose–α-Naphthol Complex

Figure 1 shows the morphology obtained when the crystals were sampled from a suspension which had been cooled slowly from 95°C to room temperature and allowed to age for a few days. These micrographs show that the crystals have a square habit different from those of the *n*-butanol and isopropyl alcohol complexes and that they consist of stacks of small thin lamellae. The thickness of each lamella is estimated from the shadow length to be about 100 Å. Dislocation-centered spiral growth was not observed in these crystals, but the crystals thicken by epitaxial growth oriented on the lower lamellae. The small grainlike particles surrounding the lamellar crystals are uncrystallized amylose which precipitates when the solvent is evaporated.

In Figure 2 are shown the interesting morphologies obtained when the crystals from the suspension are sampled at various temperatures during cooling from the crystallization temperature of 95°C. These micrographs show that the square crystals shown in Figure 1 are not formed directly from solution. The crystals in these micrographs seem to have been formed when drops of solution cooled to room temperature or evaporated on the electron microscope grid. However, crystallization does not occur if α-naphthol is added to amylose solution at room temperature. This indicates that a requirement for crystallization of amylose V is that random-coil molecules be converted to helical molecules at high temperature by complexing agent. In this respect the formation of the crystalline complex with α-naphthol is different from that of the *n*-propanol, isopropanol, *sec*-butyl alcohol or *tert*-butyl alcohol complexes, for which the greater part of the amylose in solution precipitates in the form of regular shaped lamellae at the crystallization temperature.[6,7] It may be that the difference in crystallization behavior between the α-naphthol complex and other alcohol complexes is due to a difference in the solubility of amylose. As the solubility of the α-naphthol complex in water is particularly large, crystallization occurs only at high supercooling.

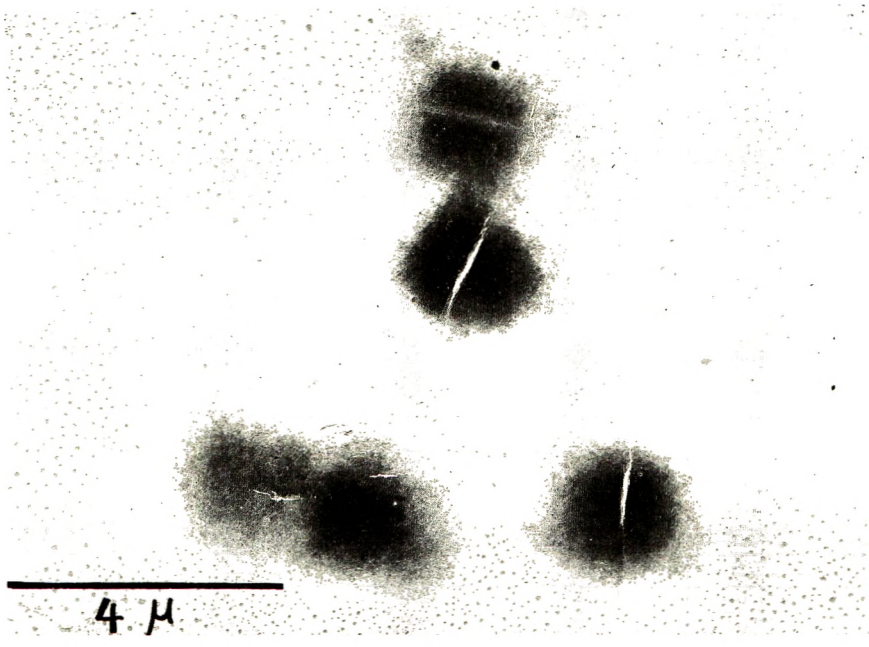

(*a*)

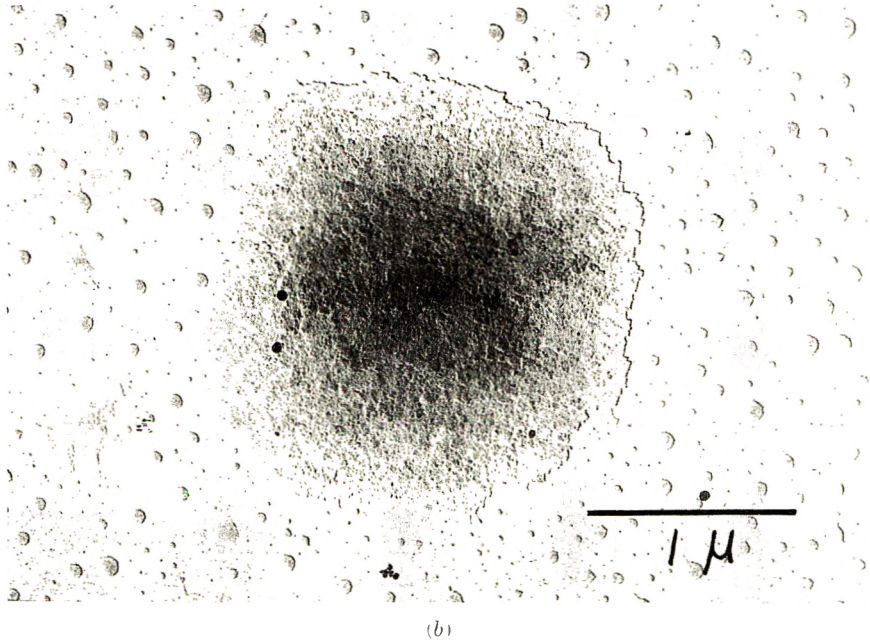

(*b*)

Fig. 1. Typical morphology of single crystals of amylose–α-naphthol complex. The crystals are from a suspension cooled slowly from 95°C to room temperature and aged for a few days: (*a*) low magnification, (*b*) high magnification.

The Crystal and Molecular Structure of the α-Naphthol Complex

A selected-area electron diffraction pattern from the lamellar crystals obtained with α-naphthol is shown in Figure 3. The position and intensities of these spots are transcribed on the reciprocal lattice in Figure 4. This pattern differs from those of the *n*-butanol complex with a 6_1 helix and the isopropanol complex with 7_1 helix shown in the previous papers.[6,7] It seems certain that these crystals precipitated with α-naphthol are composed of helical chains because α-naphthol, like *n*-butanol and isopropanol, has been reported as an agent for starch fractionation into amylose and amylopectin.[12] If the helical chains are oriented perpendicular to the lamellae as reported for the *n*-butanol and isopropanol complexes, then Figure 3 represents a two-dimensional net in the zero layer of the reciprocal lattice. It can be suggested from the symmetry of the pattern and the spacings of the spots that the unit cell of these crystals is tetragonal and the lattice constants are $a = b = 22.9$ Å, with c unknown. From the size of the unit cell it is apparent that there are two helices running through the unit cell.

If the α-naphthol complex has a tetragonal structure, the space group must belong to one of the point groups C_4, S_4, D_4. All other point groups C_{4h}, C_{4v}, D_{2d}, D_{4h} of the tetragonal system contain planes of symmetry which are not permitted to the optically active amylose molecules. Since the helical chain itself can have no fourfold axis and alternate chains must run in opposite directions on the basis of chain folding, it is deduced that the tetragonal space groups providing a satisfactory arrangement of two helices per unit cell are the enantiomorphic pair D_4^4-$P4_12_12$ and D_4^8-$P4_32_12$. In either space group $P4_12_12$ or $P4_32_12$, each helix axis is coincident with a fourfold screw axis and the molecular coordinates of two helical chains directed in opposite directions are $(0, 1/2, Z)$ and $(1/2, 0, -Z)$. Such structures are permitted by the equatorial reflections from the electron diffraction pattern, which are observed only for $h + k = 2n$. If the conformation of minimum internal steric hindrance of the glucopyranose ring is determined, the occurrence of $P4_12_12$ (right-handed helix) or $P4_32_12$ (left-handed helix) will be established. Detailed consideration of this point will be made in the future. Now the structure of the α-naphthol complex based on the space group $P4_12_12$ is shown in Figure 5.

In order to obtain information on the ordering along the *c* axis, the film obtained by filtering the crystal suspension of the α-naphthol complex was used for x-ray diffraction studies. When the x-ray beam was directed parallel to the film surface, the x-ray diffraction photograph showed a fiber-like pattern, as in Figure 6. The four principal equatorial lines can be indexed by using the lattice constants of the unit cell determined from the electron diffraction pattern, and the three lines of the first layer can also be indexed by the Bernal method. The index assignments of the lines are shown in Figure 6. It is well known that the lamellar crystals in such films

(*a*)

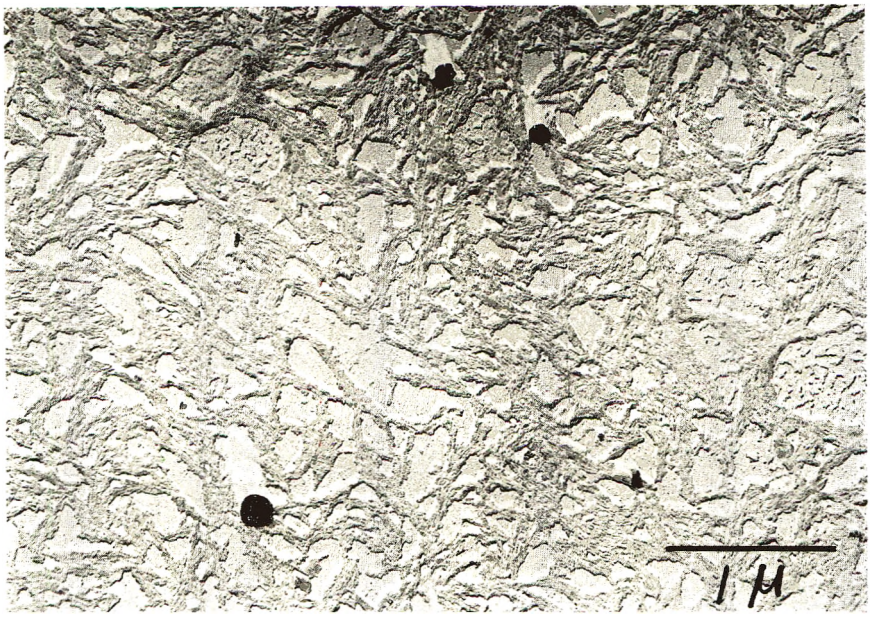

(*b*)

Fig. 2 (*continued*)

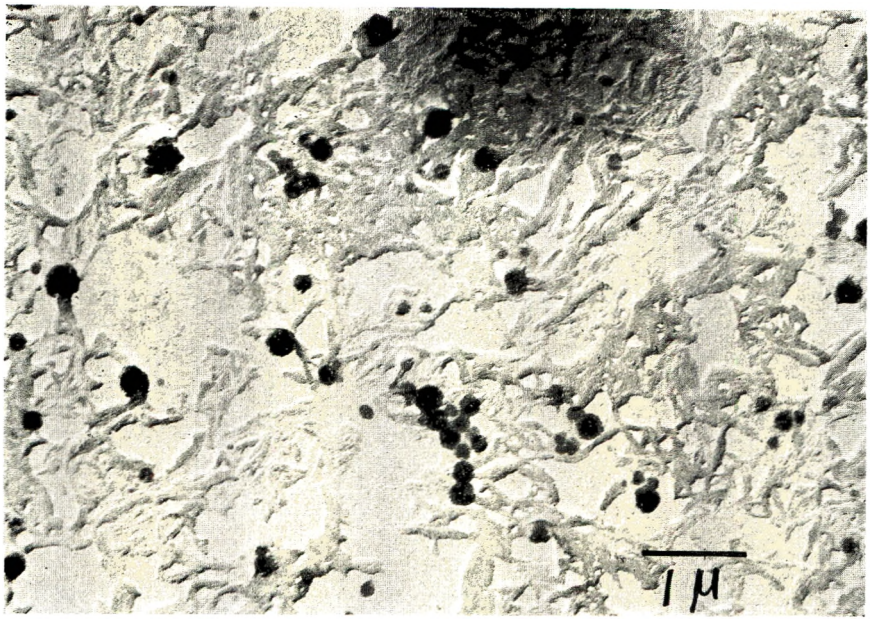

(*c*)

Fig. 2. Morphologies obtained from suspensions sampled at various temperatures during cooling from the crystallization temperature of 95°C: (*a*) 90°C; (*b*) 70°C; (*c*) 30°C.

Fig. 3. Electron diffraction pattern from single crystals of amylose–α-naphthol complex.

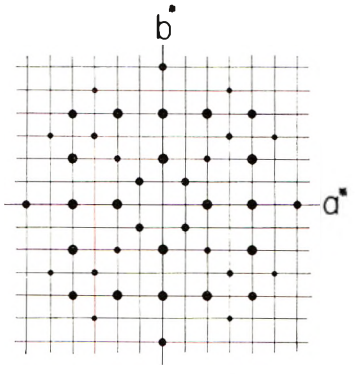

Fig. 4. Drawing showing the position and intensity of the spots in Fig. 3 on the reciprocal lattice of the equatorial plane.

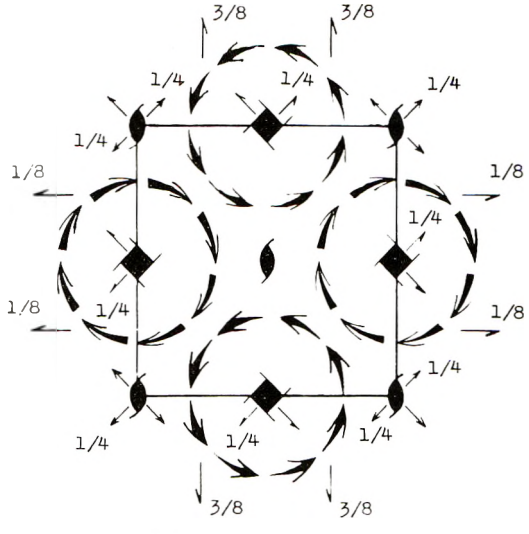

Fig. 5. Structure of the amylose–α-naphthol complex based on the space group $P4_12_12$ (right-handed). Arrows indicate the direction of the amylose molecule.

lie with their basal plane parallel to the film surface. Therefore, this fiber-like pattern clearly indicates that the helical chains are oriented perpendicular to the lamella in a manner similar to that found in other amylose V single crystals. The measurement of a layer spacing provides us with a 7.8 Å c axis spacing for this helix. This is equivalent, within experimental error, to values determined for the n-butanol and isopropanol complexes. This fact shows that the stacking of glucose residues along each helix in the three helical configurations is similar and the spacing is approximately the width of a glucose residue.

An analysis of the lattice constants and the molecular packing mode leads to a characterization of the amylose helix as larger than the 6_1 and 7_1 helices. The external diameter of this helix is 16.2 Å. From the x-ray diffrac-

tion study described above it has been found that the c axis spacing of this helix is equivalent to values for the 6_1 and 7_1 helices. Consequently, the geometry of the helical conformation requires an integral number of glucose residues per turn. In view of the equality of the c axis spacings, a comparison of true helical diameters in the three different amylose V complexes will fix the number of glucose residues per turn in the α-naphthol complex.

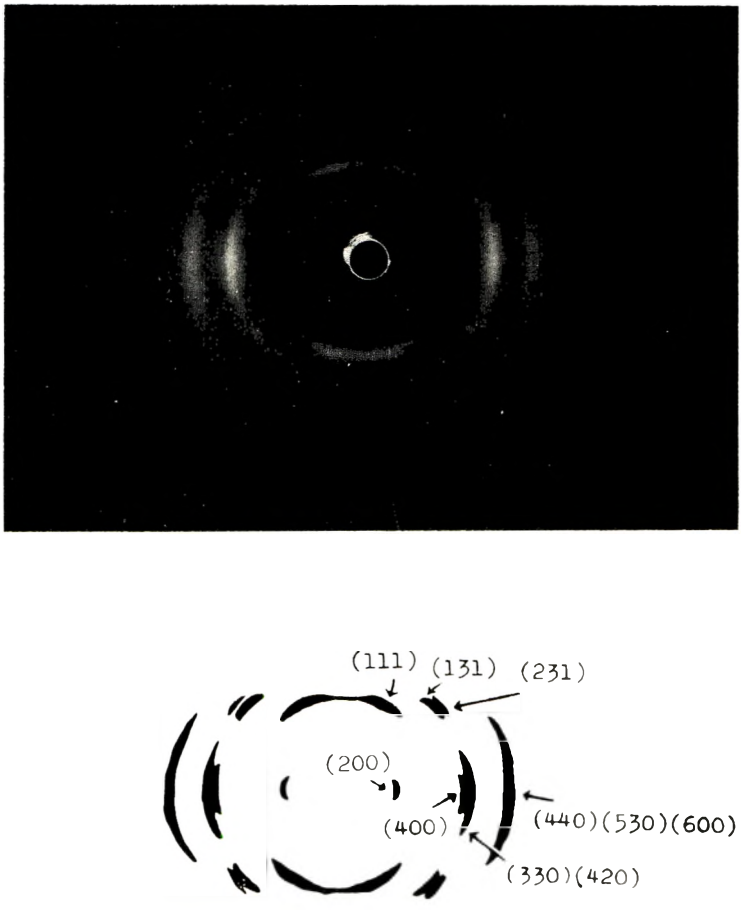

Fig. 6. X-Ray diffraction photograph obtained from film of sedimented lamellar crystals. The x-ray beam was oriented along the equator. A cylindrical camera was used.

(The term, helix diameter, has been used by us and other investigators to signify the nearest-neighbor intermolecular distance, i.e., the "external helix diameter" in the strict sense of the word.) The external helix diameters $D(6_1)$, $D(7_1)$ of the 6_1 and 7_1 helices, which were evaluated from the electron diffraction patterns for thoroughly dried specimens of the n-butanol and isopropanol complexes in our previous papers,[6,7] were 13.2 and 14.7 Å, respectively. If the radial thickness d of a glucose residue in the three

types of helix is the same, the true helix diameter can be approximately represented by D-d. Then, geometrical requirements give us the relation:

$$[D(6_1) - d]/[D(7_1) - d] = 6/7$$

Using experimental values $D(6_1) = 13.2$ Å and $D(7_1) = 14.7$ Å, we obtain $d = 4.2$ Å, a value for the radial thickness of a glucose residue close to that determined by examination of molecular models. With this value, true helical diameters of the n-butanol, isopropanol, and α-naphthol complexes are 9.0, 10.5, and 12.0 Å, respectively. The ratio 6:7:8 indicates that the helix of the α-naphthol complex has eight glucose residues per turn.

The only prior report concerned with the crystal structure of the 8_1 helical amylose is by Senti et al.[13] They suggested without experimental details that a fiber pattern from moist *tert*-butyl alcohol complex may be indexed by a monoclinic unit cell and this complex probably contains eight glucose residues per turn. However, their unit cell differs from the present one obtained by us for the α-naphthol complex. Their results are questionable in view of our finding[7] that amylose molecules in the *tert*-butyl alcohol complex form a 7_1 helix rather than an 8_1 helix.

Takeo and Kuge[14] studied the crystal structure of the γ-cyclodextrin–n-propanol complex by the x-ray powder method. They determined a two-dimensional tetragonal unit cell having $a = b = 23.7$ Å for the dry n-propanol complex. The packing diameters of the helix was calculated to be 16.75 Å. This value is close to the external diameter of 16.2 Å obtained for 8_1 helical amylose. Furthermore, comparison of the diffraction data suggests a structural analogy between the γ-cyclodextrin-n-propanol complex and the amylose–α–naphthol complex. For the former, the assigned indices for the equatorial reflections indicate that the $(hk0)$ reflections are missing when $h + k$ is odd. This extinction of the equatorial reflections is the same as that of the electron diffraction pattern in the α-naphthol complex. This fact is of interest as supporting the concept of oligomer analogy.

We do not suggest it is sufficiently documented, by the data presented here that the helix of the α-naphthol complex has precisely eight glucose residues per turn. However, it does seem clear that the multiplicity is close to eight. Then, we can venture to speculate about the diversity of helical conformations in amylose V. At present, we have obtained three crystal polymorphs with different helical configurations. We have confirmed[15] that each form is stable, even on annealing at 250°C, although transitions between the forms occur under special conditions.[7,16] It is now established both theoretically and experimentally that the glucopyranose residues in amylose exist only in the C1 conformation.[17] Since there is rotational freedom about the ether linkage C_1-O-C'_4, the helical configuration of the amylose chain is determined principally by a set of internal rotation angles (τH_1-C_1-O-C'_4, τC_1-O-C'_4-H'_4 the atoms C_1, H_1 belonging to the first residue and C'_4, H'_4 to the second residue) which is the same at all ether linkages. However, various sets of internal rotation angles can be considered even if the identity period is determined. Hence, the possible

conformations are limited by the minimum conformational energy. The nonbonded (van der Waals) energy has been computed for isolated helical amylose chains as a function of the internal rotation angles by Sundararajan and Rao.[17] Their result do not indicate that integral helices are preferred. On the other hand, the existence of 6_1, 7_1, and 8_1 helices in the molecular configuration of amylose V show that variation of the helix diameter occurs stepwise with the number of glucopyranose residues and integer. Therefore, the relative position of residues between one turn and the next can be expected to be similar. It may be speculated that the hydrogen-bonding forces operating between successive turns play an important role in determining the possible configuration of V amylose.

The authors wish to thank Mr. S. Takata for significant contributions to this work.

References

1. R. Bear, *J. Amer. Chem. Soc.*, **66**, 2122 (1944).
2. R. E. Rundle, L. Daasch, and D. French, *J. Amer. Chem. Soc.*, **66**, 130 (1944).
3. R. E. Rundle and D. French, *J. Amer. Chem. Soc.*, **65**, 1704 (1943).
4. R. E. Rundle and F. C. Edwards, *J. Amer. Chem. Soc.*, **65**, 2200 (1943).
5. R. E. Rundle, *J. Amer. Chem. Soc.*, **69**, 1769 (1947).
6. Y. Yamashita, *J. Polym. Sci. A*, **3**, 3251 (1965).
7. Y. Yamashita and N. Hirai, *J. Polym. Sci. A-2*, **4**, 161 (1966).
8. F. Schardinger, *Zentr. Bakt. Parasitenkunde Infkt.*, **22**, 98 (1908).
9. D. French, D. W. Knapp, and J. H. Pazur, *J. Amer. Chem. Soc.*, **72**, 5150 (1950).
10. D. French, M. L. Levine, J. H. Pazur, and E. J. Norberg, *J. Amer. Chem. Soc.*, **71**, 353 (1949).
11. J. M. G. Cowie and C. T. Greenwood, *J. Chem. Soc.*, **1957**, 2862.
12. T. Kuge and K. Takeo, *Agr. Biol. Chem.* (Japan), **32**, 1232 (1968).
13. F. R. Senti, and S. R. Erlander, *Non-stoichiometric compounds* by L. Mandelcorn, Ed., Academic Press, New York, 1964, p. 567.
14. K. Takeo and T. Kuge, *Agr. Biol. Chem.* (Japan), **34**, 568 (1970).
15. Y. Yamashita, unpublished data.
16. K. Takeo and T. Kuge, *Agr. Biol. Chem.* (Japan), **33**, 1174 (1969).
17. P. R. Sundararajan, and V. S. R. Rao, *Biopolymers*, **8**, 313 (1969).

Received October 6, 1970
Revised February 2, 1971

JOURNAL OF POLYMER SCIENCE: PART A-2 VOL. 9, 1483–1494 (1971)

Transport Properties of Methylene Chloride in Drawn Polyethylene as a Function of the Draw Ratio

J. L. WILLIAMS and A. PETERLIN, *Camille Dreyfus Laboratory, Research Triangle Institute, Research Triangle Park, North Carolina 27709*

Synopsis

The sorption and diffusion constants of CH_2Cl_2 at room temperature in quenched polyethylene film drawn at 60°C to different draw ratios λ between 6 and 25 drop drastically between $\lambda = 8$ and $\lambda = 9$ and then remain nearly constant, dropping only slightly up to $\lambda = 25$. Also, the exponential dependence of diffusion constant on concentration of sorbent increases abruptly in the same draw interval and then remains constant at the higher draw ratios. The data may be explained well by a composite madel: a low-permeability fiber structure embedded in a high-permeability spherulitic matrix. As the draw ratio is increased, the initially spherulitic film is gradually transformed into the fiber structure with the transformation being completed between $\lambda = 8$ and $\lambda = 9$. During subsequent drawing to $\lambda = 25$ the mutual arrangement of microfibrils, the basic elements of the fiber structure, changes by longitudinal sliding. However, their transport properties remain nearly constant. The diffusion constant drops a little as a consequence of the increased fraction of tie molecules which reduces the number of unperturbed sorption sites.

Introduction

The substantial reduction in the equilibrium sorption and the drastic reduction in the diffusion of organic vapors in drawn polyethylene has been previously reported by Peterlin, Williams, and Stannett.[1] The plastic deformation reduces the number of sorption sites and increases the activation energy of diffusion but it does not change the energy conditions at the sorption sites. These changes in the sorption and transport properties were considered as being a direct consequence of the denser packing and ordering of the tie molecules in the amorphous regions brought about by the cold-drawing process. This rearrangement of tie molecules results in blocking the easy passage of sorbent and causes a reduction in the number of unaffected chain folds where the sorption primarily occurs. Similar effects have been noted by other investigators using different penetrant–polymer systems.[2–6] For example, Davis and Taylor[4] have shown that the diffusion of dyes into nylon 66 is greatly reduced upon drawing, Takagi[5,6] found that in nylon 6 the radial diffusion increases up to a draw ratio of 1.6 and subsequently decreases to about 10% of the initial value. The axial diffusion shows only a decrease and is always smaller than the radial diffusion. All investigators have also noted that the activation energy increases considerably for diffusion into the drawn material.

In the present paper, the influence of the degree of deformation on the rate of sorption and on the equilibrium sorption has been measured over a wide range of draw ratios. The results of this investigation appear to complement the findings reported previously by Peterlin and Olf[7] and by Peterlin and Meinel[8-10] on the effect of draw ratio on various physicl parameters of drawn polyethylene such as heat content, density, chain mobility, and fraction of tie molecules. The experimental data support Peterlin's[11-15] molecular model for plastic deformation of crystalline polymers with the emphasis on the discontinuous transformation of the spherulitic structure of the starting material into the final fiber structure. The basic elements of the former structure are the well stacked lamellae with only a few interlamella links and of the latter, the strong microfibrils consisting of folded-chain blocks connected in the axial direction by a great many tie molecules.

Experimental

All measurements were made on a linear polyethylene, Fortiflex A-60-500 (Celanese Corporation), which has $\bar{M}_n$ = 5,500 and $\bar{M}_w$ = 80,000. Films of 0.5 mm thickness were made by compression molding at 150°C of pellets as obtained from the supplier followed by immediate quenching in ice water. From the resulting sheet, strips 5 mm wide were cold-drawn at 60°C in a water bath at a draw rate of 1 cm/min. The draw ratio was measured from the displacement of ink marks printed on the strip at 1mm intervals before drawing. Only the regions of the drawn material which corresponded to the exact draw ratio being investigated were used for the sorption studies. Clarity of the drawn samples was taken as being indicative of the absence of voids.[16] In Table I the density ρ and crystallinity α are given for the starting material and for the drawn samples.

Sorption experiments were carried out in a quartz helix microbalance assembly thermostatted by a jacketed bath controlled to ±0.01°C. A quartz helix having a sensitivity of 3 mm/Mg was employed along with an

TABLE I

Density ρ, Mass Crystallinity α, Regain c, Specific Regain $c_{sp} = c/(1 - \alpha)$ and Relative Specific Regain $c_{sp\lambda}/c_{sp,1}$ of Methylene Chloride at Vapor Activity p/p_0 = 0.2, 0.9 for Polyethylene Films Drawn at 60°C

Draw ratio λ	ρ, g/cc	α[a]	c, g/g		c_{sp}		$c_{sp}/c_{sp,1}$	
			p/p_0 = 0.2	p/p_0 = 0.9	p/p_0 = 0.2	p/p_0 = 0.9	p/p_0 = 0.2	p/p_0 = 0.9
1 (Undrawn)	0.949	0.718	0.60	4.59	2.13	16.21	1.00	1.00
λ = 6	0.952	0.735	0.80	4.20	3.02	15.85	1.42	0.98
7	0.953	0.741	0.80	3.92	3.09	15.14	1.45	0.93
8	0.955	0.753	0.67	3.08	2.71	12.47	1.27	0.77
9	0.962	0.793	0.11	0.64	0.53	3.09	0.25	0.19
25	0.968	0.826	0.09	0.45	0.52	2.59	0.24	0.16

[a] $\alpha = \rho_c(\rho - \rho_a)/[\rho(\rho_c - \rho_a)]$.

optical comparator reading to 0.001 mm, which was attached directly to the helix chamber. With such a micro-balance assembly, the accuracy of measurement is directly dependent on sample size, which was approximately 100 mg for the present study. In order to obtain a sample of this size for the drawn material several individually drawn strips were required. By use of several strips in the sorption experiments, to any small differences in sample history of the drawn material tend to be averaged out. In the case of the undrawn material, the sample is representative of only one film. From the initial time dependence and the limiting value, respectively, the diffusion constant and the equilibrium sorption were derived.

Methylene chloride was used as penetrant. It is a relatively small molecule with a high diffusion constant and sorption, which shortens the duration of the experiment and reduces the demands on balance sensitivity. These considerations are particularly important in experiments with drawn samples where sorption and diffusion are so drastically reduced.

To avoid grease problems, rubber O-ring joints and stopcocks were used throughout the system.

Results and Discussion

In Figure 1 the equilibrium concentration c_∞ of methylene chloride in undrawn polyethylene and in samples with draw ratios 6, 7, 8, 9, and 25 are plotted as functions of relative pressure p/p_0 of sorbent vapor. In all cases strong departures from the linear Henry's law are evident with higher penetrant activities. The departure from a straight line through the origin is most conspicuous for the undrawn sample but is still detectable even at the largest draw ratio. The isotherms obtained are of the normal mixing rather

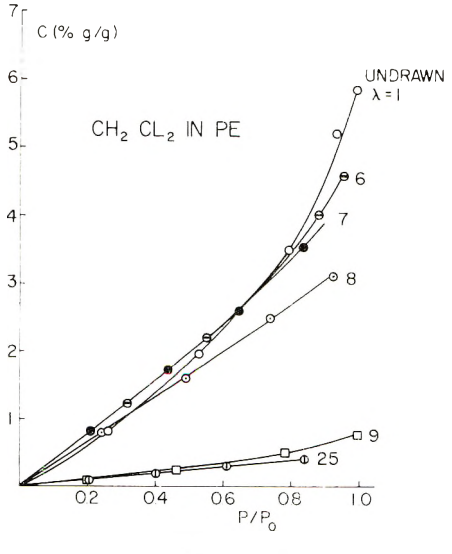

Fig. 1. Methylene chloride sorbed at 25°C in undrawn quenched polyethylene, and in films drawn at 60°C to the draw ratios indicated, vs. vapor acrivity p/p_0 (p_0 = 412 torr).

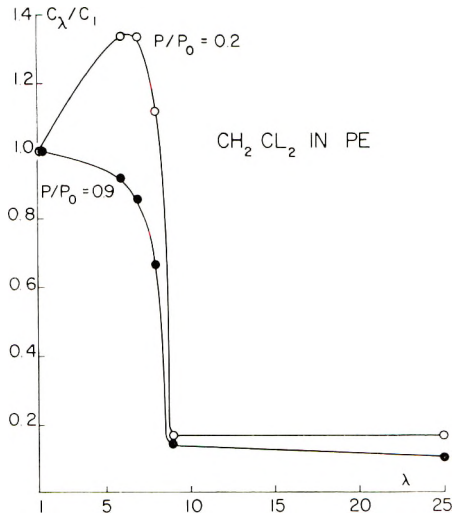

Fig. 2. Influence of drawing on the relative sorption c_λ/c_1 of methylene chloride in polyethylene at penetrant activities of 0.2 and 0.9.

than hole-filling (Langmuir) type for both the drawn and undrawn material.

A drastic reduction in equilibrium concentration of sorbent is caused by the drawing if the draw ratio λ is 9 or higher. In the sample with $\lambda = 9$ the sorption at p_0 is reduced to less than 13% of the value in the undrawn sample. The initial slope corresponding to the validity of Henry's law is reduced to about 15%. Subsequent drawing to $\lambda = 25$ has very little additional effect on sorption, as the experimental points are on very nearly the same curve as the points for the sample with $\lambda = 9$. This fact is in good agreement with former experiments on water sorption in drawn polyethylene.[17] It was shown that there is a drastic reduction in equilibrium sorption with drawing but very little change beyond $\lambda \approx 9$. For water, the normal Henry's law relation for the solubility was found to exist in both the drawn and undrawn material.

The surprising new fact, however, is the very small reduction of sorption up to a draw ratio 8. In fact, there is even a small increase of sorption at low penetrant activities, but it is not far enough above the error limits of measurement (as discussed in the experimental section) at such low sorption and activity to be worthy of special attention. The general dependence of sorption on draw ratio is best seen in Figure 2, where the relative concentration $c(\lambda)/c(\lambda = 1)$ is plotted as function of draw ratio λ for penetrant activities p/p_0 of 0.2 and 0.9. The most conspicuous feature is the small dependence on draw ratio up to $\lambda = 8$ and then the abrupt drop at $\lambda = 9$ to a new value which hardly changes with increasing λ. One has the impression that at λ between 8 and 9 the material is transformed into a new structure which does not change appreciably with further drawing.

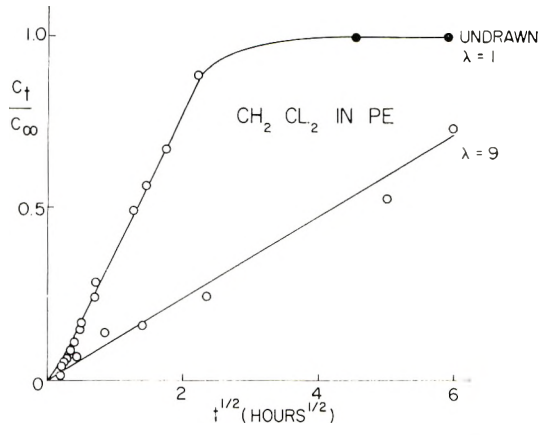

Fig. 3. Typical sorption transient curve: $c_t/c_\infty = Q_t/Q_\infty$ vs. $t^{1/2}$ for methylene chloride in undrawn and drawn ($\lambda = 9$) polyethylene at 25°C.

Since the drawing also changes the density and hence the mass crystallinity $\alpha = (\rho_c/\rho)(\rho - \rho_a)/(\rho_c - \rho_a)$ of the sample and the sorption occurs almost exclusively in the amorphous regions, one has to introduce the specific concentration $c_{sp} = c/(1 - \alpha)$, i.e., the amount sorbed per gram of amorphous component. These data are collected in Table I for penetrant activities 0.2 and 0.9. It was assumed in these calculations that the density of amorphous and crystalline components of drawn polyethylene are those of a supercooled melt and ideal crystal, respectively. One knows that this is a rather rough approximation because the density of the crystalline component decreases and that of the amorphous component increases with drawing. There is no drastic change in the draw-ratio dependence of the specific regain as compared with the directly measured data at the low draw ratios because the density and hence the crystallinity of the quenched sample remain very nearly constant up to $\lambda = 8$. The increase in density at $\lambda = 25$ and the ensuing decrease in amorphous fraction $1 - \alpha$ very nearly compensates for the concurrent drop in c so that the specific weight gain remains nearly constant between $\lambda = 9$ and $\lambda = 25$. The small irregularity of c_{sp} at $\lambda = 9$ and $p/p_0 = 0.2$ is most likely a consequence of the limited accuracy at such small weight gains. The specific regain hence shows the same type of dependence on draw ratio as c, i.e., an initial increase, a rapid drop between $\lambda = 8$ and $\lambda = 9$, and very little change at higher λ. Although the density increases and the amorphous fractions decrease with increasing draw ratio it is clear that considerably more than crystallinity changes are involved in the drastic drop of sorption brought about by the drawing process.

Typical sorption–time transient curves for the diffusion of methylene chloride are shown in Figure 3 for the drawn and undrawn material. The initial slope of the plot of relative weight gain $c(t)/c(\infty)$ versus $t^{1/2}$ was used for the calculation of the mean diffusion constant over the concentration

range from 0 to c_∞. The extreme slowness of the sorption process is apparent in that equilibrium is only reached after approximately one week for the drawn sample as compared with half a day for the undrawn polyethylene in spite of the fact that the thickness of the latter is three times that of the former ($\lambda = 9$).

The diffusion constants during the sorption process are shown in Figure 4 for the highly drawn materials as function of sorbent concentration in the polymer. The value extrapolated to zero concentration of penetrant for

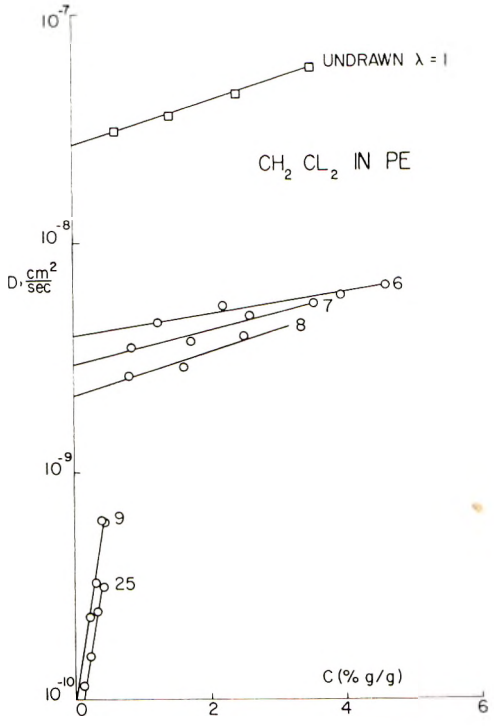

Fig. 4. Diffusion constant of methylene chloride at 25°C in undrawn and drawn polyethylene film vs. concentration of penetrant. The values are derived from the initial slopes of sorption transient curves (Fig. 3). The extrapolated values D_0 are given in Table I.

undrawn PE is 2.7×10^{-8} cm²/sec which is larger by a factor of 270 than the corresponding value 1.0×10^{-10} cm²/sec for the sample with $\lambda = 9$. Again it can be seen that upon drawing to $\lambda = 25$ only a small additional reduction of the diffusion constant, to about 58% of the value at $\lambda = 9$, is obtained. Also, the dependence of the diffusion constant on concentration is nearly 20 times higher than with undrawn material and is essentially the same for samples drawn 900% and 2500%. The diffusion constants for the drawn material with $\lambda = 9$ and $\lambda = 25$ are 270 and 370 times lower than for the undrawn material at zero concentration and 50 and 70 times lower for $c = 0.45\%$, respectively.

The situation is much less drastic for draw ratios between 6 and 8. The extrapolated zero concentration values for the diffusion constant are 3.9, 2.94, and 2.13×10^{-9} cm^2/sec for $\lambda = 6$, 7, and 8, respectively. The concentration dependence is practically the same as with the undrawn material. There is an obvious gap in experimental data between the undrawn sample and the sample with draw ratio 6 on one hand and a similar gap between the samples with the draw ratios 8 and 9 on the other hand. Both gaps are difficult to bridge because it is practically impossible to obtain sufficiently large samples with a draw ratio below 6 and the precision of draw

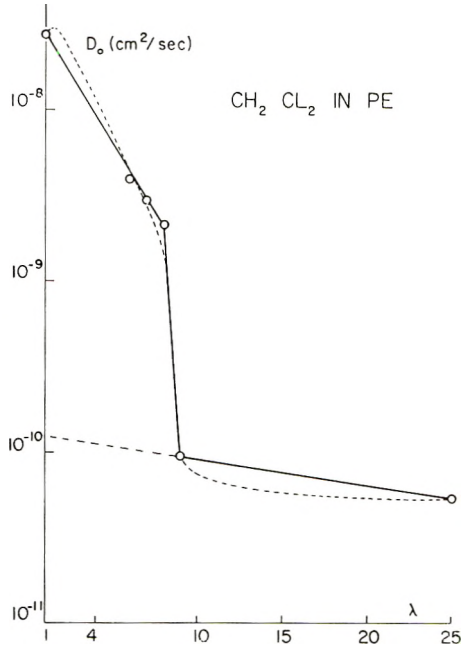

Fig. 5. Extrapolated diffusion constant of methylene chloride in drawn polyethylene at zero concentration of sorbent as a function of drawn ratio. The broken line represents the diffusion constant in the intermediate points according to the model for plastic deformation of crystalline polymers.

ratio measurements is not good enough for a proper definition of draw ratios between 8 and 9.

The dependence of the extrapolated diffusion constant D_0 at zero concentration of penetrant is given in Figure 5 as function of draw ratio. In the semilogarithmic plot the initial drop seems to be nearly linear with the draw ratio up to $\lambda = 8$. After that an abrupt decrease by a factor of 20 occurs in going from $\lambda = 8$ to $\lambda = 9$. The further decrease in diffusion is small, in fact much smaller than in the initial stages of drawing. The value of D_0 for $\lambda = 25$ is still 54% of the value for $\lambda = 9$. The few experimental points do not allow a detailed curve to be drawn, but one clearly sees the initial abrupt drop which comes to a stop at $\lambda = 9$ where a new morphological structure

seems to appear and persist with apparently only small modifications up to the maximum observable draw ratio.

The linear relation between the logarithm of the diffusion constant and the concentration of penetrant in Figure 4 is in line with results reported for vapors in polyethylene[1,18] and other polymers.[19] The dependence of the diffusion constant on concentration can be expressed by

$$D = D_0 \exp(\gamma c)$$

The resulting values of γ obtained for the various draw ratios are presented in Figure 6. From these values it is apparent that the concentration dependence of the diffusion constant as measured by the coefficient γ remains

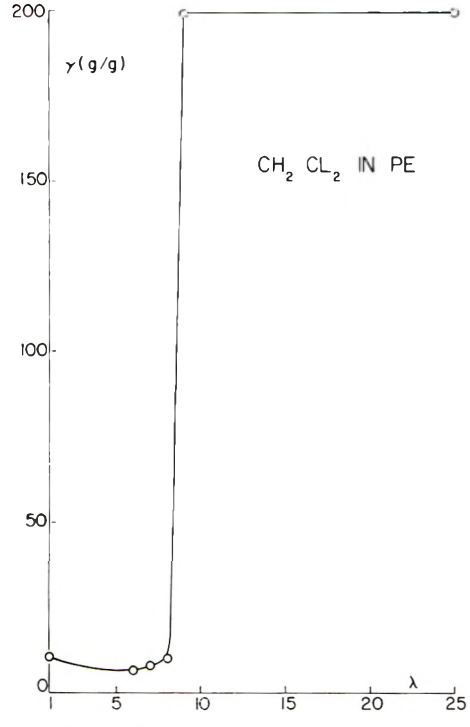

Fig. 6. Coefficient γ of the concentration dependence of the diffusion constant as a function of the draw ratio λ.

constant or even decreases slightly up to $\lambda = 8$, jumps abruptly to a value nearly 20-fold larger at $\lambda = 9$, and remains constant up to $\lambda = 25$. There is hardly any indication of a substantial variation of γ between $\lambda = 9$ and $\lambda = 25$, so that one is permitted to draw a straight horizontal line between the two experimental points. The main effect is again the abrupt increase of γ between $\lambda = 8$ and $\lambda = 9$ occurring in the range where S and D_0 also exhibit drastic changes. Beyond $\lambda = 9$, changes in all three parameters are insignificant.

Correlation with the Peterlin Model for Drawing of Crystalline Polymers

The drastic decrease of sorption and diffusion constants, along with the concurrent increase in the dependence of the diffusion constant on sorbent concentration, between draw ratios of 8 and 9 and their near constancy at higher draw ratios is a sure indication of far-reaching structural changes of the drawn material. One can safely conclude that at $\lambda = 9$ the drawn polyethylene film has, at least as far as material transport phenomena are concerned, fully acquired the fiber structure with no detectable remains of the microspherulitic structure of the starting material. At this draw ratio, the transformation of stacks of crystalline lamellae into microfibrils by micronecking seems to be completed. The subsequent drawing from $\lambda = 9$ to $\lambda = 25$, proceeding by longitudinal sliding of microfibrils, does not change the structure of the microfibrils but only changes their mutual location.[20]

The sorption and diffusion data in the high range of λ are hence characteristic for the microfibrils which consist of folded chain crystal blocks connected in the axial direction by a great many tie molecules passing through the amorphous layers separating the crystal cores of adjacent blocks. The amorphous layers contain the rather disoriented irregular chain loops, the partially oriented free chain ends (cilia), and the nearly completely oriented and extended tie molecules. In the presence of small change (or even no change) of orientation in the loops, the same type of sorption sites are available as in the lamellae of the undrawn material, but their number is reduced by the partial orientation of the cilia and particularly by the tie molecules. Hence, one can use the reduction of sorption per unit volume of amorphous material as a rough estimate of the unchanged fraction of the amorphous component. From Table I one can see that the specific sorption decreases very slightly (by about 20% at $p/p_0 = 0.9$) in the range of high draw ratios between 9 and 25, i.e., in the pure fiber structure. This can be interpreted as an indication of small changes in the amorphous component of the microfibrils, particularly of an increase of the fraction of tie molecules with increasing draw ratio from 15% up to a maximum value of 30%.[21] This reduces the contribution of folds and cilia from 85 to 70%, a reduction of about 20% in good agreement with the reduction of sorption. The microfibrils, indeed remain very much the same as they were formed in the micronecking process and are not significantly influenced by the substantial deformation of the fiber structure effected by the sliding motion of microfibrils past each other.

On the assumption of constancy of structure of microfibrils after their formation by micronecking of stacked lamellae, the rapid drop of specific sorption in the early stages of drawing reflects the progressive destruction of the original microspherulitic structure. The initial increase even indicates that during the first stage of deformation the specific sorption increases. Such an effect in permeability and sorption has already been observed in the range of elastic deformation and interpreted in terms of increased free volume.[22] Even in the plastic domain, small-angle x-ray scattering has re-

vealed a physical separation of lamellae perpendicular to the draw direction.[23] By such an effect, increasing the free volume of the amorphous component, the number of available sorption sites and hence the specific sorption become larger.

All of the initial increase of specific sorption has to be explained by such a mechanism up to the point where the transformation into the fiber structure starts, i.e., up to a draw ratio about 2. From then on, the specific sorption of the plastically strained spherulite material very likely remains constant so that the observed decrease in the specific sorption of the sample is a consequence of a transformation of the morphology which replaces the spherulitic material of high specific sorption $S_{sp,s}$ by the microfibrils with a substantially smaller $S_{sp,f}$. Unfortunately, no data are available in the low draw-ratio range which would permit a quantitative evaluation of experimental values of Figure 2 and Table I in terms of the transformed fraction of the material.

The decrease in the diffusion constant with increasing draw ratio is still more drastic than the change of sorption. Again the value for the fiber structure between $\lambda = 9$ and $\lambda = 25$ decreases very little, indicating that only relatively small changes occur in the structure of microfibrils for this range of λ. The huge reduction of D_0, by a factor of several hundred as compared to the value of the undeformed spherulitic structure, must be the consequence of a drastically changed structure of the highly oriented amorphous component of the microfibrils. The more densely packed, strained tie molecules enormously reduce the probability for formation of a sufficiently large hole for diffusion of penetrant molecules. Such an entropy effect characterized by a reduction of free volume is enhanced by the increase in activation energy for diffusion which was found previously and tentatively interpreted as a consequence of an increase of jump length for diffusion caused by the reduction in the number of available sorption sites.[1] The low sorption and the still smaller diffusion constant characterize the microfibril as a very impermeable structure element, sharply contrasting with the rather permeable spherulitic structure of the original undrawn material.

In the range of low draw ratios, the decrease in the diffusion constant is very rapid and becomes nearly catastrophic between $\lambda = 8$ and $\lambda = 9$. Again one suspects very little change in D_0 or eventually an increase at very low λ as a consequence of structure expansion preceding the necking process, followed by a subsequent reversal as the transformation to fiber structure sets in. Such a behavior is best explained by a two-component model: the nearly impermeable microfibrils generated in micronecks imbedded in a rather permeable matrix of the moderately deformed spherulitic structure. In such a composite material diffusion will take place mainly in the strained permeable spherulitic matrix and will avoid the impermeable microfibrils. The decrease of diffusion constant with increasing draw ratio is hence a consequence of the reduced amount of the as yet untransformed spherulitic structure and of increased tortuosity since the diffusant has to bypass the

growing number of impermeable microfibrils. The former effect reduces the cross section for the diffusion current, and the latter lengthens the diffusion path. The situation becomes catastrophic when all the matrix has disappeared so that the sample contains impermeable microfibrils only: the permeable fraction and hence the diffusion area go to zero and the tortuosity to infinity (Fig. 7). The contribution by the permeable matrix is nil, and all that remains is the low but still finite permeability of the microfibrils of the fiber structure.

The enormous dependence of diffusion constant on the concentration of the permeant in the fiber structure is very difficult to explain in simple terms. One must assume that every sorbed molecule plasticizes the amorphous component in the drawn sample to a much larger degree than in the spherulitic material. The main difference between the two structures is in the number and strain of tie molecules connecting the crystal lamellae or

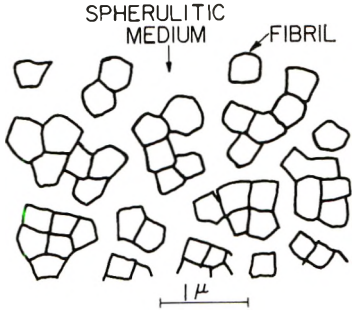

Fig. 7. Schematic model of distribution of fibrils (bundles of microfibrils) embedded in the as yet untransformed spherulitic material in a cross section of the polyethylene film with a moderate draw ratio between 1 and 8. The diffusion proceeds through the permeable embedding medium and avoids the nearly impermeable fibrils.

folded-chain blocks so that one expects that they must be primarily affected by the sorbent. On the other hand, one knows from the temperature dependence of sorption that the sorption sites are not changed by drawing as far as energy requirements are concerned. Thus, the unperturbed, and hence unoriented, irregular loops are most likely to accommodate sorbent molecules. It is possible, however, that the sorbed molecules mobilize the loops and the cilia to such an extent that they can assume more relaxed positions in spite of the compression forces of the highly strained tie molecules and by the resulting increase in occupied volume enforce some displacement of tie molecules, if not even some relaxation, by pulling them partially out of the crystal lattice. Every such relaxation eases the mass transport, i.e., increases the diffusion constant. However, one must not forget that relaxation which requires chain pulling through the crystal lattice is irreversible. Such irreversible changes were indeed formerly observed during sorption at saturation pressure of the sorbent. The drawn material after such a sorption experiment did not return to its original properties; its

sorption and diffusion constants were larger than before the saturated sorption.[1]

We would like to thank the Camille and Henry Dreyfuss Foundation for their support of this work and Mr. Harry Sugg for his expert help with all sample preparations.

References

1 A. Peterlin, J. L. Williams, and V. Stannett, *J. Polym. Sci. A-2*, **5**, 957 (1967).

2. H. J. Bixler and A. S. Michaels, paper presented at 53rd Natl. Meeting AICE, Pittsburg, Pa., May 1964.

3. A. S. Michaels, W. R. Vieth, and H. J. Bixler, *J. Appl. Polym. Sci.*, **8**, 2735 (1964).

4. G. T. Davies and H. S. Taylor, *Text. Res. J.*, **35**, 405 (1965).

5. Y. Takagi and H. Huttori, *J. Appl. Polym. Sci.*, **9**, 2167 (1965).

6. Y. Takagi, *J. Appl. Polym. Sci.*, **9**, 3887 (1965).

7. A. Peterlin and H. G. Olf, *J. Polym. Sci. A-2*, **4**, 587 (1966).

8. A. Peterlin and G. Meinel, *J. Polym. Sci. B*, **3**, 783 (1965).

9. A. Peterlin and G. Meinel, *J. Appl. Phys.*, **36**, 3028 (1965).

10. A. Peterlin and G. Meinel, in *Thermoanalysis of Fibers and Fiber-Forming Polymers* (*Appl. Polym. Symp.*, 2), R. F. Schwenker, Ed., Interscience, New York, 1966, p. 85.

11. A. Peterlin, in *Structure and Properties of Polymers* (*J. Polym. Sci. C*, **9**), A. V. Tobolsky, Ed., Interscience, New York, 1965, p. 61.

12. A. Peterlin, in *U.S.–Japan Seminar in Polymer Physics* (*J. Polym. Sci. C*, **15**), R. S. Stein and S. Onogi, Eds., Interscience, New York, 1966, p. 427.

13. A. Peterlin, in *The Meaning of Crystallinity in Polymers* (*J. Polym. Sci. C*, **18**), F. P. Price, Ed., Interscience, New York, 1967, p. 123.

14. A. Peterlin, *Kolloid-Z. Z. Polym.*, **216–217**, 129 (1967).

15. A. Peterlin, *Polym. Eng. Sci.*, **9**, 172 (1969).

16. O. Kratky and K. Schwarzkopf-Schier, *Monatsh. Chem.*, **94**, 714 (1963).

17. J. L. Williams and A. Peterlin, *Makromol. Chem.*, **120**, 215 (1968).

18. C. E. Rogers, V. Stannett, and M. Szwarc, *J. Polym. Sci.*, **45**, 61 (1960).

19. S. Prager and F. A. Long, *J. Amer. Chem. Soc.*, **73**, 4072 (1951).

20. A. Peterlin, *J. Mater. Sci.*, in press.

21. G. Meinel, A. Peterlin, and K. Sakaoku, in *Analytical Calorimetry*, R. S. Porter and J. F. Johnson, Eds., Plenum Press, New York, 1968, p. 15.

22. H. Yasuda, V. Stannett, H. Frisch, and A. Peterlin, *Makromol. Chem.*, **73**, 180 (1964).

23. A. Peterlin and F. J. Balta-Calleja, *J. Appl. Phys.*, **40**, 4238 (1969).

Received October 22, 1970
Revised February 11, 1971

JOURNAL OF POLYMER SCIENCE: PART A-2 VOL. 9, 1495–1507 (1971)

ESR Single-Crystal Study of Radical and Radical-Pair Formation in Some γ-Irradiated Vinyl Monomers

T. GILLBRO, P. -O. KINELL, and A. LUND,
Section for Nuclear Chemistry, AB Atomenergi and The Swedish Research Councils' Laboratory, Studsvik, Fack, S-611 01 Nyköping 1, Sweden

Synopsis

Single crystals of methyl methacrylate (MMA), methyl acrylate (MA), and acrolein (A) have been prepared by a low-temperature technique. After irradiation with γ-rays at 77°K the paramagnetic species were identified by ESR spectroscopy. MMA gave a seven-line single spectrum from radicals formed by hydrogen addition. The hyperfine coupling constants are slightly anisotropic with a mean value of 22 G. Radical pairs were observed as $\Delta M_S = 1$ and $\Delta M_S = 2$ transitions; the hyperfine coupling was 11 G. From the strongly anisotropic dipolar interaction, upper limits for the distances between the pair components were calculated to be 5.45 Å and 6.3 Å. MA gave a five-line main spectrum with the same hyperfine coupling values and two radical pairs, one with a distance 5.9 Å between the components. In A there was also a strongly anisotropic interaction. The hyperfine coupling of the $\Delta M_S = 2$ transition was 9.8 G. The number of radical pairs compared to the total number of radicals increases only slightly with the radiation dose. This makes it likely that pair formation occurs in the spurs and blobs formed by the γ-radiation. At an increased temperature the radical pairs disappeared; the spectrum of MMA changed to that characteristic of propagating polymer radicals.

INTRODUCTION

Investigations of radiation-induced polymerization in the solid state have met with steadily increasing interest during the last decade.[1–3] Systems studied so far show some variety in behavior. Monomers like trioxane[4] and styrene[5] polymerize readily upon irradiation in the crystalline form. On the other hand, monomers like methyl methacrylate and methyl acrylate are more difficult to polymerize in the crystalline state.[3] The importance of crystal imperfections as reaction sites has been pointed out.[6,7]

In connection with some polymerization experiments the initiating radicals have been examined in detail under trapping conditions. Especially when single crystals were used[8–11] valuable information was gained about the structure and localization of the trapped radicals. Even the conformation of propagating polymer radicals has been studied.[9,12]

One great obstacle in ESR studies of radical formation in the most common vinyl monomers has been the difficulty of preparing single crystals

at low temperature. One of our aims has thus been to overcome this by devising a method for producing such crystals. The monomers chosen for this work were expected to give stable primary radicals at low temperature and thus to polymerize slowly in the crystalline state. The monomers were methyl methacrylate, methyl acrylate, and acrolein. These crystallize at −50°C, −81°C and −88°C respectively and they do not form glasses when frozen.

Recently several authors[13−20] have found that radical pairs will form in organic crystals irradiated at low temperature. These studies have mostly been restricted to compounds solid at room temperature. Some low molecular weight hydrocarbons, irradiated at 77°K, have been reported to show radical pair formation both in polycrystalline[17] and the single-crystal[20] state. In this work we have studied radical pairs formed in the above vinyl monomers irradiated at 77°K. The radicals forming the pairs are believed to have the same structure as those generally formed in vinyl monomers by hydrogen atom addition. This shows that the mechanisms generally proposed for radical-pair formation involving a hydrogen abstraction process[17] are not always applicable.

EXPERIMENTAL

The vinyl monomers, methyl methacrylate (MMA), methyl acrylate (MA), and acrolein (A), provided by Fluka AG, were of "purum" grade and stabilized with hydroquinone. Before use, the monomers were freed from the stabilizer, dried, and distilled under vacuum. About 0.1 ml of liquid monomer was filled into a Suprasil quartz tube, one end of which was elongated into a thin capillary. The samples were degassed several times before they were sealed off at about 10^{-4} torr and 77°K.

Most of the single crystals were prepared by a freezing technique. The capillary end of the tubes was submerged in a cooling bath at a speed of 1.5 mm/hr. The temperature of the bath was kept about 10°C below the melting point of the monomer to be crystallized. The apparatus used is described in some detail elsewhere.[21] The crystals were then cooled to 77°K, slowly to avoid cracking. It is also possible to grow single crystals in the cool gas stream over liquid nitrogen in a dewar. This method, however, gives a more uneven crystal quality.

The irradiation was performed in a ^{60}Co γ-source at a dose rate of 180 or 800 krad/hr. The total dose given to the samples was 2 Mrad at 77°K unless otherwise is stated.

The ESR spectra were recorded with a Varian-V-4502-11 X-band spectrometer. Variable temperature was achieved by means of a regulated cool nitrogen gas stream around the sample in the cavity. Weak $\Delta M_S = 2$ transitions in polycrystalline samples were recorded by a Varian E3 spectrometer at 77°K. For anisotropy studies the single crystals were rotated around an axis perpendicular to the magnetic field vector. The orientation of the crystals in the tube could not be determined with the present tech-

nique. Various crystals of the same compound did not show consistent angular behavior, probably due to the fact that the crystals had grown along different axes in the sample tubes.

CRYSTAL STRUCTURES

The MMA structure is c-centered monoclinic with space group C_c or $C_{2/c}$ and dimensions $a_0 = 14.46$ Å, $b_0 = 6.30$ Å, $c_0 = 13.51$ Å and $\beta = 68°$. The unit cell contains eight molecules. The x-ray diffraction data were

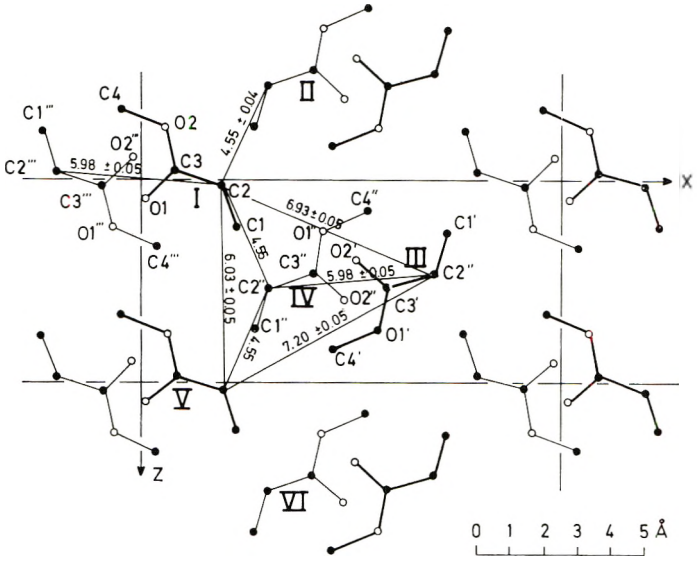

Fig. 1. Crystal structure of methyl acrylate. The molecules are situated in two planes perpendicular to the b axes. The molecules with atoms joined by heavy strokes are in plane $y = 0.75$, those joined by thin strokes are in plane $y = 0.25$. O stands for oxygen atoms and C for carbon atoms.

collected at about $-100°$C. The analysis of the structure has not yet been completed.

MA forms an orthorhombic unit cell,[20] at $-120°$C, space group P_{nma}, with the dimensions $a_0 = 12.77 \pm 0.07$ Å, $b_0 = 6.30 \pm 0.05$ Å, and $c_0 = 6.03 \pm 0.03$ Å. The cell contains four molecules. These are planar and

TABLE I

	Distance, Å	Number of nearest-neighbor carbons
C_2''-C_2	4.55 ± 0.04	4
C_2''-C_2'	5.98 ± 0.05	2
C_2''-C_2''	6.03 ± 0.05	2
C_2''-C_2''	6.30 ± 0.05	2
C_2''-C_2'''	6.93 ± 0.05	2
C_2''-C_2'''	7.20 ± 0.05	2

arranged in two planes with $y = 1/4$ and $3/4$ perpendicular to the b-axis (Fig. 1).

The distances between carbon atoms and the number of nearest neighbors are given in Table I.

The shortest distance is C_1''-$C_2 = 3.71$ Å.

There are no signs of phase transitions in the crystals of MMA and MA during gentle cooling from the melting point to liquid nitrogen temperature.

RESULTS

Methyl Methacrylate

Irradiation of polycrystalline MMA at 77°K (Fig. 2) gives a spectrum with seven equidistant broad lines. The line profile computed for a radical possessing six equivalent protons with a coupling constant $a = 22.4$ G and a line width of 12.5 G is in reasonable accord with the experimental shape. In single-crystalline form MMA shows a complicated spectrum (Fig. 3) with a central part consisting of five main lines, which undergo a slight change, indicative of anisotropy of the coupling in the radical, upon rotating the crystal in the magnetic field.

In addition to the central part of the spectrum several outer lines showing very strong anisotropy were observed. This spectrum is considered to be composed of four groups of lines forming the pairs marked (A_1, A_2) and (B_1, B_2) (Fig. 3*b*). Due to overlapping from the central spectrum the true intensity distribution among the lines of (A_1, A_2) is hard to measure. The outer pair (B_1, B_2) contains an odd number of lines showing a splitting of 11.2 G (Fig. 3*c*). The intensity distribution was calculated from the mean values of the peak heights of the lines symmetrically disposed around the

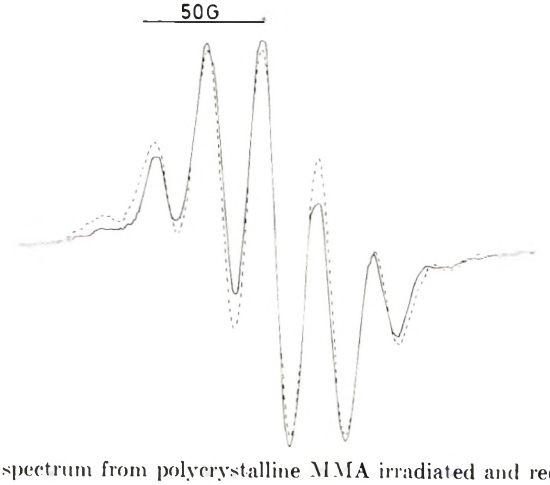

Fig. 2. ESR spectrum from polycrystalline MMA irradiated and recorded at 77°K. Dose 4 Mrad. The dashed spectrum represents simulation with a Lorentzian line shape, width $\Delta H = 12.5$ G measured between the maximum and minimum points of the derivative absorption. The splitting constant for six equivalent protons is $a = 22.4$ G.

central line in the B_2 group and was found to be 1.0:0.81:0.55:0.23: 0.07:0.04:<0.01. The binomial intensity distribution for a 13-line spectrum is 1.0:0.853:0.536:0.238:0.071:0.013:0.001. A computed spec-

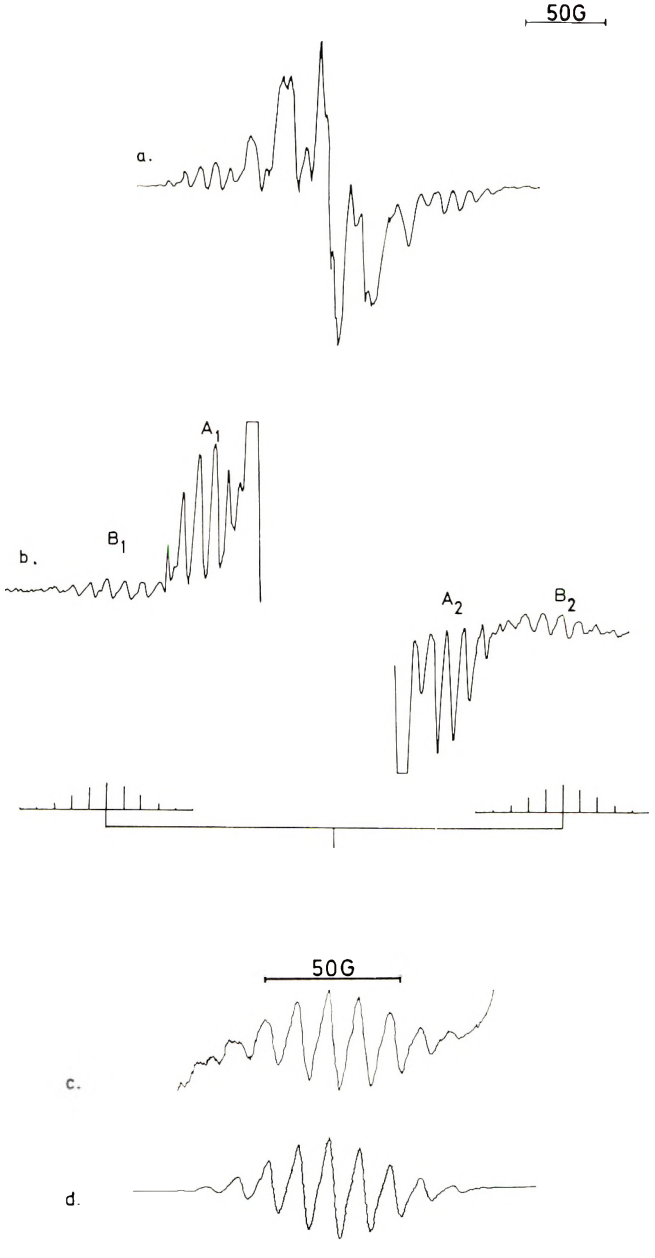

Fig. 3. ESR spectra: (*a*) from an irradiated single crystal of MMA; (*b*) with the same orientation and at higher gain; (*c*) the groups of lines B_2 at the crystal orientation where the interference with the other absorptions is at a minimum; (*d*) computed spectrum with $\Delta H = 5$ G (Lorentzian) and $a = 11.2$ G.

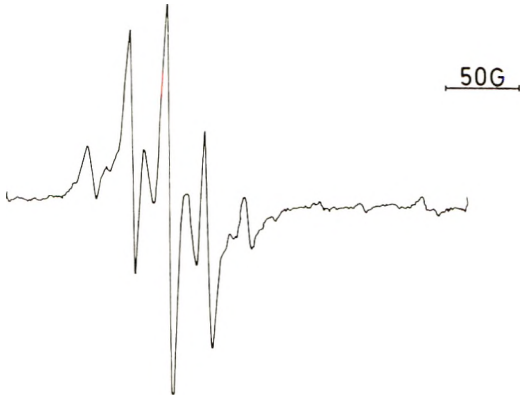

Fig. 4. ESR spectrum of the MMA crystal used to record the spectra of Fig. 3*a*, 3*b*, after annealing at 223°K.

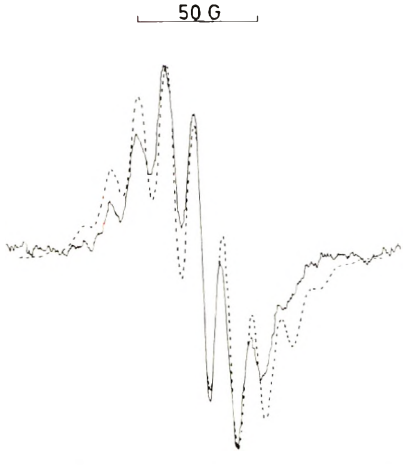

Fig. 5. ESR spectrum of the $\Delta M_S = 2$ transition in polycrystalline sample of MMA irradiated and recorded at 77°K. Dose 4 Mrad, dose rate 800 krad/hr. The dashed curve is a simulated spectrum with $\Delta H = 10$ G, (Lorentzian shape) $a = 11.2$ G (12 protons).

trum with a line width of 5 G fits the experimental line shape very well (Fig. 3*d*). The angular variation of the splitting of the components of the pair (B_1, B_2) could not be estimated due to overlap from the central spectrum. However, the maximum splitting, D, found was 343 G.

The two groups A_1 and A_2 (Fig. 3*b*) have a line splitting of 10.5 G. The number of lines was difficult to enumerate because of the overlap. The maximum splitting between the groups was 220 ± 10 G. The error arises from the difficulty in locating the centers of A_1 and A_2.

When the temperature of the crystal was increased, the outer groups B_1 and B_2 disappeared at about −140°C, while A_1 and A_2 were still clearly detectable. At the melting point, −50°C, the A pair had disappeared. The central part had then also changed (Fig. 4).

A weak absorption, at half field strength,[15,16] ascribed to a $\Delta M_S = 2$ transition, was observed both in powdered and single crystals (Fig. 5). The line shape can be reasonably approximated with a profile of 13 lines separated by 11.2 G and with a line width of 10 G.

The ratio between the amplitudes of the transitions $\Delta M_S = 2$ and $\Delta M_S = 1$ displays a slight decrease in the dose interval investigated. The spin concentration corresponding to the $\Delta M_S = 2$ transition in polycrystalline samples has been estimated relative to the $\Delta M_S = 1$ absorption. A correction for the difference in the transition probabilities was applied.[15,16] The number of radical pairs was estimated to be 5–10% of the total number of radicals. A crude estimate of the spin concentration of the $\Delta M_S = 1$ absorption intensity in single-crystal samples corroborated this value. The $\Delta M_S = 2$ transition was present also when the samples were heated for a few minutes to −140°C. The shape of the signal remained unchanged but the intensity of the absorption decreased to about 60% of the original value.

Methyl Acrylate

A γ-irradiated single crystal of MA showed a spectrum consisting of five main lines with a splitting of 22 G (Fig. 6). The anisotropy of the couplings were not sufficiently resolved to allow a study of their angular variation.

Besides the central 5-line spectrum there were four groups of lines forming the pairs (C_1, C_2) and (D_1, D_2) (Fig. 6). Anisotropy and overlap pro-

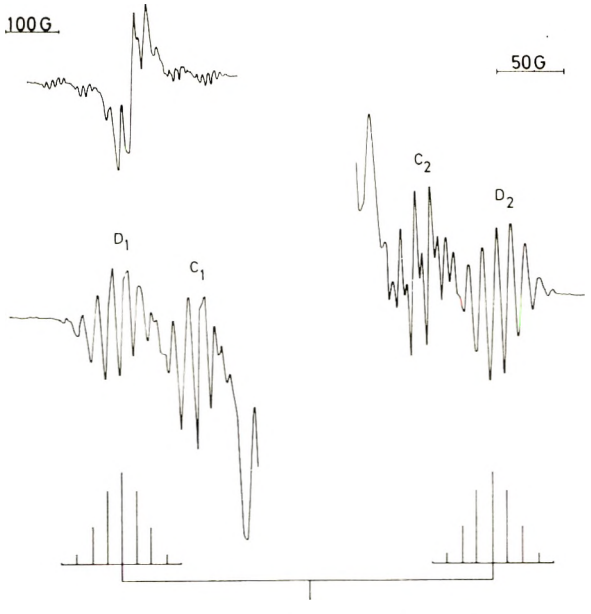

Fig. 6. ESR spectrum from an irradiated single crystal of MA. Temperature 77°K at irradiation and recording. Dose 3 Mrad.

hibit a definite estimate of the number of lines and of their intensities. The mean value of the hyperfine coupling constant is 10.8 G. A weak $\Delta M_S = 2$ transition was observed at half field strength (Fig. 7). This displays an odd number of lines, seven of which are clearly recognized in the recorded

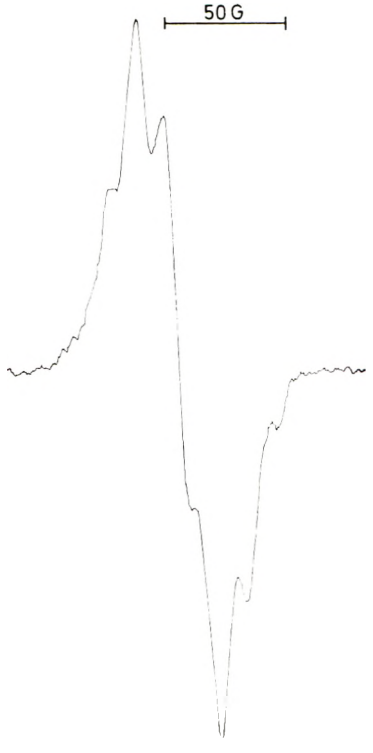

Fig. 7. $\Delta M_S = 2$ transition in a powdered MA crystal. Microwave power 25 mW, modulation amplitude 4 G.

spectrum. The line splitting is 11.5 G. The maximum separation of the groups D_1 and D_2 was found to be 275 ± 10 G, that of the groups C_1 and C_2 could not be estimated with any certainty.

Acrolein

The ESR spectra of an irradiated acrolein single crystal were strongly anisotropic and for most orientations exhibited an unsymmetric profile. Polycrystalline samples gave an unsymmetric, badly resolved spectrum. At certain orientations, additional lines similar to those obtained for MMA and MA were visible. The $\Delta M_S = 2$ transition observed in a polycrystalline sample at 77°K consisted of four equidistant lines with a separation of 9.8 G.

DISCUSSION

Radical Trapping in Single Crystal Matrices

The information about radical species which can be extracted from their spectra is largely dependent on the resolution. This implies that the nature of the matrix system used for studying trapped radicals influences the information that can be obtained about the radical species. Studies of paramagnetic species formed from vinyl monomers in polycrystalline samples[23,24] have been reported. Poorly resolved spectra were obtained which made unambigous assignments difficult. In a single-crystal matrix the radicals are usually oriented in a way which conforms with the symmetry properties of the crystal structure, which generally ensures high resolution. This has been proved on some vinyl compounds which are solid at or near room temperature, e. g., acrylic acid,[8] barium methacrylate dihydrate,[9] and methacrylic acid.[12]

Further, the angular variation of the hyperfine splittings can be measured, which allows the components of the coupling tensors to be evaluated. Also, extremely anisotropic transitions like those expected for a pair of radicals with interaction between the electron spins through dipolar coupling will be resolved with this technique.

The extension of the single-crystal technique to vinyl monomers with a low melting point, as has been done in the present work, has shown that very detailed information about the paramagnetic species can be obtained. In particular, the detection of species with dipolar interaction between the electron spins contributes to the clarification of the mechanism for the primary steps in the radiolysis.

Radical Structure

As is evidenced by the angular variation of the line shape in the single crystal spectra and by the difference in annealing rates, there are at least three different paramagnetic species present in irradiated MMA. The observed seven equidistant lines with binomial intensity distribution in the powdered sample[23] and the small anisotropy noted in the single crystal spectrum strongly suggest that the central absorption is caused by $(CH_3)_2\dot{C}COOCH_3$ (I) radicals. This also conforms with results obtained on acrylic acid[6] and barium methacrylate dihydrate.[9]

Similarly, the outermost line groups (B_1, B_2) are certainly due to $\Delta M_S = 1$ transitions in radical pairs composed of two units of type (I). Theoretically the radical pair should give a 13-line spectrum with a coupling equal to one half that in the isolated radical; however, the weakest lines could not be observed (Fig. 3*c*). The very strongly anisotropic splitting between B_1 and B_2 is caused by dipolar coupling of the two unpaired electron spins. The maximum separation is expected when the field is directed along the vector **R** between the two nuclei at which the electrons are localized. The

observed maximum separation $D = 343$ G corresponds to the principal tensor component along **R** only if this vector is perpendicular to the axis of rotation of the crystal. The distance between the radicals forming a pair is then less than 5.45 Å. Here the expression $R \leq 38.2\, D^{-1/3}$, derived from the point-dipolar approximation, has been used. The shape of the weak absorption attributed to a $\Delta M_S = 2$ transition also agrees with that calculated for a hyperfine structure involving 12 equivalent protons (Fig. 5).

The observation of $\Delta M_S = 2$ transitions in samples annealed at -140°C in which the group of lines (B_1, B_2) for $\Delta M_S = 1$ were absent, suggests that several types of radical pairs are present. This indicates that the absorption (A_1, A_2) is caused by a radical pair separated by a somewhat longer distance, $R \leq 6.3 \pm 0.1$ Å, than those responsible for the (B_1, B_2) set of lines. The finding that the shape of the $\Delta M_S = 2$ transition remains unchanged after thermal annealing proves that the lines (A_1, A_2) are composed of radical units of type (I).

The spectrum observed after warming to -50°C (Fig 4) is very similar to that displayed by irradiated PMMA[25] and by methacrylic acid[26] γ-irradiated at 0°C. By a detailed line-shape analysis[25] it was demonstrated that these radicals were of the type $-C_\beta H_2-\dot{C}_\alpha-(CH_3)-R$ in which the conformation angles of the two C_β—H bonds showed a Gaussian distribution around their most probable values. The possibility of a hindered oscillation around the C_α—C_β bond was also investigated.[25,26] This phenomenon seems less likely in the present case since no noticeable temperature dependence of the line shape was noted.

In MA the prominent absorption appears to be caused by $CH_3\dot{C}HCO-OCH_3$ radicals (II). The weak groups of lines, C and D, on the wings (Fig. 6) are attributed to pairs of radicals II. The evidence for this is mainly found in the $\Delta M_S = 2$ transition. The pairs of molecules in the unit cell which are related by inversion symmetry (Fig. 1) yield spectra that are indistinguishable. This leaves two symmetry-related radicals or radical pairs which are magnetically nonequivalent. It is therefore possible that the line groups C and D are caused by two differently orientated pairs. Alternatively, two types may be present with a different separation between the monomer units, as is the case for MMA. The distance between the radicals as estimated from the maximum separation between the groups (D_1, D_2) is $R \leq 5.9 \pm 0.1$ Å. The error comes mostly from the difficulty in determining the centers of the groups. There are three crystallographic C_2–C_2 distances within $R \leq 6.0$ Å. From the data available a distinction between the corresponding types of radical pairs cannot be made.

The analysis of the single crystal spectra from acrolein (A) is difficult due to the asymmetry and the poor resolution at most orientations. From the small hyperfine splittings observed in the radical and radical pair spectra it appears that the unpaired electron spin is delocalized. This would be expected for the radical H_3C—$\dot{C}H$—CHO formed by hydrogen atom addition but an assignment could not be made.

Mechanism

If the radical pairs were formed by diffusion of hydrogen atoms out of the tracks of the ionizing radiation and subsequent reaction with monomer molecules, the radical concentration would have a rather homogeneous distribution throughout the crystal. The probability of radical pair formation in such a process is expected to be low at moderate doses and increase with prolonged irradiation. Experimentally the concentration of radical pairs was found to increase in roughly the same way as the total radical concentration when a polycrystalline sample of MMA was irradiated at 77°K at different doses. Therefore, we conclude that radicals are produced in a process within the spurs or blobs formed by the γ-radiation.[27] In these regions the local concentration of paramagnetic species is expected to be almost independent of the dose.

The mechanism for the formation of radical pairs is still not well understood. In most cases so far investigated the pairs consist of two identical units. Mechanisms have been suggested involving abstraction of hydrogen atoms or ionization followed by stereospecific proton transfer[17] as primary processes. Both schemes ultimately give hydrogen molecule formation which corroborates the fact that no hydrogen atoms have been detected in hydrocarbons at 4°K except in methane.[28] Further, the importance of crystal defects as trapping sites for excitons or ion pairs has been emphasized.[29] There is no evidence in the present work for radicals formed by hydrogen atom abstraction. Therefore the radical pairs formed according to the hydrocarbon scheme[17] (1) cannot explain the experimental results.

$$\begin{vmatrix} RH \\ RH \end{vmatrix} \rightsquigarrow \begin{vmatrix} R\cdot + H\cdot \\ RH \end{vmatrix} \rightarrow \begin{vmatrix} R\cdot \\ R\cdot \end{vmatrix} + H_2 \qquad (1)$$

Possibly four adjacent molecules could be involved in a type of domain in which RH_2 radicals in pairs are much more stable than R· radicals. These latter radicals may combine or disproportionate almost instantaneously at 77°K. From the structure of the MA crystal it is quite obvious that certain molecules are very well arranged for hydrogen atom transfer. Thus molecule I (Fig. 1) has two neighboring molecules IV where the hydrogen atom on carbon C_2'' is in a favorable position with respect to the hydrogens on carbon atom C1 of molecule I for methyl group formation. Furthermore the mutual position of the carbonyl groups C_3-C_2 could give a charge distribution in conjugated bond systems, as in molecules III and IV, which has some stability. The formation of radicals in pairs has been observed in maleic anhydride[19] and in dimethyl maleic anhydride, which may give some support to a possible influence of conjugation on the mechanism of radical pair creation. At present the details of the MMA structure are not known and therefore any judgement about similar prerequisites for radical pair formation in the two structures must be postponed.

Polymerization

At higher temperature, the spectrum of MMA resembles that of irradiated PMMA.[25] This suggests the formation of secondary radicals by the addition of monomer to the initial species.[9,30–32] Whether chain propagation occurs or not could not be conclusively settled. Under similar experimental conditions the propagating radical in barium methacrylate dihydrate single crystal is most probably the dimeric species.[30] Obviously increased molecular motion is a necessity for macromolecular growth in the solid state. This corroborates previous observations on barium methacrylate dihydrate single crystals.[9] The absence of anisotropy was explained by destruction of the crystalline structure in the region where the radicals are trapped.[9] The presence of polymer radicals with different conformations[25] is also in agreement with this hypothesis. The crystal structure of MA has a molecular packing that allows scant possibility for molecular translation and rotation.[22] Therefore any polymerization is deemed impossible unless it breaks down the regular structure or occurs in defect regions or at grain boundaries.

The rate of polymerization of MMA and MA in the solid state may be influenced by the radical pair formation. The number of radicals bonded as pairs is in both cases as high as 5–10%. The decay of the radical pairs (B_1, B_2) in MMA already at -140°C may indicate the relative ease with which radicals situated close to each other recombine compared to more distant radicals. Combination of radicals would mean a lowering of the overall polymerization rate, approximately in proportion to the inverse square root of the recombination rate constant according to the mechanism of polymer formation in the liquid state.[3] However, in the solid state the mechanism could be partly changed.

One of the authors (T.G.) is obliged to AB Atomenergi for a fellowship. The use of an E-3 ESR spectrometer at the Institute of Biochemistry, University of Gothenburg, is gratefully acknowledged. The cost of part of this investigation has been defrayed by grants from the Swedish Atomic Research Council and the Swedish Board for Technical Development.

References

1. K. Oshima and Y. Tabata, *Adv. Nucl. Sci. Technol.*, **3**, 267 (1966).
2. Y. Tabata, in *Vinyl Polymerization*, Vol. 1: II, G. Ham, Ed., Dekker, New York, 1969, p. 305.
3. A. Chapiro, *Polymerizations en phase solide, Actions chimiques et biologiques des radiations*, **10**, 189–312 (1966).
4. S. Okamura, K. Hayashi, and Y. Nakamura, *Isotop. Radiat* (Tokyo), **3**, 416 (1960).
5. A. Chapiro and V. Stannet, *J. Chim. Phys.*, **57**, 35 (1960).
6. C. H. Bamford, G. C. Eastmond and J. C. Ward, *Proc. Roy. Soc.* (London), **A271**, 357 (1963).
7. C. H. Bamford, A. Biddy, and G. C. Eastmond, *Polymer*, **9**, 653 (1968).
8. Y. Shioji, S. I. Ohnishi, and I. Nitta, *J. Polym. Sci. A*, **1**, 3373 (1963).

9. J. H. O'Donnell, B. McGarvey, and H. Morawetz, *J. Amer. Chem. Soc.*, **86**, 2322 (1964).
10. H. Ueda, *J. Polym. Sci. A*, **2**, 2207 (1964).
11. G. Adler and J. H. Petropoulos, *J. Phys. Chem.*, **69**, 3712 (1965).
12. C. H. Bamford, G. C. Eastmond, and Y. Sakai, *Nature*, **200**, 1284 (1963).
13. Y. Kurita, *Nippon Kagaku Zasshi*, **85**, 833 (1964); *J. Chem. Phys.*, **41**, 3926 (1964).
14. Y. Kurita and M. Kashiwagi, *J. Chem. Phys.*, **44**, 1727 (1966).
15. M. Iwasaki, and K. Toriyama, *J. Chem. Phys.*, **46**, 4693 (1967).
16. M. Iwasaki, T. Ichikawa, and T. Ohmori, *J. Chem. Phys.*, **50**, 1984 (1969).
17. M. Iwasaki, T. Ichikawa, and T. Ohmori, *J. Chem. Phys.*, **50**, 1991 (1969).
18. W. Gordy and R. Morehouse, *Phys. Rev.*, **151**, 207 (1966).
19. M. Iwasaki and B. Eda, *Chem. Phys. Letters*, **2**, 210 (1968).
20. T. Gillbro, P. O. Kinell, and A. Lund, *J. Phys. Chem.*, **73**, 4167 (1969).
21. T. Dahlgren, T. Gillbro, G. Nilsson, and A. Lund, *J. Phys. Sci. Instr.*, **4**, 61 (1971).
22. A. Brown, T. Gillbro and B. Nilsson, *J Polym. Sci. A-2*, **9**, 1507 (1971).
23. R. Bensasson, A. Bernas, M. Bodard, and R. Marx, *J. Chim. Phys.*, **60**, 950 (1963).
24. T. Komatsu, T. Seguchi, H. Kashiwabara, and J. Sohma, in *Macromolecular Chemistry, Prague 1965* (*J. Polym. Sci. C*, **16**) O. Wichterle and B. Sedlaček, Eds., Interscience, New York, 1967, p. 535.
25. M. Iwasaki and Y. Sakai, *J. Polym. Sci. A-1*, **7**, 1537 1547 (1969).
26. M. Iwasaki and Y. Sakai, *J. Polym. Sci., A-1*, **7**, 1749 (1969).
27. A. Mozumder and J. L. Magee, *Radiation Res.*, **28**, 203 (1966).
28. D. Timm and J. E. Willard, *J. Chem. Phys.*, **73**, 2403 (1969).
29. G. C. Eastmond, E. Haigh, and B. Taylor, *Trans. Faraday Soc.*, **65**, 2497 (1969).
30. M. J. Bowden and J. H. O'Donnell, *J. Phys. Chem.*, **72**, 1577 (1968).
31. M. J. Bowden and J. H. O'Donnell, *Macromolecules*, **1**, 499 (1969).
32. M. J. Bowden, J. H. O'Donnell, and R. D. Sothman, *Macromol. Chem.*, **122**, 186 (1969).

Received November 3, 1970
Revised February 18, 1971

JOURNAL OF POLYMER SCIENCE: PART A-2 VOL. 9, 1509–1515 (1971)

Crystal Structure of Methyl Acrylate

ALLAN BROWN and TOMAS GILLBRO, *AB Atomenergi, Studsvik, S-611 01 Nyköping, Sweden*, and BO NILSSON, *Crystallography Group, University of Gothenburg, Gothenburg, Sweden*

Synopsis

Methyl acrylate, $CH_2CHCOOCH_3$, has been crystallized, and x-ray data have been collected at −120°C. The crystals are orthorhombic, space group *Pnma*, with four molecules in the unit cell. The structure has been determined by using symbolic addition procedures, and refined to a final residual R factor of 0.10. The molecule is planar, and the intramolecular bond distances and angles are in good agreement with values obtained for the liquid monomer by electron diffraction techniques. Considerations of crystal geometry indicate that the packing hardly permits dimerization or polymerization of the molecules in regions of crystal perfection.

INTRODUCTION

This investigation has been carried out concurrently with an ESR study of radicals produced in methyl acrylate and methyl methacrylate crystals on γ-ray irradiation at 77°K.[1] There is considerable variation in the degree of radiation-induced polymerization in the crystalline state of different monomers.[2] Trioxane and styrene, for example, polymerize easily, whereas methyl acrylate and methyl methacrylate give no indication of polymerization at moderate radiation doses. It has been shown by various techniques that the geometry of the monomer packing determines, to some extent, the chain propagation involved in the polymerization process.[3,4] So far, however, few crystal structure determinations have been carried out for monomers which are liquid at room temperature.

EXPERIMENTAL

Crystallization and Data Collection

The methyl acrylate was provided by Fluka A. G. The liquid monomer was freed from stabilizer, dried and distilled under vacuum immediately before use. It was then fed into a thin glass capillary of 0.5 mm diameter, which was subsequently mounted on a goniometer head. A special freezing technique[5] was used to grow crystals in the capillary at the melting point of the monomer, i. e., −81°C.

The x-ray diffraction patterns were recorded in a Weissenberg camera at $-120°C$ with the use of Cu Kα radiation (λ for Cu Kα = 1.5418 Å). Analysis of the symmetry elements and systematic absences indicated that the crystals were orthorhombic with cell dimensions $a = 12.77 \pm 0.07$ Å, $b = 6.30 \pm 0.05$ Å, $c = 6.03 \pm 0.03$ Å and with extinction conditions corresponding to those of the space groups *Pnma* and *Pn2a* ($h = 2n + 1$ in $hk0$ and $k + l = 2n + 1$ in $0kl$). The crystals invariably grew with the short b axis as rotation axis. Comparison of the first four Weissenberg layers obtained with this crystal orientation demonstrated that identical intensity distributions were given by the $h0l$ and $h2l$ reflections and also by the $h1l$ and $h3l$ reflections. This suggested that the carbon and oxygen atoms, largely responsible for x-ray scattering, are restricted to the mirror planes at $y = \pm 1/4$ in *Pnma*. These atoms are accordingly located in fourfold positions and the unit cell would appear to contain four molecules. The density of 1.18 g/cm^3 calculated on this basis is reasonable in view of the density of the liquid.

A total of 385 independent reflections was recorded for the four Weissenberg layers hkl, $0 \leq k \leq 3$, by using the multiple film technique. A common exposure time was used for all the layers. The reflection intensities were estimated visually by comparison with a precalibrated strip.

Structure Determination

The intensities were corrected for Lorentz and polarization effects but not for extinction or absorption. The signs of 60 normalized structure factors were determined by symbolic addition procedures.[6] Using these as coefficients, a Fourier synthesis was prepared, which revealed the positions of the nonhydrogen atoms. After some cycles of full matrix, least-squares, anisotropic refinement of these atomic positions, the six hydrogens were obtained from a difference synthesis as peaks of height 0.50–0.67 electrons/Å^3. However, since hydrogen parameters based on visually estimated x-ray data are not very precise, inclusion of these atoms in the molecule was made on the basis of their expected positions.

The nonhydrogen positions were then refined as before until the parameter shifts were less than their standard deviations. The final residual R factor, defined as $\Sigma||F_o| - |F_c||/\Sigma|F_o|$, was then 0.10, and a difference synthesis demonstrated no peaks outside the range -0.5 to $+0.5$ electrons/Å^3. Unobserved reflections were not included in the data.

RESULTS AND DISCUSSION

Atomic Parameters

The table of observed and calculated structure factors is omitted here. The atomic parameters are given in Table I. The molecule is quite planar except for two methyl hydrogens, the plane being at $y = \pm 1/4$. In liquid methyl acrylate, however, electron diffraction studies[7] reveal that the

TABLE I
Atomic Positions and Vibrations[a]

Atom	x	(σ)	y	z	(σ)	U_{11}	U_{22}	U_{33}	U_{12}	U_{13}	U_{23}
C_1	23079	(41)	75000	23761	(82)	27	53	32	0	−4	0
C_2	19866	(35)	75000	2667	(89)	17	66	30	0	43	0
C_3	8565	(34)	75000	−3609	(76)	21	46	21	0	36	0
C_4	−3446	(40)	75000	−34073	(84)	22	68	19	0	20	0
O_1	1209	(24)	75000	9644	(50)	18	58	19	0	24	0
O_2	7361	(24)	75000	−26037	(51)	19	57	18	0	29	0
H_{11}	17350		75000	37160							
H_{12}	31420		75000	27550							
H_{21}	25730		75000	−10470							
H_{41}	−3470		75000	−52150							
H_{42}	−7470		89120	−28030							
H_{43}	−7470		60870	−28030							

[a] Positions are given as fractional coordinates ($\times 10^5$). The standard deviations ($\times 10^5$) of refined coordinates are given in parentheses. Allowance was made for anisotropic thermal vibrations by use of the expression

$$\exp - 2\pi^2[h^2a^{*2}U_{11} + k^2b^{*2}U_{22} + l^2c^{*2}U_{33} + 2hka^*b^*U_{12} + 2hla^*c^*U_{13} + 2klb^*c^*U_{23}]$$

The values of U for the nonhydrogen atoms are in units of $\text{Å}^2 \times 10^3$.

methyl group is inclined at 25° with respect to the molecular plane. The hydrogen atoms are placed in assumed positions, the C-H distance being chosen as 1.09 Å. The two hydrogens H_{11} and H_{12} at C_1 are located so as to subtend bond angles of 120° at this atom. The hydrogen H_{21} at C_2 is on the bisector of the C_1-C_2-C_3 angle. The hydrogens at C_1 are so distributed as to give tetrahedral configuration around this atom, i. e. all bond angles are 109.47°. The hydrogen H_{31} is in the molecular plane, continuing the zig-zag chain, whereas H_{32} and H_{33} lie outside this plane. In space group *Pnma*, any atom which is not located in one of the two mirror planes at $y = \pm 1/4$ has eight equivalent positions in the unit cell. There should accordingly be eight of each of these two hydrogens, but only four of each of the other atoms. These hydrogens are mirror images of each other, however, and thus occupy eight sites altogether or four each.

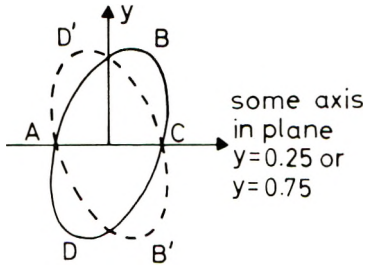

Fig. 1. In the absence of mirror symmetry across the molecular plane a vibrational ellipsoid ABCD generates a second ellipsoid AB'CD'.

The standard deviations σ of the nonhydrogen x and z coordinates given in Table I are obtained from the inverted normal-equation matrix of the last cycle of refinement. The elements of the anisotropic vibration tensors are also given in Table I. As might be expected, the out-of-plane vibrations (U_{22}) are heavier than those in the plane (U_{11} and U_{33}), corresponding to B values in the ranges 3.6–5.4 Å^2 and 1.4–2.5 Å^2, respectively. Since each of these atoms is in a mirror plane, the terms U_{12} and U_{23} must be zero. If they were not, the vibrational ellipsoid of the atom would not have mirror symmetry across the plane but would be inclined, as illustrated by the full-line ellipsoid ABCD in Figure 1. This ellipsoid, however, would generate its mirror image AB'CD', that is there would be two ellipsoids. On the average, therefore, each ellipsoid has an orientation perpendicular to the molecular plane. This may not be strictly true for all atoms, but departures are too small to influence the symmetry, as is evident from the diffraction patterns.

Molecular Geometry

Figure 2 shows intramolecular bond distances and angles. Values of the esd (estimated standard deviation) for these quantities were obtained from

the standard deviations σ of the coordinates given in Table I.[8,9] The values of σ indicated in the diagram correspond to 3 esd for 99.7% confidence limits. The distances and angles obtained by electron diffraction studies[7]

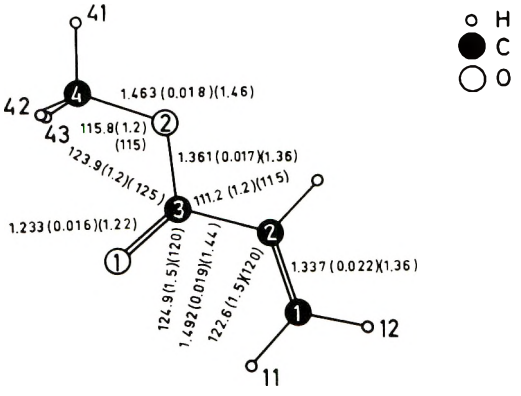

Fig. 2. Atomic numbering and bond distances (Å) and angles (degrees). Each distance and angle is given in the following sequence: mean value, 3 esd, and value relating to the liquid state.

are also given in Figure 2 for purposes of comparison. On the whole, there is good agreement between the geometry of the molecule in the liquid and in the solid states.

Crystal Geometry

The molecular packing is illustrated in Figure 3. There are no C-O distances small enough for hydrogen bonding; the molecules are therefore held together by van der Waals forces only. The C_1–C_2 double bonds are stacked in sheets perpendicular to the x axis. The shortest intermolecular $C_1 \ldots C_2$ distance in these sheets is 3.711 Å (3 esd = 0.012 Å) and is formed between adjacent molecules in the layers at $y = \pm 1/4$. If polymerization had occurred, the chains would have propagated along the path $\ldots [C_2 = C_1]_{y=1/4} \ldots [C_2 = C_1]_{y=-1/4} \ldots$ in the y and z directions. The lack of polymerization on γ-ray irradiation at low temperature is, generally speaking, due to too great a hindrance for the necessary translational and rotational molecular motions in the lattice.[3] Thus in the event of dimerization of molecules I and IV in Figure 3 a shortening of the $C_{1,I} \ldots C_{2,IV}$ distance of 3.71–1.54 = 2.17 Å would be necessary. This would in turn necessitate translations of I and IV mainly along y and z, combined with rotations of the whole or parts of the two molecules. Assuming a van der Waals radius of 2.0 Å for the methyl group and 1.4 Å for the oxygen atom, the $O_1 \ldots C_4$ distance of 3.49 Å indicates a contact, although loose, even between unmoved molecules.

Thus movement along y in either direction will rapidly lead molecule IV into collision with molecule III. Similarly IV will collide with II or VI if it

moves along z. Migration of IV along x is also hindered by the presence of molecules in its own plane ($y = {}^1/_4$). By similar reasoning, it can be deduced that rotational movements are also hindered by the prevailing mode of packing. Since the molecules have identical environments restrictions in the movement of IV are equally relevant to molecule I. It is

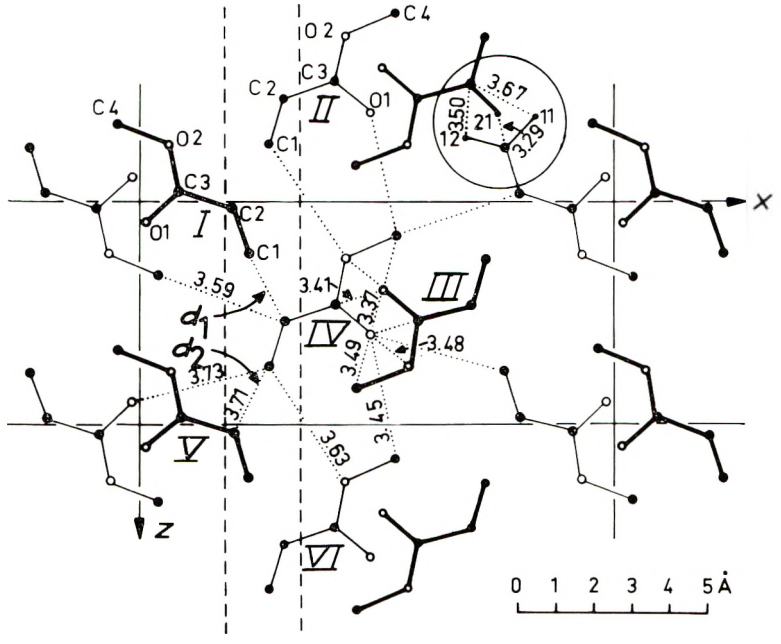

Fig. 3. Molecular packing viewed down the y axis. Intramolecular distances to molecule IV < 3.75 Å are indicated by dotted lines. Each such line occurs twice by symmetry, but the distance (Å) is only given once. For example, d_1 and d_2 are identical. Molecules in thin lines are at $y = 0.25$, those in thick lines at $y = 0.75$. A dotted line between a "thin" and a "thick" molecule is actually a duplicate, protruding from the "thin" to the "thick" molecules in the adjacent layers above and below. Hydrogens are omitted for clarity, except in the encircles area. The two dashed lines enclose a sheet in which $C_1{=}C_2$ double bonds are stacked.

therefore unlikely that a reduction in the 2.17 Å $C_1 \ldots C_2$ distance is attainable even for dimerization. It should be even harder to achieve polymerization when one of the molecules is locked to the chain. It should be pointed out that this reasoning is valid only for regions of crystal perfection. Some dimerization or polymerization may be possible in the vicinity of defects or at the junction of mosaic blocks. For acrylic acid, however, the crystal geometry[10] is such as to allow the necessary molecular movements without accumulation of a prevailing amount of strain. This compound shows solid state polymerization.[10–12]

References

1. T. Gillbro, P.-O. Kinell, and A. Lund, *J. Polym. Sci. A-2*, **9**, 1495 (1971).
2. A. Chapiro, *Polymérisations en phase solide. Actions chimiques et biologiques des radiations*, Monogr. Sér. 10, Masson & Cie Éditeurs, Paris, 1966, pp. 189–312.
3. F. L. Hirshfeld and G. M. J. Schmidt, *J. Polym. Sci. A*, **2**, 2181 (1964).
4. H. Morawetz, *Acta Cryst.*, **A25**, S223 (1969).
5. I. Olovsson, *Arkiv Kemi*, **16**, 437 (1960/61).
6. J. Karle and I. L. Karle, *Acta Cryst.*, **21**, 849 (1966).
7. T. Ukaji, *Bull. Chem. Soc. Japan*, **32**, 1275 (1959).
8. F. R. Ahmed and D. W. J. Cruickshank, *Acta Cryst.*, **6**, 385 (1953).
9. S. F. Darlow, *Acta Cryst.*, **13**, 683 (1960).
10. Y. Chatani, Y. Sakata, and I. Nitta, *J. Polym. Sci. B*, **1**, 419 (1963).
11. A. J. Restaino, R. B. Mesrobian, H. Morawetz, D. S. Ballantine, G. J. Dienes, and D. J. Metz, *J. Amer. Chem. Soc.*, **78**, 2939 (1956).
12. C. H. Bamford, G. C. Eastmond, and J. C. Ward, *Nature*, **192**, 1036 (1961); *Proc. Roy. Soc. (London)*, **A271**, 357 (1963).

Received November 3, 1970
Revised February 18, 1971

JOURNAL OF POLYMER SCIENCE: PART A-2 VOL. 9, 1517–1523 (1971)

Vibrational Analysis of Poly(vinylidene Fluoride)

F. J. BOERIO and J. L. KOENIG, *Division of Macromolecular Science, Case Western Reserve Univeristy, Cleveland, Ohio 44106*

Synopsis

A vibrational analysis has been carried out for the two crystalline forms of poly(vinylidene fluoride) (PVF_2). The Raman spectrum of the planar form of PVF_2 is also reported. The band assignments are made on the basis of the spectral properties including the infrared dichroism and Raman intensities. A force field is derived based on a force constant refinement procedure utilizing the frequency data for both crystal forms.

Introduction

Poly(vinylidene fluoride) (PVF_2) exists in at least two crystalline forms, the planar form 1 and the nonplanar form 2.[1] Planar PVF_2 is known to have one monomer in a repeat distance of 2.57 Å and CCC angles of 112°.[1] Recent work by Doll[2] indicates that form 2 has a TGTG* conformation, two monomers in the repeat unit, and CCC angles of 115°36′.

The infrared absorption of PVF_2 has been reported by Cortili and Zerbi[1] and by Enomoto et al.[3] Cortili used the infrared spectrum to deduce chain conformations while Enomoto reviewed the spectra and carried out a vibrational analysis using force constants transferred from polyethylene and tetrafluoroethylene. The results of these two investigations are in agreement but for two points. Cortili assigned a CH_2 rocking mode to a medium intensity band at 797 cm^{-1} in form 2, while Enomoto suggested that since this band is weak, it is not a fundamental. Cortili assigned a CF_2 rocking mode at 298 cm^{-1} in form 1, while Enomoto assigned this mode at 490 cm^{-1}.

We have previously reported[4] the Raman spectrum of form 2 PVF_2 and offered tentative band assignments. In this paper we present the Raman spectrum of planar (form 1) PVF_2 and discuss band assignments based on vibrational analysis.

Experimental

The sample of form 1 PVF_2 was a copolymer prepared by the Diamond Shamrock Co. and characterized by Doll.[2] The sample contained 93 mole-% percent vinylidene fluoride and 7 mole-% tetrafluoroethylene. The crystallinity was 64% by density and 59% by wide-angle x-ray diffraction. The sample was found to have the planar conformation by x-ray methods.

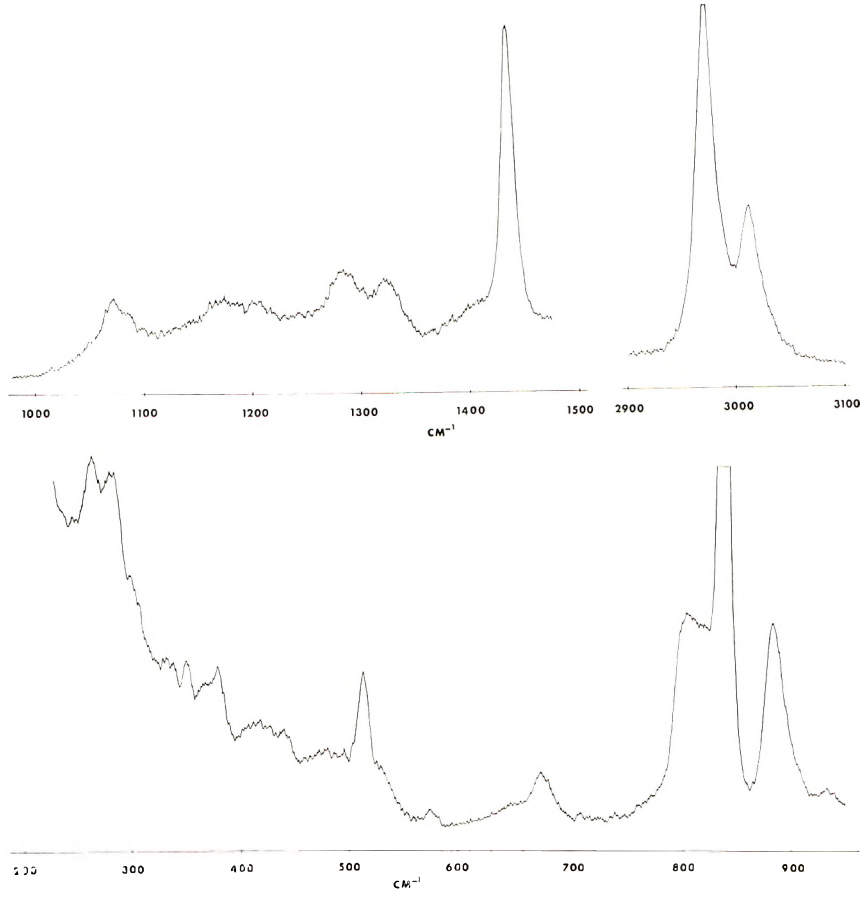

Fig. 1. Raman spectrum of planar poly(vinylidene fluoride).

The spectrum of form 1, excited with the 4880 Å line of a Coherent Radiation Laboratories, Model 52A, argon-ion laser and recorded by a Spectra Physics Model 700 Raman spectrometer, is shown in Figure 1.

Details of Calculation

For the vibrational analysis the CH bond length was taken as 1.09 Å, the CF bond as 1.34 Å, and the CC bond as 1.54 Å. The FCF and HCH bond angles were assumed to be 109°28′. In planar PVF_2 the angle CCC was taken as 112° while in TGTG* PVF_2 this angle was 115°36′.

The analysis was carried out in steps. First, force constants were transferred from polyethylene[5] and polytetrafluoroethylene.[6] Assignments for the A_1, B_1, and B_2 modes in form 1 and for some prominent bands in form 2 were made. New force constants were computed and additional assignments were made. This process was repeated several times until only a few bands remained unassigned. The calculation tended toward singularity on all iterations but application of a damping factor of 0.02 enabled a

TABLE I
Calculated and Observed Frequencies and Potential Energy Distribution (PED) for Planar PVF_2[a,b]

Species	Frequency, cm^{-1} Obsd	Frequency, cm^{-1} Calcd	PED, %
A_1	2984	2980	CH(100)
	1435	1434	CHH(72) + CCH(17)
	1180	1185	CC(43) + CCC(47) + CF(45)
	879	886	CF(59)
	509	516	CFF(77)
A_2		990	CCH(144)
	(265)	270	CCF(131)
B_1	3020	3020	CH(100)
	1274	1256	CF(93) + CCF(27)
	840	844	CCH(58) + CF(26)
	490	483	CCF(67)
B_2	1400	1398	CCH(71) + CC(47)
	1070	1063	CC(71) + CCH(27) + CCF(29)
	480	484	CCF(79)

[a] Because of contributions from interactions, the PED among the diagonal force constants may be greater than 100%.

[b] Observed frequencies in parentheses were not used to compute force constants.

fast convergence to be achieved. The final assignments for forms 1 and 2 of PVF_2 are given in Tables I and II along with elements of the potential energy distribution. The final force constants are given in Table III.

Discussion

The factor group of the line group of an isolated chain of planar PVF_2 is isomorphous to the point group C_{2v}. The normal modes are distributed among the symmetry species as $5A_1$, $3B_1$, $2A_2$, and $4B_2$ and have the following approximate descriptions:

A_1: $\nu_s(CH_2)$, $\delta(CH_2)$, $\nu_s(CF_2)$, $\delta(CF_2)$, $\nu_s(CC)$
A_2: $\gamma_t(CH_2)$, $\gamma_t(CF_2)$
B_1: $\gamma_w(CH_2)$, $\gamma_w(CF_2)$, $\nu_a(CC)$
B_2: $\nu_a(CH_2)$, $\gamma_r(CH_2)$, $\nu_a(CF_2)$, $\gamma_r(CF_2)$

All of the normal modes are active in the Raman effect, but the A_2 modes are inactive in the infrared spectra. The B_1 modes have parallel infrared dichroism, and the A_1 and B_2 modes are perpendicular.

For form 2, PVF_2 having the TGTG* structure, the factor group is isomorphous with the point group C_s. Each of the line-group normal modes of the planar molecule splits into two components, the A' modes where the two monomers in the repeat unit vibrate in phase and the A'' modes where the two monomers vibrate out of phase. The A'' modes have perpendicular infrared dichroism, while the A' modes are a mixture of parallel and perpendicular.[1]

TABLE II
Calculated and Observed Frequencies and Potentia
Energy Distribution (PED) for TGTG* PVF_2[a,b]

Species	Frequency, cm^{-1} Obsd	Calcd	PED, %
A'	3022	3020	CH(100)
	2984	2980	CH(100)
	1428	1424	CHH(73) + CCH(17)
	1404	1404	CCH(76) + CC(33)
	1294	1285	CF(77) + CCF(24) + CC(13)
	1149	1161	CC(62) + CCH(22) + CCF(22) + CF(21)
	1070	1071	CF(48) + CCH(41) + CC(26)
	976	961	CCH(102)
	876	870	CC(31) + CF(21) + CCC(13)
	845	825	CCH(54) + CF(18)
	611	601	CFF(24) + CCF(24)
	488	498	CCF(45) + CFF(30)
	413	420	CCF(52)
	289	299	CCF(84)
	214	218	CCF(79) + CCC(34)
		63	CCC(37) + τ(36) + CCF(25)
A''		3020	CH(100)
		2980	CH(100)
	(1440)	1432	CHH(60) + CCH(26)
	1384	1383	CCH(53) + CC(18) + CF(17)
	1213	1251	CF(68) + CCH(36)
	1182	1175	CF(41) + CCH(38) + CC(24) + CCC(21)
	1059	1058	CC(91)
	(943)	948	CCH(103)
	(907)	909	CC(47) + CCH(18)
	799	811	CCH(72)
	768	757	CCF(35) + CF(29) + CCC(23)
	538	517	CFF(66)
		400	CCF(84)
	357	365	CCF(68)
		272	CCF(71)
		113	CCC(63) + CCF(41)

[a] Because of contributions from interactions, the PED among the diagonal force constants may be greater than 100%.

[b] Observed frequencies in parentheses were not used to compute force constants.

The assignment of the bands observed for form I PVF_2 is fairly straightforward. The bands at 3020 cm^{-1} and 2984 cm^{-1} may be assigned to B_2 $\nu_a(CH_2)$ and $A_1\nu_s(CH_2)$, respectively. The strong Raman line near 1435 cm^{-1} is assigned to $A_1\,\delta(CH_2)$. The band at 1400 cm^{-1} in the infrared spectrum has parallel dichroism and is assigned to $B_1\gamma_w(CH_2)$. The broad, weak Raman band near 1180 cm^{-1} is assigned to $A_1\nu_s(CC)$ by analogy with other planar polymers, and $B_2\nu_a(CF_2)$ is then assigned to the strong infrared band at 1274 cm^{-1}. The weak Raman line near 1070 cm^{-1} has parallel

TABLE III
Valence Force Constants for PVF_2

Constant	Coordinate(s) involved	Common atom(s)	Calculated value[a]
1	CH		4.902
2	CC		4.413
3	CC,CF	C	0.740
4	CC,CC	C	0.148
5	CC,CCH	CC	0.206
6	CC,CCC	CC	0.273
7	CC,CCF	CC	0.567
8	CH,CH	C	0.058
9	CF		5.960
10	CF,CF	C	0.621
11	CF,CFF	CF	0.674
12	CCH		0.615
13	CCH,CCH	CC	0.105
14	CCH,CCH	CH	0.074
15	CHH		0.481
16	CCC		1.248
17	CCC,CCC(t)	CC	−0.036
18	CCF		1.262
19	CFF		1.280
20	τ	CC	0.050[b]
21	CF,CCF	CF	0.500
22	CCF,CCF	CC	0.178
23	CCF,CCF	CF	0.143
24	CCC,CCC(g)	CC	−0.064
25	CCC,CCH(g)	CC	0.106
26	CCC,CCH(t)	CC	0.207
27	CCC,CCF(g)	CC	−0.085
28	CCC,CCF(t)	CC	0.239
29	CCH,CCF(t)	CC	0.063
30	CCH,CCF(g)	CC	0.055

[a] Stretch constants have units of md/A; Stretch-bend interactions have units of md/rad; bending constants have units of md-Å/rad^2.

[b] Torsional force constant constrained to this value.

infrared dichroism and is assigned to $B_1\nu_a$(CC). The medium intensity Raman line at 879 cm^{-1} is very strong in the infrared and is assigned to $A_1\nu_s(CF_2)$, while the intense Raman line at 839 cm^{-1} is assigned to $B_2\gamma_r$ (CH_2). The line at 509 cm^{-1} is assigned to the $A_1\delta(CF_2)$ mode while the infrared bands[3] at 490 and 480 cm^{-1} are assigned to $B_2\gamma_r(CF_2)$ and $B_1\gamma_w$ (CF_2), respectively.

One of the two Raman lines at 282 and 265 cm^{-1} must be assigned to the $A_2\gamma_t(CF_2)$ mode. The line at 282 cm^{-1} is close to the $\gamma_t(CF_2)$ mode in PTFE (291 cm^{-1}) and may be due to monomer reversal during polymerization or to the tetrafluoroethylene comonomer. The $A_2\gamma_2(CF_2)$ mode is assigned at 265 cm^{-1}.

The lack of intensity of modes such as ν_s(CC) and ν_a(CC) in planar PVF_2 is remarkable. These modes are the strongest lines in the Raman spectra

of paraffins and polyethylene but appear very weakly in planar PVF_2. Perhaps this weakness may be understood by comparing the eigenvectors for $\nu_s(CC)$ and $\nu_a(CC)$ in planar PVF_2 with the eigenvectors for the corresponding modes in polyethylene. In polyethylene, all carbon atoms move with the same amplitude during these vibrations but in planar PVF_2 the carbon atoms to which the fluorines are bonded move with considerably smaller amplitudes than do the carbon atoms bonded to the hydrogen atoms. This leads to smaller derived polarizabilities and intensities in planar PVF_2.

On the other hand the broad, medium-intensity band near 810 cm^{-1} in planar PVF_2 can not be assigned to a line-group mode of the isolated molecule and must be related to monomer reversal or the amorphous fraction of the sample.

The assignment of the modes of form 2 PVF_2 is aided by the infrared dichroism and analogy with form 1. The $\delta(CH_2)$ modes are found at 1428 cm^{-1} (A') and 1440 cm^{-1} (A''). The parallel infrared band at 1404 cm^{-1} is assigned to $A'\gamma_w(CH_2)$; the A'' mode is assigned at 1384 cm^{-1}. The assignment of the $\nu_a(CF_2)$ modes is not so unambiguous. A band at 1294 cm^{-1} is observed in Raman spectra reported here and in infrared spectra reported by Cortili. Enomoto did not observe this band in infrared spectra but did observe a band near 1270 cm^{-1}. A very weak shoulder is seen near 1278 cm^{-1} in the Raman spectra. This band is near a band found in the planar molecule and may be due to short planar segments in the TGTG* molecule. The $\nu_a(CF_2)$ modes are assigned at 1294 cm^{-1} (A') and 1213 cm^{-1} (A''). The Raman line at 1149 cm^{-1} has parallel infrared dichroism and is assigned to $A'\nu_s(CC)$. The $A''\nu_s(CC)$ mode may be assigned to the infrared band at 1182 cm^{-1} or the Raman line observed at 1198cm^{-1}. One of these two bands would then have to be assigned to irregular monomer addition of the comonomer.

The $\nu_a(CC)$ modes are assigned to the infrared band at 1070 (A'), which has parallel infrared dichroism, and the Raman band at 1059 cm^{-1} (A'').

The $\gamma_r(CH_2)$ modes, not observed in the Raman spectra of form 1, PVF_2, are assigned to the medium intensity Raman line at 976 cm^{-1} (A'') and to the weak band observed at 943 cm^{-1} (A') in infrared by Enomoto. The band at 879 cm^{-1} in the planar molecule appears to correspond to the strong Raman line at 876 cm^{-1} (A') and a weak infrared band near 907 cm^{-1} (A'') observed by Enomoto. The $\gamma_r(CH_2)$ modes are found at 799 cm^{-1} (A'') and 845 cm^{-1} (A').

The $A'\gamma_w(CF_2)$ mode is assigned to the band at 611 cm^{-1} which has parallel infrared dichroism, and the $A''\gamma_w(CF_2)$ mode is assigned to the weak Raman line near 768 cm^{-1}. These bands are at considerably higher frequencies than the wagging mode in planar PVF_2(480 cm^{-1}) as a result of strong coupling with motions such as $\delta(CF_2)$ and $\delta(CCC)$. The A'' $\delta(CF_2)$ mode is assigned to the medium intensity Raman band at 538 cm^{-1}. The A' mode may be assigned to the medium intensity Raman line at 488 cm^{-1} but, as noted above, this band is a coupling of the $\delta(CF_2)$ and $\gamma_w(CF_2)$

modes. The $A'\gamma_r(CF_2)$ mode is assigned to the strong Raman line at 413 cm^{-1}, but the A'' mode is not located. This mode may be the weak infrared band at 374 cm^{-1},[1] observed as a weak shoulder near 365 cm^{-1} in Raman spectra, but a definite assignment cannot be made. The $A'\gamma_t(CF_2)$ mode is assigned to the intense Raman line at 289 cm^{-1} and the A'' mode is assigned to the weak Raman line near 357 cm^{-1}.

The band observed at 214 cm^{-1} in infrared spectra is assigned to the A' δ(CCC) mode although it is highly coupled. The A'' mode is not located. The torsional modes, calculated at 63 cm^{-1} (A') and 113 cm^{-1} (A''), are similarly not located.

The diagonal force constants found for PVF_2 may be compared with results of perfluorocyclobutane (PFCB)[7] and polytetrafluoroethylene (PTFE).[6] The CF stretching constant of 5.960 md/Å in PVF_2 is in excellent agreement with values of 6.095 md/Å in PTFE and 6.06 md/Å in PFCB. The CCF bending constant is 1.262 md − Å/rad^2 in PVF_2, 1.086 md − Å/rad^2 in PTFE, and 1.17 md − Å/rad^2 in PFCB. The CFF bending constants for these molecules are curiously different. Values of 1.628, 1.44, and 1.282 md − Å/rad^2 are found respectively for PTFE, PFCB, and PVF_2.

The CC stretching and CCC bending constants of 4.413 md/Å and 1.248 md − Å/rad^2 are closer to values usually found for hydrocarbons[5] than to values for PTFE.[6] The CCH and CHH constants are found to be 0.615 and 0.481 md − Å/rad^2, close to the usual hydrocarbon values.[5]

In general, the off-diagonal force constants are considerably different from corresponding constants in either hydrocarbons or PTFE. This is presumably the result of coupling between motions of the CH_2 and CF_2 groups. The extent of the coupling may be observed in the potential energy distributions in Tables I and II.

References

1. G. Cortili and G. Zerbi, *Spectrochim. Acta*, **23A**, 285 (1967).
2. W. W. Doll and J. B. Lando, *J. Macromol. Sci. Phys.*, **B4**, 309 (1970).
3. S. Enomoto, Y. Kawai, and M. Sugita, *J. Polym. Sci. A-2*, **6**, 861 (1968).
4. F. J. Boerio and J. L. Koenig, *J. Polym. Sci. A-2*, **7**, 1489 (1969).
5. R. G. Snyder, *J. Chem. Phys.*, **47**, 1316 (1967).
6. F. J. Boerio and J. L. Koenig, *J. Chem. Phys.*, **52**, 4826 (1970).
7. H. H. Classen, *J. Chem. Phys.*, **18**, 543 (1950).

Received October 13, 1970
Revised February 5, 1971

NOTES

Application of Positron Lifetime Measurement to the Study of Solid-State Polymerization of Dimethyl Itaconate

Over the past 20 years, extensive studies of positron annihilation in matter have been carried out. Recent books and reviews provide accounts of this work.[1-3] The application of positron annihilation as a probe in the study of the physics and chemistry of solids has proved to be very fruitful.[4,5]

Here, we report lifetime measurements of positrons in a solid monomer in which polymerization is initiated by ionizing radiation.

Lifetime measurements were performed with a conventional experimental set-up, with Naton 136 scintillators coupled to Phillips 56 AVP photomultipliers and a time-to-amplitude converter of the Weissberg type.[6] The resolution of the time analysis, as defined by the full width at half maximum of the time spectrum of ^{60}Co γ-rays, was 0.7 nsec.

Dimethyl itaconate (DMI, mp -35°C) was purified by recrystallization from methanol and dried over silica gel. A positron source, about 10 μCi of ^{22}NaCl enveloped in thin Mylar film, was placed in the center of a glass ampoule. The monomer was introduced into the ampoule, which was sealed off under vacuum (1×10^{-4} torr) after repeated melting and freezing of the monomer. The solid monomer was polymerized at 30°C by ^{60}Co γ-rays. The lifetime was measured at 0°C before and after irradiation.

Positron lifetime spectra after various irradiation doses are shown in Figure 1. It is clear from the figure that the intensity I_2 of the long-lived component in the decay curve (resolved as usual into two components), increases with the irradiation dose, while the lifetime τ_2 remains unchanged. The slow component in unirradiated solid DMI is small, and values of τ_2 and I_2 are difficult to determine exactly because the statistical accuracy is poor. In this case, τ_2 was taken equal to the value obtained for irradiated DMI in order to evaluate I_2. Figure 2, in which I_2 is plotted against monomer conversion, shows how I_2 increases with increasing conversion. In the initial stage of polymerization, only trace amounts of polymer were detected. However, after the induction period, the conversion increased rapidly.

The volume change in solid DMI during polymerization was measured by dilatometry; and, as is shown in Figure 3, the volume of the system increases during polymerization. This indicates that the free volume is greater in the amorphous polymer phase than in the crystalline monomer phase.

If the increase in I_2 is related to increase in free volume, I_2 should also increase when the crystallization of monomer is hindered. Polymer obtained by radiation polymerization of solid DMI was dissolved in the monomer in various concentrations, and the solutions were solidified quickly at -196°C. The lifetime of positrons in these solid mixtures was measured at 0°C, with the result shown in Figure 2, whence it is clear that I_2 is increased by the presence of dissolved polymer chains. When a monomer–polymer mixture was annealed at room temperature for ten days, I_2 was observed to decrease appreciably (Fig. 2).

Therefore it may be concluded that I_2 is determined by the amount of free volume. In the free volume *ortho*-positronium (the long-lived component) is annihilated by slow pick-off, but in crystalline regions of the monomer it is presumably annihilated rapidly.

The above conclusion agrees with some earlier results. When polytetrafluoroethylene was heat-treated to increase the amorphous content, I_2 was found to increase.[4]

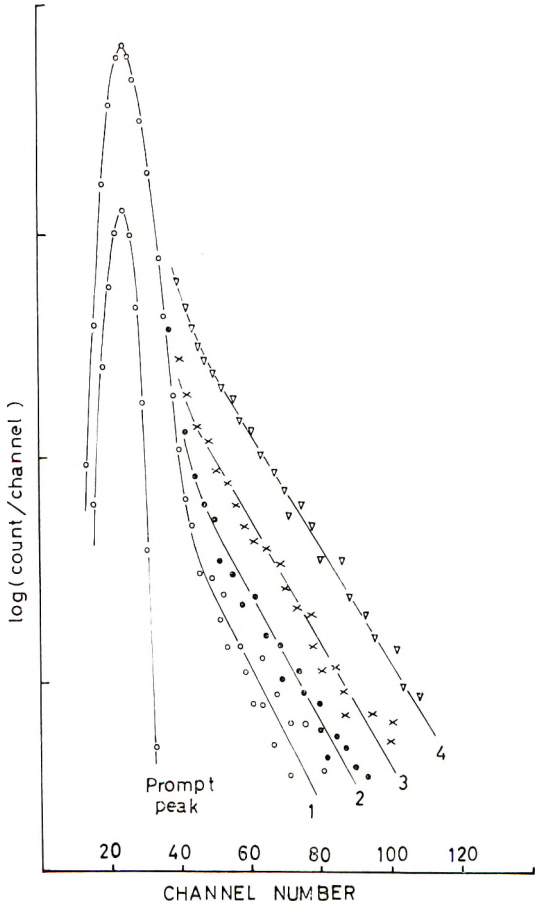

Fig. 1. Lifetime spectra in irradiated DMI for various irradiation doses: (*1*) before irradiation, (*2*) 4.5 Mrad, (*3*) 11.7 Mrad, (*4*) 17.0 Mrad.

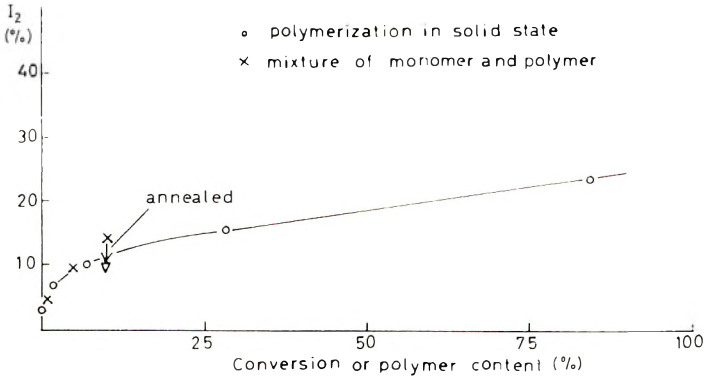

Fig. 2. I_2 as a function of conversion during radiation polymerization of DMI in the solid state. The change from × to ▽ represents the effect of annealing.

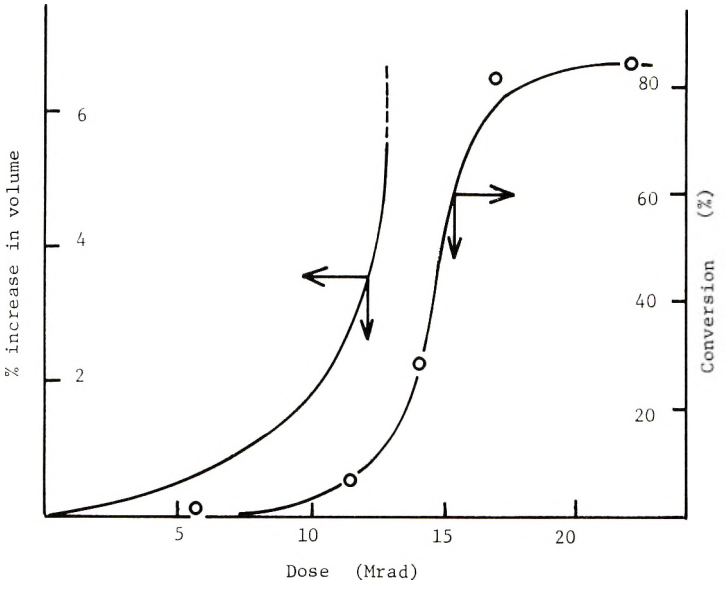

Fig. 3. Conversion to polymer and volume change in solid DMI as a function of irradiation dose.

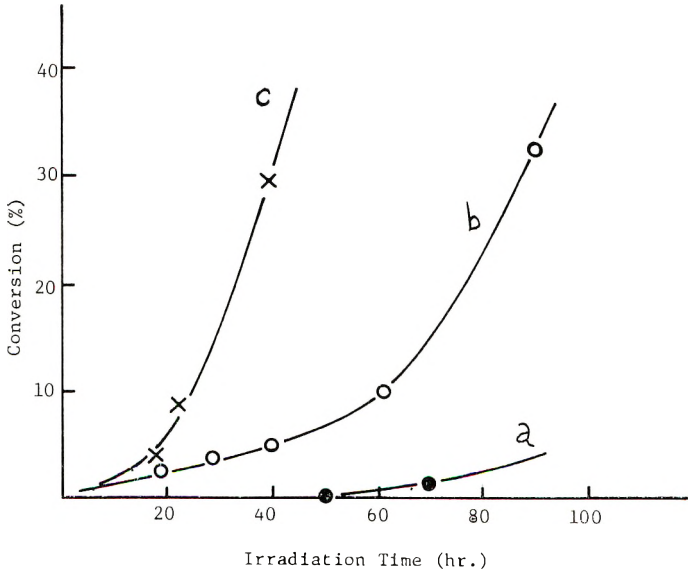

Fig. 4. Kinetic curves for polymerization of samples of solid DMI prepared under different conditions: (*a*) single crystal, (*b*) DMI solidified at room temperature, (*c*) DMI shock cooled at −196°C. Dose rate, 6×10^4 r/hr. Irradiation temperature, 30°C.

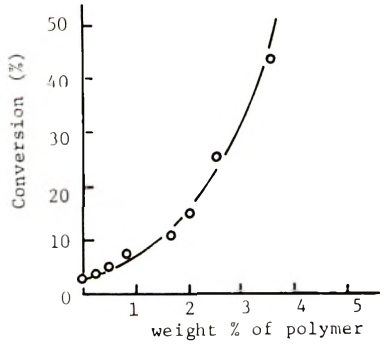

Fig. 5. Conversion in monomer–polymer mixtures as a function of initial polymer concentration: irradiation at 6×10^4 r/hr at 30°C for 20 hr.

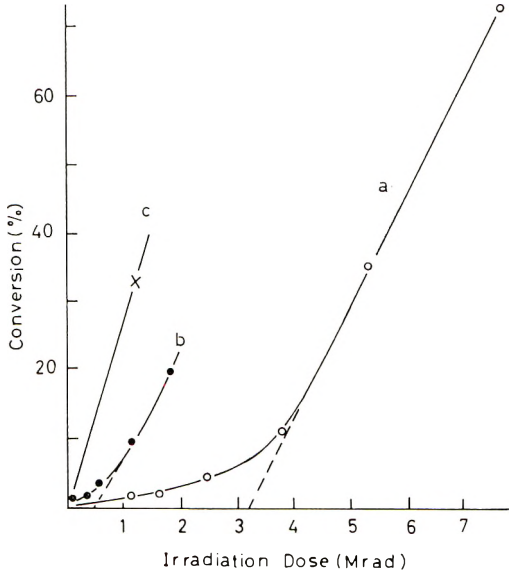

Fig. 6. Kinetic curves in solid monomer-polymer mixtures: (*a*) pure solid monomer; (*b*) 1.3% polymer (initially); (*c*) 3.0% polymer. Dose rate, 6×10^4 r/hr. Irradiation temperature, 30°C.

It was also shown by the temperature dependence of lifetimes spectra of polyethylene that the value of I_2 increases with increasing temperature.[5] In these two studies, *ortho*-positronium, which is formed in the crystalline regions, is thought to be annihilated at a rapid pick-off rate. Therefore, annihilation in the crystalline regions does not contribute to the slow component. The increase in I_2 both in polymerizing solid DMI and in monomer–polymer mixtures can also be explained by the increase of amorphous regions in the solid monomer due to the polymerization. The small I_2 value in solid DMI before irradiation ($I_2 = 3\%$) may be related to the fact that very little *ortho*-positronium is formed in disordered regions such as defects or surfaces of crystallites. When polymer nuclei are formed in the crystalline monomer phase by irradiation, the extent of the disordered region increases and the *ortho*-positronium fraction increases with the number of nuclei.

It is interesting to note that I_2 increases rapidly during the induction period in polymerization when conversion is below 10%. Above 10% conversion, I_2 increases linearly and slowly with conversion, and the transition in I_2 corresponds to that in the conversion curve shown in Figure 3. This indicates the autocatalytic nature of the polymerization.

Some kinetic studies have been made in connection with those mentioned above. Figure 4 shows the kinetic curves of several samples of solid DMI prepared under different conditions. In a nearly perfect crystal, the rate of polymerization is very slow (curve *a*), but in disordered crystal formed by shock-cooling at −196°C from the liquid state, polymerization is fast.

Conversion of monomer as a function of the initial amount of polymer in various monomer–polymer mixtures is shown in Figure 5. These solid mixtures were irradiated at a dose rate of 6×10^4 r/hr at 30°C for 20 hr. The polymerization rate increased with the amount of polymer in the mixture. Figure 6 shows kinetic curves for the mixture. The induction period is shortened by introduction of polymer into solid monomer and is not observed at all in monomer including 3% polymer. Therefore, it can be concluded that polymerization takes place more easily in the disordered state of the monomer, and that the autocatalytic propagation of polymerization starts when there is sufficient disorder in the crystal. Phenomena of this type can be detected by positron lifetime measurement, and it is expected that detailed studies will yield important information concerning the mechanism of solid-state polymerization.

References

1. J. H. Green and J. Lee, *Positronium Chemistry*, Academic Press, New York, 1964.
2. A. T. Stewart and L. O. Roellig, Eds., *Positron Annihilation*, Academic Press, New York, 1967.
3. V. I. Goldanskii, *Atomic Energy Rev.*, **6**, 3 (1968).
4. S. J. Tao and J. H. Green, *Proc. Phys. Soc.*, **85**, 463 (1965).
5. W. Brandt and I. Spirn, *Phys. Rev.*, **142**, 231 (1966).
6. H. Weissberg, *Nucl. Instrum. Methods*, **32**, 33 (1965).
7. Y. Tabata, Y. Ito, and K. Oshima, *Proceedings of Symposium Organic on Solid State Chemistry*, BNL, USA, 1968.

YASUO ITO
SHINGO KATSURA
YONEHO TABATA

Department of Nuclear Engineering
Faculty of Engineering
University of Tokyo,
Tokyo, Japan

Received December 4, 1969
Revised February 2, 1971

Technique of XYZ Photographic Light Scattering as Applied to Uniaxially Drawn Polyethylene

The photographic light-scattering (LS) technique, first introduced by Stein et al. in 1955,[1] has, since then, only been applied to the study of thin films, the laser beam passing normal to the plane of the film. Only thin films have been used, owing to the necessity of keeping the optical density low in order to minimize the multiple scattering which might complicate interpretation of scattering patterns. For this reason, no attempt to measure such patterns from thick "bulk" samples has been made. To do so, however, could be quite valuable in investigating changing morphology through a layer of a material, or the structure at some specific location, such as a region of curvature in a molded bottle.

The difficulty of multiple scattering in thick samples can easily be overcome by "sectioning," i.e., cutting thin sections approximately 5 mils thick from the bulk material. By sectioning in different planes, it is possible to better correlate the patterns with proposed models or presumed assumptions such as the affine deformation of a spherulite under low uniaxial extension. The method also allows for a more comprehensive study of the superstructure of biaxially deformed materials, as has been carried out with qualitative success on the basis of available theory.[2]

To demonstrate that light scattering can be measured from thin sectioned films, some initial data obtained from uniaxially drawn polyethylene will be presented here. Since the results can be anticipated from previous theoretical and experimental investigations, which provides a basis to prove or disprove this application of sectioning, this material has been used.

For clarity, the standard notation denoting the arrangement of the electric vector of the polarizer P and analyzer A with respect to the stretch axis has been modified. The familiar H_H and V_V notation is no longer clear since the incident beam may also be propagated along the stretch axis. We therefore simply denote all patterns with the P, A vectors aligned and crossed as parallel polar (PP) and crossed polar (CP) patterns, respectively. In each case the relation of the sample axes to the vectors is given with the pattern as is required for proper interpretation of results. The sample axes X, Y, and Z are designated to lie along the film-normal, transverse direction, and draw direction, respectively.

An experimental Alathon polyethylene sample of density 0.933 g/cm^3 was compression-molded at 150°C into a film of about $^1/_8$ in. thickness. The molten film was then air-quenched at room temperature and cut into $^1/_2$ in. strips. One strip was left undrawn, others were drawn slowly to less than 50%. Still another was drawn on an Instron Tester until necking occurred in a sufficient portion of the material. It was estimated by use of bench marks that the material in the neck region had an imposed strain of about 150%. Knowledge of the actual strain is not of high importance in this discussion since at this point we only wish to illustrate the application of this XYZ LS technique to uniaxially drawn materials. Samples were then sectioned and scattering patterns were obtained.

Figures 1*a*–1*f* show the CP and PP patterns obtained with the incident beam directed along the X, Y, and Z axes of the undrawn sample. The PP patterns were identical, as expected with patterns of the H_H type. Figures 2*a*–2*h* show similar patterns taken from a sample which was drawn slowly to about 20% elongation. If true uniaxial deformation of the spherulites had occurred, the incident beam would have "seen" the spherulites along each axis as in the sketches in Figure 2. Figures 3*a*–3*l* show the same type of patterns taken in the neck region of the sample drawn on the Instron machine.

As is required in a uniform film, the three PP patterns of Figure 1 are equivalent. It is clear that distinct patterns can easily be obtained by sectioning along any of the three axes X, Y, or Z. In fact, if desired, patterns can be obtained at any angle to a chosen reference axis. Figure 1 also clearly shows that the sample has a uniform, truly spherulitic structure.

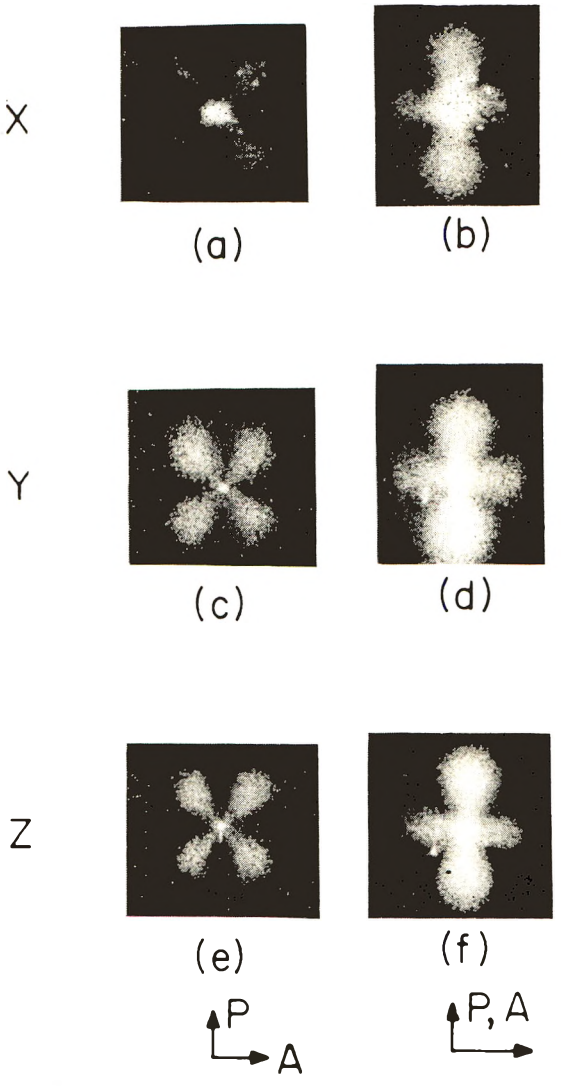

Fig. 1. Light-scattering patterns taken with beam along X, Y, and Z axes of an undrawn sample. Both CP and PP patterns are shown. The stretch axis, Z, is vertical in the X and Y patterns, the X axis is vertical in the Z patterns. (Polarizer, P, and analyzer, A, orientation with respect to the sample axes are given with the respective patterns.)

The patterns of Figure 2 allow one to see nearly what would be expected if true spherulitic uniaxial deformation had occurred. Both the X- and Y-axis patterns show nearly equivalent CP and PP patterns while those taken along the Z axis are essentially equivalent to those found when the incident beam encounters an undeformed spherulite.* It should be noted that in the unnecked material it is the symmetry of the patterns that must be compared rather than the intensities. Intensity varies between different pat-

* This is not to imply that the spherulite is undeformed, but rather that the beam "sees" a circular spherulite shape since the beam propagates along the draw axis, Z.

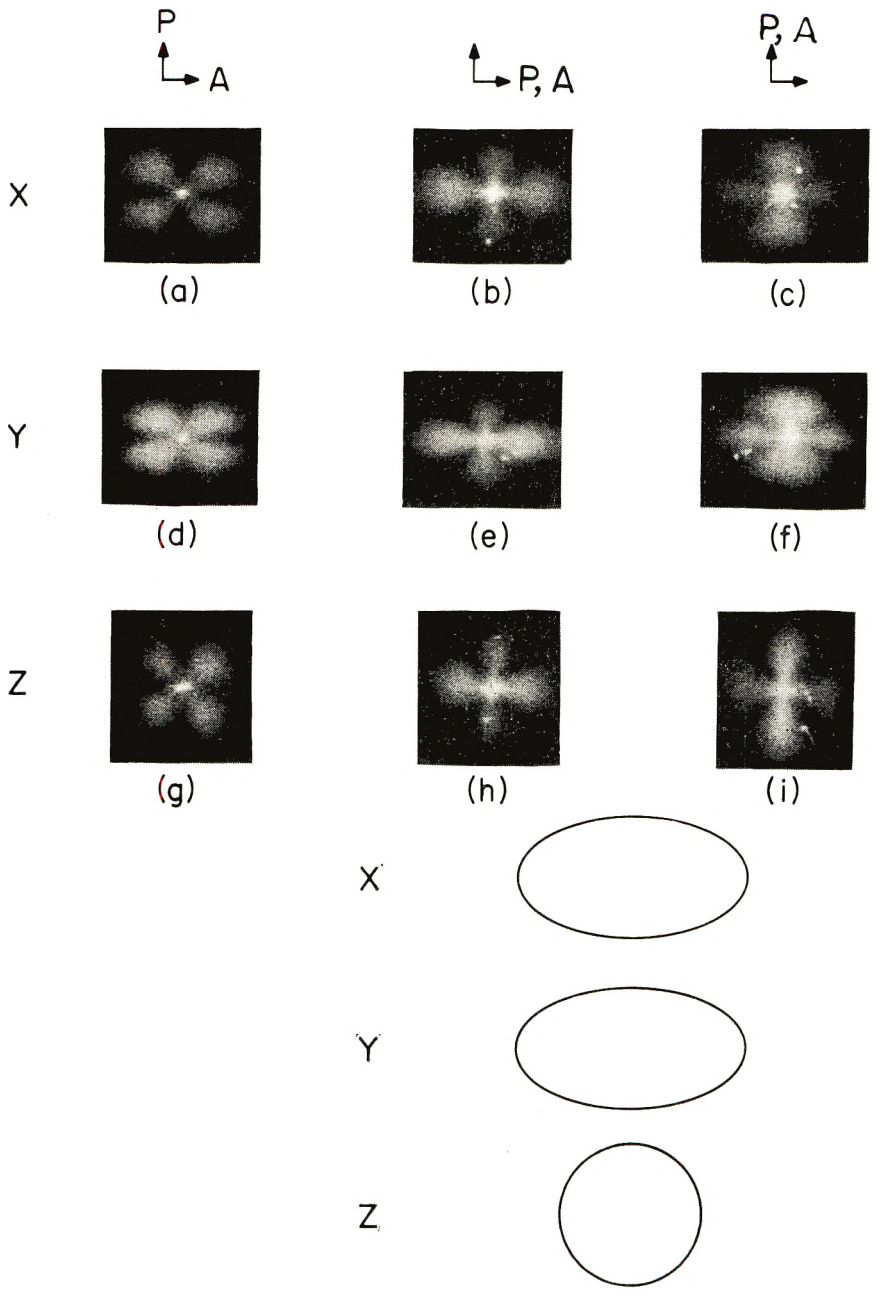

Fig. 2. Light-scattering patterns taken with beam along the X, Y, and Z axes of a sample drawn approximately 20%. Both CP and PP patterns are shown. The stretch axis, Z, is vertical in the X and Y patterns, the X axis is vertical in the Z patterns. (Polarizer P and analyzer A orientation with respect to the sample axes are given with the respective patterns.) The sketches illustrate how the laser beam "sees" the deformed spherulite.

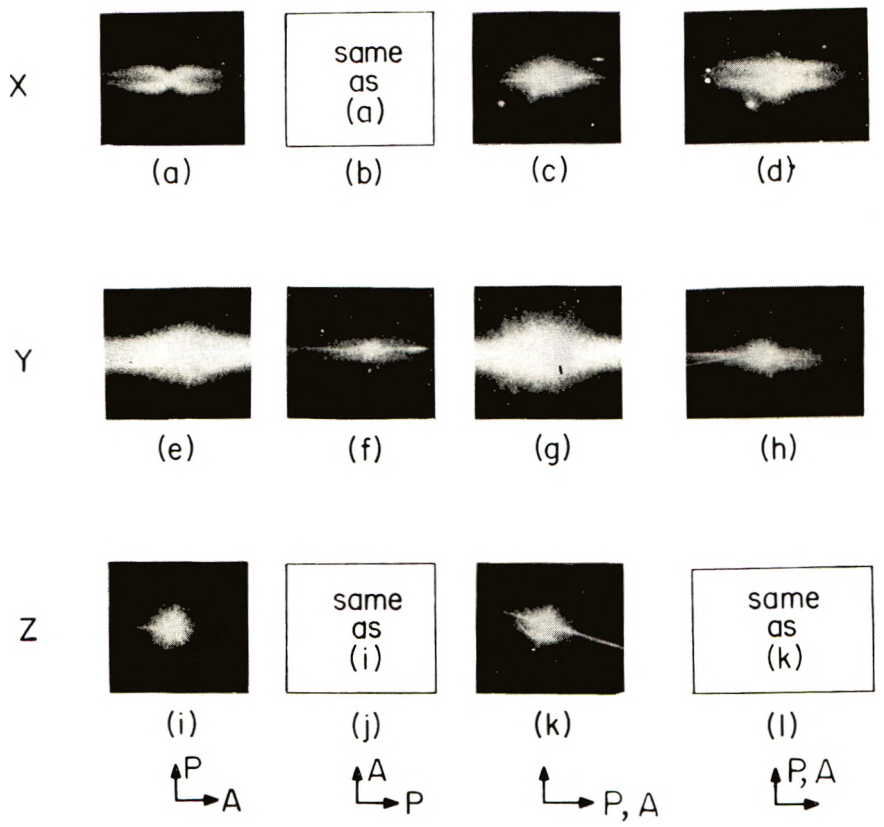

Fig. 3. Light-scattering patterns from the necked material taken with the beam along the X, Y, and Z axes. Both CP and PP patterns are shown. The stretch axis, Z, is vertical in the X and Y patterns, the X axis is vertical in the Z patterns. (Polarizer P and analyzer A orientation with respect to the sample axes are given with the respective patterns.)

terns of the same type because section thicknesses are slightly different. The patterns seem to be in excellent agreement with those expected from the theory[3] applicable to uniaxial deformation. The slight difference in degree of symmetry between the CP patterns for the X and Y axis is most likely due to the fact that since different sections are used for each pattern, differences are caused by slightly nonuniform drawing. The fact that the Z-axis CP pattern has fourfold symmetry is strong evidence, however, of uniform drawing on a local basis. From Figure 3 it is apparent that the shapes of the two types of PP patterns with the beam along either the X or the Y axes are not equivalent, as they were prior to drawing.† This is expected, since drawing induces both shape and optical anisotropy in the scattering body, i.e., the spherulite.

Turning briefly to Figure 3 and the neck region, we find that the patterns have changed quite drastically from the unnecked material (a not unexpected event since one is now dealing with a material that has been most likely transformed in morphology). During necking, a distinct spherulitic texture becomes more fibrillar in nature, owing to the partial unfolding of lamellar structure and further extension of amorphous material.

† Since we are discussing only X and Y axis PP patterns we remind the reader that the two types of patterns correspond to the familiar V_V and H_H types.

The theoretical interpretation of the resulting LS patterns becomes more complex because of the possible combination of scattering from different origins. For example, the patterns of Figure 3 are not described at all well by the scattering from deformed spherulites; they have some similarities to the patterns expected from rod scattering,[4] but are certainly not in total agreement. Further theoretical efforts using the rod model however, might be helpful. There is also the additional possibility that existing internal strain fields could have contributed to the scattering, thus adding to the complexity of these patterns. The simplest stages of this problem have been considered,[5] but much more theoretical work is necessary where nonuniform strain fields are imposed, as in multiaxial deformation.

Presently, we speculate that rod scattering or rod scattering combined with strain scattering may well be the primary cause of the patterns in Figure 3 since all the Z-axis patterns were very weak in intensity relative to the X- or Y-axis patterns and were circular. Such results would be expected if one were propagating the beam down a rod axis where the maximum internal strain and principal polarizability axes were parallel to the incident beam. We consider the standard scattering equation, eq. (1):

$$E = \int_V (\mathbf{M} \cdot \mathbf{O}) \cos K(\mathbf{r} \cdot \mathbf{s}) d\mathbf{r} \tag{1}$$

which, when applied to the scattering from anisotropic rods, leads to eq. (2)

$$E = C(\mathbf{M} \cdot \mathbf{O})L \frac{\sin (KaL/2)}{(KaL/2)} \tag{2}$$

where E is the amplitude of the scattered light, $\mathbf{M}$ is the induced dipole moment in the scattering volume-element and $\mathbf{O}$ is a unit vector parallel to the electric vector of the analyzer. The parameters L and a are, respectively, the length of the rod and a term dependent on the orientation of the rod with respect to the incident beam and to the analyzer electric vector; K is equal to $2\pi/\lambda$, where λ is the wavelength in the scattering medium, and C is a constant. Simple qualitative consideration of eq. (2) supports the data found specifically in the patterns in the necked region (Fig. 3). This follows from the fact that in such a case little scattering would be induced with the beam along Z since the magnitude of the scattered beam depends on the dot product $\mathbf{M} \cdot \mathbf{O}$. In the rod or strain scattering considered here, this dot product would be essentially zero, since the principal polarizability axis lies along the beam axis, i.e., the electric vector of the analyzer is normal to the polarizability axis. However, a lack of scattering would not be expected in all patterns with the beam along X or Y as is experimentally observed. It might be added that the intensity is less for the X- or Y-axis LS patterns in the neck region, relative to the unnecked regions, particularly in the PP patterns. This, however, is expected since, upon necking, the material transforms from a somewhat turbid state to a more transparent material. This is due to a decrease in the magnitude of the two terms which give rise to the majority of scattering by polyethylene.[6,7] These terms arise from (a) the correlation of density fluctuations and (b) the correlation of orientation fluctuations. It is reasonable to assume that both types of fluctuations would decrease in number for medium-density polyethylene "necked" at room temperature. The result is a decrease in turbidity of the sample and thus less scattering per unit volume of material.

The XYZ light-scattering technique, then, can give rise to distinct patterns when applied to such polymeric "bulk" samples. It is also apparent that in this case of uniaxial drawing, the results, at least for the unnecked material, are in excellent agreement with those expected from previous theory for scattering from undeformed and deformed spherulites. Certainly, a systematic study is warranted in uniaxially deformed materials by this technique, e.g., for studying the validity and limits of an affine deformation mechanism in such spherulitic materials under different deformation conditions.

References

1. R. S. Stein and M. B. Rhodes, *J. Appl. Phys.*, **31**, 1873 (1960).
2. G. L. Wilkes, *J. Materials Sci.*, in press.
3. R. S. Stein, P. Erhardt, J. J. van Aartsen, S. Clough, and M. Rhodes, in *Small Angle Scattering from Fibrous and Partially Ordered Systems* (*J. Polym. Sci. C*, **13**), R. H. Marchessault, Ed., Interscience, New York, 1966, p. 1.
4. M. B. Rhodes and R. S. Stein, ONR Tech. Rept. No. 48, Project NR 056-378, Contract NONR 3357(01), Polymer Research Institute, Univ. of Mass., Amherst (1968).
5. R. S. Stein and G. L. Wilkes, *J. Polym. Sci. A-2*, **7**, 1695 (1969).
6. R. S. Stein and P. R. Wilson, *J. Appl. Phys.*, **33**, 1914 (1962).
7. A. E. M. Keijzers, J. J. van Aartsen, and W. Prins, *J. Appl. Phys.*, **36**, 2874 (1965).

Garth L. Wilkes

Department of Chemical Engineering
Princeton University
Princeton, New Jersey 08540

Received October 23, 1970
Revised February 3, 1971

The *Journal of Polymer Science* publishes results of fundamental research in all areas of high polymer chemistry and physics. The *Journal* is selective in accepting contributions on the basis of merit and originality. It is not intended as a repository for unevaluated data. Preference is given to contributions that offer new or more comprehensive concepts, interpretations, experimental approaches, and results. Part A-1 *Polymer Chemistry* is devoted to studies in general polymer chemistry and physical organic chemistry. Contributions in physics and physical chemistry appear in Part A-2 *Polymer Physics*. Contributions may be submitted as full-length papers or as "Notes." Notes are ordinarily to be considered as complete publications of limited scope.

Three copies of every manuscript are required. They may be submitted directly to the editor: For Part A-1, to C. G. Overberger, Department of Chemistry, University of Michigan, Ann Arbor, Michigan 48104; and for Part A-2, to T. G Fox, Mellon Institute, Pittsburgh, Pennsylvania 15213. Three copies of a short but comprehensive synopsis are required with every paper; no synopsis is needed for notes. Books for review may also be sent to the appropriate editor. Alternatively, manuscripts may be submitted through the Editorial Office, c/o H. Mark, Polytechnic Institute of Brooklyn, 333 Jay Street, Brooklyn, New York 11201. All other correspondence is to be addressed to Periodicals Division, Interscience Publishers, a Division of John Wiley & Sons, Inc., 605 Third Avenue, New York, New York 10016.

Detailed instructions on preparation of manuscripts are given frequently in Parts A-1 and A-2 and may also be obtained from the publisher.

Two Professional Journals from Wiley-Interscience

JOURNAL OF APPLIED POLYMER SCIENCE

Board of Editors: H. Mark, W. Cooper, M. Morton, B. Ranby, P. Weiss

A necessary complement to the *Journal of Polymer Science*, the *Journal of Applied Polymer Science* is a convenient, comprehensive source of information on polymer research. Articles concentrate on systems, compounds, and products of technological significance in the field. Major areas treated include the analysis of polymers, including instrumentational methods; testing of plastics, elastomers, films, and fibers; adhesion and adhesives; emulsions and latex; mechanical properties; ion-exchange; diffusion and permeability; aging of polymers; extrusion and molding; and reinforcement and vulcanization. The journal's Symposia volumes contain proceedings of important borderline fields.

A Selection of Forthcoming Articles to be published in the *Journal of Applied Polymer Science*—

- *Crack Initiation in PVC for Subsequent Linear Elastic Fracture Mechanics Analysis*—P. G. Faulkner and J. R. Atkinson
- *Crease Recovery and Cuprammonium Solubility of Some Cross-Linked Cotton Fibers*—Frank S. H. Head
- *Non-Newtonian Flow and the Steady State Shear Compliance*—W. M. Prest, Jr., Roger S. Porter, and J. M. O'Reilly
- *Oligomer of O-Xylene as a Heat Stabilizer for Isotactive Polypropylene*—John Boor, Jr.
- *The Relation between Melt Flow Properties and Molecular Weight of Polyethylene*—Shigeru Saeda, Junji Yotsuyanagi, and Kinya Yamaguchi
- *Characterization of Ethylene Propylene Rubber and Ethylene Propylene Diene Rubber Networks* —A. M. Hassan and L. N. Ray, Jr.

Volume XV-Monthly, plus Symposia
Subscription Price: $150.00
Foreign Postage: $6.00
Back Volume prices on request

The journal is also available in a microfilm edition. Volume 1 (1959) through Volume XIII (1969) is available for $320.00. (This price applies only to subscribers to the journal. Prices for non-subscribers available on request.) Prices for individual volumes are available on request.

BIOPOLYMERS

An International Journal of Research on Biological Macromolecules

Editor: Murray Goodman, *Polytechnic Institute of Brooklyn*

Editorial Board: Elkan Blout, *Harvard Medical School;* D. F. Bradley, *Polytechnic Institute of Brooklyn;* Ephraim Katchalski, *The Weizmann Institute of Science, Rehovot, Israel;* Arthur Peacocke, *St. Peter's College, Oxford, England;* I. Tinoco, Jr., *University of California, Berkeley*

Biopolymers includes original research papers on biological macromolecules, related synthetic macromolecules, as well as relevant model compounds. The studies of such macromolecules involve their physical chemistry, organic chemistry, and biophysics. Covered in these three broad fields are synthesis, including biosynthesis, structure, chemical modification and reactions, catalytic function (in molecular terms) and other reaction mechanisms, macromolecular interactions, and organization. Three main types of articles are published in *Biopolymers*: manuscripts based on original research, short communications containing significant and novel results, and perspectives in biopolymer research. In the latter type of article, contributors present pertinent historical background, discuss and correlate current views, and suggest possible lines of development in future work.

A Selection of Forthcoming Articles to be published in *Biopolymers*—

- *A Model of the Orientation Symmetry of Water Molecules in the Biopolymers (by NMR Spectra)* —A. A. Khanagov
- *Optical Rotatory Dispersion of Mucopolysaccharides. III. Ultraviolet Circular Dichroism and Conformational Specificity in Amide Groups*— Audrey L. Stone
- *A Comparison of Helix Stabilities of Poly-L-Lysine, Poly-L-Ornithine and Poly-L-Diaminobutyric Acid*—M. J. Grourke and Julian H. Gibbs
- *Simple Methods for the Orientation of DNA Molecules in Films Suitable for Optical Studies*—T. Kurucsev and J. R. Zdysiewicz
- *Optical Rotatory Dispersion of Polypeptides in the Near Infrared Region*—Yu. N. Chirgadze, S. Yu. Venyaminov, and V. M. Lobachev
- *Molecular Beams of Macroions. III. Zein and Polyvinylpyrrolidone*—G. A. Clegg and M. Dole

Volume X-Monthly
Subscription Price: $70.00
Foreign Postage: $4.00
Back volume prices on request

WILEY-INTERSCIENCE

a division of JOHN WILEY & SONS, Inc.

605 Third Avenue, New York, N.Y. 10016

In Canada: 22 Worcester Road, Rexdale, Ontario